An investigation of bacterial composition and biofilm structure in mixed-community bioanodes

Dorin-Mirel Popescu

A thesis presented for the degree of
Doctor of Philosophy

Chemical Engineering and Advanced Materials
Newcastle University

April 2016

Abstract

Microbial fuel cells (MFC) are devices that convert chemical energy in soluble organic matter into electrical energy. They can be used for wastewater treatment coupled with energy production as well as for sensing, hydrogen production, electrosynthesis and metal recovery. Implementing these technologies is hindered by low current production. Currently, little is known about anodic communities regarding growth, electrode coverage, bacterial composition, biofilm structure, metabolism and how are they affected by operational factors. Such knowledge is needed to engineer MFCs that can overcome current limitations.

The subject of the present study is the mixed-community bioanode. The effects of light, anode-to-cathode surface ratio (A/C), substrate composition and anode potential on bioanodes were investigated. Two types of substrates were used: the first was based on sodium acetate and the second was a synthetic wastewater which simulated the chemical composition of real wastewater. First bioanodes were studied in presence and absence of light. A different set of bioanodes were grown at 9 different A/C ratios in single-chamber MFCs. Another set of bioanodes were grown in half-cells at 3 different anode potentials (-400 mV, -200 mV and 0 mV vs Ag/AgCl). The development of anodic biofilms and their long-term dynamics were investigated using a multi-anode reactor which allowed for better replication of running conditions.

Geobacter was identified in all bioanodes but its abundance was highly variable and dependent on running conditions. Over time the bacterial composition of bioanodes under constant conditions continuously changed during the first 33 days but stabilised by the 67^{th} day. Bioanodes fed on acetate had higher cell counts, *Geobacter* percentage, and current output than bioanodes fed on synthetic wastewater. Light exposure decreased coulombic efficiency by almost 14 times and favored growth of *Rhodopseudomonas* species in the detriment of *Geobacter*. Abundance of *Geobacter* increased with anode potential when fed on acetate (from 609.98×10^6 cells/gram at -400 mV to 5212.38×10^6 cells/gram at 0 mV) but decreased when fed on synthetic wastewater (from 200.6×10^6 cells/gram at -400 mV to 49×10^6 cells/gram at 0 mV). Current density and *Geobacter* density decreased by an order of magnitude when A/C ratio was varied from 1:12 to 1:1 but remained relatively constant when A/C was increased further to 8:1. Uneven biomass coverage on bioanodes and a decrease of biofilm volume with depth inside bioanodes were observed suggesting that anodes were only partially used by electrigenic bacteria. Results reported here have important implications for future reactor designs, on the use of three-dimensional bioanodes and on long-term applications of Microbial Fuel Cells.

Acknowledgments

I owe my thanks and gratitude to many people that have supported me in different ways while doing research and then during writing the thesis. First of all I thank to my supervisors Prof. Keith Scott and Dr. Eileen Yu for offering the opportunity to conduct research in the field of Microbial Fuel Cells for which I had acquired a passion and interest long before I started this PhD. Thank you both for your confidence, feed-back and patience.

To my group colleagues, Edward Milner and Martin Spurr I am grateful for being good friends and for creating a very productive environment at work where ideas were discussed and knowledge was shared. To Edward Milner thank you for reviewing all my experimental chapters and for teaching me to play Squash (one day I will beat you).

To the university workshop staff Steward Latimer, Ian Strong, Simon Daley and Brian Grover thank you for fitting my tasks in your extremely busy schedule. Thank you Rob Dixon for you reliability and for being the first person to ask whenever I needed technical help.

To my parents thank you for your encouragements and for moral support. To my girlfriend Ioana, many thanks and appreciation for your moral support and for listening to my ceaseless discourses about my work. Your love and patience mean alot to me.

Table of Contents

List of Figures

List of Tables

List of Abbreviations

A/C Anode to cathode surface area ratio

AcCA Acetate and Constant Anode Area

AcCC Acetate and Constant Cathode Area

AEM Anion Exchange Membrane

Ag/AgCl Standard Potential of the Silver Chloride Reference Electrode

APB Anoxygenic Photosynthetic Bacteria

ARB Anode Respiring Bacteria

ATP Adenosine Triphosphate

BES Bioelectrochemical System

BOD Biochemical Oxygen Demand

bp base pairs

CA Chronoamperometry

CI Current Interrupt

CNT Carbon Nanotubes

COD Chemical Oxygen Demand

CP Chronopotentiometry

CSCA Complex Substrate and Constant Anode Area

CSCC Complex Substrate and Constant Cathode Area

DET Direct Electron Transfer

DNA Deoxyribonucleic Acid

dNTP Deoxynucleoside Triphosphate

DO Dissolved Oxygen

EIS Electrochemical Impedance Spectroscopy

ET Electron Transfer

ETM Electron Transfer Mechanism

GDE Gas Diffusion Electrode

LSV Linear Sweep Voltammetry

MEA Membrane Electrode Assembly

MER Multi-Electrode Reactor

MES Microbial Electrochemical System

MET Mediated Electron Transfer

MIC Microbial Induced Corrosion

MTED Microbial Terminal Electron Donor

OC Open Circuit

OCP Open Circuit Potential

OECD The Organisation for Economic Co-operation and Development

OTU Operational Taxonomic Unit

PCoA Principal Coordinate Analysis

PCR Polymerase Chain Reaction

PI Propidium Iodide

PTFE Polytetrafluoroethylene

RE Reference Electrode

SHE Standard Hydrogen Electrode

TEA Terminal Electron Acceptor

Chapter 1. Introduction

1.1 Academic and industrial interest in bioelectrochemical systems

Human society and industry need to move away from the use of fossil fuel and embrace sustainable and environmental-friendly energy resources. Wastewater and other organic wastes contain huge amounts of energy which unfortunately are not normally accessible for society's needs [1]. Electricity producing microbes are attractive because they can tap such sources of energy. They are grown inside reactors called Bioelectrochemical system (BES) that are used for energy production and waste removal. BESs have found other niches in the wastewater treatment industry such as sensing and recovery of resources. BESs can also be integrated with anaerobic digestion for the purpose of polishing resulting effluent [2].

BESs that use microbes as catalyst for electricity production are also known as microbial electrochemical systems (MES). Production of electricity by bacteria in MES is known as electrigenicity. Bacteria with this ability are called electrigenic bacteria, electrigens, exoelectrigens or anode-respiring bacteria (ARB). Electrigenicity has also been observed outside MES where it represents an important mechanism of charge transfer between bacteria [3]. The study of electrigenicity becomes of practical interest because it extends the sphere of knowledge in environmental microbiology and ecology with the benefits of clean industries and environmental remediation. Furthermore, bacterial components involved in bacterial electrigenicity have shown transistor and supercapacitor properties, opening the door to new biomaterials.

The most common type of MES is the microbial fuel cell (MFC). The MFC uses a bioanode to convert chemical energy within organics to electricity. The microbial electrolysis cells (MEC) is another type of MES and is used for producing hydrogen or other useful chemicals. The third type of MES is the microbial half-cell where the anode or cathode potential is maintained at a constant value. The microbial half-cell is used for sensing, resource recovery and fundamental studies on electricity-producing bacteria.

MESs are of interest due their high number of industrial applications including energy production, wastewater treatment, soil remediation, sensing and production of useful compounds. Applications

of different types of MES are summarised below:

1. Lowering energy requirements for waste water treatment
2. Lowering the energy input in hydrogen production by electrolysis
3. Microbial electrosynthesis of useful compounds [4]
4. Biological oxygen demand (BOD) and/or toxicity sensors [5]
5. Bioremediation of conductive soils [6]

Academic interest on MES and bacterial production of electricity includes:

1. Culturing method in microbiology [7]
2. Lab-scale systems for studying Microbial Induced Corrosion (MIC) [8]
3. Bacterial production of electricity is important in many anaerobic microbial processes [9]
4. Electrigenicity is considered as signature for life in astrobiology [10]
5. Biomaterials [11]

1.2 The bioanode as an important component of MESs and a source of limitations

The bioanode is present in many MESs and its importance stems from its ability to convert soluble organics to electrical energy. In BOD and toxicity sensors the bioanode represents the sensing component of the device. In systems used for waste removal and/or electricity generation the bioanode is responsible for oxidation of organic waste. In MECs used for electrosynthesis at the biocathode, electrons are generated at the bioanode from oxidation of organic molecules. A chemical anode would need a constant supply of a redox active chemicals to provide the electrons. The disadvantages of this approach include increased costs associated with the production of oxidisable chemicals and managing resulting products. By comparison, a bioanode-based MEC extracts reducing power from wastewater which is inexpensive and available in huge quantities, with the added benefit of (partial) treatment.

MESs are currently not ready to be implemented mainly because their current output does not meet industry expectations. The bioanode is one of the factors responsible for limited current output. This could be solved with a better understanding of the anodic biofilm regarding its bacterial species composition, how it develops, varies with time and reacts to local conditions and reactor design. Increasing performance in MESs requires new designs that address chemo-physical limitations including mass transfer and electrical resistances. Equally important, MESs should

also accommodate for the dynamic nature and complexity of electrigenic biofilms. An integrated approach that combines microbial ecology with electrochemistry opens the door to bacterial community engineering applied on MESs.

1.3 Aims and objectives

The aim was to characterise the bacterial community of bioanodes under different operational conditions and across time from colonisation to maturity. Bioanodes were characterised by community analysis, confocal microscopy, epifluorescence microscopy, imaging biomass on entire bioanodes and electrochemical methods. Bioanodes were assessed in different reactor types, growth conditions and through time. The result is an integrated picture of bacterial ecology of bioanodes which can be used by engineers for future designs.

The objectives of this study and the rationale behind each are described below:

1. Establish what are the effects of exposing bioanodes to light
    - Before conducting other experiments it is important to assess the effect of light on bioanodes. This is because light is pervasive, can drive bacterial photosynthesis and some studies have successfully integrated light with MESs suggesting a positive effect. However, here it was hypothesised that light favours growth of photosynthetic bacteria which outcompetes ARBs for substrate and anode area. Establishing the effect of light on mixed-community bioanodes is important for deciding if MESs used in the current investigation should be protected from light exposure or not.
2. Develop a multi-electrode reactor (MER) which allows growth of bioanodes under identical conditions
    - The MER was designed with the purpose of improving replication of running conditions. It was used for studying bacterial community dynamics.
3. Investigate on the colonisation and growth pattern of anodic biofilms on three-dimensional (3D) electrodes
    - Colonisation and long-term dynamics of bioanode communities are poorly understood. Monitoring community composition is important for understanding system stability. Observing biofilm growth and morphology on 3D electrodes through time is important for assessing use efficiency of 3D anode materials by ARBs.
4. Investigate on the effect of anode potential on anodic biofilms

- The polarised bioanode is frequently used as a model for studying electron transfer processes and was also proposed as a culturing method in microbiology. It was hypothesised that energy gained by ARBs increases with anode potential.

5. Investigate on the effect of anode-to-cathode surface area (A/C) ratios on anodic biofilms

    - The (A/C) ratio was hypothesised to influence system performance and bacterial density on bioanodes.

6. Assess the effect of substrate type on bioanodes

    - The simplest organic substrate is acetate. It is non-fermentable and cannot sustain microbial growth in absence of a terminal electron acceptor. Acetate is readily available and consequently is the preferred substrate for ARBs. By comparison, wastewater is a complex mixture of proteins and carbohydrate polymers which require many steps before substrate can be used by ARBs. However results on bioanodes fed on acetate are frequently extrapolated to wastewater. 2 anolyte composition were used. The first uses sodium acetate 1 g/L as substrate and the second is based on the recipe recommended by The Organisation for Economic Co-operation and Development (OECD) to simulate the chemical composition of domestic wastewater. Comparing the communities associated with each type of feed when one operational factor is systematically varied, provides valuable information about the interaction between ARBs and other bacteria. It also allows to differentiate between the effects of anolyte type and those of anode poised potential, anode-to-cathode surface area ratio and exposure to light.

1.4 Outline of chapters

The thesis is structured on 9 chapters which includes 4 experimental chapters. All are briefly described below:

1. Introduction

2. Literature review on bioanodes

3. Materials and methods

4. Anodic Biofilms exposed to light: effect on community composition and performance

    - This is a case study on the competitive advantage of ARBs over anaerobic phototrophic bacteria. Both categories compete for organic substrate and anode surface. Results establish the effect of light on bioanodes and will impact all future reactor designs used in the next chapters.

5. The effects of substrate and anode potential on anodic bacterial communities, growth and electron transfer mechanism

    - Bioanodes were grown at 3 different anode potentials using both acetate and OECD anolyte recipes. Community analysis and bacterial abundance show how anode potential and substrate type impacts on bioanodes in terms of bacterial composition and abundance, electron transfer, current production and gained energy.

6. Effect of anode-to-cathode ratio on anodic community, performance and biofilm distribution

    - Bioanodes were grown in reactors with different A/C ratio and on two types of substrates. Results explain why current densities are higher for smaller anode areas.

7. Colonisation and development of anodic biofilms on 3D electrodes assessed with a specially designed multi-anode reactor

    - The development of a multi-anode reactor and its validation are described. Then it was used to investigate on the anodic biofilm colonisation and long-term dynamics. The reactor was run for 67 days with electrodes being sampled in pairs at different moments in time and investigated by confocal microscopy imaging and community analysis.

8. Conclusion

9. Appendix

Chapter 2. Literature review on bioanodes

The purpose of this literature review is to establish the role of microbial bioanodes in bioelectrochemical systems (BES), their limitations and possible strategies to solve for these. This chapter is structured in 6 subsections. First subsection describes the general layout of BES. Second subsection summarises common applications of BESs and the role of the bioanode in each. Third subsection describes fundamental aspects of bioanodes. These include electron transfer mechanisms, bacterial composition of bioanodes and the role of bacterial electricity production in nature. The latter aspect is important for better understanding what roles electrigens play in important microbiology processes, what are their required growth conditions and what is their relation to other bacteria. Forth subsection treats separately on the effects of light, anode potential and anode surface area on bioanodes. Fifth section treats on colonisation and community dynamics of bioanode communities. Subsection 6 treats on bioanode replication and the utility of multi-electrode reactors to increase replication. This chapter ends with a summary of common limitations associated with bioanodes, their origins and approaches to circumvent them.

2.1 Microbial Electrochemical Systems and electricity-producing bacteria

Microbial Electrochemical Systems (MES) are a type of BESs that work using electrical current generated by bacteria. There are many types of MESs each with a particular application. Some are in prototype phase and others have already been implemented or await optimization. A typical MES is the microbial fuel cell which is schematically shown in figure 2.1. Both the anode and the cathode are covered in electrigenic biofilms. The anodic and cathodic chambers are separated by an ion-exchange membrane. Electrodes are connected to each other using an external resistor. Bacteria on the bioanode perform oxidation of organics using the anode as electron acceptor. Electrons result from the oxidation process occurring at the bioanode and are transferred to the cathode. To maintain charge balance, protons are transported through the membrane to the cathode. Other cations can be transported or even anions in which case they are transported in opposite direction. Electrons are conveyed from the anode to the cathode where they are used to reduce oxygen or other electron acceptors such as nitrate or CO_2.

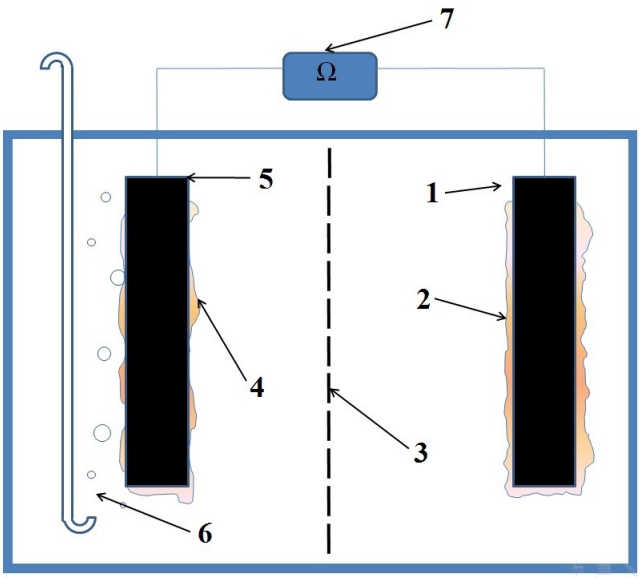

Figure 2.1: Diagram of Microbial Fuel cell with both bioanode and biocathode to show the main components of a typical MES: 1 - anode; 2 - anodic biofilm; 3 - ion-selective membrane; 4 - cathodic biofilm; 5 - (bio)cathode; 6 - air sparger; 7 - external resistor;

From this basic layout all other types of MESs are derived by changing one of the bioelectrode with a chemical electrode and/or by replacing the external resistor with a power supply or potentiostat. The MES is a very flexible technology with many variations for particular applications. Current can be used directly as energy, synthesis of hydrogen or other useful chemicals, reducing contaminants or as a signal for measuring organic content.

2.2 Applications bioelectrochemical systems and the role of bioanodes

2.2.1 Integration of MES with wastewater treatment and energy production

Activated sludge is one of the most frequently used systems for COD removal. One of its disadvantages is the conversion of soluble fraction into suspended biomass which then obturates equipment. Furthermore biomass accumulates toxins present in wastewater making its use problematic [12]. Inside the anodic chamber of a MES, oxidation occurs at potentials lower that the reduction potentials of typical electron acceptors such as oxygen or nitrate. This results in lower biomass yield inside MES which can be used to circumvent problems associated with high sludge production [12].

It is estimated that the energy residing in all municipal wastewater can cover around 2% of a country's consumption [13]. Aeration is the main energy-intensive step in the wastewater treatment and can reach 0.5 kWh per m^3 of sewage. On the other hand it is estimated that chemical energy residing within the untreated wastewater is approximately 9 times higher than the energy input used for its treatment [14]. The MFC is a candidate for replacing secondary treatments. Its purpose

is to lower the energy input required for wastewater treatment. The main advantage of MFCs is their ability to use water-soluble non-combustible fuels which contain high amounts of energy that cannot be harvested by any other means.

So far, most wastewater treating MFCs reported are lab-scale. Recently there have been reports of pilot-scale reactors able to treat real wastewater with no amendments [15, 16]. Such systems produced enough energy to power a pump used to circulate wastewater through the system achieving the purpose of self-powering. One of this reactor showed little performance degradation over a period of 6 months [15]. Furthermore it was found that the use of multiple modules ensured constant current and reduced fluctuations caused by temperature.

Upscaling is not required for MFCs powering small remote devices or sensors. These systems are characterized by small dimensions and an ability to use *in situ* organics making them maintenance-free. Small devices that can be powered by MFC include temperature-monitoring system and chemical sensors [17, 18]. Recent progress has lead to the development of low-power sensors and actuators [19]. This makes the MFC a feasible power source for remote and independent small robots with the advantage of using environmentally friendly components. Implantable medical devices are small and require power in the range of μW to mW. However their disadvantage is the need for battery replacement which sometimes require surgery. This can be circumvented by using an MFC for powering the device [20]. Currently the use of MFC-powered medical devices is limited by lack of biocompatible materials and need to assess power production for longer times.

Irrespective of application, using MFCs is limited by small voltages and erratic current production which is sensitive to organic loading and temperature. Current variations can be lowered by the use of multiple MFCs connected in parallel [15]. Production of small voltages can be circumvented by use of voltage converters. It was also shown that DC power from an MFC can be converted to AC power with less than 5% loss [21]. Capacitors can also be used for storing energy and then to donate it in a controlled manner [22].

2.2.2 Removal of toxic components and recovery of useful compounds

Wastewater contains toxic components which need to be removed before discharging. Removal of toxic chemicals and recovery of useful compounds occurs at the cathode. In these MESs the bioanode plays the role of counter electrode. Among toxic chemical that can be removed from wastewater by MESs are dyes commonly used in the paper, paint and textile industries. Azo dye is the most common type present in wastes. This can act as an electron acceptor and therefore can be reduced at the cathode of an MFC [23, 24]. Other dyes can be used as mediator to enhance current production and COD removal rates in MFCs such as azure A and azure B [25]. Rbu160 textile dye (reactive blue 160) was also removed at a cathode in a MFC [26]. Up to a concentration of

600 mg/L it has beneficial effects on current production but above that it became toxic for electrigens. Chlorine containing compounds are another class of toxic chemicals that can be removed by reduction at cathode [27].

Metal recovery as an application has gathered momentum recently. Conventional methods for metal recovery from wastes are not efficient at concentrations below 100 mg/L [28]. MFCs can be used under this threshold. Metals that can be recovered in MFCs include copper, gold, zinc, arsenic, vanadium, cobalt, selenium and uranium [28]. Metal recovery occurs at the cathode without the participation of a biological catalyst. The bioanode plays the role of counter electrode.

MFCs can also be used for denitrification of wastewater [29]. Nitrate and nitrite can be used as electron acceptors at the cathode of an MFC [30]. This results in nitrate removal with energy generation. Nitrogen removal rate was found to be proportional to current and a decrease in cathode potential resulted in lower nitrogen loading [31]. By comparison with oxygen, nitrate has a lower reduction potential but much higher solubility. Oxygen concentration is usually around 8 mg/L and nitrate can be hundreds of times higher. Therefore the nitrate reducing biocathode is advantageous compared with the oxygen biocathode. This suggests that using nitrate as terminal electron acceptor can lower aeration costs [32].

2.2.3 MFC-based sensors

Biosensing MFCs are used for measuring biochemical oxygen demand (BOD) levels. MFC sensors can also be applied for monitoring toxic heavy metals like Cu(II) and arsenic [33, 34] or can be integrated with the process monitoring system used in anaerobic digestion [35]. The bioanode plays the role of the sensing electrode. Advantages of using MFCs for sensing include their faster response time compared with standard procedures, low-cost and ability for continuous monitoring [34]. Other methods require expensive instrumentation (atomic spectroscopy, mass spectrometry) and frequent sampling coupled with the need for sample preparation. The principle of sensing is based on the response of ARBs to BOD loading and/or to concentration of toxic compounds. Electric current results from the ARBs activity which is measured and used as the sensor signal [36, 37]. The response to BOD loading vary greatly in terms of peak current and the shape of current profile. Regressions reported in the literature are inconsistent to each other. Although current shows a relation to BOD loading this response is complex and depends on many factors. It was therefore propose that BOD sensors be integrated with artificial neural networks for signal transducing [38]. Sensing can be improved by using a flow-through anode instead of flow-by anodes and by using fixed-potential anodes instead of fixed resistor [33].

2.2.4 Soil remediation

The occurrence of contaminated soils is increasing with the expansion of human activity. Contaminated soils can in time clean themselves naturally but at a very low rate. During this time local biodiversity decreases and negative effects on the environment accrue. Mass transfer limitations and spatial separation between electron donors and electron acceptors are responsible for the small rates of natural bioremediation. Bacteria consume oxygen faster that it can diffuse through soil resulting in a spatial separation between an anoxic high-organic loading region and an oxic region. The interface of these two regions is where bacteria can oxidise organics and it is called the oxidation interface. The process can be accelerated by injecting electron acceptors (oxygen or nitrate) or by applying a potential difference to drive transport of charged species [39]. Nitrate addition to contaminated soil is particularly not attractive due to permeability of soil matrix, costs and the possibility of generating secondary contaminants [40].

Degradation in anaerobic conditions is slower that in presence of oxygen or other soluble electron acceptors. However it was observed that inserting the anode of an MFC in contaminated soil resulted in better degradation of phenol compared with a non-MFC control and even better that oxygen injection [41]. The reason is that charge can be transported faster than oxygen. *Viggi et al.* reported a simplified version of sediment MFC consisting of one rod made of conductive material. [42]. Its upper half was in contact with oxygen-rich upper layers above petroleum contaminated sediments. The rod is also called cleaning electrode or microbial electrochemical snorkel and is depicted in figure 2.2. It exhibits polarity having one end immersed in the anoxic contaminated region which becomes a bioanode and the other end in contact with the oxic region which plays the role of the cathode. Anodic bacteria grow on electroconductive media introduced in soils contaminated with organic material. Organic contaminants are oxidised by anodic bacteria and the resulting electrons are conveyed to the cathodic part of the cleaning electrode. To close the circuit positive charge is transported through the soil. The entire system works as a microbial fuel cells with a very low resistance. It was reported that power increases with anode depth and anode potential was lower deeper in the sediment [43]. This shows that conditions for ARB growth improve with depth mainly due to a decreases of both oxygen concentration and redox potential. Closer to the surface, higher redox potential signal the presence of alternative electron acceptors which can inhibit electrigenesis.

This suggests that for bioremediation purposes the main condition for coupling oxidative and reductive processes is the insertion of conductive medium in contaminated soil or sediment. The bioanode part of the cleaning electrode is responsible for removing contaminants. Besides remediation, the sediment MFCs was proven to enhance the COD removing capacity of wetlands [44] and also increased the survival rate of the submerged macrophyte *Potamogeton malaianus* [45].

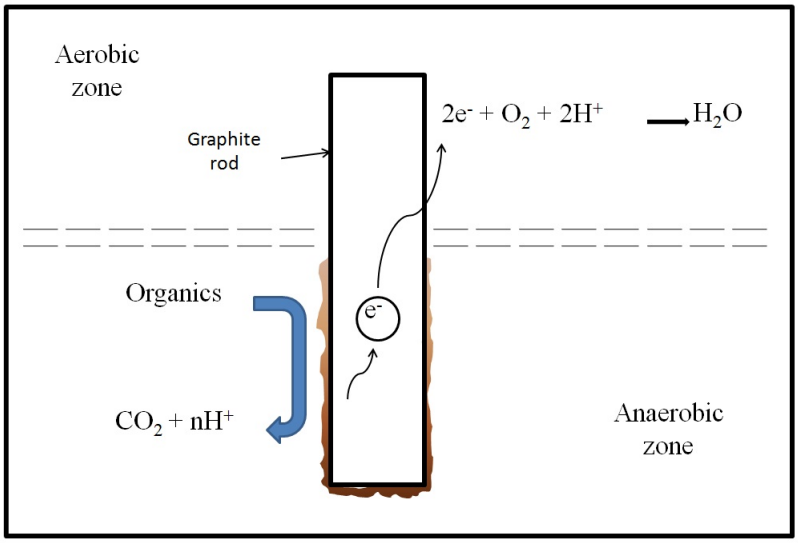

Figure 2.2: Graphical concept of the microbial electrochemical snorkel/cleaning electrode. This is a device proposed for sediment/soil bioremediation.

2.2.5 Electrosynthesis of hydrogen and other useful chemicals

Electrosynthesis is accomplished in Microbial Electrosynthesis Cells (MEC). Currently the list of chemicals that can be obtained by electrosynthesis includes only a few such as acetate, formate, methanol, methane and ethanol [46]. Hydrogen is another useful product that can be obtained using MEC technology. Hydrogen production occurs by proton reduction at the cathode. This can be either abiotic or a biocathode. A hydrogen producing biocathode can be created by reversing the hydrogen-oxidation reaction in a bioanode [47]. This conversion is achieved in 3 steps: a bioanode is grown on acetate, substrate is switched to hydrogen and the hydrogen oxidation reaction is reversed to proton reduction by lowering anode potential. However hydrogen production at abiotic stainless steel cathodes is more economically feasible due to its simplicity and ease of scale-up. Using a bioanode has a series of advantages over chemical anodes. First wastewater provides for an inexpensive and easily available source electron donors. Additionally the anodic process does not result in toxic products. Furthermore it decreases energy input and has the advantage of decreasing BOD in wastewater in parallel with hydrogen production. Compared to domestic wastewater, industrial wastewaters have higher organic loading and their use in MEC result in higher hydrogen yields [48].

2.2.6 The bioelectrochemical system as a tool for microbiology

The polarised bioanode and the MFC have been proposed as culturing methods in microbiology [7]. Problems of replicating environmental conditions for the culture and isolation of new species are well known. Only a very small proportion of bacteria can be currently cultured [49]. This is espe-

cially true for bacteria involved in syntrophic associations, many of which perform inter-electron exchange [9]. For these bacteria the polarised electrode of a MES acts as the syntrophic partner. With the introduction of MES as a culture procedure new types of environments can now be replicated in laboratory conditions. This strategy has already led to the discovery of new species of bacteria in the case of biocathodes [50] and will probably lead to further discoveries in terms of new species, microbial processes and interactions. After the discovery of the role of electrigenicity in methanogenesis, there has been an increased interest in further exploring electrigenicity in microbes. The expected benefit is a deeper knowledge of microbial electrochemistry which can accelerate implementation of MESs [51]. It can also lead to an improvement of industrial processes that rely on electroactive bacteria such as anaerobic digestion and remediation of polluted soils.

2.3 Fundamentals of bioanodes and electrigenic bacteria

Bacteria that transfer electrons to an electrode are known as electrigens or exoelectrigens [52]. Due to their ability of using an anode as a terminal electron acceptor (TEA) these bacteria are also known as anode respiring bacteria (ARB). More generally they are called electrigens [53]. The last name emphasizes their current producing ability and applies to both anodic and cathodic bacteria. The defining component of a MES is the bioelectrode which is an electrode that interacts by electron exchange with a bacterial community. The bacterial community can be either fixed forming a biofilm covering the electrode or free as a planktonic community. It can be mixed or based on single strains. The mixed community is composed of many species of bacteria of which only some are responsible for electricity production and are called electrigens. The other species perform other functions and are called non-electrigens. The metabolic functions they perform can be coupled or decoupled from electricity production.

2.3.1 Electron transfer mechanisms in bioanodes

Electron transfer (ET) from ARBs to the anode occurs either directly or by use of diffusible mediators. The first mechanism is called direct ET (DET) and uses extracellular conductive structures that bridge bacteria and the anode. The second type is called indirect or mediated ET (MET) and relies on bacterial or artificially produced mediators. Mediators are reduced inside bacterial cells and are oxidised at the anode surface. Current production by DET is higher compared to MET [53]. Both MET and DET are schematically shown in figures 2.3A and 2.3B respectively.

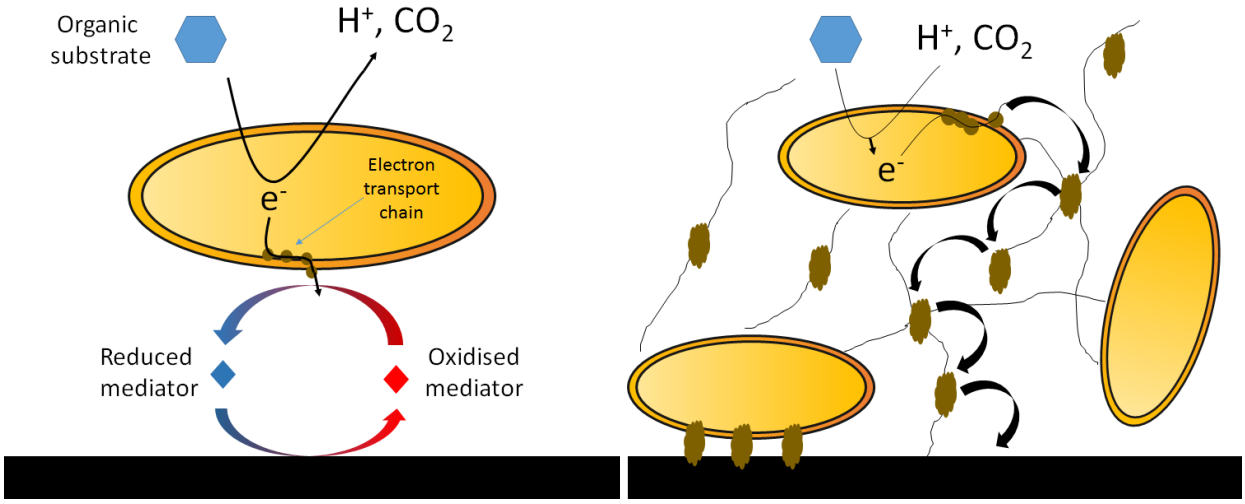

Figure 2.3: Electron transfer mechanisms in bioanodes. A: mediated electron transfer; B: direct electron transfer;

MET is typical for planktonic bacteria because it does not require proximity between electrigens and electrode. The mediator is produced by bacteria or is added to the reactor [54]. Mediators must be non-toxic, reversible and highly-diffusible. The mediator must be able to reversibly accept and donate electrons in order to act as an electron shuttle. Production of mediators requires energy consumption on the part of bacteria. Furthermore mediator concentration has to be high enough to support bacterial growth. Mediators can get diluted or be washed away from reactors during medium change. This can be avoided by chemical attaching the mediator to the surface of the anode. In one case riboflavin was immobilized on anode surface leading to increase in power density [55]. EIS measurements showed a decrease in charge transfer resistance (R_{ct}). On the long term this procedure suffers from slow leaching of riboflavin from the anode surface.

Shewanella species are the most studied bacteria performing MET. *Shewanella oneidensis* transfer electrons to the anode using flavins as mediators [56]. In one study riboflavin was the most common mediator and it was found that it can be adsorbed on the surfaces of anodes and other minerals commonly used as TEA such as Fe^{3+} and Mn^{4+} oxides. Other natural mediators include pyocyanin and phenazine-1-carboxamide [57]. Measurements of phenazine in *Pseudomonas aeruginosa* biofilms showed that the concentration of this mediator is higher inside biofilms compared to bulk solution [58]. Within biofilms its concentration profile increased from biofilm surface to anode surface. This shows that some ARBs overcome dilution limitation associated with MET by confining mediators inside the biofilm. Another strategy is the simultaneous release of mediators by the entire community controlled by quorum sensing [59]. When the population is small, mediators are diluted or can diffuse far from bacteria. Quorum sensing circumvents this problem by allowing bacteria to coordinate mediator release. This shows that MET requires collaboration between bacteria.

DET requires the electrigens to be in close contact with the electrode. Bacteria involved in DET form biofilms. This has been observed with many bacteria including *Geobacter* species and even in *Shewanella putrefaciens* [60]. *Kim et al.* reported that in *Shewanella putrefaciens* biofilms current production was only possible with anaerobically grown cultures but not with aerobically grown cultures suggesting physiological changes are required for current production [60]. DET occurs by direct contact between bacteria and anode using cytochromes, conductive pili or both [61]. Electrons result from oxidation processes inside the cell and are used for reducing NAD+ to NADH. Electrons are pulled away from NADH by a membrane-bound enzymatic complex called NADH-dehydrogenase. Its role is to couple electron transport with proton-gradient formation across bacterial membranes, required for energy conservation. In electrigens NADH-DH donates electrons to a series of cytochromes. Electrons leave the cells and are transported through a network of outer-membrane cytochromes and/or conductive bacterial appendages [62].

The electron transport network forms a conductive matrix which allows the electrigens to form thick biofilms performing long-distance ET. The concentration of reduced cytochromes decreases from the exterior of the biofilms towards the anode surface, while the concentration of oxidised cytochromes follows the opposite distribution. Several cytochromes involved in DET were identified. MacA is a di-heme cytochrome present in the periplasmic space of *Geobacter sulfurreducens* [63]. Its presence is necessary for using insoluble electron acceptors. PpcA is a tri-heme cytochrome present in the periplasmic space and is also involved in ET. OmcB and OmcE are multiple cytochromes associated with the outer membrane and OmcZ is associated with extracellular material [62]. Multi-heme OmcS is associated with *Geobacter* pili. This cytochrome is involved in the transfer of electrons to Fe^{3+} and electrodes [64]. Flocs of *Geobacter* that express high amounts of OmcS, show electric conductance when placed between 2 electrodes [64] suggesting that OmcS is involved in ET.

Electrons can also be transported through conductive appendages that connect bacteria with each other and with the electrode. Non-motile tube-like bacterial appendages are known as pili [65]. These structures are diverse and are involved in many processes including inter-bacteria communication and transfer of genetic material. Fibrous proteins that make up pili are called pilins. Conductive pili in electrigenic bacteria are called nanowires. They form a network which acts as a scaffold for outer-membrane cytochromes, but some were found to have intrinsic conductive properties. Measurements on nanowires showed the average width is 7-12 nm and average length is 6 μm, although they depend on growth conditions [66].

It was suggested that pili have mainly a structural role in organising c-type outer membrane cytochromes and not necessarily directly involved in ET [67]. However a comparison between 2 strains of Geobacter differing in their current producing properties, showed that the better performing strain produced thicker biofilms with a higher density of nanowires and a lower concentration

of outer membrane cytochromes [68]. This suggests that pili have intrinsic conductive properties. Furthermore, it was shown that in some instances nanowires can convey electricity without cytochromes. For example some iron reducing bacteria such as *Pelobacter* do not exhibit cytochromes but only pili showing that these are enough for ET [69]. Also *Desulfovibrio desulfuricans* can produce nanowires in response to presence of insoluble electron acceptors [66]. Type IV pili are electrically conductive and were found to be involved in reduction of Fe^{3+} oxides [69]. Measurements conducted on isolated pili revealed that high conductivity is an intrinsic property of the pili. Current to voltage relation was found to be linear showing that pili have ohmic resistance [66, 69]. However *El-Naggar et al.* reported that nanowires conductivity is not constant but is a function of applied voltage [11]. Pili are also involved in cell to cell ET [69] and are important in colonising surfaces of solid electron acceptors [62]. Their structural function is to hold cells together in biofilms grown around solid electron acceptors. The wide range of pili functions in electrigenic bacteria suggests a high diversity of pili types. Some are electrically conductive while others have pure structural roles keeping the biofilm together and providing a physical support for attachment of outer-membrane cytochromes.

Charge separation occurs inside electrigenic biofilms. This results in formation of pH gradients across *Geobacter* biofilms [62,70]. Proton concentration inside a *Geobacter* biofilm can be an order of magnitude higher that the bulk concentration. The magnitude of pH gradient increases when current is produced and relaxes when the electrodes are disconnected. Lower pH inside the biofilm limits ET and bacterial cell growth. However, in a different study using *Shewannela oneidensis* biofilms, pH gradients were not observed and it was proposed that this is not a limiting factor to current production [71]. The existence of pH gradients and their effect on current production seem to depend on ET type. In MET protons may not be produced because the mediator acts as a charge-transporting agent. Instead, only redox gradients were measured across MET biofilms [71]. These showed similar relation to current production as the pH gradient in DET biofilms. Redox gradients were also measured across *Geobacter* biofilms [67].

2.3.2 Microbial composition of anodic communities and the identification of electrigens

A survey of 74 strains isolated from a mixed-community bioanode, identified 25 electrigenic bacteria [72]. These included species from *Vibrio*, *Enterobacter*, *Citrobacter* and *Bacillus* genera. Studies of single strains identified a wide range of ARBs such as *Geoalkalibacter ferrihydriticus* [73], *Enterobacter cloacae* [74], *Clostridium butyricum* [75], *Lactobacillus pentosus* [76], *Escherichia coli* [77], *Pseudomonas sp.* [78], *Caloramator australicus* [79], *Desulfobulbus propionicus* [80], *Desulfovibrio desulfuricans* [81], *Geothrix fermentans* [82], *Thermincola ferriacetica* [83, 84], *Ochrobactrum anthropi* [85], Aeromonas [86] and *Enterobacter cloacae* [34]. Out of these only 4 are gram-positive (*Bacillus stratosphericus*,*Thermincola ferriacetica*, *Lactobacillus pentosus* and

Caloramator australicus) while the majority of known electrigens are gram-negative.

There is general agreement that mixed species outperform pure cultures [19, 52, 87]. It was suggested that this is due to protection of ARBs from oxygen by anaerobes or to a wider pool of ARBs from which the best are selected [88]. Other studies showed that non-electrigens perform hydrolysis and fermentation processes resulting in low molecular weight organic species used by ARBs [87, 89]. This shows an important relation between ARBs and fermenters. Mixed communities may also contain species that negatively impacts on current production or directly on ARBs. Hydrogenotrophic bacteria and methanogens were found to compete for substrate with ARBs [87, 90]. Grazing protozoans were found to be responsible for performance degradation in sediment MFCs [91]. While protozoa grazing on electrigens has only been detected in sediment MFCs, it could be possible they occur in scaled-up systems treating wastewater.

The most common species of bacteria identified in bioanodes from field MESs (sediment/benthic/plant MFCs) and laboratory MES (MFCs and half-cells) are summarised in table 2.1. *Geobacter* is the most commonly identified ARB in bioanodes grown in laboratory and field conditions. Field MFCs such as benthic or sediment MFCs show different community composition compared to laboratory MFCs. Bioanode communities of field MFCs can have other electrigens than *Geobacter* such as *Pseudomonas putida* and *Ochrobactrum anthropi* [40]. Bioanodes from field MFCs show more diverse communities including members from *Actinobacteria*, *Acidobacteria* and *Epsilonproteobacteria* which are not usually detected in laboratory MFCs. Their presence can be explained by the permanent contact of the bioanode with the environment which is inherently biodiverse and shows fluctuating conditions. Conversely, conditions in laboratory MFCs are constant and feeds are sterile. This can explain why bioanode communities from laboratory MFCs show consistently the same common genera including *Pelobacter*, *Arcobacter*, *Cloacibacillus*, *Dysgonomonas*, *Alcaligenes*, *Clostridium*, *Desulfovibrio*, *Pseudomonas*, *Aeromonas*, *Azospira*, *Comamonas*, *Sedimentibacter* and *Paludibacter*. Currently there is not enough data to establish if the above are electrigenic or what is their role in relation to electricity generation. If they are involved in syntrophic aggregations performing electron exchange with the ARBs, they could act as electron sinks. Identifying such phenomena is important because it would mean syntrophies in bioanodes should be inhibited.

Table 2.1: Most common bacterial general identified in field MFCs (sediment, benthic or plant MFCs), and MFCs and H-cells grown in laboratory conditions. For each category the number in brackets indicates number of articles reviewed that reported on species composition on bioanodes from that type of MES.

Genus	Field MFCs (9)	Lab MFC (34)	Lab H-cell (17)
Geobacter	7 [45, 89, 92–96]	15 [88, 97–110]	12 [90, 101, 111–120]
Clostridium	4 [40, 93–95]	12 [99, 104, 107–109, 121–127]	3 [113, 116, 128]
Pseudomonas	2 [40, 92]	11 [97, 99, 106, 107, 109, 121, 122, 125, 126, 129, 130]	5 [90, 111, 112, 114, 128]

continued ...

. . . continued

Table 2.1: Most common bacterial general identified in field MFCs (sediment, benthic or plant MFCs), and MFCs and H-cells grown in laboratory conditions. For each category the number in brackets indicates number of articles reviewed that reported on species composition on bioanodes from that type of MES.

Genus	Field MFCs (9)	Lab MFC (34)	Lab H-cell (17)
Comamonas	2 [40, 89]	7 [88, 102, 103, 106, 109, 122, 123]	3 [112, 128, 131]
Desulfovibrio	0	10 [97, 102, 107, 110, 123, 125, 129, 130, 132, 133]	1 [131]
Acinetobacter	1 [92]	6 [97, 106, 109, 129, 130, 134]	3 [114, 128, 135]
Desulfuromonas	3 [45, 92, 136]	4 [99, 104, 105, 137]	3 [116, 117, 135]
Pelobacter	3 [45, 94, 136]	3 [99, 100, 105]	3 [90, 117, 119]
Stenotrophomonas	2 [40, 92]	6 [84, 102, 109, 124, 126, 130]	1 [128]
Bacillus	3 [40, 93, 136]	5 [84, 109, 121, 125, 138]	1 [135]
Spirochaeta	1 [45]	7 [84, 100, 106, 122, 123, 130, 133]	0
Ochrobactrum	1 [40]	6 [100, 102, 121–123, 130]	0
Sedimentibacter	1 [40]	5 [88, 109, 125, 129, 130]	1 [112]
Dysgonomonas	0	6 [97, 122, 123, 126, 129, 130]	1 [112]
Arcobacter	0	4 [104, 123, 125, 130]	2 [112, 128]
Eubacterium	0	6 [88, 97, 104, 121, 123, 130]	0
Geothrix	3 [45, 93, 94]	3 [102, 107, 127]	0
Desulfobulbus	2 [45, 94]	4 [98, 110, 125, 132]	0
Mycobacterium	2 [40, 93]	3 [98, 122, 130]	1 [112]
Thiobacillus	3 [93–95]	2 [122, 139]	1 [128]
Enterococcus	0	6 [99, 108, 121, 125, 129, 130]	0
Sphingobacterium	0	5 [99, 109, 126, 130, 137]	1 [128]
Acidovorax	0	6 [99, 102, 106, 109, 126, 130]	0
Proteiniphilum	0	4 [100, 122, 129, 130]	1 [111]
Flavobacterium	3 [45, 93, 95]	2 [106, 137]	0
Hydrogenophaga	0	2 [109, 137]	3 [112, 114, 128]
Azospirillum	2 [40, 96]	3 [122, 127, 130]	0
Bradyrhizobium	2 [93, 136]	3 [109, 122, 130]	0
Thauera	0	4 [102, 109, 127, 139]	1 [135]
Achromobacter	1 [40]	3 [109, 124, 130]	1 [112]
Chryseobacterium	0	2 [97, 123]	3 [112, 128, 135]
Rhodococcus	0	3 [122, 123, 132]	1 [120]
Paludibacter	0	4 [88, 124, 129, 130]	0
Azospira	1 [45]	2 [106, 107]	1 [128]

continued . . .

... continued

Table 2.1: Most common bacterial general identified in field MFCs (sediment, benthic or plant MFCs), and MFCs and H-cells grown in laboratory conditions. For each category the number in brackets indicates number of articles reviewed that reported on species composition on bioanodes from that type of MES.

Genus	Field MFCs (9)	Lab MFC (34)	Lab H-cell (17)
Gemmatimonas	3 [40,45,93]	0	1 [128]
Cloacibacillus	0	4 [104,106,109,122]	0
Lactococcus	0	4 [105,121,122,130]	0
Bacteroides	0	4 [97,105,122,129]	0
Longilinea	2 [45,93]	1 [129]	1 [135]
Alcaligenes	1 [40]	3 [88,109,121]	0
Aeromonas	1 [92]	3 [105,107,140]	0
Brevundimonas	0	3 [126,130,137]	1 [128]
Paracoccus	1 [94]	2 [106,125]	1 [128]
Diaphorobacter	0	4 [102,109,125,139]	0
Enterobacter	1 [40]	3 [104,122,130]	0
Erysipelothrix	0	4 [87,109,130,134]	0
Dechloromonas	1 [45]	3 [97,102,139]	0
Desulfobacca	3 [45,93,95]	0	0
Afipia	1 [136]	2 [122,130]	0
Victivallis	0	3 [102,109,130]	0
Pseudoxanthomonas	1 [40]	1 [139]	1 [128]
Gordonia	1 [40]	1 [109]	1 [112]
Trichococcus	0	3 [105,109,125]	0
Acetoanaerobium	0	3 [100,105,129]	0
Desulfatirhabdium	1 [45]	2 [110,129]	0
Parabacteroides	0	3 [109,129,130]	0
Parvibaculum	1 [40]	1 [130]	1 [112]
Holophaga	0	3 [87,102,137]	0
Anaerovorax	1 [40]	2 [109,129]	0
Aquamicrobium	0	2 [102,130]	1 [128]
Ignavibacterium	2 [45,93]	0	1 [112]
Sphingomonas	1 [136]	1 [109]	1 [131]
Petrimonas	0	1 [129]	2 [111,128]
Desulfocapsa	3 [92,93,136]	0	0
Terrimonas	2 [45,93]	1 [102]	0

continued ...

...continued

Table 2.1: Most common bacterial general identified in field MFCs (sediment, benthic or plant MFCs), and MFCs and H-cells grown in laboratory conditions. For each category the number in brackets indicates number of articles reviewed that reported on species composition on bioanodes from that type of MES.

Genus	Field MFCs (9)	Lab MFC (34)	Lab H-cell (17)
Sphingopyxis	0	2 [122, 130]	1 [128]
Arthrobacter	1 [93]	2 [123, 141]	0
Acetobacterium	0	2 [97, 129]	1 [90]
Hyphomicrobium	2 [93, 95]	1 [130]	0
Dehalogenimonas	2 [45, 93]	0	1 [112]
Lactobacillus	0	3 [121, 125, 134]	0
Syntrophus	3 [92, 93, 95]	0	0
Burkholderia	0	3 [84, 97, 139]	0
Treponema	1 [95]	1 [133]	1 [112]
Bellilinea	1 [45]	1 [109]	1 [135]
Azoarcus	0	2 [107, 127]	1 [135]
Bosea	1 [136]	1 [102]	1 [128]
Rhodopseudomonas	0	2 [109, 125]	1 [90]

Big differences in community composition between inocula and mature bioanodes have been observed [121, 129, 142]. Wastewater that is often used to inoculate bioanodes is dominated by members of *Epsilonproteobacteria*, *Gammaproteobacteria* and *Bacteroidetes* [101]. Conversely bioanode composition changes dramatically being dominated by *Deltaproteobacteria*, *Bacteroidetes*, *Firmicutes*, *Synergistetes* and *Clostridia* . *Deltaproteobacteria* are usually represented by *Geobacteraceae*, *Desulfuromonadacea* or *Desulfobulbaceae*. Their abundance is particularly higher on better performing MFCs and on poised potential bioanodes and increases with time concomitantly with increase in performance. Community composition at bioanodes is impacted by anode material [87, 106], substrate [99, 142] and external resistance [89, 99]. Furthermore bioanode communities are different communities sampled from other parts of the MFC reactor such as the anolyte [129, 143] or ion-exchange membrane [143].

2.3.3 Electrigenicity in nature

Bacterial electricity production has been mainly described in man-made systems such as MESs. This has lead to a better understanding of many important aspects of electrigenicity such as electron transfer mechanisms, energy conservation and identification of many electrigenic bacteria. The

literature body describing electrigenicity outside MESs has grown considerably in recent years. Understanding electrigenicity in nature is important for a number of reason. First tt can help in identifying suitable environments for inocula extraction and explain why activated sludge is a particular good source of electrigens. It can lead to finding new ways of harnessing energy produced by electrigens. Furthermore it can have far-reaching implications as electrigenicity was also considered as a biosignature for finding life on other planets [28] and was found responsible for geological structures previously unexplained [144].

Recently one study has described in nature what seems to be microbial electrigenesis [3]. This was the first finding where sulfide oxidation in the anoxic part of a marine sediment and oxygen reduction at the water-sediment interface was coupled by bacterial activity. Pyrite minerals together with bacterial nanowires and outer membrane cytochromes were suggested to be involved in electron transfer that couples sulfide oxidation to oxygen reduction [144]. Transported ions included protons, Ca^{2+} and Fe^{2+}. Gradients of oxygen, pH, sulfide and electric potential were measured across the sediment.

Bacteria from the *Desulfobulbaceae* family were found to be responsible for electric coupling between sulfide oxidation deeper in sediments and reduction of oxygen [145] or nitrate [146] at the surface of the sediments. Electric coupling was associated with the presence of pH gradients and a spatial separation between electron donors (sulfide) and electron acceptors (oxygen or nitrate). These bacteria were called cable bacteria. They have a filamentous morphology and their cell wall shows ridges parallel across the cell length and uniformly distributed. It was found that the ridges correspond to periplasmic filaments with electron conductive properties. These filaments span multiple cells connected in series and are thought to be responsible for electric coupling of oxidation and reduction processes in sediments. Cable bacteria can adapt to changes in spatial separation of sulfide and oxygen by directed growth and movement. They form a continuous community connected simultaneously with the deeper anoxic zone and the oxic zone above [146].

Cable bacteria are responsible for both oxidation and reduction processes. In their case the purpose of electron transport is to overcome spatial separation between electron donors and electron acceptors. However in other microbial communities oxidation and reduction do not occur in the same bacterial cell. To allow metabolic coupling, these bacteria form syntrophic associations [147]. Recent findings suggests that direct exchange of electrons between syntrophic partners is responsible for metabolic coupling. For example, *Geobacter sulfurreducens* is able to grow on acetate in syntrophic aggregations with hydrogen-oxidising bacteria [148]. Metabolic coupling consists in the transfer of reducing equivalents from one partner to the other. Interspecies exchange of molecular hydrogen is incompatible with low partial pressure of hydrogen and its removal rate. Also hydrogen becomes inhibiting for acetate oxidation at very low partial pressure. It was therefore proposed that hydrogen is transferred as electrons and protons which have higher mobility compared to molecular

hydrogen.

Direct inter-species electron transfer was proven to be responsible for metabolic coupling in a syntrophic consortia of methane oxidisers and sulphate reducers [149]. Neither of these 2 processes could occur in isolation. Therefore exchange of reducing equivalents between oxidisers and reducers was thought to be responsible for metabolic coupling in syntrophic associations. Models based on diffusion of H_2 could not explain the high metabolic rates. Furthermore within syntrophic associations the 2 partners are spatially separated. Methane metabolic rates were found to be independent of inter-species distance which is incompatible with hydrogen diffusion-based model. Staining with 3,3'-diaminobenzidine identified cytochromes on the membranes of both partners and dispersed in the intercellular space suggesting coupling by DET.

DET between *Geobacter metallireducens* and *Geobacter sulfurreducens* forming aggregates was demonstrated [64]. *G. metallireducens* can oxidise ethanol using Fe^{3+} as electron acceptor and producing hydrogen in the process. *G. sulfurreducens* cannot metabolise ethanol but can oxidise hydrogen using fumarate as electron acceptor. In this association oxidation and reduction are not separated by partners. Instead the association's purpose is to keep hydrogen partial pressure low which could otherwise inhibit the entire bacterial activity. Direct electron exchange does not couple oxidation within one partner with reduction within the other. Instead this is a mechanism of avoiding transfer of molecular hydrogen which would require gradients that are incompatible with bacterial activity. Addition of conductive minerals to a syntrophic association of *Geobacter sulfurreducens* and *Thiobacillus denitrificans* enhanced metabolic coupling of acetate oxidation and nitrate reduction [150] showing the role of electron interspecies exchange in metabolic coupling.

Electrigens can be enriched from a wide variety of natural sources like river sediments [151, 152], ocean cold seep [92] and seafloor [153]. It was suggested that electrigens are more ubiquitous in nature than previously thought [154]. Activated sludge is a common inoculum used for growing bioanodes. Activated sludge contains flocs which are conglomerations of bacteria and organic waste. At the surface of these flocs, steep oxygen and redox gradients were measured [155]. It is possible that electrons are being produced inside the flocs as a result of oxidation of organics catalysed by anodic bacteria. Electrons are then transported at the surface of the floc where cathodic bacteria use them for catalysed oxygen reduction. Thus flocs are natural MFCs explaining the suitability of activated sludge as inoculum for both bioanodes and oxygen reducing biocathodes. Bacterial aggregations from anaerobic digestion effluent were found to be 3-fold more electrically conductive than artificial associations [156]. Community analysis revealed presence of *Geobacter* species and methanogens. This shows why wastewater is a good inoculum for MESs.

With the acknowledgment of electrigenicity as a newly discovered bacterial function, the list of biomaterials and biocatalysts has increased to include components from electrigenic bacteria [11].

Such components include electron-conveying structures such as pili and outer-membrane cytochromes and enzymes endowed with electronic gates that can act as interface through which their activity can be controlled and powered. In the light of these new findings it seems electrigenicity plays important roles in many microbial processes. These include (electro-)methanogenesis, oxidation in anaerobic environments, iron reduction/oxidation and corrosion.

2.4 The effects of operational factors on bioanodes

2.4.1 Effect of light

There have been many reports on using light to drive electricity in different MESs. These vary in terms of inoculum, anode material, substrate and which of the electrodes was subjected to light. A review from 2010 by *Rosenbaum et al.* identified 5 strategies for harnessing light energy using MESs [157]. The first uses photosynthetic bacteria at the anode with added artificial mediators. Second is hydrogen production by anaerobic photosynthetic bacteria and oxidation of the resulting hydrogen at a platinum anode. Third is the use of a mixed consortium of electrigens and photosynthetic bacteria at the anode. Photosynthetic bacteria produce organics during light periods which are then used by electrigens during night periods. Forth is the use of photosynthetic bacteria to generate oxygen at the cathode. Fifth is DET between photosynthetic bacteria and anode.

In light-exposed cathode MESs, the anode is usually protected from light. In these systems the purpose of light is to drive the cathodic reaction. For example using a phototrophic community, CO_2 was reduced in presence of light at the biocathode [158]. Light is also used for oxygen generation by photosynthetic organisms in the cathodic chamber [159]. In these systems light-dark cycles were observed with current increasing during the day. These are explained by oxygen production under light. *Chlorella vulgaris* produced oxygen during light periods which was then used as electron acceptor at the cathode [160]. The anode was fed with artificial wastewater containing glucose and fructose. This design has the added advantage of growing *Chlorella* which is valued for its lipid content in the fuel production industry [159, 161]. In another study algal biomass produced in the cathodic chamber was used as feed in the anodic chamber [162]. These suggest that wastewater treatment can be coupled with algal biomass production at the cathode which also decreases aeration costs. Catholyte can be recirculated between the cathodic chamber and an external bioreactor where algae are exposed to light while the MFC itself is protected from light [163]. This set-up was proposed as replacement for aeration.

In anodes exposed to light, the community can be mixed or based on single strains. Many species of cyanobacteria were shown to be electrically active at the anode [164]. Cell voltages ranged from 3 to 30 mV on a 1 kΩ external resistor for an anode surface area of 50 cm^2 which is equivalent

to a current density between 0.6 and 6 mA/m^2. A relatively higher current density of 300 mA/m^2 was reported using *Anabaena* [165]. It was suggested that electricity production in cyanobacteria is a mechanism of avoiding photo-oxidation by discharging excess reducing equivalents formed during excessive illumination [164]. ET mechanism in cyanobacteria remains unknown. However nanowires have been observed in *Synechocystis* [166]. *Badalamenti et al.* reported that also green sulfur bacteria were able of producing current at an anode, but the mechanism remains unknown [167]. Current decreased in the dark periods and increased in light exposure. Inoculum was previously enriched for green sulfur bacteria. Community analysis identified green sulfur bacteria at high percentages however it also showed presence of *Geobacter*. It is possible that *Geobacter* was not affect by light directly but it can be replaced by other bacteria which have a competitive advantage under light conditions.

Another mechanism of converting light to electricity at anodes is based on *in situ* oxidation of photobiological produced hydrogen. In these MESs a bacterium uses light to convert organic substrate to hydrogen which is then oxidised at platinum anodes. The advantage of this approach is direct utilisation of biologically produced hydrogen. One of the disadvantages of this approach is anode performance degradation caused by microbial byproducts [168]. Bacteria capable of hydrogen production as pure strains in an anodic chamber include *Rhodobacter sphaeroides* [168, 169] and *Chlamydomonas reinhardtii* [170].

Lastly, bioanodes can be fed with organics synthesized by photosynthetic organisms under light. The producer can be a plant with its roots inserted in the anodic chamber of an MFC [171]. Organics released by plant root account for 10-20 % of photosynthetic output. In this design the bioanode is not directly exposed to light. Producers can also be represented by photosynthetic microorganisms grown in the anodic chamber [172]. In this case current decreased in light conditions but recovered in the dark. Oxygen production by algae in light was the proposed cause of current inhibition. This was confirmed by another study which measured oxygen production in light periods [173]. Organics were produced by photosynthetic bacteria in light, and were oxidised in the dark by electrigens. This set-up was a closed system where carbon was continuously recycled between organic molecules and CO_2. Therefore it is not suitable for wastewater treatment but is a proposed device for conversion of light energy to electricity.

Although the literature suggests that light has a positive effect on MESs it should be noted that few studies have directly investigated on the effect of light on mixed-community bioanodes. Wastewater can carry many types of bacteria. Such communities, due to their high biodiversity, have the potential of changing in response to growth conditions. Purple non-sulfur bacteria are particularly important due their versatile metabolic capabilities which potentially allows them to dominate a community in presence of light. For example, *Rhodopseudomonas palustris* and *Rhodobacter capsulatus* can perform anaerobic respiration using Fe^{3+} minerals or anodes as electron accep-

tors [174]. However due to the lower reduction potential of these TEAs, they gain less energy and at a lower rates compared with using light. This suggests that purple non-sulfur bacteria can change their metabolism in response to growth conditions, choosing light over insoluble TEA. Therefore inside MFCs in presence of non-fermentable substrates and light exposure, purple non-sulfur bacteria can grow without using the anode, leading to a decrease in performance. *Rhodobacter* and *Rhodopseudomonas* were identified in a bioanode performing MET [175]. The inoculum was previously enriched for non-sulfur bacteria. However no dark controls were provided thus it remained unknown if other electrigens could develop in absence of light capable of higher performance. It was suggested that a strain of *Rhodopseudomonas palustris* is capable of DET reaching a current density of 9900 mA/m^2 [176]. This means that some non-sulfur bacteria are capable of producing high currents but not when exposed to light when other metabolic activities prevail such as hydrogen production.

2.4.2 Effect of anode potential

Anode potential is an important factor that influences current output, biomass production and ET mechanism in bioanodes. It can be controlled using a potentiostat or by changing external resistance in MFCs. Higher anode potential can lead to faster start-up [177]. Regarding its effect on biomass growth it was proposed that anode potential controls the amount of energy gained by electrigens [151]. A review on the effect of anode potential revealed that most often current increases with anode potential, with some exceptions reported [178]. In one instance it was observed that the effect of anode potential on current depends on anode material [179]. This was shown by using 2 anode potentials (-200 and +200 mV) and 2 anode materials (glassy carbon and tin-doped indium oxide). Current was highest at +200 mV on glassy carbon but lowest at the same anode potential when tin-doped indium oxide was used as anode material. It was proposed that other factors which influenced current dependence on anode potential, include growth conditions and inoculum [178].

Current as a function of anode potential in DET can be modeled using the Nernst-Monod equation, proposed for the first time by *Marcus et al.* in 2007 [180]:

$$J = J_{max} \cdot \left(\frac{1}{1 + e^{-\frac{F}{RT}(E - E_{ka})}}\right) \cdot \left(\frac{S}{K_{half} + S}\right) \tag{2.1}$$

where F is Faraday constant (96485 C), R is the gas constant, T is temperature (°K), E is anode potential, E_{ka} is the half-saturation potential, J is current density, J_{max} is maximum current density, S is substrate concentration and K_{half} is the half-saturation substrate concentration. Most often substrate concentration is in excess which means that the Monod term (second expression in brackets in equation 2.1) can be dropped off. The resulting equation has been applied for calcu-

lating the mid-potential of bioanodes using low scan LSVs [181, 182]. However, it was reported for a bioanode during its growth phase, that as current increased higher deviations from Nernst-Monod behavior were noticed [183]. This changes are characterised by decreasing mid-potential and decrease of the slope at the middle of the current curve.

Deviations from Nest-Monod behavior can be explained by the existence of multiple ET pathways. Two redox species with redox potentials at -60 mV and +380 mV were identified in *Geobacter* biofilms, responsible for current production [184]. The first was more active on bioanodes grown at +200 mV while the second was more active on bioanodes grown at +600 mV. These redox peaks were attributed to outer membrane cytochromes, each associated to a different ET pathway. Investigating a wider anode potential range identified 7 peaks in *Geobacter* [185]. Bioanodes based on *Geoalkalibacter ferrihydriticus* showed 4 peaks each attributed to a different electron transfer pathway [73]. The activity of each pathway was found to depend on poised anode potential [73]. OCP values depend on the electrochemically active components in contact with the electrode and its measurements can reveal modifications to ET mechanism induced by anode potential. It was found that OCP in 3 benthic MFCs increased with poised anode potential which was set at -58, +103 and +618 mV [151]. OCP varied with poised anode potential when using a commercially available *Geobacter* strain [186]. However OCP become independent of anode potential in new bioanodes obtained by using anolyte from previous MFCs as inoculum. This showed that electrigens can suffer long-term physiological changes possibly explaining contradicting reports. It seems that electrigens can adapt to the TEA potential by expressing different cytochromes. Furthermore it was found that the activities of each ET pathway are not additive [183]. Instead *Geobacter* showed preference for the ET pathway with a redox potential closer but not higher than the anode potential. It was proposed that the higher-potential redox activity allows *Geobacter* in nature to reduce vanadate which has a redox potential of 1.1 V [184].

It was suggested that *Geobacter* can adapt its electron transport chain (ETC) to anode potential in order to maximise energy gain [187]. ETCs are branched, modular and inducible [188]. The ETC is composed of protein complexes which are found in the inner membrane of gram-negative bacteria. Energy is acquired by oxidising organic substrate and transferring resulting electrons to a suitable electron acceptor. The electron acceptor can be sulfate, nitrate, oxygen, CO_2 or insoluble minerals in the case of electrigens. The purpose of the ETC is to transport electrons from donors to acceptors. As a result of electron flow through an ETC component, protons are pumped outside the cells resulting in a proton gradient across the bacterial membrane. This can be used directly for powering other membrane proteins (such as motor protein at the base of flagellum) or it can be used for ATP synthesis. The number of components in a ETC varies depending on TEA potential. Oxygen-reducing ETCs have 4 complexes. For lower redox TEAs such as nitrate and sulfate, bacteria use shorter ETCs. Thus the energy a bacterium can harness is not arbitrary, but is constrained by the accumulated potential drop at each complex.

Anode potential control energy gain for bacteria according to the following equation 2.2:

$$\Delta G^{0'} = -nF(E^{0'}_{donor} - E_{anode}) \tag{2.2}$$

where $\Delta G^{0'}$ represent change in Gibbs free energy, F is Faraday constant, $E^{0'}_{donor}$ is substrate biological potential and E_{anode} is anode potential. Equation 2.2 predicts higher energy gains with increasing anode potential. Consequently biomass yield is expected to increase with anode potential. However the structure of ETC suggest that energy is harnessed in discrete steps and not continuously. In a study using bioanodes grown at -400, -200 and 0 mV it was found that biomass yield was smaller for the bioanode grown at the lowest anode potential while the other bioanodes showed equal biomass yield [189]. A similar trend was observed with anode potential poised at -160, 0, and 400 mV [187]. Biomass increased only for the first 2 anode potential values. On the other hand maximum current was linear with biomass yield. Also biomass yield per gained energy was smaller for the bioanodes grown at the lowest potential (-160 mV). This shows that growth efficiency is also affected by anode potential. Lower growth efficiency at smaller anode potential may be due to a need of oxidising more substrate for energy production leaving less substrate to be assimilated as biomass. In another study total biomass increased with anode potential at -250, -90 and 210 mV and decreased at 510 and 810 mV [190]. These studies show a trend of increasing biomass yield with anode potential until a certain value but they differ in terms of the anode potential range investigated and the biomass-limiting value of anode potential. Biomass measurement were done by subsampling the bioanodes which could affect results if biomass coverage was uneven. Furthermore by using mixed-community inoculum to start the bioanodes real abundance of electrigens was not accessible. This precluded the investigation of electrigen abundance correlation to gained energy.

Regarding the effect of anode potential on bacterial community composition there are contradicting reports. In one study it was reported that anode potential had no effect on community composition [114]. However this was acquired using DGGE-based sequencing which compared to new-generation sequencing methods, has a much lower resolution. Community analysis based on pyrosequencing showed that anode potential had little impact on community composition [190]. Variation in *Geobacter* percentages were observed but due to lack of replication it could not be established if these differences are consistent with anode potential. Another study reported that anode potential had a high selective pressure on bioanode communities [105]. Although *Geobacter* was identified on all bioanodes (grown at -400, -250 and -100 mV) different phylotypes were associated with each.

2.4.3 Anode surface area

Bacteria adhere to the anode surface forming electrigenic biofilms. Anode material must have high surface area to improve colonisation, be biocompatible and conductive. Electron transfer from bacteria to anode is a limiting step in current production. Increasing electrode conductivity can decrease charge transfer resistance (R_{ct}) which in turn can lead to higher current densities. Decreasing (R_{ct}) can be done by surface modification of anode materials. The simplest methods of modifying anode surface are heat and acid treatment. Following these treatments anode surface can become hydrophilic which favours attachment of bacteria. Also these treatments can induce surface modifications that include higher N/C ratio and a decrease in C-O bonding which are associated with smaller R_{ct} [191].

Current output can also be enhanced by the attachment of nanoparticles made from conductive materials on the anode surface. These can be nitrogen-doped carbon [192], titanium oxide [193], gold [194] or palladium nanoparticles [195]. Palladium is particularly attractive due to its catalytic properties comparable to platinum. Furthermore biocompatible palladium nanoparticles can easily be synthesized by many species of bacteria [196]. These are deposited on the outer membrane of bacterial cells allowing their easy separation. Stability of nanoparticles can be improved by combining them in emulsion with carbon nanotubes (CNT) [197, 198]. This approach can also increase the list of nanoparticle materials that can be attached to anode surfaces. Using conductive nanoparticles resulted in all cases in higher current density, longer batch cycles, and higher coulombic efficiencies and COD removal rates.

CNTs exhibit high conductivity themselves and can be employed directly for anode surface modifications. *Erbay et al.* (2015) reported that applying CNTs directly on stainless steel anode led to an increase in current density by 7.4 times compared to carbon cloth anode of the same projected area [199]. This was a promising result because stainless steel is cheaper and physically more robust than carbon cloth. Most of the time the support is less conductive that the applied CNTs. This was exploited in one study by completely removing the support and creating a three-dimensional (3D) sponge made entirely of CNTs [200]. This showed higher current density and a decrease in R_{ct} by 13 times compared to carbon felt anode of equal dimensions. Furthermore, production of the 3D CNT sponge proved to be cost effective (0.1 $ per gram).

Higher conductivity and porosity of anodes allows for higher performance due to improved colonisation and electron transfer. Cheap anode materials can be obtained by carbonising at high temperature materials that already have a highly porous structure. These include corrugated cardboard [201] or plant stems such as kenaf [202], bamboo [203] and palm kernel [204]. Plant stems are particularly attractive because they are cheap to produce and exhibit hierarchical natural porosity allowing for efficient colonisation by bacteria. Furthermore, as a result of the carbonisation process, an in-

crease in C-N bonds occurred on the surface of the materials which is associated with a decrease in R_{ct} [203]. 3D macroporous carbon is suited as an anode material because it improves ion transport, is less prone to clogging than microporous carbon and provides high surface area for bacterial colonisation. Increasing anode area by using low pore size does not increase power output because bacteria cannot colonise the small pores. For example a porous carbon material with smaller pore size and higher surface produced lower power compared to a carbon material of bigger pore size and smaller surface area [205].

Increasing anode area was suggested for increasing power and COD removal efficiency [15]. Graphite granules were proposed as anode material due to their high surface area. It was found that increasing granule bed led to an increase in current [206]. However this also decreased anode to cathode distance which in turn resulted in smaller internal resistance explaining the increase in current. Other studies however reported reduced or no enhancement in power with increasing anode dimensions. For example doubling anode area in a sediment MFC brought no increase in performance [207]. Also while increasing the number of anodes in a pilot scale reactor increased power, this was associated with a decrease in power density reported to total anode area [203]. In this case the explanation provided was that anodes further from the cathode had poorer performance.

In one instance, the use of 3D electrodes increased current only marginally [208]. Compared to flat electrodes, they had a surface area around 10000 times bigger but the current density projected to surface area increase only 2 to 3 times. Looking closer at the relation between current and anode area it was noticed in one instance that these are not proportional even when cathode area was not a limiting factor [209]. This was confirmed by another study which reported an increase in power density with higher cathode to anode ratio but which plateaus above a certain ratio [210]. The ratio where power density levels off was found to depend on cathode activity, being smaller for a more active cathode. The limiting ratio was 27 for an air-cathode and 4 when a ferricyanide cathode was used. For a constant cathode area, increasing anode area leads to a decrease in internal resistance [211, 212]. In these cases the MFC with the smallest anode area showed the highest power density but also the highest internal resistance.

A general decrease in power density with increasing anode area has important practical implications. It can affect comparison between anode materials. For example *Chen et al.* (2012) reported that current density decreased with increasing anode area which was varied between 1.16 and 7.35 cm^2 [202]. Because these were flow-through bioanodes, it was proposed that substrate depletion occurs close to the anode outlet. However, bigger flow rates and substrate concentration did not lead to any increase in current density. This observation was left unexplained although the current density at the smallest anode was chosen for comparing the novel anode material with others from the literature.

Other factors were proposed to replace power density as a parameter to describe performance of

MESs such as normalised energy recovery [213]. This can be expressed as J/m^3 (energy per cubic meter of treated wastewater) or J/kgCOD (energy per kg COD removed). MES upscaling is limited by cathode ativity, ohmic resistances and potential gradients on the surface of bioanodes which leads to power dissipation as a result of local currents. To overcome these limitations, it was suggested that upscaling reactors can be done by stacking multiple MFCs [19, 214, 215].

2.5 Anodic biofilms: colonisation and dynamics

Bacterial colonisation of anodes is one of the least understood aspect of MES engineering. The composition of bacteria in the inoculum is important in defining the composition of mature bioanodes. Despite this, the community of mature bioanodes is very different from that of the initial inoculum [121, 129, 142]. Colonisation begins with bacteria establishing contact with the anode which might rely on Brownian motion or bacterial active swimming. It was found that *Shewanella oneidensis* strain MR-1 actively swims towards solid electron acceptors and anodes [216]. This property was called electrokinesis. The rate of migration was found to be influenced by the potential of the conductive mineral/anode. Mutants deficient in outer membrane cytochromes did not show electrokinesis. Initially cells swam towards the conductive surface in a touch-and-go manner. Contact between cells and the solid was maintain for 1 second. It was observed that within 24 hours cells of *Shewanella oneidensis* remained in contact with the solid eventually forming biofilms. While this was only described for just one electrigenic strain, it offers one possible mechanism of electrode colonisation. Study of electrokinesis could help understand biofilm formation by ARBs. Surface charge of bacteria is important for attachment on electrode. Gram-negative bacteria, which includes most of ARBs known to date, have a negatively charged surface [217]. This allows them to colonise positively charged solid surfaces [218].

After colonisation, bacteria grow on the surface of the anode, eventually forming a continuous mono-layer biofilm. Multi-layer thick biofilms produce higher currents than thin or mono-layer biofilms [219]. However thickness can become a limiting factor to current production [220]. Several authors have divided growth of *Geobacter sulfurreducens* biofilm in 3 phases ([70, 220]): lag phase, an exponential phase and finally a mature phase. In the lag phase cells are small and tightly packed, and concentration of c-type cytochromes is small. In the exponential phase, biofilms become multi-layered and the concentration of c-type cytochromes increases. In the mature phase biofilms are thick and exhibit high porosity, a characteristic which is thought to improve transport of ions and substrate. *Geobacter* biofilm morphology also differs with anode materials. For example *Nevin et al.* (2008) showed that xylose-fed *Geobacter* biofilms were 3-18 μm thick and relatively uniform on carbon cloth while on flat graphite electrodes biofilms were 50 μm thick and showed pillar-like structures [221]. Although carbon felt biofilms were in general thinner, due the proximity of carbon threads in this materials, biofilms were frequently contiguous between neigh-

boring threads.

Dead biomass has been frequently observed on anodic biofilms [111, 221–223]. Its accumulation might be a limiting factor to current production as suggested by *Bridier et al.* [111]. In their study they proposed a renewal procedure for bioanodes which favoured production of thinner biofilms that can produce higher current. They found that in MFCs fed on real wastewater, anodic biofilms increased in thickness over time which was considered as the leading cause of performance degradation. The renewal procedure consisted of placing a fresh piece of anode material close to an old bioanode. After 2 days, the old bioanode was removed and the new bioanode was left in its place. Serial bioanode replacement led to better performance and to a decrease of *Firmicutes* bacteria which are not known as electrigens. Such observations show great promise in biofilm engineering.

In general, anodic biofilms showed clear separation between regions with dead cells and regions with live cells [111, 221–223]. Biofilm morphology is different between 3D and bi-dimensional anodes. It was observed that on carbon paper during stable current production, visualised biofilms were thin and composed of maximum 2 layers with more than 50% dead cells [222]. *Nevin et al.* reported that biofilms grown on flat graphite showed inner layers composed of live cells and outer layers containing many dead cells [221]. Conversely, a bioanode made from hierarchical porous material showed increasing ratio of dead cells with depth [223]. It is possible that deeper within bioanodes, bacteria experience higher death rates possible due to accumulation of metabolites and limited substrate diffusion. Uneven biomass coverage and biofilm thickness across the surface of bioanodes was reported by *Harrington et al.* [208]. In their study wastewater feed was circulated through the bioanodes. Biofilms were thicker closer to the feed entry point, decreased in thickness at the middle and was lowest at the exit point. Being a flow-through anode, mass transport cannot be the reason for biofilm thickness distribution.

Understanding bacterial community dynamics holds promise for community engineering but this has rarely been investigated. In sucrose-fed bioanodes grown for 91 days it was observed that biodiversity increased over time and showed good correlation to power production [224]. Community dynamics on glucose-fed bioanodes was studied over a period of 21 days using carbon felt and graphitised Berl saddles as anode materials [225]. For the latter anode material, it was noticed that *Clostridium* decreased over time while for the former no clear trend could be observed. Community analysis was limited to a predefined set of of bacteria for which specific probes were developed, possibly leaving an important part of the entire community undetermined. *Commault et al.* (2015) reported on anodic community resilience by adding soil to mature MFCs [226]. It was observed that in general communities were resistant to addition of competing bacteria. Furthermore the communities on acetate-fed bioanodes were more stable compared to ethanol-fed bioanodes. The effects of substrate switching on community dynamics were assessed by *Zhang et al.* (2014) [110].

The MFC used in their study was fed on acetate for the first 7 cycles and on a mixture of acetate and landfill leachate for the following 5 cycles. *Geobacter* abundance continually increased during acetate feeding, reaching 78%. After substrate switching *Geobacter* decreased to 32%. This was accompanied by an increase in biodiversity and of protein-consuming bacteria from the phylum *Synergistetes*.

2.6 Multi-electrode reactor design and bioanode replication

Multi-anode reactors can serve several purposes. They were proposed as a scale-up design, having multiple anodes in contact with wastewater [227, 228]. The anodes are usually connected to the same cathode and they act as baffles to improve mass transfer. Placement of anodes in relation to the cathode was found to influence distribution of oxygen and substrate with an effect on power and COD removal efficiency [228]. When placing multiple bioanodes in the same reactor at different distances from the cathode, it was observed that performance decreased with distance from the cathode [203]. Multi-anode designs were also used for sediment MFCs [229]. The purpose was to ensure a higher surface to volume ratio. Such designs allow a better distribution of solid electron acceptors in sediments or wastewater, compensating for low mass transfer rates.

Multi-electrode designs were also used for increasing bioanode replication and ensuring similar running conditions. Concerns have been raised regarding potential losses and voltage-reversal in modular MFCs [230, 231], however these apply for MFCs that are electrically connected in series. On the other hand, connecting the anodic chambers of 4 SCMFCs showed no interference between the units [232]. When all MFCs were connected in parallel, total power was equal to the sum of powers from each individual MFC. Also, each MFC produced overlapping power curves. Another study using a SCMFC with 2 anodes and 2 cathodes connected in pairs, showed bacterial community composition was similar on both bioanodes [134]. A multi-anode reactor having 4 anodes connected to the same cathode was used for anode material testing [107]. The purpose of this design was to increase bioanode replication. One system was run for each of the 2 anode materials. Multi-anode reactors were also used as half cells with multiple bioanodes connected to the same counter electrode, sharing the anolyte and the reference electrode. In these systems bioanodes can all be poised at the same potential [233] or each can be poised individually at a different potential [120]. These observations show that shared anolyte does no lead to interference between electrode pairs. Multi-anode reactors show good replication of bioanodes with the added advantages of decreasing maintenance and using only one reference electrode.

The use of multi-electrode reactors can be beneficial for many studies by increasing bioanode replication. Figure 2.4 summaries a literature survey regarding bioanode replication. It shows that at least 57% of the studies did not replicate the bioanodes. The survey was done on 339 articles ran-

domly chosen from the literature. These were filtered by removing studies referring to stacking, proof-of-principles, scale-up, probing strains, fundamental studies on metabolism and ET, new designs as tools, modeling, reviews and μMFCs. After filtering, 170 studies were kept. The topics in the remaining studies included anode materials and assessing the effect of different operation factors such as substrate, buffers, anode potential or light. These studies were analysed for replication regarding bioanode. Replication of chemical/electrochemical analysis were not considered as bioanode replication. Figure 2.4 shows the percentage of no-replication, duplicates, triplicates and higher replication.

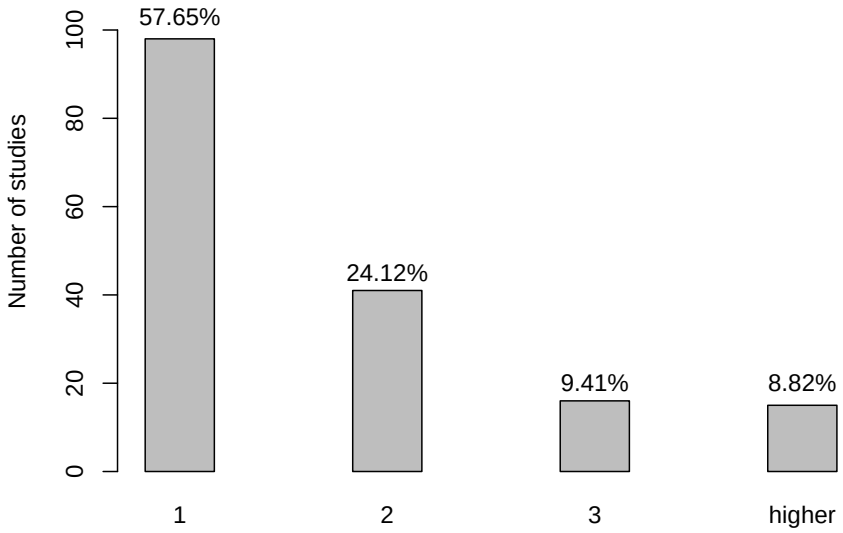

Figure 2.4: Literature survey of bioanode replication

2.7 Summary

The amount of current produced by MESs is limited and this puts a barrier on their applications. In recent years there has been an increase of reports on pilot MFC reactors that were used for treating wastewater while being energy independent. These reports are encouraging and they signal that the field of MES is making progress. It is expected that more pilot-reactors will be reported in the future.

Anode materials are becoming more diverse and begin to specialise by applications. Some can be obtained by carbonisation from plant materials and have the advantage of being cheap and easy to manufacture. Others are obtained by applying conductive nanoparticles or CNT on carbon and stainless steel anodes. Three-dimensional materials have a higher surface area that can harbor electrigens and are therefore able to supply higher currents compared to bi-dimensional materials. Power density in MFCs decreases with anode area. Most probably this is due to cathode limitations. How the anodic community is influenced by anode to cathode ratio remains unknown.

ARBs use the anode as terminal electron acceptor. Biomass density increases with anode potential until a value between 0 and +200 mV. Any further increase in anode poised potential does not result in increase in biomass density. The increase of biomass with anode potential was explained by the ability of ARBs to harness more energy which resulted in higher biomass yields. However no study had access to both total bacterial abundance and relative abundance of ARBs. This precluded investigating if biomass yields of electrigens increase with anode poised potential.

Bacterial composition of bioanodes grown in laboratory condition is very consistent across many studies. It is very different from communities developed in wastewater or other parts of an MFC. Mixed community bioanodes produce higher current densities compared to single-strain bioanodes. Furthermore single-strains are not applicable on real wastewater because they can be replaced by invading bacteria. Light can be used to power different MESs. However the effect of light on mixed-community bioanodes has been insufficiently investigated. The anode community is dynamic and changes over time and with operational conditions. Anodic communities take long times on the order of weeks to reach a stable composition and current production. During this time biodiversity increases. Community composition is sensitive to changes such as substrate switching or adding a source of competing bacteria. Anodic biofilms are composed from dead and live regions and their morphology vary with anode material. Uneven distribution of biomass has been reported on a few occasions. In studies on community dynamics and colonisation the same bioanode was subsampled without considering the possibility that community can vary across the bioanode.

Anodic biofilm morphology and composition, and its relation to operation factors and anode materials still remain poorly understood. Analyzing bacterial community dynamics on bioanodes is important for understanding interactions between bacteria that lead to better performing bioanodes. This knowledge can help with inocula selection or controlling growth conditions that favour ARBs. Engineering communities requires an understanding of what makes mixed communities perform better. Community resilience to unforeseen factors also needs to be investigated together with strategies of reversing damaging effects.

Chapter 3. Materials and Methods

3.1 Reactor Designs

Three types of reactors were used for the current study. These are the double-chamber half-cell (H-cell), the single-chamber microbial fuel cell (SCMFC) and a multi-electrode reactor (MER). Anion-exchange membrane was used for all reactors due to its low price and because anion-exchange membranes were proved to be better suited for MES [234].

3.1.1 H-cells

Each H-cell was constructed from 2 bottles with lateral flanges. One of the bottles played the role of the anodic chamber an the other played the role of the cathodic chamber. The chambers were separated by a 20 cm^2 anion exchange membrane (AEM) which was placed between the flanges. A fully assembled H-cell is shown in figure 3.1. The flanged bottles are made from modified 250 ml Duran bottles. After addition of the lateral flange the filled volume of each increased to 330 ml. Each flange was fitted with a square plate with holes at the corners to allow joining by use of threaded bolts. The cap of the anodic chamber was drilled to allow connection to the reference electrode (RE) and anode current collector. The H-cell was used for anode poised potential studies.

3.1.2 Single Chamber Microbial Fuel Cells

The single chamber microbial fuel cell (SCMFC) reactor was made from the same type of modified Duran bottle as the H-cell. Figure 3.2 shows a diagram of the SCMFC design. A membrane-electrode assembly (MEA) composed of carbon paper cathode and AEM, was placed on the lateral flange and held in place with a square end-plate with holes at the corners corresponding to similar holes in the square plate fixed to the flange. The MEA was sandwiched between two silicon ring gaskets to prevent leaking.

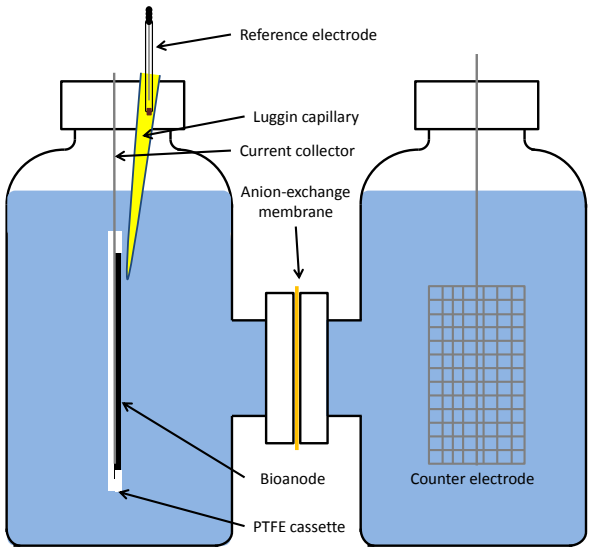

Figure 3.1: H-cell diagram

A thin plastic tube was placed between the 2 gaskets opening next to the anolyte-facing side of the MEA. This tube was used as a port through which a Luggin capillary was inserted when cathode potential was being measured ensuring low uncompensated resistance during the acquisition of polarisation curves. When the Luggin capillary was removed, the tube opening was covered with a silicon cap to prevent evaporation and oxygen influx into the anolyte. The bottle cap was drilled to allow fitting of two small rubber buns. One of the buns was pierced with a wire which was connected to the anode's current collector and the other bun had a Luggin capillary going through it. The Luggin capillary was placed with its tip as close as possible to the bioanode and was used for measuring anode potential.

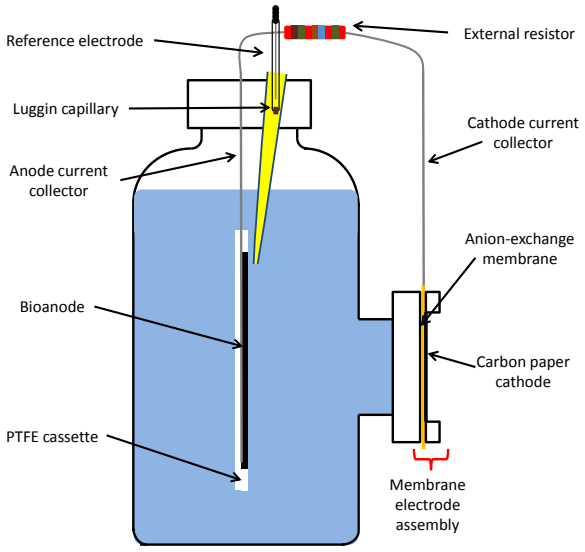

Figure 3.2: Diagram of SCMFC

3.1.3 Multi-electrode reactor

The multi-electrode reactor (MER) was designed with the aim of improving replication of running conditions. It was designed using the 3D modeling program SketchUp. A 3D perspective of the design can be seen in figure 3.3A. Each anode-cathode pair forms one cell making the MER a system of 8 cells with shared catholyte, anolyte, AEM and RE. The anodic and cathodic chambers are cylindrical. The cathodic chamber was covered with a ring-shaped lid which will be referred to as the outer lid. The anodic chamber was covered with a round lid which will be referred to as the inner lid. The inner lid fits exactly within the outer lid. To assemble the system the anodic chamber was placed inside the cathodic chamber and was held in place by the outer lid which can be fasten to the rims of both chambers. When the MER is assembled the cathodic and anodic chambers are concentric.

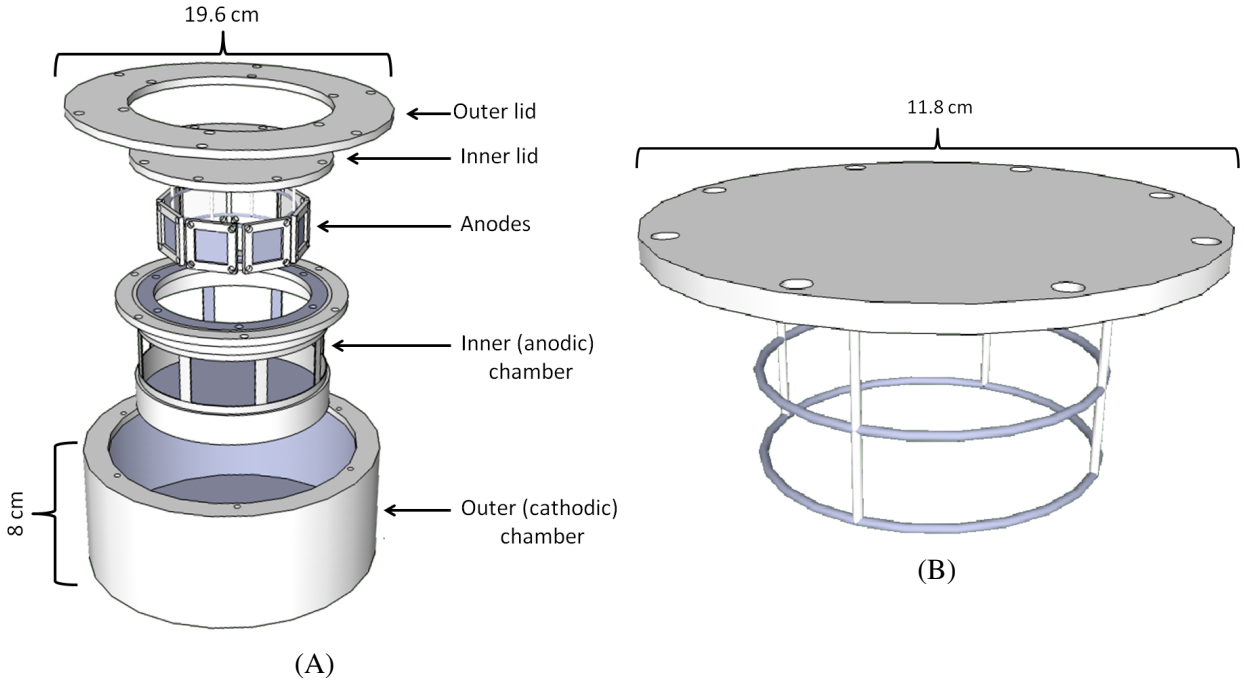

Figure 3.3: A: 3D perspective view showing all components of the multi-electrode reactor and how they are assembled; B: 3D perspective of inner lid with 2 horizontal hoops used as a electrode holder

The anodic chamber's vertical wall is circular and has 8 equally-sized windows to fit a AEM separator. Instead of using individual AEM pieces for each window, one band of AEM was used to cover all the windows which was held in place using a PTFE belt. Applying the AEM band and the PTFE belt around the inner chamber are shown in figure 3.4. The AEM was cut as a band of equal length with the circumference of inner chamber and then wrapped around the windows. Next the PTFE belt was applied and fixed in place with PTFE screws and silicon glue.

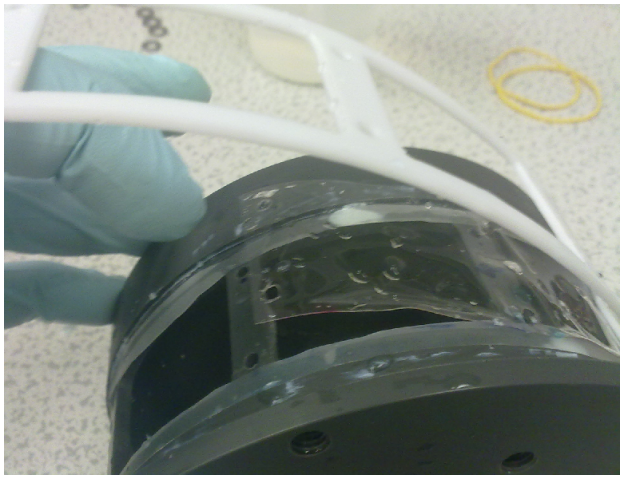

Figure 3.4: Inner chamber with band of membrane around it

On its anolyte-facing side the inner lid was fitted with a system for anchoring 8 anodes as shown in figure 3.3B. The anchoring system is made of 4 vertical bars to which 2 horizontal stainless steel hoops are attached. Each anode was placed in a PTFE cassette with 2 small appendages at the back allowing the anode to be hooked to the horizontal hoops.

Anodes are placed in a circular symmetric manner. Their hooks can slide on the hoops allowing their repositioning when needed such as when some anodes are taken out altering placement symmetry.

The inner lid is also fitted with 8 ports placed in a circular fashion. They allow for the anode wires to come out of the anodic chamber. Anode wires were made from titanium wire insulated with heat shrink (RS Electronics, Cat. no.: 170-2684) except at the ends. One end was connected to the current collector of an anode and the other end was connected to the external resistor. Each anode wire was pushed through a port which was then sealed with silicon glue. The cathodes were connected in a similar fashion using the same type of insulated titanium wires. The outer lid has ports through which the cathode connections and sparging tubes ran.

There were a total of 8 anodes and 8 corresponding cathodes connected in pairs. To avoid cluttering of wires and to allow change of external resistor during acquisition of polarisation curves, 2 connection boxes were build. These are depicted in figure 3.5. Each connection box has 16 connectors placed in two parallel rows. Each connector from a box was connected to its corresponding connector on the other box by means of an external wire. The resulting 16 wires were kept in a common shielded cable that connected the 2 boxes. Each wire was individually insulated to avoid interference between pairs of electrodes. One box was used to connect the cathodes and the anodes; one row of connectors were connected to the anodes and the other row was connected to the corresponding cathodes. The other box was used to connect the external resistances and the data-logger.

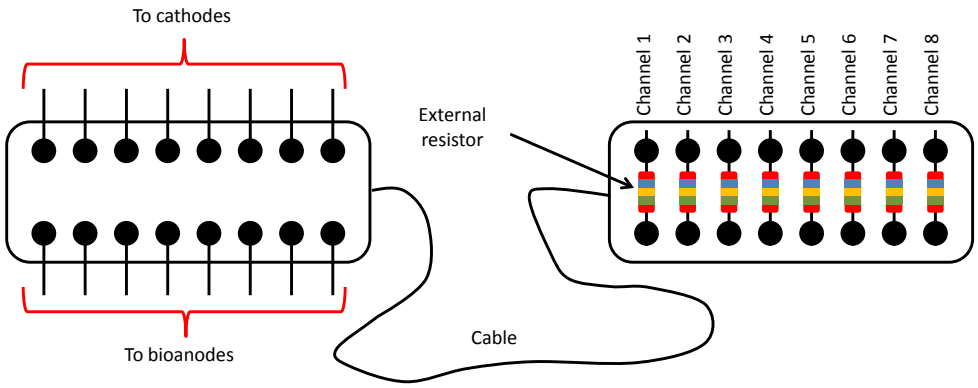

Figure 3.5: Diagram of the connection boxes

3.2 Electrodes

3.2.1 Anodes

Anodes were made from carbon felt (Cat. number: 43200.RF, Alfa Aesar, UK) and carbon cloth. The FTIR spectra for both materials are shown in figure 3.6. These are similar and suggest their surfaces do not carry functional groups. Anodes were cut out from a sheet of carbon material. To allow good reproducibility of electrode sizes, PTFE sheets were used as templates to cut out anodes of required dimensions.

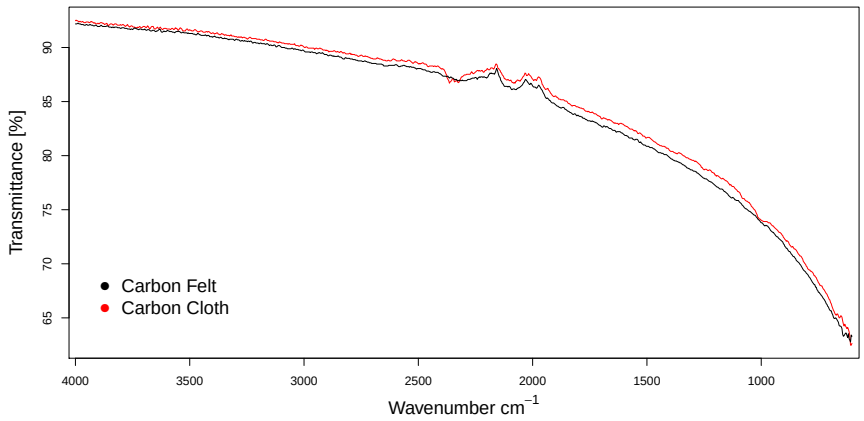

Figure 3.6: FTIR spectra of carbon felt and carbon cloth

Carbon felt is a mechanically weak material and shakes when handled which can cause biofilms to slough off. To prevent this all anodes were placed in PTFE cassettes. These were composed of three parts called back-plate, frame and window as shown in figure 3.7. The current collector was a piece of stainless steel mesh of the same size as the anode. A titanium wire was tied to the current collector. The order in the assembly is: back-plate, current collector, carbon felt anode, frame and last is the window. The entire assembly is held in place with PTFE screws. Good contact is ensured

by pressing the anode against the current collector. The titanium wire protrudes outward through a small groove in the frame. The exposed surface area of the anode is determined by the window sizes. The window has a grove on its front upper side to allow for the Luggin capillary.

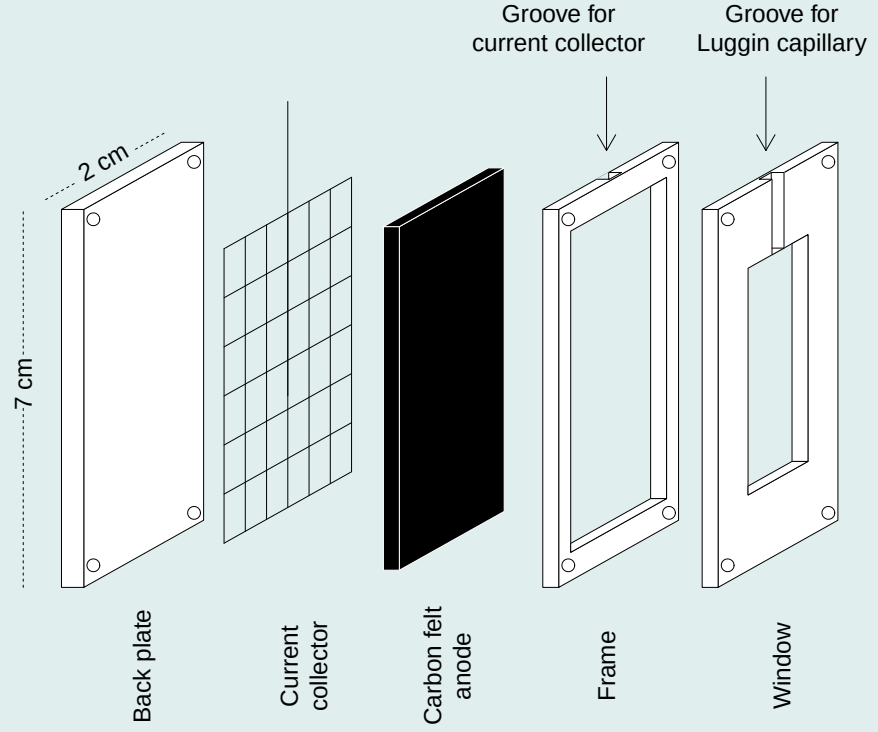

Figure 3.7: Anode assemble components

3.2.2 Counter electrodes

Counter electrodes were of one of the two types: platinum-covered titanium mesh or gas diffusion electrodes (GDE). The former were used inside H-cells and the latter were used in SCMFCs. To make the first type of counter electrodes, pieces were cut out from a sheet of platinised titanium mesh. Each piece was connected to stainless steel wire.

3.2.3 Gas Diffusion Electrodes

The GDE was made from carbon paper with catalyst ink applied on the catholyte facing side. Carbon paper (250 μm, air permeability: 70 $Pa \cdot s$) was purchased from Freudenberg FCCT SE & Co. KG (Cat no.: H2315 I2 C6). One side of the paper is teflonized and hydrophobic and the other side has a hydrophilic porous carbon layer. To make the cathodes, round pieces of carbon paper of 19.6 cm^2 were cut out using a PTFE template. A catalyst ink was applied on the porous layer with a pipette and left to dry. To prepare an aliquot of ink necessary for one electrode the following

were mixed in a glass tube: 50 mg Pt 5% in black carbon powder, 2 ml absolute ethanol and 87 µl of Nafion. The preparation steps are described below:

- add 50 mg catalyst powder in a tube
- tilt the tube at 45° and add ethanol on the side wall of the tube slowly and carefully to avoid sparks that may ignite the mixture. For safety this is done in a fume cupboard.
- add 87 µl Nafion
- add 5 Zirconium balls
- vortex for 30 minutes
- sonicate for 30 minutes
- cut out a 19.6 cm^2 piece of carbon paper and placed it on a heating plate set to 50°C with the porous side upside
- apply the ink on the porous side of the electrode with a pipette to ensure uniform distribution and let it dry

When fitted to a SCMFC, the teflonized side is exposed to the air and the catalyst layer is facing the anolyte from which is separated by AEM. Oxygen enters through the teflonized side and is reduced inside the catalyst layer by platinum within the catalyst ink. The GDE and the membrane are sandwiched between 2 gaskets and the resulting assembly is fitted on a flanged Duran bottle.

3.2.4 Cathodes for multi-electrode reactor

A typical cathode used for MER is shown in figure 3.8. The cathode was made from a rectangular piece of carbon paper with Pt catalyst applied on the catholyte-facing side as described in section 3.2.3. After the catalyst ink dried, the cathode was placed inside a PTFE cassette. To avoid corrosion the current collector was made of graphite. This was placed together with the cathode in PTFE cassette.

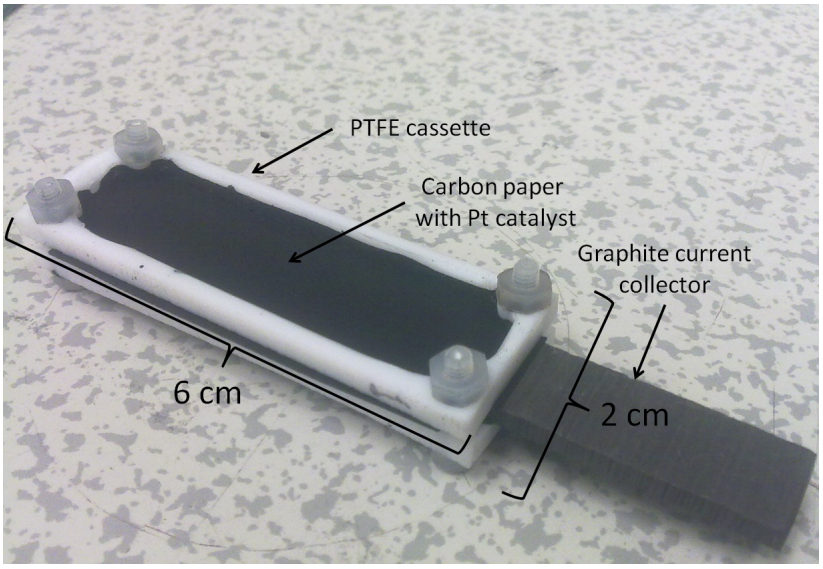

Figure 3.8: Cathode used in the multi-electrode reactor

3.2.5 Reference electrodes

Reference electrodes (RE) (Ag/AgCl in 3M NaCl, +205 mV vs NHE) were purchased from IJ Cambria Scientific Ltd (RE-5B). If an RE is left for long periods of time in liquids of different compositions than their inner filling solutions, it experiences potential drift. It was considered that this happened due to transportation of solutes through the RE plug changing the inner filling composition which modifies the potential of the silver wire. To avoid drift and to minimize the uncompensated resistance, REs were fitted with Luggin capillaries. These were made from Pasteur pipettes partially filled with agar gel as shown in figure 3.9. The small tip of the Pasteur pipette ensures small uncompensated resistance and the 3M NaCl reservoir keeps the RE from drifting. The agar bridge was made by filling the Pasteur pipette with molten agar gel using a syringe. The gel was prepared by dissolving 8.366 g of NaCl and 2 g of agar in 50 ml deionised water on a heating plate. When the composition is molten it forms a gel. This was pushed inside a Pasteur pipette using a syringe. The Pasteur pipette was then transferred to a beaker of deionised water at room temperature to solidify the agar gel inside. Air bubbles could form inside the Luggin capillary during gel solidification which could fragment the salt bridge. New Luggin capillaries were tested by measuring the potential between 2 REs one of which was placed in the reservoir of the freshly prepared Luggin capillary. A stable potential reading signaled that the Luggin capillary was good while noisy potential reading signaled fragmentation of salt bridge.

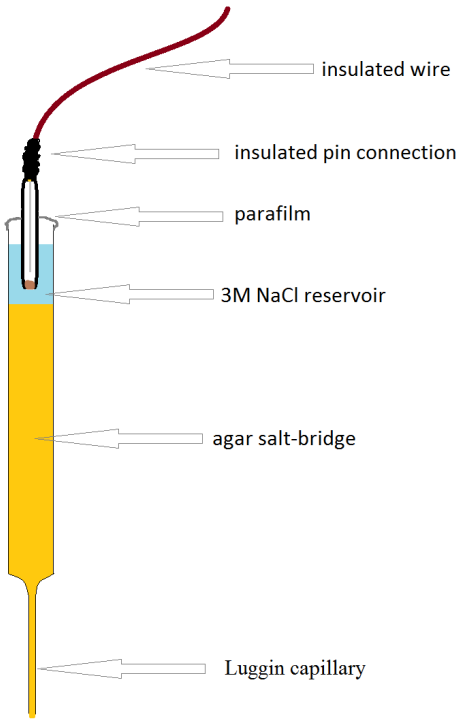

Figure 3.9: Diagram of reference electrode in Luggin capilarry with salt bridge and 3M NaCl reservoir

3.3 Reactor Operation

3.3.1 Anolyte

Two anolyte compositions were used. The first uses sodium acetate as substrate and its recipe is based on [235]. To prepare 1 liter of acetate anolyte, 1 g of sodium acetate, 2 ml of micronutrient solution, 10 ml of macronutrient solution and 50 ml of 1 M PBS buffer are mixed and the volume is brought to 1 L by adding deionised water. The composition of the second anolyte is based on the OECD recipe for synthetic sewage [235]. The only modification is the addition of 4 g/L NaCl for increased conductivity. For each anolyte type the ingredients and their final concentrations are shown in table 3.1.

pH, conductivity and COD content of both the acetate and OECD anolytes are shown in table 3.2. Acetate anolyte was not amended to equate its COD content to that of the OECD medium. This was because acetate is commonly used at a concentration of 1 g/L. The OECD recipe was not altered in terms of COD content because it was designed to approximate the chemical composition of typical domestic wastewater. The only amendment to the OECD recipe was the addition of 4 g/L NaCl to increase conductivity. Wastewater has small conductivity in relation to MFC requirements. Addition of NaCl to the OECD anolyte solves for this. It has been pointed before that integration of MES in the waste treatment industry might require ancillary tanks for anolyte titration with different

Table 3.1: Recipes for acetate anolyte and OECD complex substrate anolyte

Acetate anolyte			Complex substrate anolyte	
Component	Concentration	Solution	Component	Concentration
Sodium acetate	1000 mg/L	NA	Pepton	160 mg/L
NaCl	4000 mg/L	NA	NaCl	4000 mg/L
HK_2PO_4	5024 mg/L	1 M PBS buffer	H_2KPO_4	28 mg/L
H_2KPO_4	2877 mg/L	1 M PBS buffer	Urea	30 mg/L
NH_4Cl	280 mg/L	Macronutrients	Yeast extract	110 mg/L
$CaCl_2 \cdot 2H_2O$	5.7 mg/L	Macronutrients	$CaCl_2 \cdot 2H_2O$	4 mg/L
$MgSO_4 \cdot 7H_2O$	100 mg/L	Macronutrients	$MgSO_4 \cdot 7H_2O$	2 mg/L
$FeCl_2 \cdot 4H_2O$	4 mg/ L	Micronutrients		
$CoCl_2 \cdot 6H_2O$	2 mg/L	Micronutrients		
$MnCl_2 \cdot 4H_2O$	1 mg/L	Micronutrients		
$ZnCl_2$	0.1 mg/L	Micronutrients		
H_3BO_3	0.1 mg/L	Micronutrients		
$CuCl_2 \cdot 2H_2O$	0.08 mg/L	Micronutrients		
$(NH_4)_6Mo_7O_{24} \cdot 5H_2O$	0.14 mg/L	Micronutrients		
$NiCl_2 \cdot 6H_2O$	2 mg/L	Micronutrients		
$Na_2SeO_3 \cdot 5H_2O$	0.32 mg/L	Micronutrients		
Pyridoxine	1 mg/L	Vitamins		
Nicotinic acid	0.5 mg/L	Vitamins		
Riboflavin	0.25 mg/L	Vitamins		
Thiamine	0.25 mg/L	Vitamins		
Biotin	0.2 mg/L	Vitamins		
Folic acid	0.2 mg/L	Vitamins		
Vitamin B_{12}	0.01 mg/L	Vitamins		

purposes [12]. Addition of 4 g/L NaCl translates to a concentration of 68 mM. By comparison the salt concentration of sea water is around 600 mM.

Table 3.2: pH, conductivity and COD content of acetate and OECD anolytes measured at 20°C.

	Acetate anolyte	OECD anolyte
pH	6.97	7.27
Conductivity (mS/cm)	7.86	7.31
COD (mg/L)	853.3	387.5

3.3.2 Catholyte

Catholyte composition was similar to that of the anolyte used with the exception that organic substrate was avoided in the catholyte. When acetate anolyte was used the catholyte lacked acetate and when OECD anolyte was used the catholyte lacked peptone and yeast extract. The reason for having the same ion species in both the anolyte and the catholyte of the same cell was to avoid

concentration potential difference across AEM. Organic substrate in the catholyte was avoided also because in presence of oxygen it promotes biofouling.

3.3.3 Inoculation procedure and inocula types

Two methods of inoculation were used: at closed-circuit and at open circuit potential. In the first method the anode chamber is filled with inoculum with 1 g/L added acetate. Connections are established and the cell is run for the first cycle on the mixture of substrate and inoculum. In the second method the anode is pre-incubated in inoculum for 2 days without being connected to the cathode. After this step the anode is transferred into a cell with freshly prepared anolyte. All reactors that were run on OECD anolyte were pre-fed on acetate for the first cycle after inoculation. This is because it was not possible to start bioanodes directly on OECD medium.

Two types of inocula were used: primary and secondary. Primary inoculum was a 1:1 mixture by volume of activated sludge and wastewater collected from a trickling filter from the treatment plant in Tudhoe Mill. Secondary or enriched inoculum was represented by anolyte collected from mature cells at the end of each cycle.

3.3.4 Feeding cycles

Feeding was done in two modes: batch and continuous. In the batch mode reactors were run for several cycles with medium change after each. This was applied to H-cells and SCMFCs. Continuous feeding was ensured by flowing anolyte through the anodic chamber and was applied on the MER.

The number of cycles was used as the standardization parameter to allow running of bioanodes that were compared under similar conditions. Allowing all reactors to run for the same amount of time introduces big differences among them due the subjective nature of deciding when a cycle has stopped, and due to differences in cycle length with substrate type and design.

3.3.5 H-cells: running, maintaining and current monitoring

H-cells were used for studying the effect of anode potential and light on bioanode communities and their performance. A 4-channel potentiostat purchased from Whistonbrook Technologies Limited (Quad Potentiostat) was used for poising anode potential and for current data-logging. All anode potentials reported in this thesis are relative to the silver-chloride (Ag/AgCl) RE. All H-cells were run in batch mode by changing the entire anolyte when substrate was depleted. Bioanodes using

complex substrate were run during their first cycle on acetate for pre-feeding. All cells were kept on a heating mat inside a insulating box with temperature controlled at 27°C.

3.3.6 Single-chambered MFCs: running, maintaining and current monitoring

SCMFCs were used for studying the effect of anode to cathode area ratio (A/C) on the bioanode community and current production. Cells were temperature-controlled at 27 °C on a heating mat inside a insulated box. All cells used a 500 Ω external resistor and were run in batch-mode. Anode potential and cell voltage were recorded every 10 minutes using a multi-channel data-logger (NI USB-6225, National Instruments).

3.3.7 Multi-electrode reactor: running, maintaining and current monitoring

The multi-electrode reactor (MER) was run in continuous mode in order to avoid substrate depletion in the anolyte. This was done by recirculating the anolyte between the anodic chamber and an external reservoir. The anolyte recirculation system is shown in figure 3.10. A peristaltic pump was used for this purpose with the flow rate set to 2 ml/min. The inner lid of the reactor was fitted with two ports, one for anolyte outflow and one for anolyte inflow. Through each port a 50 cm long piece of oxygen impermeable tubing was inserted with the external opening connected to the anolyte reservoir. To avoid emptying the anodic chamber, the outflow tubing opened at the top of the anodic chamber. The inflow tubing opened at the bottom of the anodic chamber. With this design old anolyte was pumped out from the top of the anodic chamber and fresh anolyte entered at the bottom of the reactor.

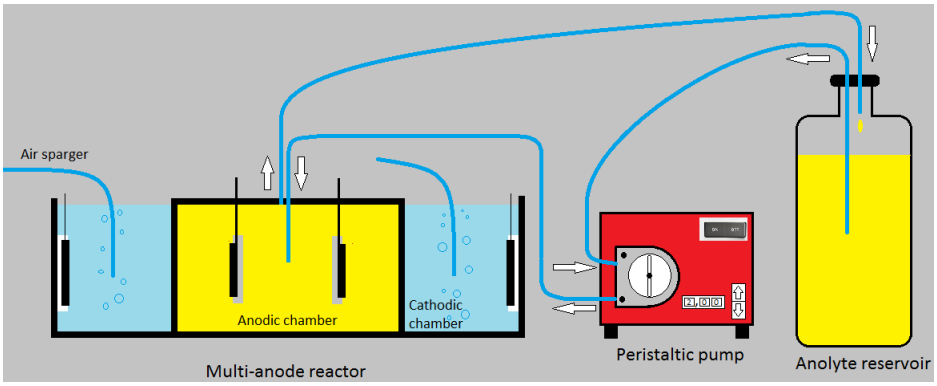

Figure 3.10: Anolyte recirculation and catholyte sparging with air in the ME reactor

The flow of anolyte was designed firstly to avoid the accumulation of old anolyte at the bottom of the anodic chamber and secondly to avoid the immediate re-collection of fresh anolyte before it diffuses through the anodic chamber. Furthermore this also avoided anolyte being drained in case of pump failure or unbalanced inflow. Anode potentials and cell voltages were recorded every 10

minutes using a National Instruments data-logger. Each cell had its own external load and was logged independently from the rest. Temperature was controlled at 27°C by keeping the reactor on a heating mat inside an box with polystyrene insulation.

3.4 Sampling methods

3.4.1 Electrode sampling and storing

At the end of an experiment, bioanodes were removed from their reactors. The part of carbon felt that was exposed to the anolyte was cut out from the PTFE cassette with a sterile razor. The resulting part was then cut in smaller pieces and transferred to a labeled 2 ml Eppendorf tube. The bioanode pieces were then crushed inside the tube using a stainless steel rod. During crushing anolyte entrapped in the spongy structure of the bioanodes was released giving the homogenate a liquid consistence. After this step, bioanode samples became like a slurry which could be handled with pipettes. Entire bioanode homogenisation ensured the entire community from the bioanode was characterized. The reason was to avoid subsampling which due to uneven distribution of biomass on electrodes could introduce random variance. For long-term storage, homogenised bioanode samples were kept in the freezer at -20°C.

3.4.2 COD measurement

Anolyte samples were taken at the end of each cycle. Collected sample were filtered through a 0.2 µm filter and stored in the freezer at -20°C. Chemical oxygen demand (COD) was determined by a photometric method using kits (Spectroquant®Test kits, Merck Millipore) and a colorimeter (Spectroquant®Multy Colorimeter 173630, Merck Millipore).

3.5 Cell counts

0.2 grams of homogenised bioanode was dispersed in 12 ml of PBS pre-filtered through a 2 µm Millipore filter. The resulting solution was diluted to 20x by mixing 50 µl sample and 950 µl PBS. Samples from bioanodes fed on OECD were further diluted by 10x (total dilution 200x) by mixing 100 µl of 20x sample and 900 µl PBS. Samples from bioanodes fed on acetate anolyte were further diluted by 100x (total dilution 2000x) by mixing 10 µl of 20x sample and 990 µl PBS.

50 µl of SYBR Gold (S11494, Life Technologies, diluted to 100x in sterile PBS) was added to 1000 µl diluted bioanode sample. Then the sample was filtered on a membrane using the following steps:

1. a Millipor filter holder is connected to a vacuum pump
2. a 13 mm membrane filter (Isopore^{TM} 0.2 μm, EMD Millipore) is transferred in the holder
3. the sample is pipetted on the membrane filter and the vacuum pump is switched on
4. allow sample to be draw through the membrane filter
5. wash 3x with sterile PBS by pipetting 1 ml PBS on the membrane filter and allow each time the liquid to be sucked away
6. place a small drop of CitiFluor^{TM} on a microscopic slide
7. transfer membrane filter on microscopic slide
8. place another small drop of CitiFluor^{TM} on the filter membrane and place coverslip on filter membrane

The microscopic preparation was visualised with an epifluorescence microscope (Olympus BX40) at 400x magnification. 20 fields of view were randomly chosen and pictures of each were taken with an Olympus digital camera (E-400). Membrane filter area was 70.88 mm^2 and field of view area was 0.0252 mm^2. Bacterial cell numbers per field of view were extracted using ImageJ image analysis software, and were averaged for all 20 images per bioanode sample. Average cell number per field of view was converted to total bacterial cells per gram of bioanode using the following steps:

- multiply average cell counts per field of view with ratio of membrane filter area to field of view area (2812.6)
- multiply result by dilution factor (200x for acetate bioanodes and 2000x for OECD bioanodes) and then multiply by volume of PBS used to disperse bioanode sample (12 ml)
- divide result by weight of bioanode homogenate initially used

3.6 Electrochemical methods for characterizing bioelectrochemical systems

3.6.1 Cyclic voltammetry

Cyclic voltammetry (CV) is a sweep method during which the potential of an electrode is changed at constant scan rate back and forth between two points while recording the current. It was done in a 3-electrode set-up. Positioning the RE is very important and has to be as close as possible to the working electrode to minimize uncompensated resistance. Current plotted against potential forms a cyclic voltammogram. CVs were run at different scan rates (1, 3, 5, 7, 9, 20, 40, 60, 80 and 100

mV/s) starting from -500 mV up to +200 or +400 mV (vs Ag/AgCl RE). This range was chosen to include the anodic peak which results from the activity of the cytochromes involved in microbial catalyzed electron transfer [205].

3.6.2 Current Interruption for measuring the uncompensated resistances

Current interruption (CI) is a technique used for measuring ohmic resistances in fuel cells [236]. CI was applied as faster alternative to EIS to measure uncompensated resistance. However compared to EIS, CI overestimates uncompensated resistance because it is not able to separate charge transfer resistance. The principle of the method is based on applying a potential on the working electrode vs RE or across the cell (between the working and the counter electrode) for a short time ($< 10\mu s$) and then let the system relax. The ohmic part of the potential relaxes almost instantly compared to non-ohmic contributions because current stops immediately. Potential is recorded after the current is stopped and the data is fitted to identify the part of potential drop associated with the ohmic resistance. It can be applied either in 2-electrode set-up when used for measuring cell resistance or 3-electrode set-up when used to measure uncompensated resistance of the working electrode.

3.6.3 Electrochemical impedance spectroscopy

Electrochemical Impedance Spectroscopy (EIS) is a technique used for characterizing the electrode-electrolyte interface. Its advantage over current interrupt method is that it can split a resistance into its contributions. The method is performed by applying a small amplitude disturbance at frequency that decreases over time. In the present study EIS was run in potentiostatic mode by maintaining anode potential constant and superimposing on current an oscillation of small amplitude (10 μA). Frequency was scanned from 10000 Hz down to 0.1 Hz in 30 steps. Frequencies higher than 10000 Hz showed inductance-like behavior (negative impedance) while frequencies lower than 0.1 Hz were sensitive to noise and extend unnecessarily the procedure time. When run in 3-electrode set-up EIS was used to measure accurately the uncompensated resistance, charge-transfer resistance and contact resistance between anode and current collector.

3.6.4 Power Curves

Power curves were performed as described in [237]. External load was changed every 20 minutes after which anode potential, cathode potential and cell voltage were measured. The procedure was started at open circuit potential (OCP) which is equivalent to infinite external load. After that loads are applied in decreasing order. The range of loads was varied according to anode surface area

and substrate type. Power curves were used for determining peak-power resistance and identifying limiting electrodes.

3.7 Imaging Techniques

3.7.1 Fluorescence Microscopy

Preliminary investigation on biofilm morphology and its distribution on anodes was performed using a fluorescence microscope (Olympus BX40). Epi-illumination was applied because carbon felt is not a transparent material. Samples were prepared by cutting small pieces from mature bioanodes and placing them on glass slides. Samples were incubated for 30 minutes in dead-live staining mixture (SYBR Gold and PI) under dark. SYBR Gold is cell permeable and stains DNA (deoxyribonucleic acid). Under blue light it emits green fluorescence which is enhanced if bound to DNA. Propidium iodide (PI, P3566, Life Technologies) emits red fluorescence when illuminated with green light and shows enhanced fluorescence when it binds to DNA. PI is not cell permeable and will only stain DNA within membrane-compromised cells. To remove noisy background the samples were then washed briefly by holding them with a pair of tweezers and dipping a few times in fresh 50 mM PBS buffer. During washing, excess unbound stain is removed. The sample was then placed on a microscopic glass slide with a coversplip on top. Samples were then visualised under the microscope.

3.7.2 Confocal Microscopy

A confocal microscope from Leica Microsystems Heidelberg GmbH (TCS SP2 UV AOBS MP) was used for investigating on growth, morphology, coverage and distribution of dead and live biomass in anodic biofilms. Confocal microscopy is an imaging technique which allows the acquisition of images at different depths within the sample. Its optical systems allows collection of light from a thin region within the sample also called a focal plane. By setting the required depth only light from a single focal plane will reach the detector while light from the rest the field of view is filtered out. Acquiring images from serial focal planes is called optical slicing or z-scan. Images from a z-scan can be used to reconstruct the 3D structure of the sample. Optical slicing avoids formation of artifacts which are typically introduced by physical slicing or other sample preparation procedure required for other microscopy techniques.

Bioanode samples were placed in a PTFE cassette as in shown in figure 3.11. The cassette is made from 3 components: back plate, frame and front plate. The samples were sandwiched between the back and front plates. The frame acts as a spacer between back and front plates allowing the

samples to be investigated with minimal mechanical stress which would otherwise alter the sample structure. Bioanode samples were placed with their anolyte-facing side upwards. Coverslips were carefully placed on the samples. The front plate has 2 windows corresponding to each sample. The coverslips are slightly pressed against the sample by the front plate. The cassette is useful for microscopy investigations of electrigenic biofilms on 3D electrodes with reduced disturbance and sample handling. It also keeps the sample in place during z-scans.

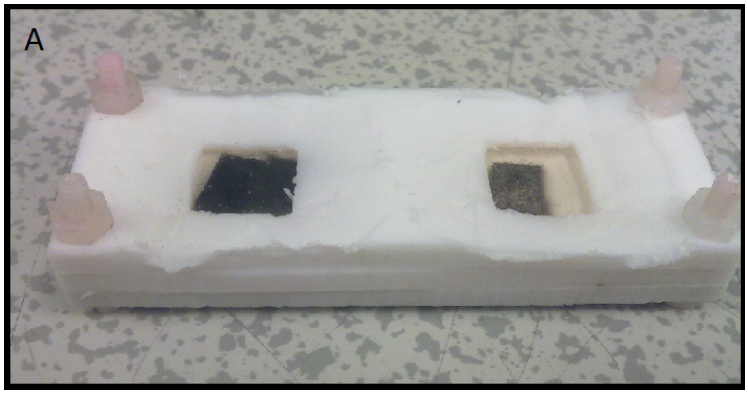

Figure 3.11: Picture of a holder-cassette with two carbon felt samples inside.

3.7.3 Dead-live staining: procedure and controls

Dead-live staining kit (FilmTracer™ LIVE/DEAD®) purchased from Life Technologies was used to monitor time variation of dead and live cells in anodic biofilms. The kit contains two dyes: SYTO 9 and PI. Both show affinity for DNA. Their fluorescence is enhanced when bound to DNA. The mechanism of dead-live staining relies on the different membrane permeabilities of both dyes and on the overlap of SYTO 9 emission spectrum with PI absorption spectrum. SYTO 9 is cell permeable and will bind to any DNA in the sample. Conversely PI is not cell permeable and will not enter bacterial cells with integral membranes. It will therefore stain only extraneous DNA which includes DNA present in cells with compromised membranes. All live cells have integral membranes while dead cells have membranes with compromised integrity. The emission spectrum of SYTO 9 overlaps the absorption spectrum of PI. Consequently when both dyes are in close proximity, PI will quench SYTO 9 emission. This condition applies to DNA that is either extraneous or present inside dead cells.

The cassette with samples was placed on the microscope stage. 3 fields of view were randomly chosen for each sample. Magnification was 400x and each field of view captured an area of 375 x 375 µm. Z-scan was conducted in each field of view reaching on average a depth of 200 µm. The scan starts from the upper most limit of the sample and continues downwards in increments of 5 µm. For each optical section 3 images (channels) were recorded. The first channel visualised SYTO 9 (live biomass), second channel visualised PI (dead biomass) and third channel visualised

reflectance (from carbon threads). Settings and targeted structures for each channel are shown in table 3.3.

Table 3.3: Confocal microscope settings for each acquisition channel

Channel	Mode	Colour	Excitation	Emission	Targeted objects
1	Fluorescence	Green	488 nm	498-517 nm	Live cells
2	Fluorescence	Red	543 nm	587-697 nm	Dead cells and extraneous DNA
3	Reflectance	White	478-498 nm	478-498 nm	Carbon threads

Dead-live controls were prepared from a culture of a strain of *Shewannela oneidensis*. After the culture reached lag phase 2 aliquots were taken. One was killed by a treatment as described in [238] and the other was stained as it is. The killing procedure is based on exposing the culture to a high concentration of isopropanol. This chemical solubilises lipid components of cell membranes compromising their integrity causing death to cells. Pictures of controls were taken with the confocal microscope using the same settings that were used in biofilm investigation. Controls are shown in figure 3.12. The dead control shows fluorescence in the red channel and none in the green channel confirming the existence of dead cells. The live control shows the opposite pattern. Also the dead control shows fewer cells than the live control. This is explained by the effect of isopropanol treatment which eventually causes total disintegration of cells. The SYTO 9/PI mixture proved to be suited for differentiating dead from live cells. It is important to note that exposed DNA will bind both dyes which cause PI to quench SYTO 9 fluorescence due to spectra overlap. This results in DNA emitting only red fluorescence with the used dead-live staining.

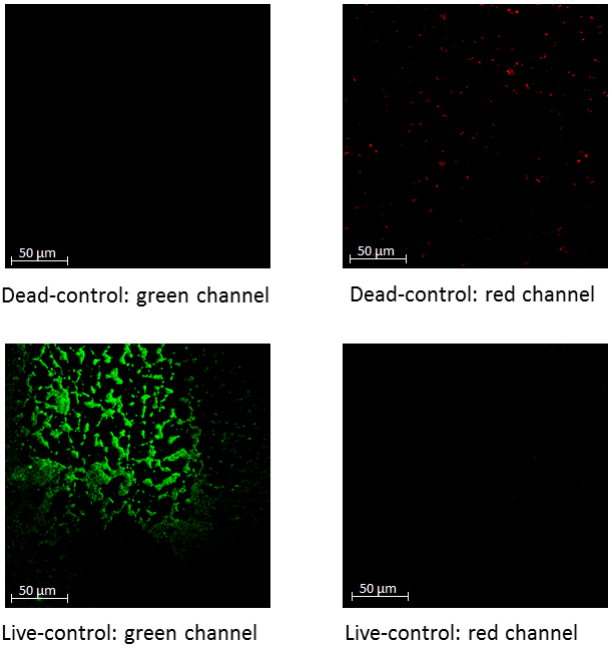

Figure 3.12: Dead-live controls

3.7.4 Imaging biomass distribution on electrodes

Biofilm distribution on electrodes was assessed by an imagining technique derived from the method used for visualizing electrophoresis gel slabs. The bioanode was taken out of the reactor at the end of the experiment. The anolyte-exposed side of the bioanode was cut out and stained with SYBR-Green (S11494, Life Technologies). The staining solution was prepared by adding 5 µl of 10000x SYBR-Green stock solution to 50 ml PBS (50 mM). The bioanode was incubated for 30 minutes in the staining mix in a Petri dish ensuring the solution covered the entire bioanode. The bioanode was then rinsed in fresh 50 mM PBS buffer and placed in a clean Petri dish. The Petri dish with one or more stained bioanodes was then placed inside a gel documentation system (iBOX®, UVP). Excitation light (480 nm) was applied in epi-illumination mode. Emission was imaged using a band-pass filter (485-655 nm).

3.8 Molecular biology methods

3.8.1 Background

Community analysis is a method used for identifying the core composition of a bacterial community. First DNA is extracted and the 16S rDNA gene is amplified. Origin of DNA sequences is determined by using different barcoded primers for each sample during amplification. Bacteria are identified by comparing the 16S DNA sequences against a database. Bacterial composition is then obtained and is used for downstream analysis for comparing bioanode communities.

3.8.2 DNA extraction and quantification

PowerSoil® DNA Isolation Kit purchased from Cambio (Cat. no. UC-12888-100) was used for DNA extraction. Bioanode samples were taken out of the freezer and thawed. 0.2 grams from each sample was transferred to a separate labeled tube. These were placed in a homogeniser (FastPrep®-24) and run for 60 seconds. Tubes contain small beads ensuring bacterial cell rupture by mechanical means during homogenisation. The next steps followed the manufacturer's protocol which is not detailed here. DNA concentration and quality factors for each DNA sample were measured with a NanoDrop spectrometer (3300, Thermo Fisher Scientific, USA).

3.8.3 Choice of target amplicon and the use of barcoded primers

Identification of bacterial species and phylogeny studies use 16s rDNA gene as a marker due to its presence in all bacteria. This gene is composed of alternating hypervariable and conserved regions.

The sequence composition in the hypervariable region is a signature specific down to species or sometimes to strain level. Hypervariable regions accumulate mutations with high frequency and vary among species as opposed to conserved regions that are the same across wide groups of bacteria. Each hypervariable region is different in terms of identification resolution and what bacteria can differentiate. For most studies only a segment of the 16S rDNA gene is sequenced due to PCR limitation of amplicon length.

The targeted segment was composed of V4 and V5 hypervariable regions separated by a conserved region. The V4/V5 region was recommend for wastewater, activated sludge and soil samples because it can differentiate both Archaea and Eubacteria [239]. Furthermore *in silico* and practical studies showed this region outperformed all others when sequenced on Illumina and Ion-Torrent platforms [240].

The V4F forward primer (515R) and the V5R reverse primer (926R) were used [241]. The forward primer was the same for all samples. The reverse primer was specific for each bioanode sample. For this purpose the reverse primer was modified by appending an adapter and a barcoded sequence [242]. A different barcode was used for each sample.

Although the used primers are considered universal care should be taken when generalizing results obtained with just one pair of primers. It has been shown before that using different pairs of primers leads to different conclusion when analysing wastewater communities [243]. Different pairs of primers may show different fractions of the total community. In the current study only one pair of primers were used but they were consistent for all the samples so the same fraction of the communities was analysed in all samples.

3.8.4 DNA amplification

After extraction DNA was amplified by PCR (Polymerase Chain Reaction) in a thermocycler (TC-512, TECHNE) for 30 cycles. The amplicons include V4 and V5 regions separated by a conserved region. Reaction mix was prepared in PCR tubes by adding 22.5 µl Megamix Blue (Cambio, Cat. no.: 2MMB-25), 2.5 µl DNA template, 2.5 µl forward primer and 2.5 µl reverse primer. The PCR program is detailed in table 3.4.

Table 3.4: PCR program

Step	Temperature (°C)	Time
1. Initial elongation	95	4 min. 0 s
2. Denaturation	95	1 min. 0 s
3. Primers alignment	55	0 min. 45 s
4. Amplicon elongation	72	1 min. 0 s
5. Final extension	72	10 min 0 s
6. Final hold	4	Indefinite

3.8.5 Purification of amplicons

Amplification results were checked by agarose gel electrophoresis. Agar gel was prepared by mixing 1.5 grams of agar in 100 ml 1x TAE buffer (2 M Trix-Acetate, 0.05 M EDTA, pH=8.3, Eppendorf Scientific Inc.) The mixture was heated for 5 minutes in a microwave oven. When temperature allow touching by hand 15 µl SYBR® SAFE (ThermoFisher Scientific) was added and the gel was poured in the cast. Electrophoresis was run for 40 minutes at 100 V/m. Gel slabs were visualised with a gel documentation system (iBOX®, UVP). Electropherograms showed presence of amplicons together with primer-dimers, genomic DNA and dNTPs.

Amplicons were purified by AMPure from Agencourt. This procedure is size-selective for DNA sequences. AMPure reagent to sample volume ratio controls for size selection. Expected size of amplicons is around 564 base pairs and this is selected by using a ratio of 1.1 to 1. Purification was validated by a second agarose gel electrophoresis.

3.8.6 DNA sequencing

DNA concentration in each sample was determined by Qubit fluorometric quantification. All samples were then pooled together to a final concentration of 100 pM. Sequencing was done using ion torrent technology with H-Qi chemistry on a 316 chip. The sequencing machine was an in-house PGM™ Sequencer in the Environmental Engineering department at the School of Civil Engineering and Geosciences, Newcastle University.

3.9 Data Analysis

3.9.1 Community analysis

Sequence data was stored in a file in binary format which was then converted to a fastq file. The fastq file contains all sequences tagged with a unique identifier and with a corresponding string of

quality scores for each nucleotide identified in the corresponding sequence. Analysis of raw data was done in QIIME (Quantitative Insight Into Microbial Ecology) [244]. Analysis steps and their corresponding commands are shown in order:

1. **convert_fastaqual_fastq.py**: Splits the fastq file into a fasta file that contains the sequences and a qual file that contains the quality scores.

2. **split_libraries.py**: Sorts all sequences by sample names and applies filtering based on minimum quality score and length range. Sequences shorter than 200 base pairs and with an average quality score smaller than 20 are filtered out during this step. Each sample identifier and its corresponding barcode are written in a mapping file. Barcodes are used for identifying the sample of origin for each sequence.

3. **pick_otus.py**: Clusters sequences using usearch method at a similarity threshold of 97%. The resulting groups are known as OTUs (operational taxonomic unit). The threshold of 97% is standard for OTU identification. A new fasta file is created that stores all sequences with unique identifiers that includes information on the OTU affiliation and sample origin.

4. **pick_rep_set.py**: Selects one representative sequence for each OTU and stores the resulting list in a new file. Selection was done based on abundance criteria.

5. **assign_taxonomy.py**: Establishes taxonomy for all OTUs down to the lowest possible taxonomic level. Most OTUs were identified down to genus level and only for a few identification down to species is possible. Some OTUs were only identified at higher levels such as family, order and rarely at class level. The method checks each sequence against a curated database and uses a classifier algorithm for allotting each OTU representative sequence to a taxonomic group. The output is an OTU table in biom format [245]. It contains OTU composition for each sample and is used for downstream analysis. Both SILVA and Greengenes databases were used. One biom file was obtained based on querying each of the above databases. SILVA based taxonomy is compatible with the CopywriteR algorithm which was employed to calculate percentage data based on 16S rDNA gene copy number [246]. The Greengenes taxonomy is compatible with Tax4Fun method which was used for metabolic profiling [247].

6. **align_seq.py**: Aligns sequence using uclust method

7. **filter_alignment.py**: Filters out gaps introduced in the previous step

8. **make_phylogeny.py**: Produces phylogenetic trees

The output of community analysis includes the biom file and the phylogenetic tree file. Both were used as input for downstream analysis which include alpha diversity, clustering/ordination, metabolic profiling and to correlate composition to reactor properties.

3.9.2 Metabolic profiling

Metabolic profiling was applied for estimating microbial activities in bioanode communities. The procedure is based on retrieving the metagenome from 16S rDNA data. It checks every bacterial taxon identified in a community with the SILVA database of sequenced genomes. It then extracts identified enzymes and weighs them by the abundance values in the OTU table. This was done in R using Tax4Fun package [247]. The input is the biom file obtained after taxonomy assignment step using the SILVA taxonomy for compatibility with the genome database. The output is a table with all enzymes retrieved from the built metagenome of each sample. Enzymes were then grouped by type of metabolism.

3.9.3 Numerical ecology methods

Numerical ecological methods were used to calculate diversity of samples and identify structures in species composition data. The OTU tables were used as the starting point for all subsequent methods which are described below.

Alpha diversity is a category of indices for measuring biodiversity within each sample. They provide for a one-dimensional comparison of communities. Obtained values are sensitive to the number of sequences or sampling depth which was assessed by generating rarefied data of incremental sizes through random sampling with replacement (bootstrap). Visualisation was done by plotting diversity indices against the size of rarefied data. Sample depth was estimated based on the shape of the curves. If they level off it signals that sampling depth has caught a big portion of diversity. Conversely curves with a positive slope signal that more sampling would have resulted in higher diversity. Alpha diversity analysis including assessment of sampling depth was performed in QIIME using the following commands:

1. **multiple_rarefactions.py**: Bootstrapping method for generating rarefied OTU tables of size ranging from 100 base pairs (bp) up to the highest number of sequences in a given sample in increments of 100 bp.

2. **alpha_diversity.py**: Computes alpha-diversity indices on rarefied data.

3. **collate_alpha.py** and **make_rarefaction_plots.py**: Sorts output from previous steps and creates plots of diversity vs. size in bp of rarefied data.

Part of analysing multi-variate data is the identification of structures in the data. These fall in two categories: gradients and groups. A group is a collection of similar samples while a gradient is an ordered series of samples. Interpretation of each type of structure is done in relation to reactor properties. Sample grouping is based on similarity or distance scores. They are calculated for

every pair of samples from the OTU table and are stored as a matrix. Computation of distance matrices requires transformation of data. Data transformations were done using the R function decostand from vegan package. Distances were calculated using R function vegdist from vegan package. Distances used, corresponding data transformations and their interpretation are described below:

- **Bray-Curtis**: $BC_{ij} = 1 - \frac{2 \cdot C_{ij}}{S_i + S_j}$
  where C_{ij} is the sum of the smallest abundance values for common species and $S_i + S_j$ is the sum all abundances in both samples. This distance emphasizes the role of abundance in clustering of samples. It is applied on percentage abundance.

- **Jaccard**: For a pair of samples is calculated as the number of species in common divided by the total number of species in both samples. Prior to its application abundances must be converted to presence-absence data. Because it gives equal weight to all species rare species are equally important as abundant species in comparing samples.

- **UniFrac**: uses phylogenetic distances between species in both samples. It can be applied on presence-absence data (unweighted UniFrac) or on percentage abundance data (weighted UniFrac).

Data structures were identified by principal coordinate analysis (PCoA). This is an unconstrained ordination method that uses as input the matrix of distances. The plot is a 2-dimensional visualisation of the input distance matrix that preserves as much as possible the initial distances between samples. These plots are used for observing trends in data. Confirmed structures were correlated with reactor type and running conditions, substrate used or time of sampling in case of the multi-electrode reactor.

3.9.4 Processing and data extraction from confocal-microscopy images

Raw data was represented by image files in tiff format. For each optical section 3 mono-colour images were generated: red (propidium iodide for dead biomass), green (SYTO 9 for live biomass) and white (reflectance for carbon threads). For each field of view the images were used to create 3D projections in ImageJ. This allowed visual investigation of biofilm morphological features. All channels per each optical section were joined using PIL (Python Image Library) module in Python.

Cell coverages, biovolumes and z-profiles were extracted from the images. Cell counts (obtained in ImageJ) proved an unreliable measure because clusters of bacteria would either be identified as one bacterium or ignored if a maximum dimension was set. Biovolume and biomass coverage are commonly used for biofilm description and they can replace cell counts when this measure is not

possible due to high cell density. Biomass coverage is the percent of pixels with a colour intensity above the background threshold value representing noise level. Background threshold values were calculated by choosing regions in the images that do not include biomass. Average pixel intensity and its standard deviation was calculated for the selected regions. The limit of biomass detection was set as average pixel intensity in biomass-free regions plus 5 times its standard deviation.

Biomass coverage was calculated using PIL module in Python. Carbon threads are not optically transparent therefore their coverage decreases the visible portion of each optical slice with depth. To correct biomass coverages the area occupied by biomass was divided by the visible portion of each optical slice instead of total area of the optical slice. Carbon threads were visualised by reflectance. Individual carbon threads appeared as a bundle of parallel white stripes alternating with dark stripes. Due to these discontinuities computation of carbon threads coverage is underestimated if considering only pixels of intensity above noise level. The first step in computing the true coverage of carbon threads was to fill in the dark stripes. This step was performed with a series of alternating image dilation and erosion operators to fill in the gaps as described in [248]. The routines that were used for this are implemented in the scikit-image module of Python [249].

Plotting biomass coverage against depth creates biomass z-profiles. These allow investigation of biofilm development on 3D electrodes. Based on colour separation resulted after channel joining 3 types of biomass can be identified: live (green), dead (red), mixed (yellow). For each type of biomass, biovolumes were calculated by integrating biomass coverage over depth and multiplying the result with a geometrical correction factor to convert to mm^3 of biomass per field of view. The correction factor is the volume per optical slice and is calculated by multiplying height with are of field of view.

3.9.5 Peak analysis

Cyclic voltammetry raw data was smoothed using Fast Fourier Transform algorithm with a cutoff above 200 Hz. Position of peaks of interest were then identified. Peak detection was done in Nova 1.10 using the manual method without base subtraction. Peak heights were plotted vs scan rate and square root of scan rate. Peak analysis and CV plots were used to investigate on possible effects of operation factors on the electron transfer mechanism.

3.9.6 Calculation of Coulombic Efficiency

Coulombic efficiency (CE) is the ratio of total coulombs that passed as electric current and the total number of coulombs consumed [250] according to the equation 3.1:

$$C.E. = \frac{M \cdot \int_0^t Idt}{F \cdot b \cdot V \cdot \Delta COD} \tag{3.1}$$

where M=32 is the molecular mass of O_2, F is Faraday's constant, b = 4 is the number of exchangeable electrons per molecule of oxygen, V is the anodic chamber volume and ΔCOD is the amount of consumed COD (Chemical Oxygen Demand) during a batch cycle. Total coulombs passed through circuit ($\int_0^t Idt$) was calculated by integrating current over time. Consumed COD (ΔCOD) is the difference between COD values of fresh medium and anolyte at the end of a cycle.

3.9.7 Calculation of energy gain

Energy gain is defined as the amount of energy that the electrigenic bacteria from a bioanode are capable of harnessing as a result of current production. For one mole of substrate consumed, energy gain is calculated as the difference between the potentials of substrate and terminal electron acceptor multiplied by the number of coulombs donated by substrate required for its complete oxidation [187]. This is expressed according to equation 3.2:

$$\Delta G^{0'} = -nF(E^{0'}_{substrate} - E_{anode}) \tag{3.2}$$

where $\Delta G^{0'}$ (J/mol) represent change in Gibbs free energy, n is the number of electrons per substrate molecule, F is Faraday constant (96485 C), $E^{0'}_{substrate}$ is substrate's biological potential and E_{anode} is anode potential. The amount of energy harnessed by electrigens can be calculated by applying equation 3.2 at each point in time over the entire run of each bioanode.

For the half cell the terminal electron acceptor is represented by the anode and its potential is constant over the entire run. Therefore, energy gain for bioanodes in half cells was calculated according to equation 3.3 where current is integrated over time to get total number of coulombs:

$$\Delta G^{0'} = -(\int_0^{t_{end}} I(t) \cdot dt) \cdot (E^{0'}_{substrate} - E_{anode}) \tag{3.3}$$

where $\Delta G^{0'}$ is total energy gain, $I(t)$ is current as a function of time, $E_{substrate}$ is the biological potential of acetate, and $E_{anode}(t)$ is anode poised potential.

In MFCs the anode potential is not constant over the entire run therefore energy gain is calculated by integrating current multiplied by the difference between anode potential and the oxidation potential

of substrate at each point in time. The following equation was applied to calculate total gained energy in MFCs:

$$\Delta G^{0'} = \int_0^{t_{end}} I(t) \cdot (E_{substrate} - E_{anode}(t)) \cdot dt \tag{3.4}$$

where $\Delta G^{0'}$ is total energy gain, $I(t)$ is current as a function of time, $E_{substrate}$ is the biological potential of acetate, and $E_{anode}(t)$ is anode potential as a function of time.

For both acetate and OECD anolyte-fed bioanodes the biological oxidation/reduction potential of acetate was used for calculating energy gain. This has a value of -0.59 V vs Ag/AgCl [251].

Chapter 4. Anodic Biofilms exposed to light: effect on community composition and performance

In this chapter the effect of light on mixed-community bioanodes was investigated. It was hypothesised that the anodic community can change its composition when exposed to light, with consequences on performance. This is based on the principle of competitive exclusion which states that when 2 species are competing for the same resource(s), the one that will have a slight advantage will prevail [252]. Wastewater contains many types of bacteria including anoxygenic photosynthetic bacteria (APB). These are able to grown on non-fermentable products such as acetate by performing anoxygenic photosynthesis [253]. Consequently electrigens and APBs will compete for substrate. In presence of light, the latter will have a competitive advantage helping them to drive out the former.

The aim of this study was to investigate if light has a negative effect on performance of mixed-community bioanodes and if so, to provide an explanation for the underlying mechanism. The objectives were to investigate the effects of light on bioanodes:

- started from both primary and secondary inoculum to check if APB can be eliminated through enriching
- grown inside MFCs and half-cells to confirm that the effect does not depend on the reactor type
- fed on acetate and OECD anolyte to check if substrate is not responsible for the observed effects

4.1 Introduction

Bioanodes can be exposed to light when bioreactors are built from transparent materials such as plexiglas/glass or when the engineer purposely allows for light exposure based on the assumption that ARBs will benefit from it. The ability of photosynthetic bacteria to harness light energy can be employed for driving electricity production in MESs. Most of these MESs used single strains such

as *Rhodoferax* and *Rhodopseudomonas* at the bioanode [168, 169, 176]. These bacteria produced hydrogen photosynthetically which was then *in situ* oxidised at the anode. The anode was made of platinum or carbon covered in platinum-based catalyst. Other studies have used mixed communities of bacteria that contain both photosynthetic bacteria and ARBs [172, 254]. In these systems organic molecules were produced by the photosynthetic organism and then were used by ARBs on the anode. While a positive effect on electricity production was reported, especially when single strains were used, the same effect on mixed communities cannot be assumed. MESs are usually inoculated and fed on wastewater/sewage which are characterised by high biodiversity. Furthermore, the composition of mixed communities can change dramatically with conditions [255].

4.2 Experimental design

A set of 9 reactors were used for this study. 5 were exposed to light by placing an incandescent light bulb 20 cm away from the bioanodes. The emission intensity of incandescent bulbs is higher in the infrared region than in the visible region [256]. The other 4 reactors were protected from light and played the role of dark controls. Reactors are summarised in table 4.1.

Table 4.1: Summary of reactors used to investigate on the effect of light on bioanodes indicating type of MES, substrate, inoculum, and samples subjected to community analysis.

Reactor	MES Type	Inoculum	Light	Substrate	Community analysis
A	Half-cell	Primary		Acetate	
B	Half-cell	Primary	✓	Acetate	
C	Half-cell	Secondary		Acetate	
D	Half-cell	Secondary	✓	Acetate	
E	MFC	Secondary	✓	Acetate	✓
F	MFC	Secondary	✓	OECD	✓
G	MFC	Secondary	✓	Acetate	✓
H	MFC	Secondary		OECD	✓
I	MFC	Secondary		Acetate	✓

Reactors A and B were 2 half cells with the anodes polarised at -200 mV vs Ag/AgCl and were fed with acetate. Reactor A played the role of control and reactor B was exposed to light. Both bioanodes were started from primary inoculum. Comparison was based on current output.

Reactors C and D were also half cells with the anodes polarised at -200 mV vs Ag/AgCl and fed on acetate. Bioanodes were obtained from secondary (enriched) inoculum. Reactor C was the dark control and reactor D was exposed to light. Reactors E, F, G, H and I are SCMFCs that used a platinum catalyst based cathode. Bioanodes were obtained from secondary inoculum. Bioanodes E and F were exposed to light starting with the second cycle, allowing them to grow in dark for the

first cycle. Bioanode G was exposed to light from the first cycle. Bioanode H and I were used as dark controls. Reactors E, G and H were fed on acetate and reactors F and I were fed on OECD medium. Anolyte was collected at the end of each cycle for determining COD used for calculating coulombic efficiency. At the end of the run bioanodes were collected, homogenised and stored at -20° for community analysis.

4.3 Results and discussion

4.3.1 Start-up of bioanodes in presence of light is influenced by inoculum

Figure 4.1A shows the current output from half-cells A and B with the bioanodes started from primary inoculum. By the 3th day both started to grow and their current output was 40 µA. Current from the light exposed bioanode did not grow above this value. Current produced by the dark control increased very fast and reached a plateau by the 5th day at around 1800 µA. Anolyte was replenished with acetate on the 14th day. This was followed by a sudden increase in current for the dark control up to 6500 µA. Reactor B initially showed a growing trend in current up to 40 µA by the 5th day and then it dropped to 0 µA with no recovery even after medium change.

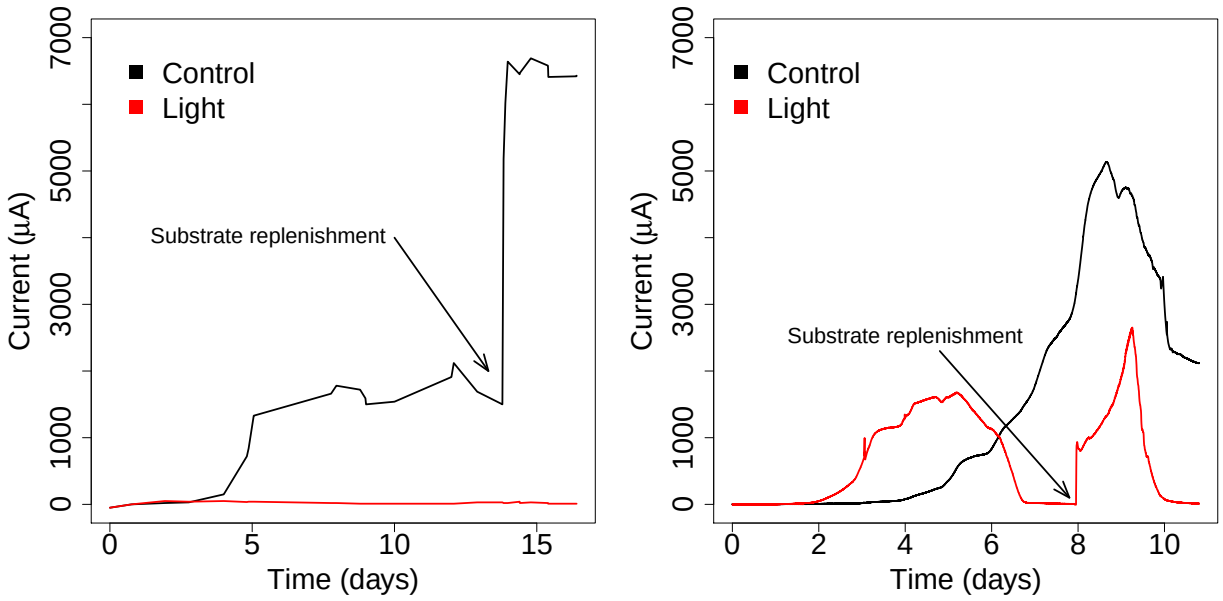

(A) Primary inoculum

(B) Secondary inoculum

Figure 4.1: CA on half-cell. A: bioanodes were started from primary inoculum; B: bioanodes were started from secondary inoculum. Red signifies exposure to light and black indicates dark controls.

Figure 4.1B shows current produced over time by bioanodes C and D which were started from secondary inoculum. Both started to produce current and actually the light-exposed bioanode showed faster growth by the 5th day. Current in the light cell reached a peak at 1620 µA on the 5th day and

then decreased within 2 days. A second cycle was started on the light-cell but this was even shorter than the first cycle. Meanwhile the dark control cell has not finished its first cycle and its maximum current was 5130 μA.

In primary inoculum and presence of light, ARBs cannot grow to form mature bioanodes. With secondary inoculum and exposure to light, ARB can grow but the cycle length and maximum current are smaller that those of the control. The faster start-up time in presence of light might be explained by temperature rise due to lamp proximity. Yet, measurements revealed no difference in temperature between the anolyte of the light-exposed cell and that from the dark cell (24°C). However, carbon felt may absorb more light due to its dark color and therefore it may experience higher temperature than the anolyte. This could explain why the light exposed bioanode D started before its dark control C. A positive effect of light on start-up cannot be concluded. Acetate is non fermentable and cannot sustain bacterial growth in absence of electron acceptors. However APBs can grow on acetate in presence of light. Their growth in the light-exposed anolyte is supported by the fact that anolyte becomes red in color as shown in figure 4.2. Secondary inoculum is thought to have a higher count of electrigenic bacteria which is why the light-exposed bioanode started from this inoculum was able to produce current, although over longer time light decreases performance. Primary inoculum is expected to have low electrigen count and higher biodiversity. When exposed to light, electrigens in primary inoculum cannot establish a biofilm because they have a lower competitive advantage compared to other bacteria.

Figure 4.2: Accumulation of red biomass in the anolyte of light-exposed half-cell

4.3.2 Effect of light on bioanodes fed on acetate and complex substrate and the possibility of excluding anaerobic photosynthetic bacteria during enrichment

When bioanodes were grown in dark for the first cycle, they did not show any degradation in performance after being exposed to light. This is shown in figure 4.3A for bioanode E and in figure

4.3B for the bioanode F. In figure 4.3 grey regions show dark periods during the first cycle and the yellow regions show light-exposure periods covering the rest of the cycles. Based on previous observations it was expected that cycle length and current output would decrease immediately upon light exposure. However this did not happen as shown by the first 2 cycles in the light regime (figures 4.3A and 4.3B). At the beginning of the 4^{th} cycle, 1 ml of primary inoculum was added to the anolyte of both cells. This was accompanied by an immediate decrease in cycle length while maximum current was not affected. Cycle length decreased from 14.64 to 4.98 days in the acetate reactor (E) and from 16.63 to 3.03 days in the OECD reactor (F). CE dropped from 27.57$\pm$ 5.7% to 9.19$\pm$1.99% in the acetate bioanode and from 23.22$\pm$1.6% to 3.23$\pm$1.23% in the OECD bioanode. COD removal rate improved for both cells (from 85.54$\pm$1.28% to 92.47$\pm$2.8% and from 77.16$\pm$0.54% to 85.1$\pm$4.89% respectively). However this should not be interpreted as a positive effect of light because the increase in COD removal rates is attributed to growth of non-electrigenic bacteria.

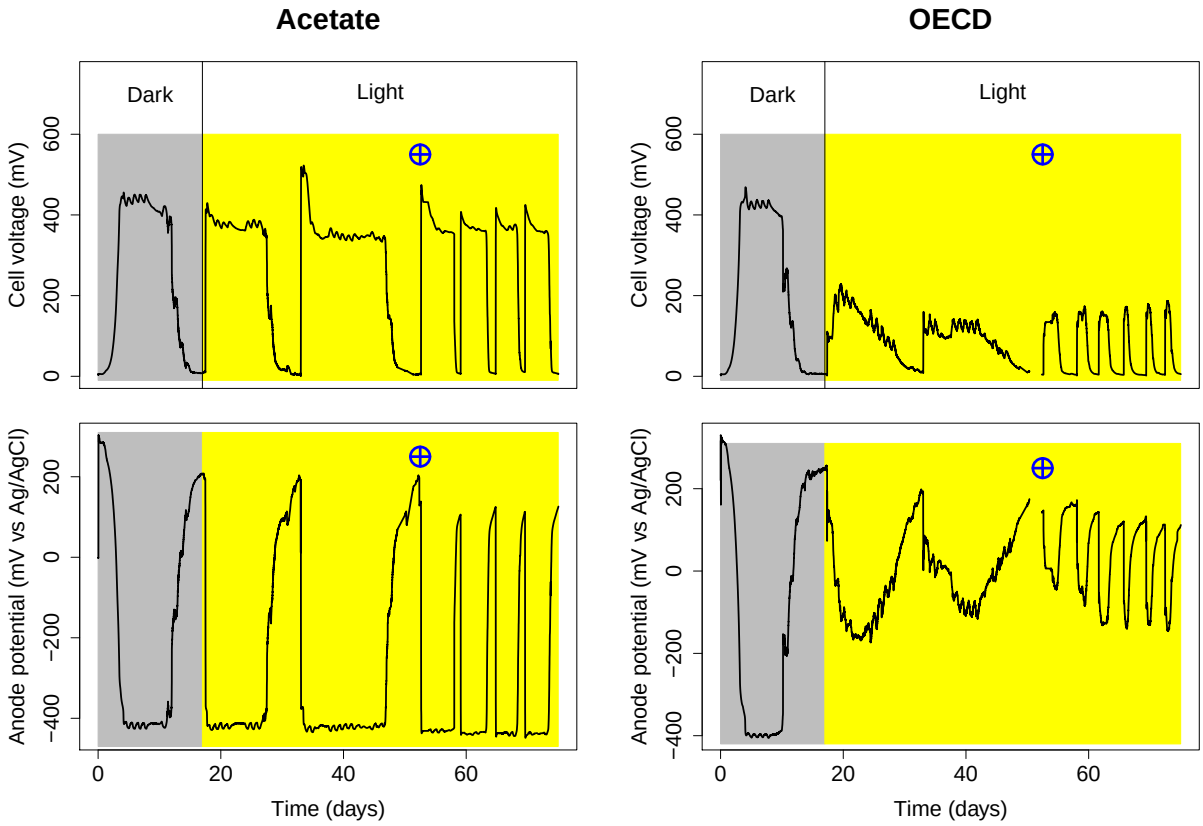

(A) (B)

Figure 4.3: CP on SCMFCs exposed to light. A: bioanode was fed on acetate; B: bioanode was fed on OECD medium. Cell voltage is plotted against time in the upper 2 graphs. Their corresponding anode potentials are plotted against time in the lower 2 graphs. Grey color signifies periods of dark and yellow color signifies periods of light exposure. The target symbols indicate the moment of adding 1 ml of a 1:1 mixture of activated sludge and wastewater.

These suggest competition for substrate between electrigens and non-electrigens. The latter group may be represented by APB. These were introduced with the addition of 1 ml primary inoculum at the beginning of the 4th cycle. It is likely they were also present at the beginning of the first cycle but lack of light did not allow for their growth. This favoured instead the electrigens to establish themselves from the beginning.

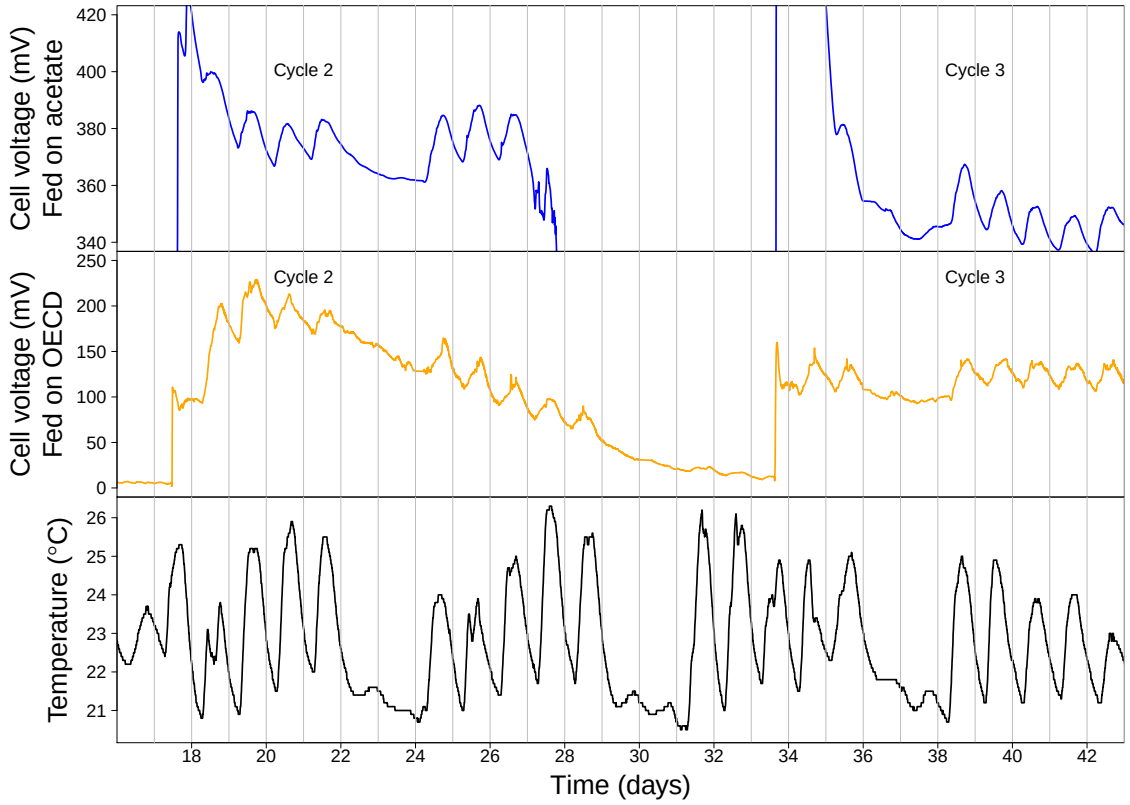

Figure 4.4: Day-night oscillations in cell voltage of acetate-fed MFC (top) and a OECD anolyte-fed MFC (middle) superimposed on temperature profile during the same time period (bottom). Cell voltages are shown during 2nd and 3rd feeding cycles of the MFCs. Temperature was logged in a sterile reactor placed in light next to the MFCs. Time axis was offset in order for the vertical gray lines to coincide with midnight.

CPs presented in figure 4.3 show regular variation in cell voltage on a night-day basis. Cell voltage drops during the night and increases during the day. Similar trends have been reported in the literature [159]. This might be due to temperature variation because the MFCs were not temperature-controlled. Temperature was logged for 33.5 days after the oscillations in cell voltages were observed. Temperature and cell voltages are plotted during the same time period in figure 4.4. This shows the same night-day variation as cell voltage, varying from 20°C during night, and up to 26°C during day. It follows that current increases with temperature. This effect is stronger for the OECD bioanode. The acetate bioanode is limited by cathode which explains its smaller night-day oscillation compared to the OECD bioanode.

Bacterial community composition is shown in figure 4.5. Percentages of *Geobacter* and *Rhodopseudomonas* and total bacterial cell abundance are shown in table 4.2.

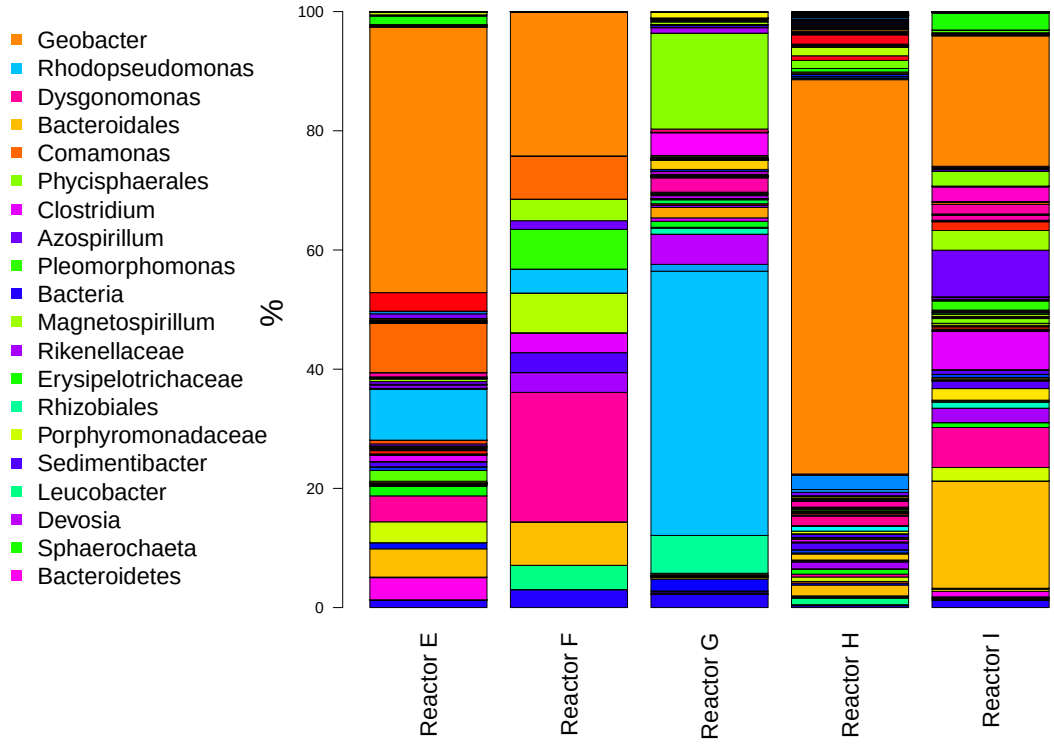

Figure 4.5: Community analysis for bioanodes E, F, G, H and I. Taxons are identified to genus level. Where this was not possible the next classification level is shown (family, order or class). Bioanodes E and F were exposed to light from the second cycle and G from the first cycle. Bioanodes H and I are dark controls

Table 4.2: *Geobacter* and *Rhodopseudomonas* percentages and total cell counts on bioanodes E, F, G, H and I. Cell counts values are expressed in units of 10^6 cells/gram of wet anode.

Reactor	Light exposure	Substrate	*Geobacter* (%)	*Rhodopseudomonas* (%)	Cell counts
E	from 2nd cycle	Acetate	45.9	9	433
F	from 2nd cycle	OECD	24.2	4	96
G	from 1st cycle	Acetate	0.18	38.2	
H	dark control	OECD	66.16	0	718
I	dark control	Acetate	21.87	0	79

Rhodopseudomonas was not detected on the bioanodes grown in dark. Both *Geobacter* percentage and total cell abundance were smaller in light exposure for acetate-fed bioanodes. The opposite trend was observed for the OECD bioanodes. In this case both *Geobacter* percentage and total cell abundance were higher on the light exposed bioanode.

Bioanode G exposed to light from the first cycle had the lowest percentage of *Geobacter* (0.18%) and highest percentage of *Rhodopseudomonas* (38.2%). Bioanodes E and F who were exposed to light from the second cycle showed a *Geobacter* percentage of 45.9% and 24.2% respectively.

Keeping these bioanodes under dark for the first cycle has allowed the electrigens to colonise the bioanode and possible it has lead to the exclusion of *Rhodopseudomonas*. This explains why performance was not degraded when light was applied in the second cycle. Furthermore the anolyte remained clear during cycles 2 and 3 but it turned red within 2 days after addition of a small quantity of primary inoculum. This suggest that the effect of light depends on the presence of APBs even in small quantities.

On the bioanodes exposed to light from the second cycle *Rhodopseudomonas* percentages were 9% and 4%. Although it is thought that any APB were removed during the first cycle, their presence on these bioanodes is explained by the addition of primary inoculum at the 4^{th} cycle. Because electrigens were already established, *Rhodopseudomonas* was not able neither to attain dominance nor to exclude electrigens. By comparison *Rhodopseudomonas* percentage on the bioanode exposed to light from the first cycle was the highest (38.2%). In this case, *Rhodopseudomonas* was able to grow faster covering the bioanodes and preventing colonisation and growth of electrigens. Its percentage was lower in OECD anolyte. This is because OECD anolyte sustains growth of more types of bacteria compared with acetate and also because OECD anolyte has lower COD content compared to acetate anolyte.

Rhodopseudomonas has been extensively studied as a model for bacterial anoxygenic photosynthesis [253]. Metabolically it is very versatile and can use many organic molecules for growth while harvesting light energy [257]. It can also grow exclusively on acetate as carbon source in the presence of light [258]. Such conditions are met inside the anodic chamber of MES made of transparent material. Artificial illumination provides for a light source and oxygen is removed by heterotrophic bacteria. The effect of light was initially noticed in half-cells with polarised anodes and fed on acetate. This effect was manifested by the anolyte changing in color to red. After medium change the anolyte was turning red even faster that in previous cycles.

4.4 Conclusions

Light alters bacterial community composition in the detriment of electrigens when fed on acetate. The effects of light exposure included drop in performance, shorter cycle length, lower CE and growth of red biomass inside the anodic chamber. These effects were influenced by inoculum type. When primary inoculum was used, the bioanode could not be started at all in presence of light. In the case of secondary inoculum and light exposure, the bioanode was able to grow but its performance was lower compared to the dark control. The negative effects of light are attributed to the growth of APBs, suggested by the red biomass growth under light and the results from community analysis. Light effects on performance were not observed for bioanodes grown in the dark for the first cycle. This is because APBs can be excluded during one cycle of enrichment.

However, reintroducing them caused an immediate drop in the performance.

The main APBs identified in bioanodes exposed to light belong to the genus *Rhodopseudomonas*. No APBs were detected in bioanodes protected from light. Metabolic versatility of the genus *Rhodopseudomonas* and its ability to grow exclusively on acetate in the presence of light suggest that competition for substrate between electrigens and APBs represents the mechanism of performance degradation in bioanodes exposed to light. It is therefore recommended that MESs based on mixed communities to be excluded from light to preserve performance.

Chapter 5. The effects of substrate and anode potential on anodic bacterial communities, growth and electron transfer mechanism

In this chapter the effects of anode poised potential on bioanodes were assessed. It was hypothesised that increasing anode potential leads to higher yields of electrigenic bacteria. This is because the amount of energy bacteria are able to harness is limited by the potential of the terminal electron acceptor (TEA). In the case of anode-respiring bacteria (ARB) the TEA is represented by the anode. Increasing its potential allows ARBs to harness more energy which in turn are able to increase in biomass.

The first aim of the present study was to investigate how the anode poised potential impacts on anodic communities in terms of composition, abundance of electrigens, electron transfer mechanism and distribution of biomass on anodes. The objectives associated with this aim are:

- investigate how current density, coulombic efficiency and COD removal rate are influenced by anode potential
- investigate if anode poised potential impacts on bacterial composition of bioanodes
- establish if electrigens abundance is correlated to gained energy
- perform cyclic voltammetry and peak analysis on bioanodes grown at different anode potentials
- check if the observed relations are substrate-independent by repeating the experiment using complex substrate anolyte
- image biomass on bioanodes grown at different anode potentials
- investigate on the effect of RE position in relation to the bioanode on the actual anode potential

The second aim was to assess the relation between biomass and performance. The objectives associated with this aim are:

- compare distribution of biomass and electrigenic activity across the depth of bioanodes
- the effect of biomass removal on performance

5.1 Introduction

The commercial implementation of MESs is hindered by their low power output. The bioanode converts chemical energy to electrical energy and is one of the main factors responsible for the limitation in power density [187]. One important reason for bioanode limitation is bacteria use some part of the energy released from substrate which is controlled by anode potential [189]. Previously it was shown that biomass on anodes increases with anode potential [187,189,190]. However in absence of community analysis the yield of electrigens was not available. The maximum theoretical energy gain is limited by substrate's potential and anode potential according to equation:

$$\Delta G^{0'} = -nF(E^{0'}_{donor} - E_{anode}) \tag{5.1}$$

where $\Delta G^{0'}$ represent change in Gibbs free energy, F is Faraday constant, $E^{0'}_{donor}$ is substrate biological potential and E_{anode} is anode potential. However not all of this energy is available for bacteria. Some of it is used for the transfer of electrons from bacteria to anode which is measurable as a potential difference between electrode and biofilm and is called over-voltage [71]. This potential difference is given by the difference between anode potential and the potential of microbial terminal electron donor (MTED).

The potential drop across anode-biofilm interface is the potential difference between MTED and TEA. The latter is represented by the anode. Increasing the TEA potential would increase the potential drop across the anodic interface consequently leading to higher current. At higher anodic potential bacteria are offered higher free energy [181] but it remains unknown if bacteria are able to harness the surplus energy. It may be possible that surplus potential could be used only to drive the current [151]. Alternatively the possibility of ETC extension as a response to an increase in TEA potential would consequently lead to higher energy gain for bacteria per molecule of substrate and therefore higher biomass yield.

The study of bioanodes at different poised anode potentials is justified by the need to understand how bacteria are influenced by this factor. This knowledge can be used to design better MES reactors for dedicated applications. Previously other studies have investigated on the effect of anode potential but they mainly have focused on performance parameters. The effect of anode poised potential could be better understood by conducting studies which determine the species composition and their abundance [151]. Integrating electrochemical characterisation with microbiology

methods allows for a better understanding of the relation between performance and the biology of bioanodes. Abundance of electrigens which was not previously available with mixed communities was extracted and compared against performance and energy gain. Imaging biomass distribution on entire bioanodes is presented here as a novel and useful technique which is recommended for future studies. Using two types of substrate can establishes how observations acquired on acetate medium can be extrapolated to wastewater and gives insight into the interactions between electrigens and non-electrigens at different anode potentials.

5.2 Experimental design

4 sets of reactors were used for this study. Details of all reactors are summarised in table 5.1 which includes information on the analyses performed on each.

The purpose of the first set of reactors was to choose a suitable acetate concentration for the anolyte composition by investigating on its relation to the current output. 2 bioanodes were grown at -400 and -200 mV vs Ag/AgCl respectively and the acetate concentration was varied while observing changes in current.

The second set focuses on community composition, cell abundance, performance and ETM. 3 anode potentials and 2 substrates (acetate and OECD anolytes) were used with each combination run in duplicate making for a total of 12 H-cell reactors. 6 were run on acetate and the other 6 were run on OECD medium. The chosen anode potentials were: -400, -200 and 0 mV vs Ag/AgCl. The smallest value is closer to the OCP of the bioanodes (-490 mV vs Ag/AgCl). This range covers common anode potential values typical for microbial fuel cells. The naming system is composed of three parts. The first indicates anode potential, the second indicates substrate and the third is a repetition index. For example the name -200AcB shows this H-cell had its anode polarised at -200 mV vs Ag/AgCl, was fed on acetate and is the second repeat of its treatment type. All reactors were run for 3 uninterrupted cycles (not including the pre-feeding cycle for OECD cells). At the end of each cycle anolyte samples were collected, filtered and analysed for chemical oxygen demand (COD) used to calculate coulombic efficiency (CE). A forth cycle was started and cells were kept running for 2 days to reach stable conditions. At this point electrochemical analysis was performed which includes current interrupt (CI) method, electrochemical impedance spectroscopy (EIS) and cyclic voltammetry (CV). EIS spectra were collected galvanostatically close to OCP and run between 0.1 and 10000 Hz. CVs were run from -500 mV to +200/+400 mV at the following scan rates: 1, 3, 5, 7, 9, 20, 40, 60, 80 and 100 mV/s. Bioanodes were collected at the end of the run, homogenised and stored at -20°C for community analysis and bacterial cell counting. A few carbon threads covered in biofilms were collected using a pair of tweezers from bioanode -200AcA and analysed under a microscope using SYBR Green staining.

In the third set of reactor biomass distribution on bioanodes was investigated. 2 anode potentials (-400 and -200 mV) and 2 substrate types (acetate and OECD) were used. Each reactor was run in duplicate making for 8 reactors. All were run for 3 cycles (not including pre-feeding for OECD cells). At the end the bioanodes were collected and placed in a Petri dish with SYBR-Green stain solution. After 30 minutes of incubation bioanodes were imaged using a gel documentation system.

The forth set was used for profiling electrigenic activity and biomass distribution across bioanode depth. 2 bioanodes were grown on acetate for 3 cycles at -200 mV vs Ag/AgCl. One of them was exposed to the anolyte on all sides and at the end of its run was sliced on its length. The resulting pieces were imaged using the same procedure as in part 3. The other bioanode was sliced on its middle line with 2 resulting thinner parts that had the same height and width as the original bioanode. Each facets of both pieces were investigated for electrigenic activity by CV and had samples taken for microscopy imaging.

Table 5.1: Bioreactors used for the study of anode potential effect on bioanodes. Double lines separate different sets of reactors which are indicated by uppercase letters: A - current vs acetate concentration; B - effect of anode potential on community composition, cell abundance, current output and ETM; C - effect of anode potential on biomass distribution on bioanodes; D - Depth profile of electrigenic activity. Single lines separate acetate bioanodes from OECD bioanodes.

Reactor set	**Reactor**	**Substrate**	**Potential**	**CA**	**Community analysis**	**Cell counts**	**Electrochemical analysis**	**Biomass imaging**	**Fluorescence microscopy**
A	ConcA	Acetate	-400	X	X	X	X	X	X
	ConcB	Acetate	-200	X	X	X	X	X	X
B	-400AcA	Acetate	-400	✓	✓	✓	✓	X	X
	-400AcB	Acetate	-400	✓	✓	✓	✓	X	X
	-200AcA	Acetate	-200	✓	✓	✓	✓	X	✓
	-200AcB	Acetate	-200	✓	✓	✓	✓	X	X
	0AcA	Acetate	0	✓	✓	✓	✓	X	X
	0AcB	Acetate	0	✓	✓	✓	✓	X	X
	-400CSA	OECD	-400	✓	✓	✓	✓	X	X
	-400CSB	OECD	-400	✓	✓	✓	✓	X	X
	-200CSA	OECD	-200	✓	✓	✓	✓	X	X
	-200CSB	OECD	-200	✓	✓	✓	✓	X	X
	0CSA	OECD	0	✓	✓	✓	✓	X	X
	0CSB	OECD	0	✓	✓	✓	✓	X	X
C	-400AcC	Acetate	-400	✓	X	X	X	✓	X
	-400AcD	Acetate	-400	✓	X	X	X	✓	X
	-200AcC	Acetate	-200	✓	X	X	X	✓	X
	-200AcD	Acetate	-200	✓	X	X	X	✓	X
	-400CSC	OECD	-400	✓	X	X	X	✓	X
	-400CSD	OECD	-400	✓	X	X	X	✓	X
	-200CSC	OECD	-200	✓	X	X	X	✓	X
	-200CSD	OECD	-200	✓	X	X	X	✓	X
D	-200AcE	Acetate	-200	X	X	X	✓	✓	✓
	-200AcF	Acetate	-200	X	X	X	X	✓	X

5.3 Results and discussion

5.3.1 Current dependence on substrate concentration

It was reported that current does not increase for acetate concentrations higher than 0.2 g/L (2.44 mM) [259–261]. The effect of acetate concentration on current output is shown in figure 5.1. When acetate was increased from 0.25 g/l to 0.5 g/l, current output from the bioanode poised at -200 mV increased from 2.83 mA to 3.12 mA. Above 0.75 g/L acetate concentration current decreases slightly suggesting substrate has an inhibiting effect at higher concentrations. The bioanode grown at -400 mV did not show any change in current output with concentration. In this case the applied potential was the determining factor.

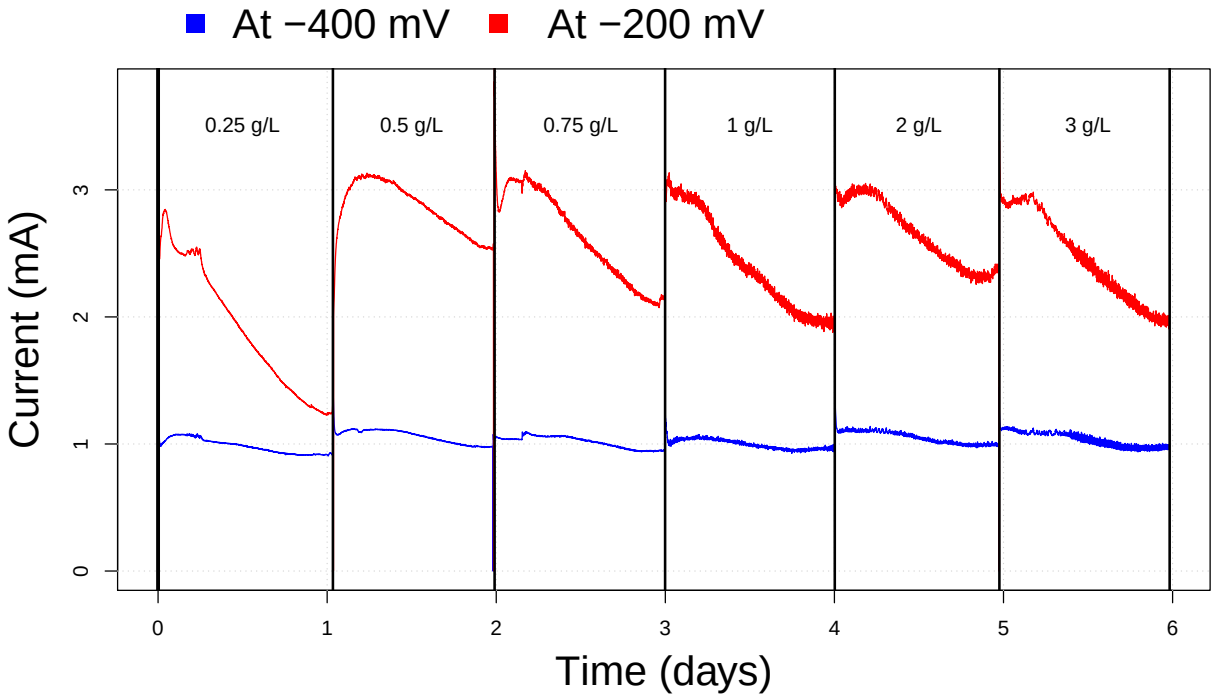

Figure 5.1: Electrical current relation to acetate concentration and anode potential. One bioanode was poised at -400 mV (red) and the other at -200 mV (blue). Each day the acetate concentration was increased.

5.3.2 Effect of poised anode potential on current output

CA profiles are shown in figure 5.2 for acetate cells and in figure 5.3 for OECD cells. Current during cycle shows differences between cells grouped by substrate type. In the case of acetate cells current increases fast at the beginning of the cycle from 0 mA reaching a maximum in less than 1 day followed by a steep decrease creating the appearance of a peak. After that current decreases

slowly until the end of the cycle. Current maxima are also present in the CA profiles of the OECD cells. Here current also experiences a sharp increase on adding substrate at the beginning of the cycle and then slows down to form a broader flatter peak and not forming a sharp peak.

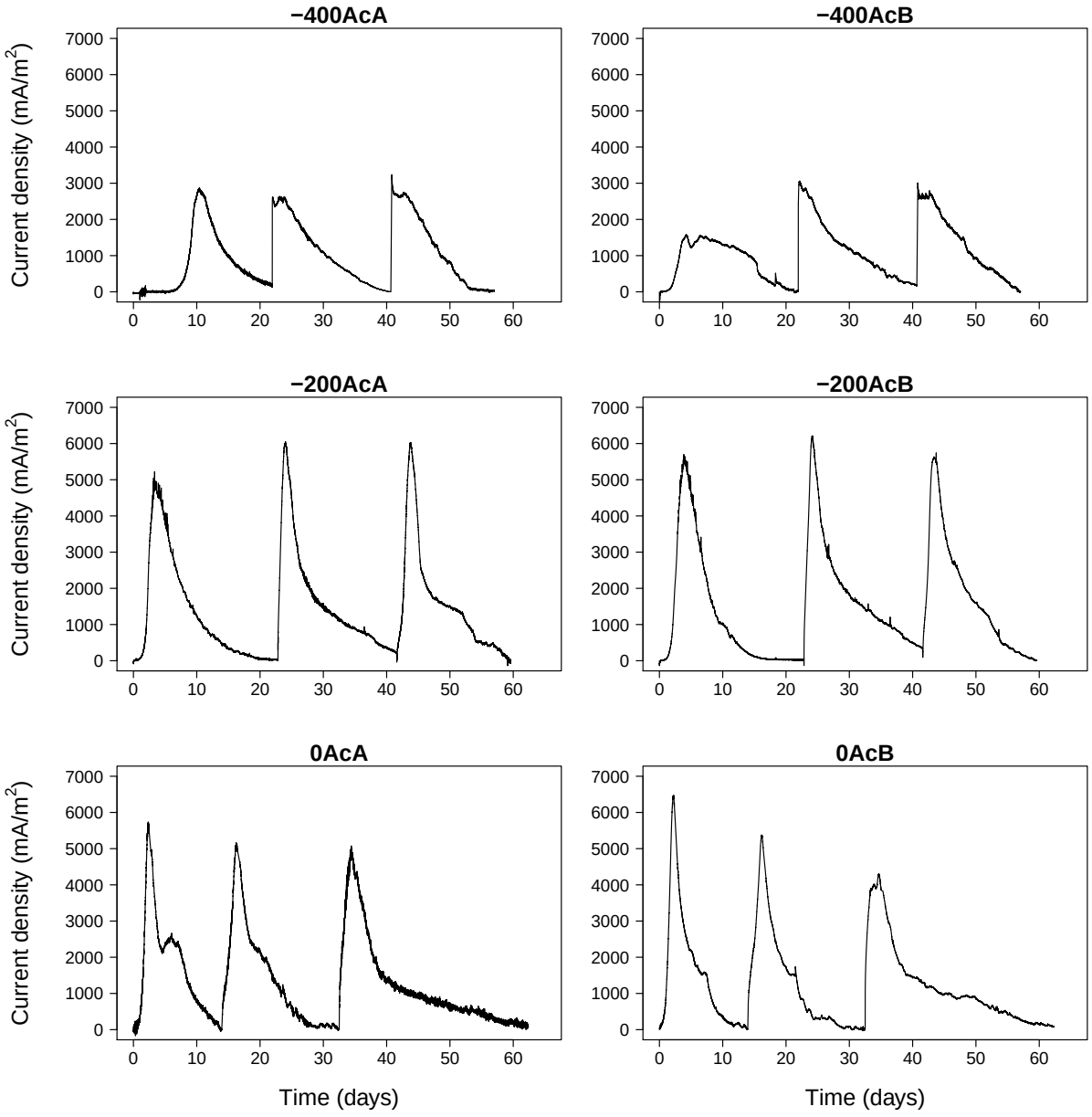

Figure 5.2: CA profiles for bioanodes grown on acetate medium. Bioanode duplicates are arranged by column. Each row shows bioanodes poised at a certain anode potential: -400 mV (upper row), -200 mV (middle row) and 0 mV (lower row).

In a half-cell reactor the anode potential is held constant and the counter-electrode (cathode) is free to produce as much current as needed (provided that its activity is not limited by supply of oxidant or other factors). Therefore changes in current output in half-cells during cycles is influenced mainly by organic substrate. Substrate concentration is highest at the beginning of the cycle. At this point the bacteria start producing current which increases very fast. Substrate starts decreasing

leading to a decrease in current.

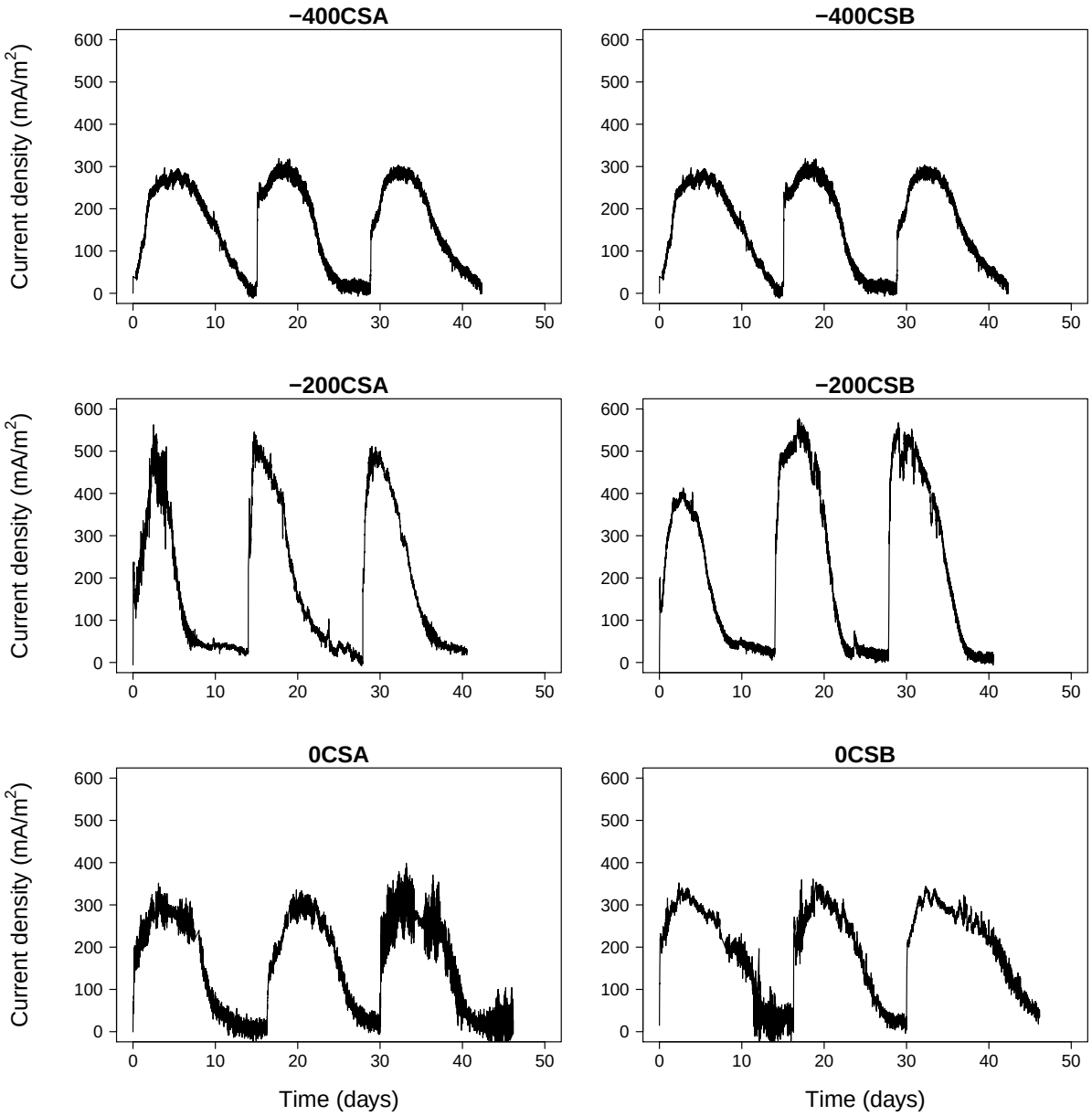

Figure 5.3: CA profiles of bioanodes grown on complex medium (OECD recipe). Duplicates are arranged by column. Each row shows bioanodes poised at a certain anode potential: -400 mV (upper row), -200 mV (middle row) and 0 mV (lower row).

The CA profiles show two other important difference between substrate groups. First the cycle length on acetate cell is 19.89±5.24 days and for OECD cells is 14.34 ±3.12 days. Secondly current densities for OECD cells are smaller by an order of magnitude compared to those from acetate cells. Because the CA profiles show sharp peaks in the case of acetate cells the maximum current density per cycle is not a good measurement for comparing reactor output. Instead current density was averaged for values higher than 90% of maximum current. The current densities extracted by this approach are shown in figure 5.4. The plot shows clearly the differences between current

output by substrate. It also shows that the average current density follows the same trend with potential for each substrate. For both groups current density is lowest at an anode potential of -400 mV. It then reaches the highest value at -200 mV followed by a decrease at 0 mV. A similar trend was reported in another study [259] where the highest current increased with applied potential until the anode potential reached 0 mV vs Ag/AgCl. This could be explained by an inhibition effect of poised anode potential above -200 mV.

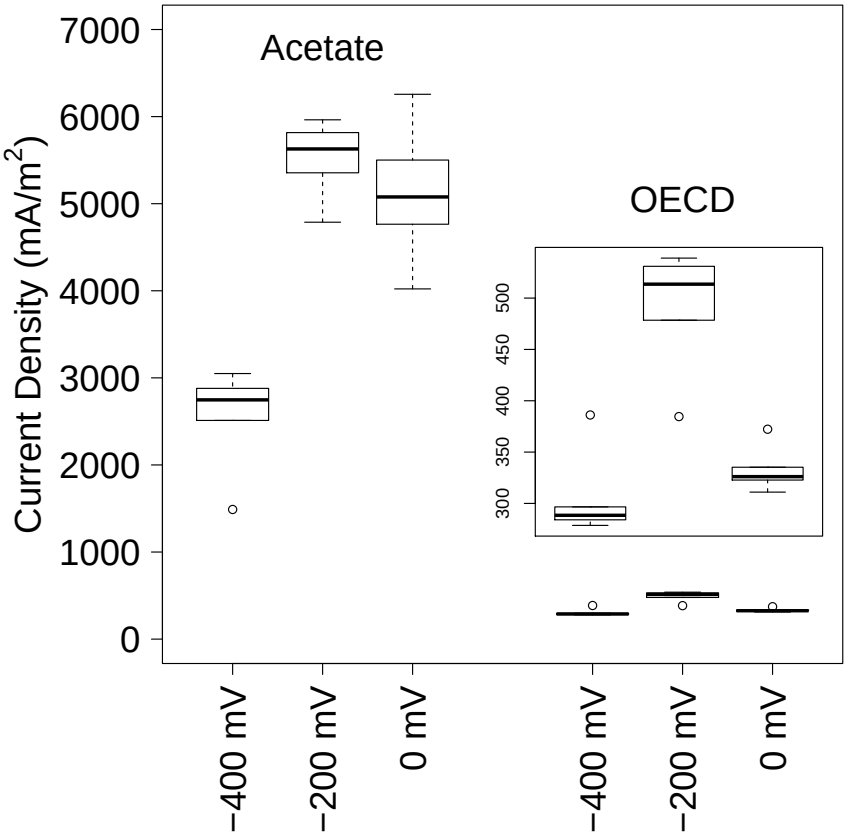

Figure 5.4: Current output shown by anode potential and substrate type. Current was extracted from the CA profiles from each cycle in the stable region. Values from duplicates are merged. The inset figure shows the same data from the OECD bioanodes rescaled for better visualisation.

Measurements showed a COD value of 387.5 mg/L for OECD anolyte and 853.3 mg/L for acetate anolyte. This can explain the shorter cycle length and smaller current densities for OECD cells. CE and COD removal rates are shown in the appendix in table 9.2 and are plotted in figure 5.5. Average CE on acetate cells was 25.81% and on OECD cell was 5.7%. CE has increased with time in acetate cells with 2 exceptions. By the third cycle CE increased with anode poised potential. COD removal rate does not follow any trend with anode potential. It is influenced by the type of substrate being higher for acetate compared to OECD cells (87.66% and 75.89% respectively). Complex substrate contains many chemical species some of which cannot be used by bacteria or take longer to be metabolised. Consequently the removal of COD in OECD medium is lower as

compared to acetate. The average COD at the end of the cycle was 88.05 $\pm$ 33.71 mg/L for acetate cells and 90.6 $\pm$ 20.17 mg/L for OECD cells.

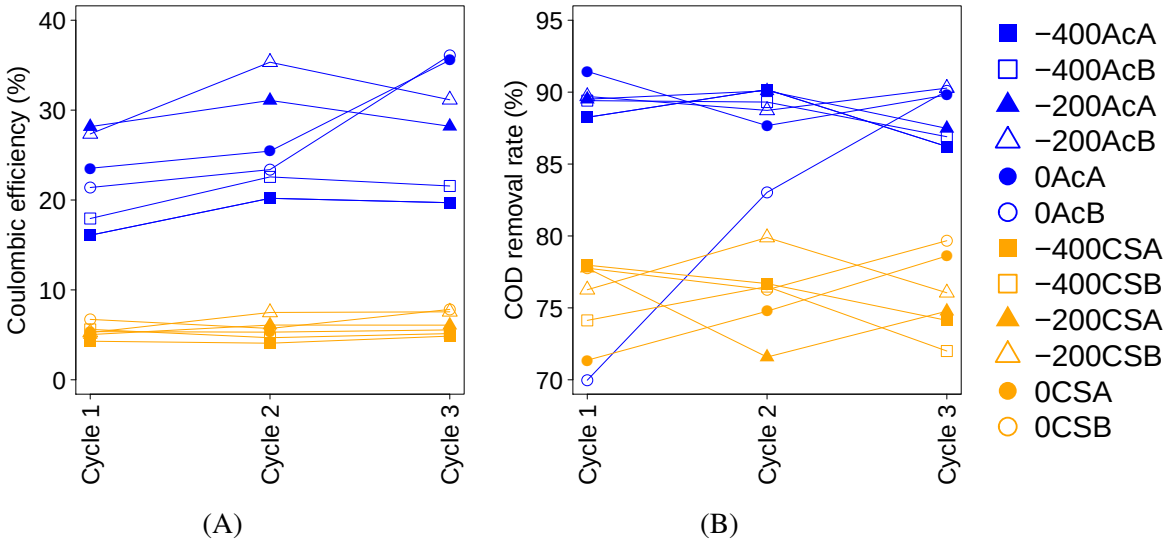

Figure 5.5: Coulombic efficiencies (A) and COD removal rates during each cycle for each bioanode. Acetate bioanodes are shown in blue and OECD bioanodes are shown in orange.

5.3.3 Bacterial community composition

Community analysis results are shown in figure 5.6. This shows that acetate half-cells are characterised by higher percentage of *Geobacter*. The bacteria communities grown on anodes fed with OECD medium show a higher percentage of fermentative bacteria. It is thought that these bacteria are important in providing the electrigens with substrate. They also lower COD content during fermentation explaining the lower CE values in OECD cells.

The most abundant class is the *Deltaproteobacteria* which at the order level is almost entirely represented by *Desulfuromonadales* and at genus level by *Geobacter*. This genus is the only known electrigen identified in the communities. The next most abundant classes are the *Bacteroidia*, *Clostridia* and *Betaproteobacteria* but these show higher diversity in terms of orders and genera they are represented by. The first of this class includes species commonly found in the environment or present in the animal gut. The *Clostridia* includes only strictly anaerobic species some of which are commonly found in anaerobic reactors like *Anaerofilum*. The *Betaproteobacteria* are mainly represented by *Comamonas*. This is a motile rod-shape bacteria commonly found in soils, mud and activated sludge [262]. It can feed on many organic acids and amino acids. Most species in this genus are aerobic but many can perform nitrate respiration as well being important members o denitrifying communities [263]. Its presence in the bioanode community is probably due to carryover from primary inoculum and its survival is due to its metabolic versatility. None of the

species in this genus were found to perform fermentation [263] so it is thought *Comamonas* is not important for electrigenesis. *Dysgonomonas* was also abundant in the bioanode communities. A strain from this genus has been previously identified and isolated from a MFC [264]. This genus includes species capable of fermenting many types of sugars but also perform respiration using a wide range of TEAs. It is thought in this study that *Dysgonomonas* is breaking down organic components providing the electrigens with suitable substrate.

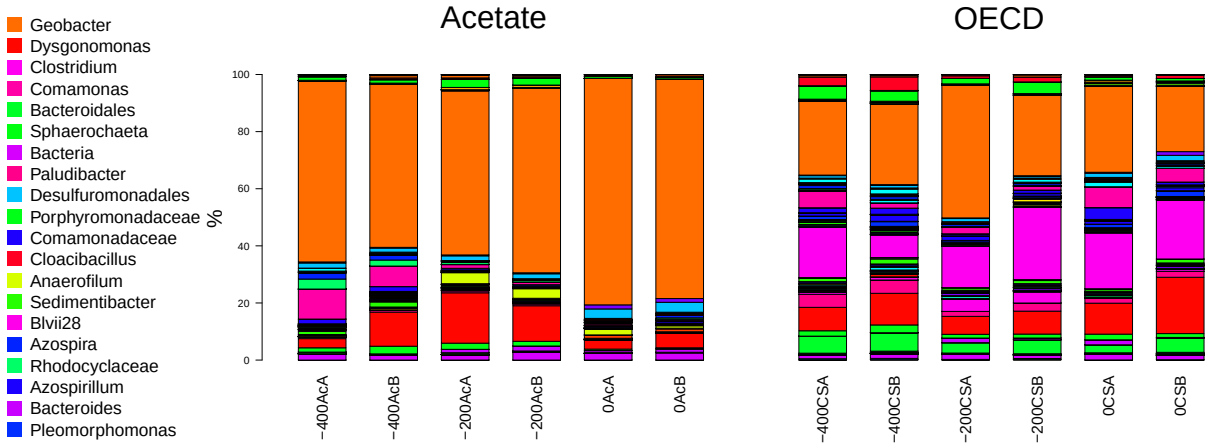

Figure 5.6: Bacterial community composition of bioanodes. Taxons are identified to genus level. Where this was not possible the next classification level is shown (family, order or class).

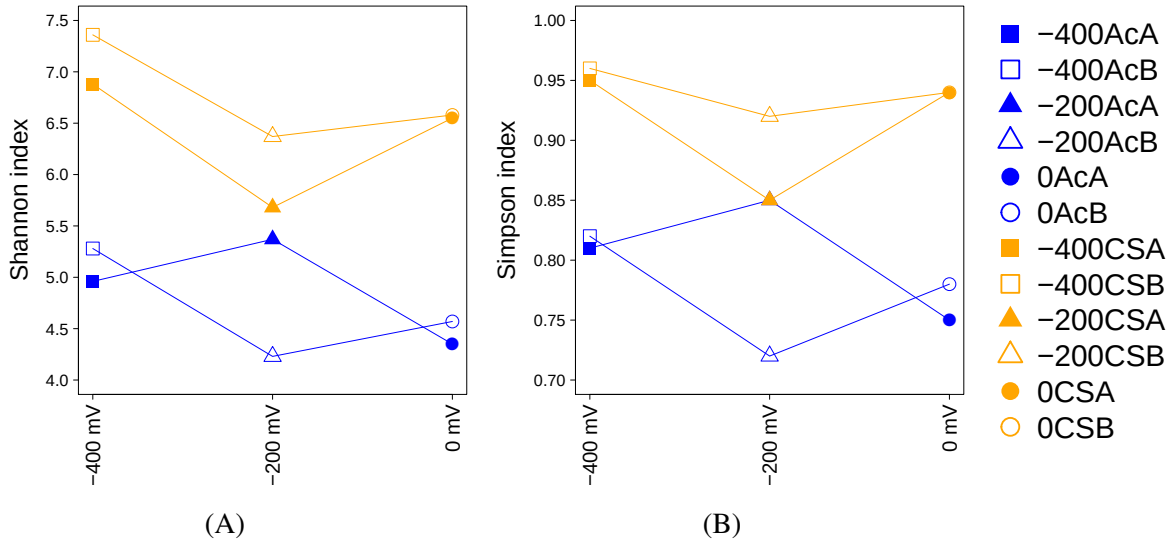

Figure 5.7: Biodiversity of anodic communities. A: Shannon index; B: Simpson index; Acetate anodic communities are shown in blue and OECD anodic communities are shown in orange.

The non-electrigenic bacteria were possible carried over from primary inoculum. In acetate bioanodes they have smaller percentage and might not be important for electrigenesis. They grow in these

reactors feeding not on acetate but on organic mass produced by *Geobacter*. On OECD bioanodes non-electrigens provide *Geobacter* with substrate as result of fermentation processes. Biodiversity was computed as Shannon and Simpson indices. These are shown in the appendix in table 9.3 and are plotted in figure 5.7. Shannon index is a measure of species richness and Simpson index is a measure of species evenness [265]. OECD bioanodes have higher biodiversity than acetate cells. This is because complex substrate provides for a higher number of niches. Both biodiversity indices show a decreasing trend with anode potential. For the acetate bioanodes this is mainly due to increasing *Geobacter* percentage.

5.3.4 Poised potential and substrate are important factors that influence community composition

Ordination of communities based on Bray-Curtis distance is shown in figure 5.8A. Each substrate group forms a linear gradient on the plot. Within each gradient samples are placed in increasing order of applied anode potential as shown by arrows in figure 5.8A. Samples forming pairs of repeats are positioned close to each other. Within the acetate group intra-pair distance decreases with applied potential. This suggests that as the anode potential increases it applies a higher selective pressure on the community composition. At lower anode potential substrate plays a bigger role in shaping the bacterial community. As the anode potential is increased the bioanode becomes a more selective environment were some species are gradually excluded.

The presence of gradient-like structures in the community analysis data shows the selective power of anode potential on the bacterial composition. As the anode potential is increased the communities converge for both substrate types. Convergence is more pronounced within the acetate group where the bioanodes grown at -200 mV and 0 mV form a cluster placed further from the bioanodes grown at -400 mV. For the OECD group convergence is also visible but the intra-pair distances are bigger compared to the acetate group. Therefore OECD allows for higher diversity and growth of bacterial species that are less influenced by anode potential.

Grouping of samples based on Jaccard distance is shown in figure 5.8B. Here no gradients are visible. Instead 3 clusters are observed grouping bioanodes by substrate type. The acetate group is represented by 2 clusters and the OECD cells by 1 cluster. Bioanodes within the OECD groups are positioned closer to each other compared to the acetate group. The acetate bioanodes grown at -400 mV and -200 mV forms a cluster and the pair grown at 0 mV cluster separately.

Comparing ordinations based on abundance data in figure 5.8A and presence-absence data in figure 5.8B shows that anode potential has a strong effect on abundance of taxons whereas substrate type has a stronger influence on the composition of communities.

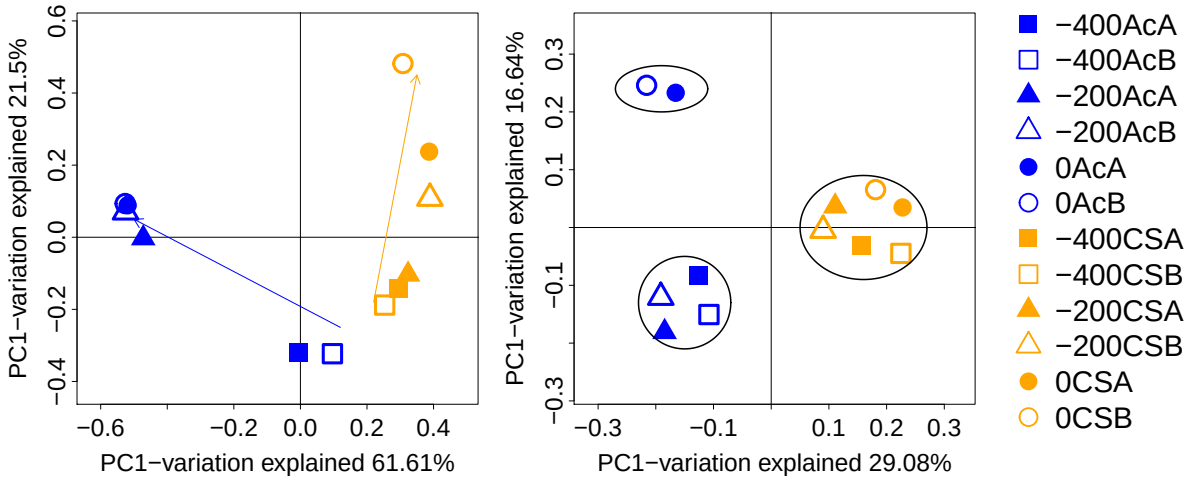

(A) (B)

Figure 5.8: Ordination of samples using Principal Coordinate Analysis. Blue color indicates acetate bioanodes. Orange color indicates OECD bioanodes. Square symbols indicates bioanodes grown at -400 mV. Triangles indicate bioanodes grown at -200 mV and circles indicate bioanodes grown at 0 mV.
A: Principal Coordinate Analysis based on Bray-Curtis distance. The blue arrow indicates the arranging direction of acetate bioanodes and the orange arrow shows the same for OECD bioanodes.
B: Principal Coordinate Analysis of bioanodes communities based on Jaccard distance. Only presence-absence of taxons are considered while their abundances are ignored.

Within the acetate group anode potential seems to influence the composition only at 0 mV due the separate clustering of bioanodes grown at this potential. This suggests that at higher anode potential some species are excluded and/or their abundance is lowered beyond detection limit due an increase in *Geobacter* abundance.

5.3.5 Bacterial abundance and its correlation to current output

The amount of energy used for growth by bacteria depends on how much substrate was used for current production. Because bioanodes fed on OECD medium had lower CE it follows that these bacteria had less energy available for growth and consequently their abundance should be lower. This expectation was confirmed by cell counts as shown in figure 5.9. OECD bioanodes have cell counts lower by almost an order of magnitude. Within the acetate group cell counts increased with applied potential. For the OECD group the trend is opposite with cell counts decreasing with applied potential. For acetate cells the relation between cell counts and anode potential is similar to the relation between biomass measured as phospholipid content per cm^2 and anode potential described by *Wei et al.* [187]. In their study biomass increased suddenly from 0.04 $\mu g/cm^2$ to 0.18 $\mu g/cm^2$ when anode potential was changed from -160 mV to 400 mV vs SHE (-360 mV and +200

mV vs Ag/AgCl respectively) and decreased to 0.13 μg/cm^2 at an anode potential of +500 mV vs SHE (+300 vs Ag/AgCl).

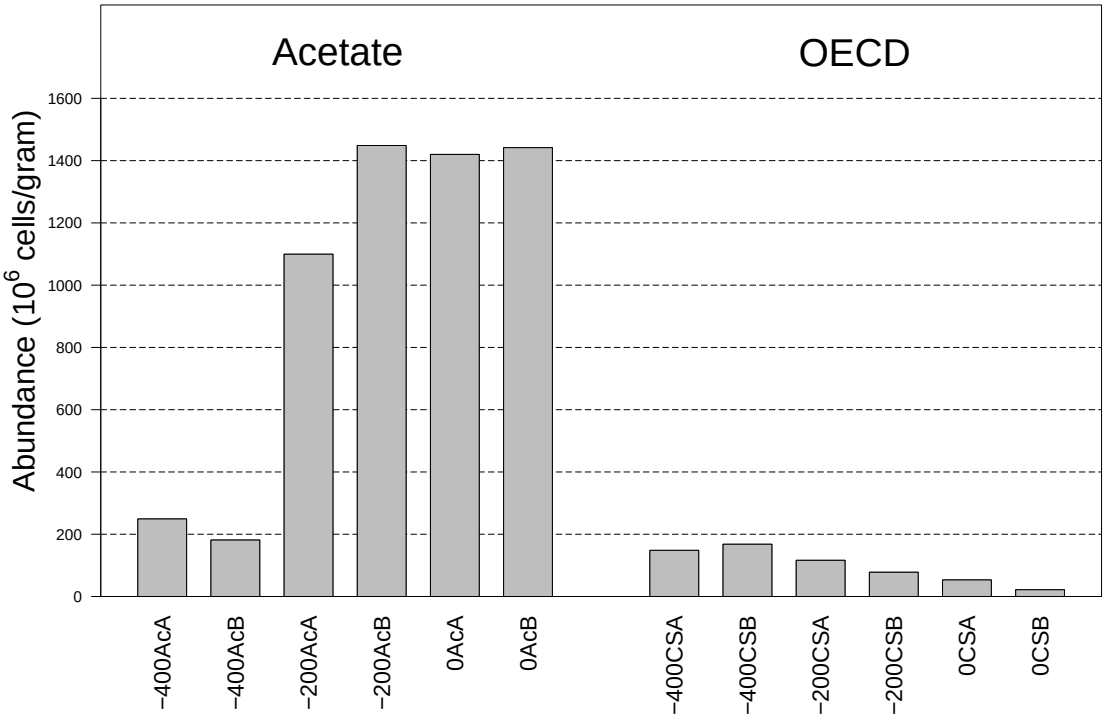

Figure 5.9: Cell abundance expressed as millions of bacterial cells per gram of electrode. The 6 samples at the left are bioanodes grown on acetate and the 6 samples at right are bioanodes grown on OECD complex substrate.

The community composition weighed by cell counts show that average *Geobacter* abundance increases with anode potential within the acetate group (215, 1273 and 1430 $\times 10^6$ cells/gram) and decreases within the OECD group (158, 97 and 37 $\times 10^6$ cells/gram). Within the acetate group there is a big jump in *Geobacter* abundance (from 215 to 1273 $\times 10^6$ cells/gram) when the anode poised potential was varied from -400 mV to -200 mV. Current density has increased between these 2 applied anode potentials from 3213 to 6912.18 mA/m^2 . At 0 mV current density has decreased slightly to 6395.41 mA/m^2 but *Geobacter* abundance has increased further. These suggest changes to the electron transfer mechanism and the amount of energy that bacteria can acquire from electrigenesis. The anode acts as the terminal electron acceptor and increasing its potential allows bacteria to extend their electron transfer chain to harness more energy per acetate molecule. This in turn leads to higher biomass yield at higher anode potentials as already shown.

Total energy gain was calculated according to equation 3.2 by integrating current over time to obtain the total coulombs produced by the electrigens and by assuming the biological potential of acetate/CO_2 is -0.59 V vs Ag/AgCl [251]. Total energy gain values are shown together with cell counts and maximum current per cycle for each bioanode in the appendix in table 9.1. Total energy gain increases with anode potential for both substrates. The bacteria grown on acetate

were able to harness the surplus energy when the anode potential was increased. If this was not the case then upon increasing the anode potential the amount of energy should not have changed. The increase of almost 6 times in cell abundance between -400 and -200 mV anode potentials can only be explained if bacteria are able to harness more energy when the anode potential is increased. Increasing gained energy with anode poised potential can be achieved by regulating the potential of the MTED [151]. The ETC conveys electrons using the potential drop for creating an electrochemical potential which is then used by ATPsynthase to produce ATP. The amount of energy an ETC can harness is constrained by the drop in potential across each of its components. This means the potential window that an ETC can use is not arbitrary wide but increases in discrete steps.

The Spearman correlations between current, total cell counts, electrigen abundance, CE and gained energy are shown in table 5.2. Within the acetate group there is strong correlation between *Geobacter* abundance and gained energy (correlation = 0.94). Correlation between total cell counts and gained energy is smaller (correlation = 0.71). These indicate that energy obtained from using the anode as terminal electron acceptor was used by *Geobacter* for growth and not by other bacteria. For OECD bioanodes energy gain is negatively correlated to total cell counts and to *Geobacter* abundance. This suggests that on OECD bioanodes higher anode potential had a negative effect on total cell abundance but the mechanism remains unknown.

Table 5.2: Spearman correlation indices between cell counts, *Geobacter* abundance, gained energy and current density

		Total cell counts	Geobacter counts	Gained energy
Acetate	Geobacter counts	0.77	-	-
	Gained energy	0.71	0.94	-
	Current density	0.83	0.49	0.43
OECD	Geobacter counts	0.83	-	-
	Gained energy	-0.94	-0.77	-
	Current density	-0.43	0.09	0.37

The relation between total and *Geobacter* abundance vs gained energy is shown for both types of substrate in figure 5.10. This shows that for acetate bioanodes there is better linearity between energy and *Geobacter* while for OECD bioanodes there is better linearity between energy and total cell counts.

Cell counts decreased with theoretical energy gain in the case of OECD cells. This can be observed from the negative trend of cell counts versus anode potential as shown in figure 5.9. The assumption behind calculating the energy gain is that electrigens in OECD medium are provided with acetate resulting from fermentation processes performed by non-electrigens. This assumption may not be correct due to the high diversity of non-electrigen and the types of fermentation they can carry.

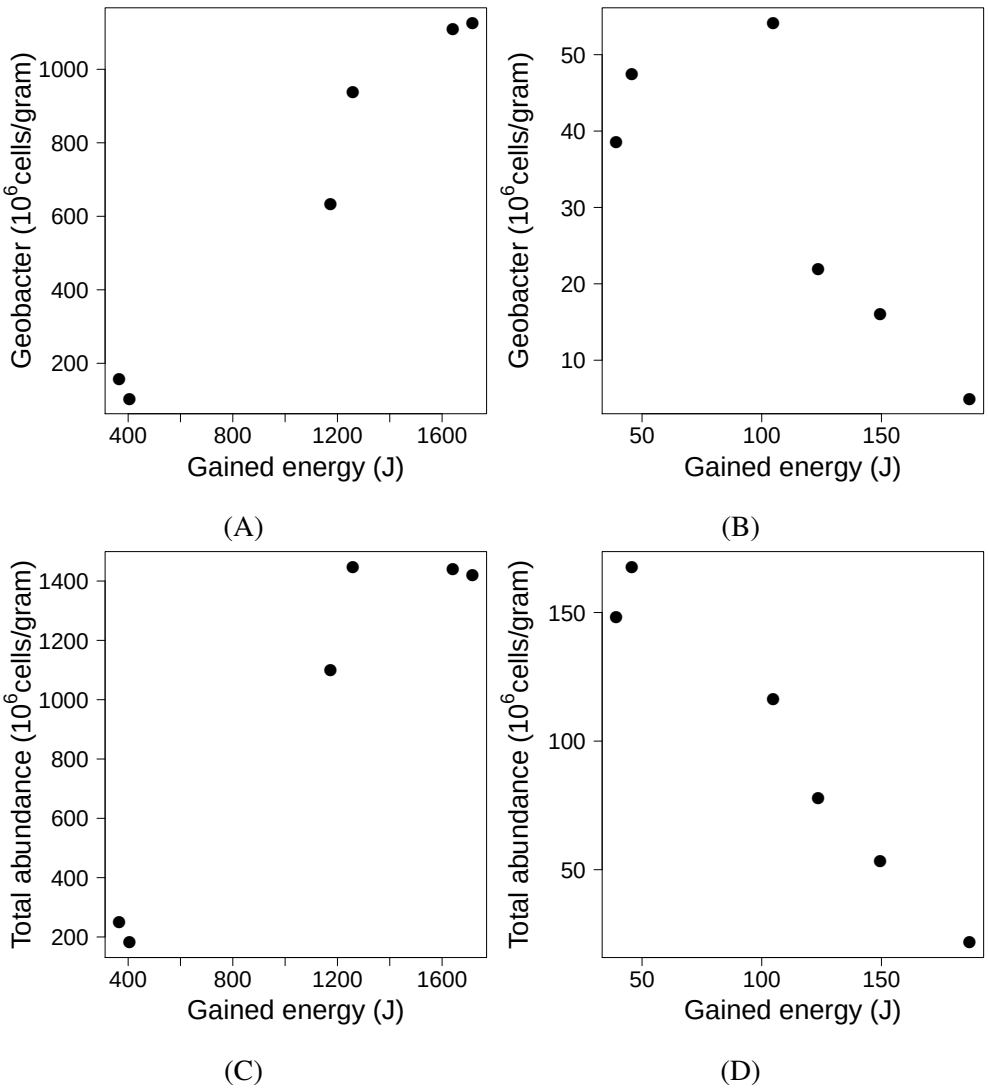

Figure 5.10: Total cell abundance and *Geobacter* abundance vs gained energy. A: *Geobacter* abundance vs gained energy for acetate bioanodes; B: *Geobacter* abundance vs gained energy for OECD bioanodes; C: Total cell abundance vs gained energy for acetate bioanodes; D: Total cell abundance vs gained energy for OECD bioanodes;

Furthermore *Geobacter* is able to use other products of fermentation. This means the calculation of energy gain should include each substrate *Geobacter* is able to use. However the results from acetate cells suggests that *Geobacter* is able to harness more energy with increasing anode potential. Therefore there is no reason to reject that energy gain has increased with anode potential also in OECD cells although their true values depend not only on acetate oxidation. The decrease in cell counts with higher energy yields may be due to accumulated dead cells in biofilms which can be removed with the expense of energy. Bioanodes grown at -400 mV do not acquire enough energy to ensure the removal of dead cells which therefore accumulate. In bioanodes grown at higher anode potentials the number of live cells increases which are therefore able to remove more of the dead cells leading to a decrease in total cell counts. Therefore it would be the abundance of the live

fraction that increases with energy gain. It may also be possible that the complex medium contain chemicals that upon oxidation at the anode becomes toxic for cell growth.

5.3.6 An investigation on electron transfer mechanism using electrochemical methods

The uncompensated resistances were measured by EIS as the high-frequency resistance in the EIS spectrum. The measured values were 7±4 Ω. For currents of 5 mA this translated into 15-35 mV shifts to the applied anode potential during scans. Uncompensated resistance increases with distance between RE and anode as shown in figure 5.11. This observation allows for an investigation on the effect of the uncompensated resistance on peak position. Figure 5.12 shows LSVs collected at 1 mV/s scan rate on the same bioanode but with two different values of uncompensated resistance. It shows that peak position has shifted by 34.5 mV when uncompensated resistance was changed from 11 Ω to 30 Ω. This aspect is not always considered in the MES field despite that some articles include pictures or diagrams of the reactors that were used showing the RE was placed half way between WE and CE [120, 190]. Such an arrangement alters the true applied potential according to equation 5.2.

$$E_{effective} = E_{applied} - iR_u \tag{5.2}$$

where $E_{effective}$ is the real applied potential, $E_{applied}$ is the applied potential, i is current and R_u is uncompensated resistance.

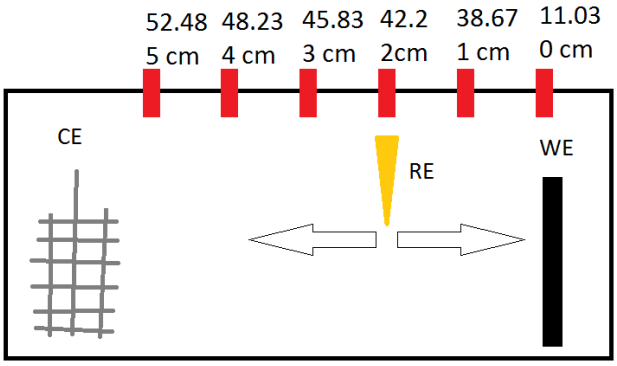

Figure 5.11: Diagram showing the effect of RE position on uncompensated resistance. Uncompensated resistance was measured by EIS and it is written for each distance between reference electrode and working electrode.

CVs were acquired at scan rates of 3, 5, 7, 9, 20, 40, 60, 80 and 100 mV/s. CVs at a scan rate of 5 mV/s are shown for all bioanodes in figure 5.13. CVs at all scan rates are plotted for the acetate bioanodes in figure 9.2 and for OECD bioanodes in figure in 9.3 in the appendix.

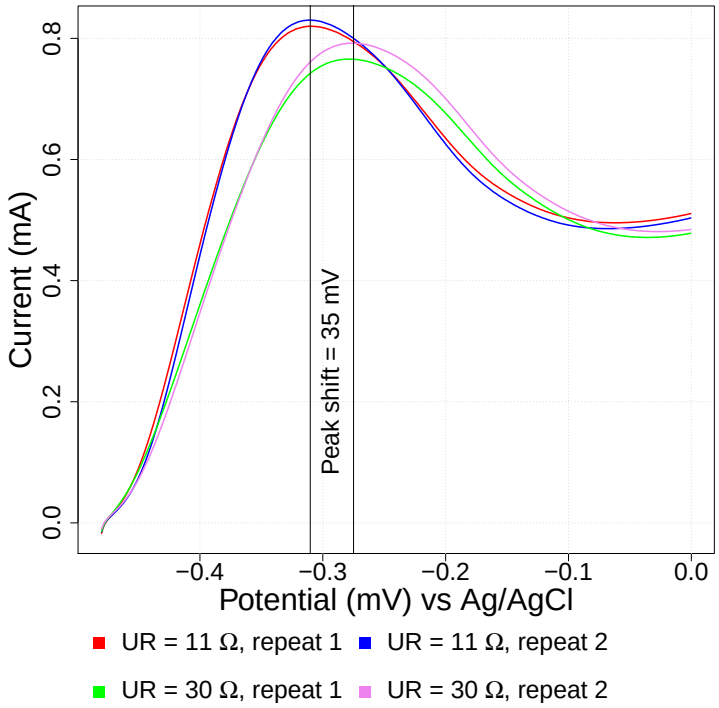

Figure 5.12: Effect of uncompensated resistance on peak position. The reference electrode was placed at 2 different distances from the bioanode. Each time 2 LSV were recorded. The values for uncompensated resistance is shown for each LSV. The vertical lines show by how much the peak has shifted between the 2 RE positions.

Voltammograms show higher currents for acetate cells up to 5 mA while for OECD cells they were an order of magnitude lower. With the exception of bioanode -200AcA all CVs show a peak positioned at around -0.2 V. This peak is considered to originate from an electroactive component involved in electrigenesis due to its height, consistent presence on bioanodes and absence from CVs taken on pristine carbon felt electrodes (shown in the appendix in figure 9.1).

For OECD bioanodes the electrigenic peak is consistently identified at -0.2 V for a scan rate of 5 mV/s. For acetate bioanodes its position varies around -0.2 V. This is because the acetate bioanodes produced more current which led to higher ohmic drop due to the uncompensated resistance. The electrigenic peak is more conspicuous on bioanodes grown at -400 mV regardless of substrate type. Furthermore the same bioanodes produce higher currents during voltage scans compared to bioanodes grown at higher anode potentials. Peak height was extracted and plotted against the scan rate and the square root of scan rate as shown in figure 5.14. Heights were measured from the baseline (at 0 mV) with no correction for capacitive currents.

For acetate bioanodes plotting the peak height against the square root of scan rate shows better linearity as compared to plotting it versus scan rate. A linear relation between peak height and scan rate would signal a surface electrode process which seems to be the case for OECD cells.

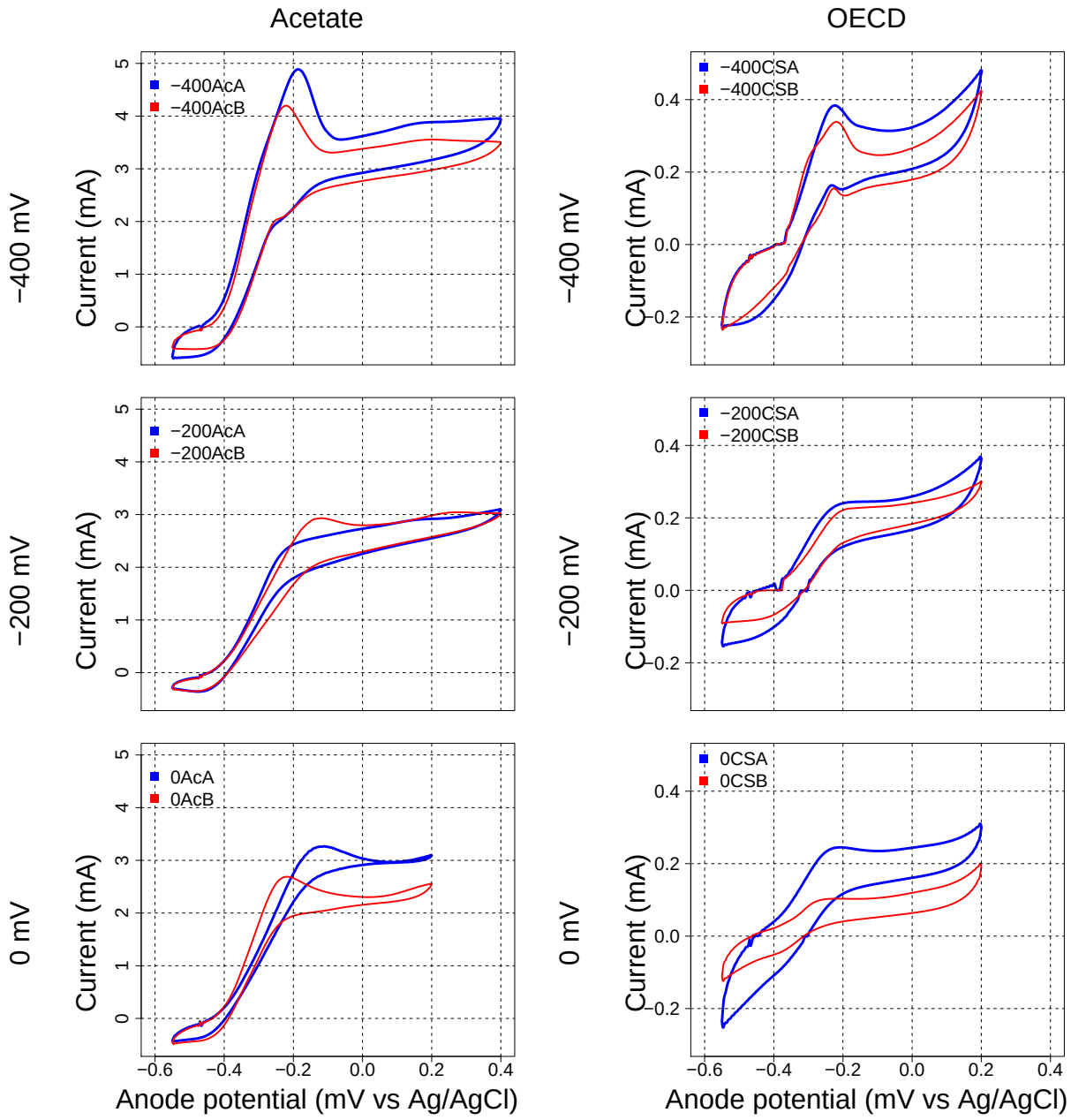

(A) CVs on acetate cells

(B) CVs on OECD cells

Figure 5.13: Cyclic voltammograms collected at a scan rate of 5 mV/s. Plots are arranged vertically from top to bottom in increasing order of poised anode potential. Each plot contains 2 CVs from duplicates. A: CVs from acetate bioanodes; B: CVs from OECD bioanodes;

R^2 values for linear fitting of peak height with scan rate and its square root are shown for both substrate types in table 5.3. Peak analysis on acetate bioanodes suggests the presence of a free diffusible electron shuttle that is reduced by bacteria and oxidised at the electrode. However a mechanism based on a diffusion is unlikely due the metabolic costs associated with producing a mediator by bacteria. Secondly upon medium change current recovered almost immediately.

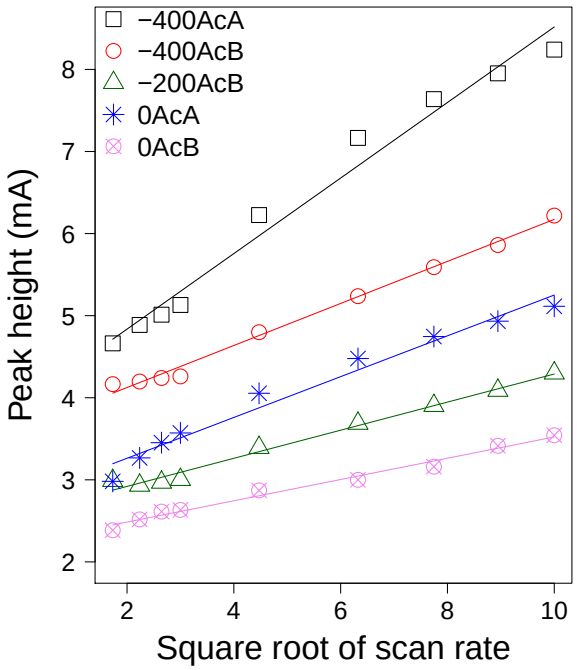

(A) Peak height vs square root of scan rate in acetate bioanodes

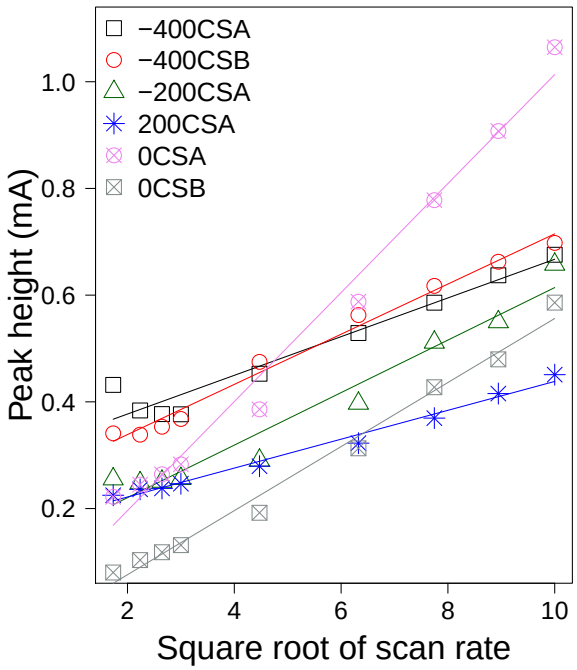

(B) Peak height vs square root of scan rate in OECD bioanodes

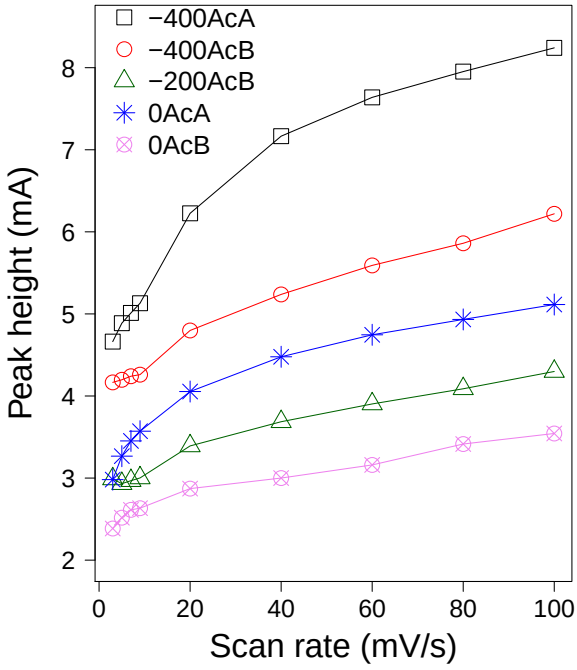

(C) Peak height vs scan rate in acetate bioanodes

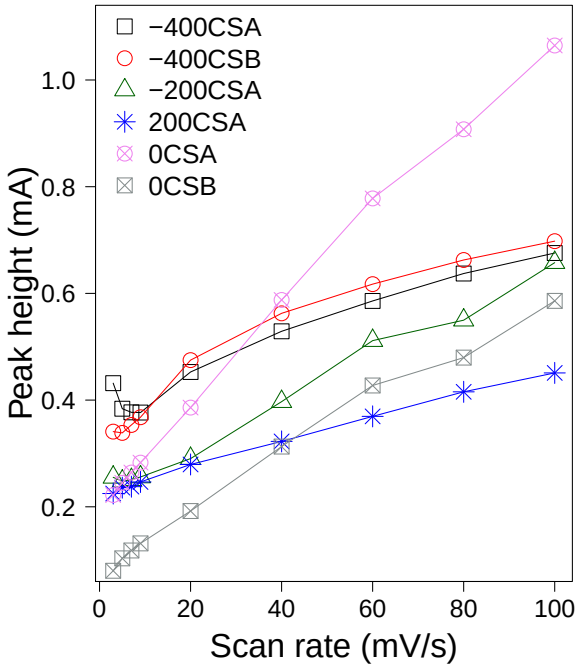

(D) Peak height vs scan rate in OECD bioanodes

Figure 5.14: Peak analysis of the the peak identified at -0.2 V vs Ag/AgCl. Left column show results for acetate bioanodes. Right column shows results for OECD bioanodes. Upper row shows peak height plotted against the square root of scan rate. Lower row shows peak height plotted against scan rate.

A diffusive mediator would be washed away during anolyte replenishment and the bacteria would take time and energy to regenerate it. Under these circumstance current would take longer times to recover upon medium changes.

Table 5.3: R^2 values for fitting peak height versus linear scan rate and square root of scan rate

Reactor	Scan rate	Square root of scan rate	Best fit
-400AcA	0.9123	0.98	Square
-400AcB	0.9732	0.9932	Square
-200AcB	0.9624	0.9871	Square
0AcA	0.8959	0.9737	Square
0AcB	0.9576	0.9855	Square
-400CSA	0.9552	0.9409	Linear
-400CSB	0.9393	0.9879	Square
-200CSA	0.9899	0.955	Linear
-200CSB	0.996	0.9864	Linear
0CSA	0.996	0.9844	Linear
0CSB	0.9909	0.9884	Linear

It was shown that fixed redox centers in a multi-layer polymeric coating applied on an electrode behave as a diffusive electrode process [266]. In this case there is no concentration gradient formed during voltage scan. Instead this is replaced by a gradient of redox states which behaves mechanistically as a diffusion process by showing a linear relation between peak height and the square root of scan rate. An electrigenic biofilm may behave as a polymer with fixed redox centers. Outer membrane cytochrome were identified to be involved in the electron transfer process in electrigenic bacteria. These cytochromes are equivalent to fixed redox centers in a polymer coating thus explaining why peak analysis on bioanodes signals a diffusive process. The apparent linear relation between peak height and scan rate in the case of OECD bioanodes is explained by lower cell abundance on these bioanodes. This means biofilms are much thinner when fed with OECD anolyte. Cytochromes are present in a thin layer very close to the surface of the anode. This would eliminate diffusion-like behavior making peak height proportional to scan rate.

Peak heights are bigger for bioanodes grown at -400mV for both substrate types with the exception of bioanode 0CSA. This trend can be explained by accepting the involvement of outer membrane cytochromes in the electron transfer process and by hypothesizing that their abundance can be regulated by bacteria in response to anode potential. In this case bacteria grown at lower anode potential would produce more outer membrane cytochromes to compensate for the lower anode potential. During voltage sweeps these bioanodes are able to produce more current as compared to those grown at higher anode potential. This is also in agreement with lower cell abundance on bioanodes grown at -400 mV; these bacteria must invest more energy in synthesizing the cytochromes thus limiting the amount of substrate used for cell growth.

Fluorescence microscopy images of samples taken from bioanode -200AcA are shown in figure 5.15. These show that biofilms grow around carbon threads and are made of a layer of dead biomass surrounded by a region of live biomass. The dead region is thicker and is in direct contact with the carbon thread. This raises an important question on the distribution of electrigenic activity across biofilm thickness. If electrigens are mostly present in the live region than they must convey the electrons over the entire thickness of the biofilm until they reach the conductive carbon thread. *Geobacter* is known to produce many outer membrane cytochrome that can convey electricity by electron hopping over long distances [62]. In this case the dead region could contain the cytochromes produced by cells that have died but are still involved in the electron transfer process.

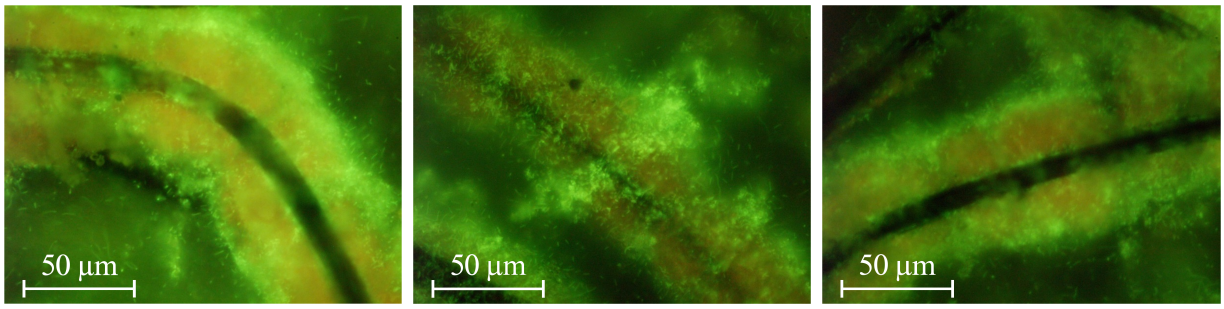

Figure 5.15: Microscopic images using dead-live staining on biofilms grown around carbon threads collected from bioanode -200AcA. Biofilms show a thicker internal regions composed of dead cells and an external thinner region composed of live cells

5.3.7 Biomass distribution on poised potential bioanodes and its relation to electrigenic activity

Biomass distribution on bioanodes is shown in figure 5.16. Although it is not possible to quantify biomass from fluorescence intensity it can be assumed that both are monotonically related as more biomass is associated to more DNA to which the SYBR-Green dye can bind and produce more fluorescence.

Overall bioanodes show a relatively uniform distribution of biomass with the exception of bioanodes -400AcD, -200CSC and -200CSD. Bioanodes -400AcD and -200CSC show more biomass at the bottom and bioanode -200CSD shows more biomass at the top. Biomass shows local concentrations showing unequal growth across the bioanodes. It remains uncertain if the regions of higher biomass density also produce more current. Although this could be true considering that bioanodes grown at -400 mV produce less current and exhibit lower biomass density compared to bioanodes grown at -200 mV. Biomass local concentrations suggest that bacteria benefit from clustering together rather then spreading uniformly on the available anode area.

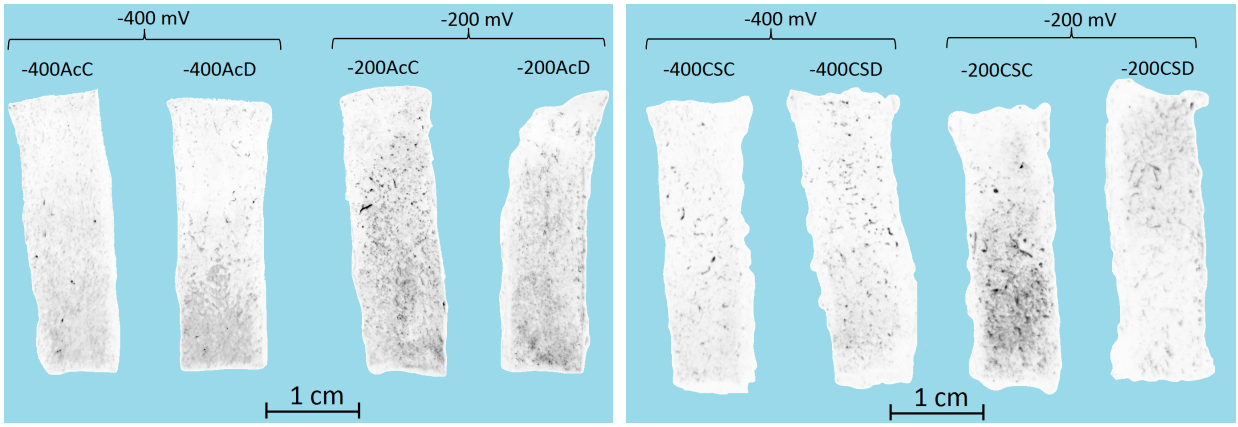

(A) Acetate cells (B) OECD cells

Figure 5.16: Biomass distribution on the anolyte-facing sides of bioanodes grown in half-cells. Anode poised potential values are shown above the bioanodes and are expressed vs Ag/AgCl reference electrode. Bioanodes were stained with SYBR-Green, incubated for 30 minutes and visualised in fluorescence mode (excitation at 480 nm; emission at 485-655 nm).

Figure 5.17 shows biomass imaging on bioanode -200AcE which was exposed to anolyte from all sides. Biomass distribution shows biofilms grown better at the surface of the bioanode and less inside it. This observation is explained by substrate mass transfer limitation. Bacteria inside the bioanode have limited access to substrate and therefore their growth is impaired.

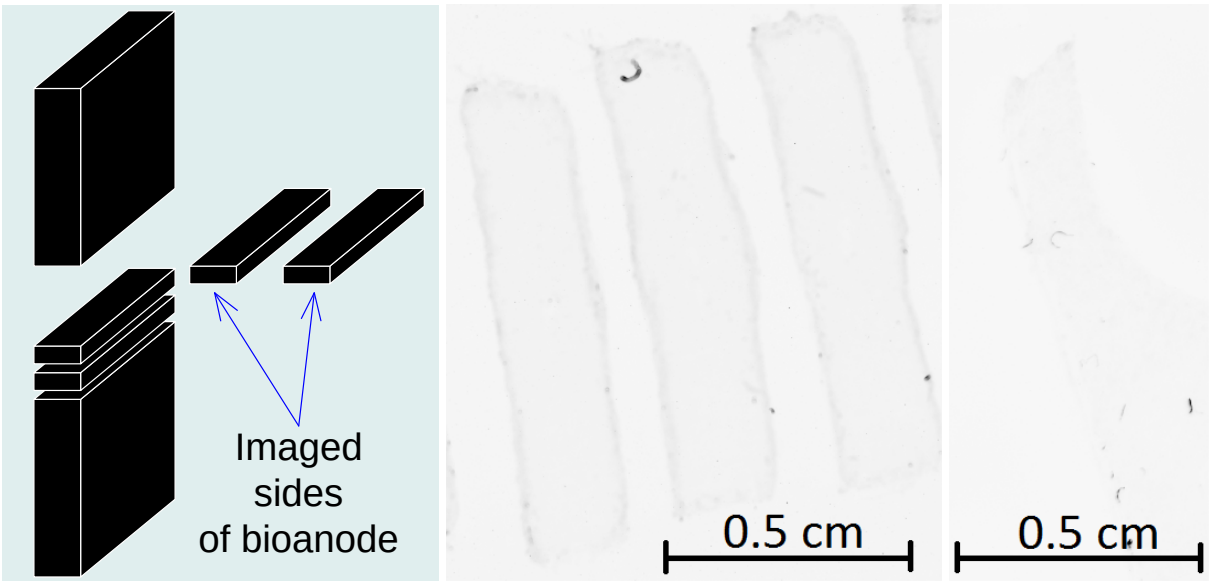

(A) (B) (C)

Figure 5.17: Biomass distribution inside a bioanode exposed to anolyte from all sides. A: bioanode was cut in slices; B: imaging shows biomass present on the periphery of slices which corresponds to bioanode exposed facets; C: control (pristine carbon felt material); Slices were incubated in SYBR-Green stain for 30 minutes. Imaging was done in fluorescence mode (excitation at 480 nm; emission at 485-655 nm)

Figure 5.18 shows the distribution of electrigenic activity with depth in bioanode -200AcF. The bioanode was cut in 2 creating 4 facets indexed by uppercase letters A, B, C and D. Facet A is the anolyte facing side while facet D is the current-collector facing side. It shows that the side directly exposed to anolyte is responsible for most of electrigenesis. Activity decreases with depth and it becomes negligible on the side that was facing the current collector. Facets B and C although are placed at the same depth in the bioanode show a big difference in activity. This is because facet B comes from the half of the bioanode closer to the anolyte. Electrigens present closer to facet A were responsible for some of the current produced when facet B was exposed to anolyte. The difference between facets A and C show that most of electrigenic activity occurs in the half of the bioanode exposed to anolyte.

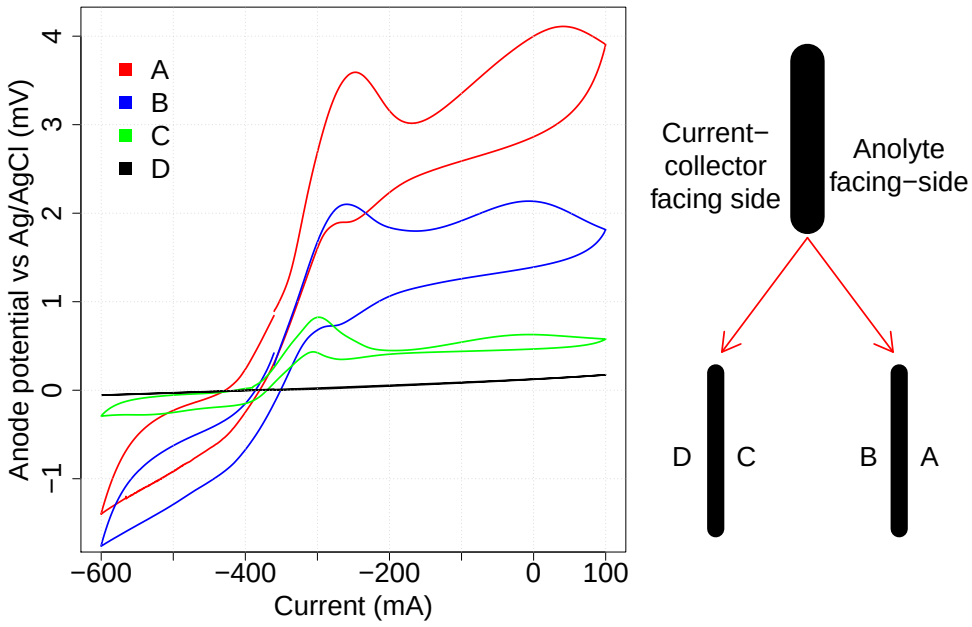

Figure 5.18: Distribution of electrigenic activity with depth. The bioanode was cut in 2 parts creating 4 sides: A, B, C and D. Voltammograms shows activity decreasing with distance from the anolyte facing side.

Microscopic images were taken on biofilm developed at the front, mid and back sides of the same bioanode (-200AcF) and are shown in figure 5.19. Although electrigenic activity is profiled for 4 facets there is not difference in depth between facet B and C. Therefore the mid-bioanode microscopic image characterises biofilms grown at the level of both facets B and C. Biofilms developed on the front side are thick. In the middle of the electrode single layer biofilms can be observed around the carbon threads. There are also numerous free living cells which by their green staining are thought to be alive. Most of the cells that are attached to the carbon threads stain in red signaling they are dead. At the back side of the bioanodes some threads are covered in biofilm but these are thin and composed of dead cells. The planktonic cells are less numerous than on the from side of the bioanode and are mostly stained in red suggesting they are dead.

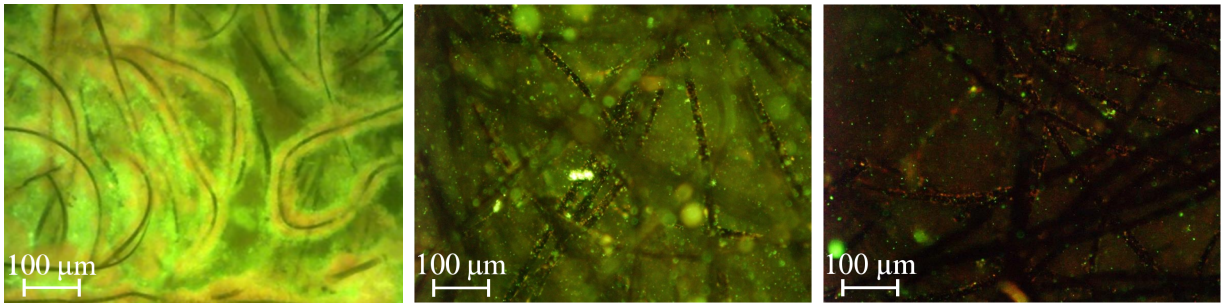

(A) Front of bioanode (B) Mid bioanode (C) Back of bioanode

Figure 5.19: Fluorescence microscopy images taken at different depths on the same bioanode. Dead-live staining was used. Dead regions are shown in red and live regions are shown in green. Biofilms grow around carbon threads (shown as black curved strips).

It is interesting to observe that biofilms grown on the anolyte facing side of the bioanode are very thick and show a dead region surrounded by a live region. If the biofilm grows in thickness with time and dead biomass accumulates than this should limit electron transfer efficiency. To support this claim it was observed that scraping the biomass off the surface of a mature bioanode leads to an increase in current as shown in figure 5.20. This suggests that the biomass on the surface of the bioanodes accumulates in time and becomes a limiting factor for electricity production.

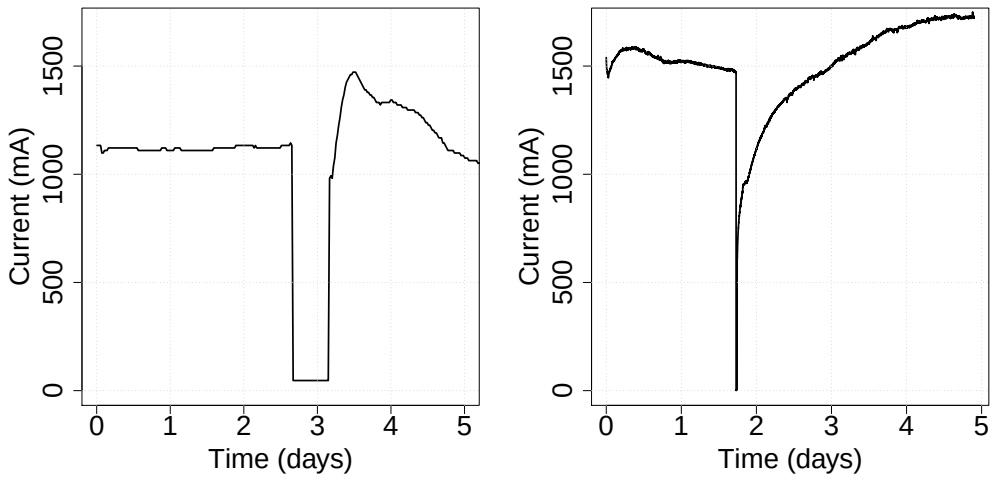

(A) (B)

Figure 5.20: Current regeneration after removal of biomass on the surface of a bioanode. Excess biomass was removed with a pair of tweezers causing the current to drop suddenly followed by an increase in current higher that before biomass removal

Although current seems to be associated with higher biomass and the place of maximum electrigenic activity coincided with the region of highest biomass it is mot likely that biomass is the effect of electricity production and not the other way around. As current is produced bacteria grown in number forming thick biofilms which then become self-limiting for current production. Figure 5.21A shows an old bioanode where biomass is visible by naked eye due its reddish colour (pos-

sibly due to cytochrome-rich biofilms). Removing some of the biomass with a pair of tweezers reveals the underneath carbon felt material as can be seen in figure 5.21B. This suggests an aging effect which may require periodic reconditioning of bioanodes by removing excess biomass.

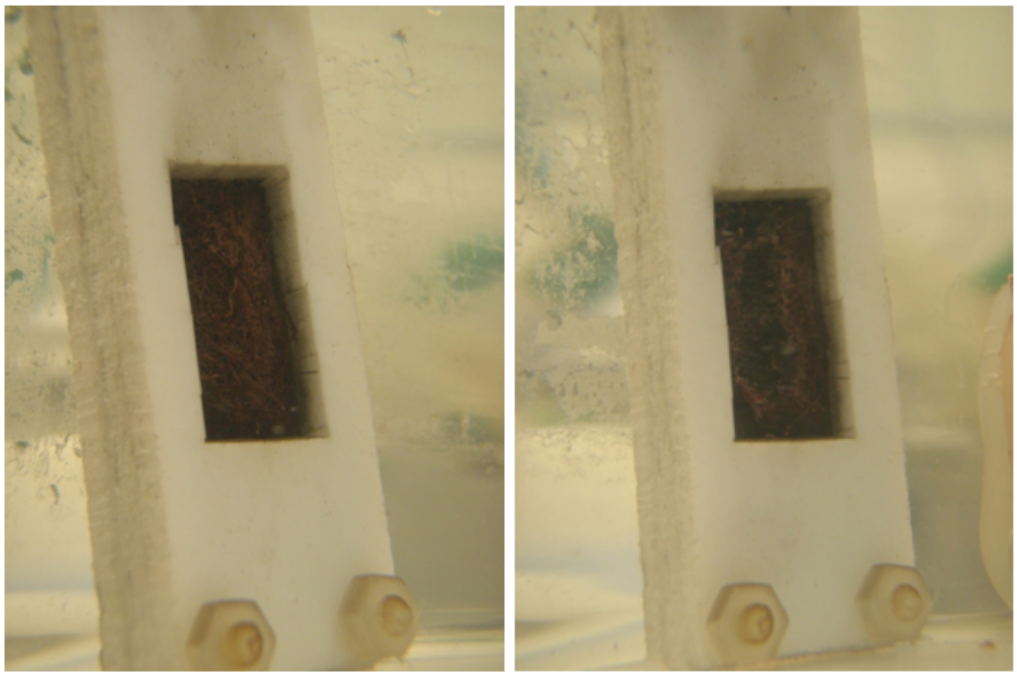

(A) (B)

Figure 5.21: Macroscopic appearance of old bioanode (>60 days) before (A) and after removal of biomass with tweezers (B). Picture taken with underwater camera submerged in the anodic chamber.

5.4 Conclusions

From a practical perspective, results presented here are important for the use of the half cell as a microbiology tool and as MESs with industrial applications. This offers important insight into how the anode potential may trigger different electron transfer mechanisms and how it impacts on current output, CE, energy gain, biomass abundance and distribution on bioanodes. The effects of anode potential on bioanodes depends on substrate type. These effects are enumerated below:

- Current was smallest at -400 mV and highest at -200 mV experiencing a small decrease at 0 mV. Coulombic efficiency follows a similar trend. Both coulombic efficiency and COD removal rate are higher for acetate half-cells.
- Cell abundance increased with anode potential on acetate bioanodes and decreases with anode potential on bioanodes grown on complex substrate.
- Regarding the bacterial community its abundance is mainly determined by anode potential

while its species composition depends on substrate type. Biodiversity is higher on bioanodes grown in complex medium.

- Cyclic voltammetry led to the identification of a peak involved in the electron transfer positioned at -0.2 V vs Ag/AgCl. Peak height is linear with the square root of scan rate for acetate bioanodes and with scan rate for complex substrate bioanodes. Peak height decreases with poised anode potential suggesting an adaptation of bacteria to lower anode potential.

- Biomass grows at the surface of bioanodes and decreases with depth. Electrigenic activity showed a similar profile. Biomass density on bioanodes increases with anode potential.

Bacteria grown at lower anode potentials exhibit strategies that allow them to increase their current production. What these strategies entail remains unclear but it is proposed here that bacteria can produce more cytochromes when limited by anode potential. This hypothesis is in agreement with observing the biggest peak heights on the bioanodes grown at the lowest anode potential. Bioanodes grown at 0 mV were able to produce higher cell abundance at lower currents compared to bioanodes grown at -200 mV. This can be explained by bacteria being able to harness more energy with increasing anode potential. One way they can achieve this is by extending the electron transport chain. The biggest changes occurred when the anode poised potential was changed from -400 mV to -200 mV. This suggests that an extension of the electron transport chain has occurred somewhere between these 2 anode potentials. This hypothesis can be verified in the future by focusing the investigation between these 2 anode potentials.

Biomass growth was limited mainly to the surface of bioanodes due to mass transfer limitations. Electrigenic activity follows the same trend. These observations imply that material costs can be lowered by using thinner anodes. They also suggest bacteria are limited by mass transfer deeper in the bioanode. The increase in current after biomass removal from the surface of bioanodes suggests that as biofilm grow in thickness they become self-limiting for current production. It also suggests that although biomass is associated with higher currents it is not desirable to aim for high biomass densities on bioanodes. Instead, for the purpose of increasing MES efficiency, a mechanism for periodic removal of excess biomass should ideally be devised and implemented.

Chapter 6. Effect of anode-to-cathode ratio on anodic community, performance and biofilm distribution

This chapter reports on how the anode to cathode surface area ratio (A/C) affects power and shapes the anodic community. In chemical fuel cells the engineer has control over catalyst loading on electrodes. This is not the case for the bioanode of an MFC. It is expected that density and abundance of electrigens are determined, among other factors by A/C ratio. The hypothesis is that increasing A/C ratio does not result in proportional increase in current because as the anode area is increased, current is limited by cathode. This means that anode area becomes in excess which results in decreasing density of both bacterial cells and power. Most studies are based on observations in acetate anolyte. To establish if the conclusions can be extrapolated to wastewater the present study also investigated the effect of A/C in complex substrate (OECD) anolyte which simulates the chemical composition of wastewater.

The overall aim was to confirm if there is a relation between power density and A/C in both acetate and complex substrate anolytes and to provide an explanation of the observed trend based on microbiological and electrochemical phenomena. The objectives are listed below:

- establish if the bacterial community composition is affected by the A/C ratio
- investigate how abundance of electrigens varies with A/C ratio
- assess how performance varies with A/C ratio in both types of substrate
- assess how biomass distribution is affected by A/C ratio

6.1 Introduction

It was previously shown that current output in MESs does not grow proportionally to anode size and that power density decreases with anode surface area [202, 209, 267]. Both current density and power density are frequently reported as quality parameters. While the effects of membrane and external load have been thoroughly investigated, the A/C ratio has been considered less frequently. However MES designs described in the literature vary greatly in terms of electrode types and sizes.

Results from different designs cannot be used to explain the relation between power density and electrode sizes. This is especially problematic because reporting a value for power density cannot be used to extrapolate performance with scale-up. For example, when A/C ratio is increased by maintaining one of the electrode surface area constant, current levels off due to cathode limitations [181]. In one particular study aimed at producing macroporous anodes, although current density decreased with anode area, the biggest current density was used for comparing material performance with other studies [202]. This approach can lead to incorrect conclusions regarding comparison of materials because reported current densities can be increased by using smaller anodes.

Investigating on A/C ratio could help in developing a theory used for predicting bacterial performance based on reactor design and for choosing the optimum A/C ratio based on application. Understanding the effect of A/C ratio may help with comparing different designs by replacing power density with other parameters as criteria for comparing performance. One such parameter could be activity per electrigenic cell. Optimising the A/C ratio for a given cathode type and constant external resistance is also important for controlling the sensing range of BOD sensors [210]. Other benefits could be on reducing material costs for building MESs by identifying the optimum A/C ratio. When the cathode is limiting, increasing anode surface is not expected to result in a proportional increase in current. Therefore, excess material used for the anode increases production cost of MES.

Anodic biofilms are composed of a mixture of electrigens and non-electrigens. Interactions between both types of bacteria are important for understanding the ecology of anodic biofilms but are currently poorly understood. For example competition for anode surface between electrigens and non-electrigens was already mentioned as a possibility [12]. So far, no study has addressed fully this prospect. Varying the A/C ratio could provide for an important angle for the study of interactions between electrigens and non-electrigens and especially their competition for anode area.

6.2 Experimental design

For this study, a total number of 23 SCMFCs were used which are summarised in table 6.1. They are separated in 2 sets according to the objectives they correspond to. Set A covers objectives 1 and 2 and its purpose was to collect community composition, cell abundance and current output data. Set B covers objectives 2 and 4 and focuses on correlating polarisation curves and biomass distribution to A/C. SCMFCs included in set B replicate the A/C ratios used in set A with the exception that the number of OECD cells in set B was reduced to 3 due to practical limitations. For each set half of the reactors were fed on acetate and the other half were fed on OECD anolyte.

A/C ratios used for acetate SCMFCs were: 1:24, 1:12, 1:6, 1:3, 1:1 and 8:1. For OECD SCMFCs the following ratios were used: 1:24, 1:6, 1:3, 2:3, 1:1, 2:1, 4:1 and 8:1. Ratios do not overlap entirely for both substrate types because it was expected that anode will become limiting at higher A/C ratios when run on OECD anolyte as compared to acetate. Ratios were obtained by combining anodes and cathode of certain surface areas. For anodes these are: 0.5, 1, 2, 4, and 8 cm^2. Cathodes were built of the following surface areas: 1, 2, 4, 8 and 12 cm^2.

For both substrate types the A/C ratios were selected to create a region of constant cathode area (12 cm^2) with varying anode area and a region of constant anode area (8 cm^2) with varying cathode area. By taking substrate type into account, all 23 SCMFCs can be separated in 4 categories. These will be referred to as AcCC (acetate substrate and constant cathode area), AcCA (acetate substrate and constant anode area), CSCC (complex substrate and constant cathode area) and CSCA (complex substrate and constant anode area).

All SCMFCs were run in batch mode for 4 cycles with temperature controlled at 27°C. OECD cells were pre-fed on acetate during the first cycle and switched to OECD anolyte starting with the second cycle. Anolyte samples were collected at the end of each cycle to measure COD used for calculating CE. The external load was 500 Ω. Anode potentials and cell voltage were monitored using a multi-channel data-logger. At the end of the run, bioanodes from set A were collected, homogenised in 2 ml tubes and stored at -20°C. Downstream analysis included community analysis and cell counting. For the SCMFCs in set B a 5^{th} cycle was started and run for 2 days after which polarisation curves were acquired by changing the external resistance and allowing each time a stabilisation period of 20 minutes. Biomass distribution was visualised only on acetate bioanodes from set B. For this purpose, bioanodes were stained with SYBR-Green dye and then imaged in UV light. OECD bioanodes from set B were homogenised and were subjected to community analysis.

Table 6.1: Summary of SCMFCs used for studying the effect of A/C ratio. The naming of reactors is composed of 3 parts: the first designates substrate (Ac for acetate and CS for complex substrate), the middle part shows the ratio and the last part is a upper case letter indicating the part of study to which the reactor belongs. For example, the name Ac1to24A indicates that this SCMFC was run on acetate at an A/C ratio of 1:24 and belongs to set A. The last 5 columns tabulates analyses with a check-mark symbol if performed and with an X sign if not.

Set of reactor	**Reactor name**	**Substrate**	**A/C ratio**	**Anode area (cm^2)**	**Cathode area (cm^2)**	**CA**	**Cell Counts**	**Biomass Imaging**	**Polarisation curves**	**Commmunity Analysis**
A	Ac1to24A	Acetate	1:24	0.5	12	✓	✓	X	X	✓
	Ac1to12A	Acetate	1:12	1	12	✓	✓	X	X	✓
	Ac1to6A	Acetate	1:6	2	12	✓	✓	X	X	✓
	Ac1to3A	Acetate	1:3	4	12	✓	✓	X	X	✓
	Ac1to1A	Acetate	1:1	8	8	✓	✓	X	X	✓
	Ac8to1A	Acetate	8:1	8	1	✓	✓	X	X	✓
	CS1to24A	OECD	1:24	0.5	12	✓	✓	X	X	✓
	CS1to6A	OECD	1:6	2	12	✓	✓	X	X	✓
	CS1to3A	OECD	1:3	4	12	✓	✓	X	X	✓
	CS2to3A	OECD	2:3	8	12	✓	✓	X	X	✓
	CS1to1A	OECD	1:1	8	8	✓	✓	X	X	✓
	CS2to1A	OECD	2:1	8	4	✓	✓	X	X	✓
	CS4to1A	OECD	4:1	8	2	✓	✓	X	X	✓
	CS8to1A	OECD	8:1	8	1	✓	✓	X	X	✓
B	Ac1to24B	Acetate	1:24	0.5	12	✓	X	✓	✓	X
	Ac1to12B	Acetate	1:12	1	12	✓	X	✓	✓	X
	Ac1to6B	Acetate	1:6	2	12	✓	X	✓	✓	X
	Ac1to3B	Acetate	1:3	4	12	✓	X	✓	✓	X
	Ac1to1B	Acetate	1:1	8	8	✓	X	✓	✓	X
	Ac8to1B	Acetate	8:1	8	1	✓	X	✓	✓	X
	CS1to3B	OECD	1:3	4	12	✓	X	X	✓	✓
	CS2to1B	OECD	2:1	8	4	✓	X	X	✓	✓
	CS4to1B	OECD	4:1	8	2	✓	X	X	✓	✓

6.3 Results and discussion

6.3.1 Effect of A/C ratio on cell voltage, anode potential and current output

Cell voltages and corresponding anode potentials are shown for acetate cells and OECD cells in the appendix in figures 9.4 and 9.5 respectively. OECD cells were fed an acetate for the fist cycle. After that, they were run on OECD anolyte for all subsequent cycles. The purpose of pre-feeding is to ensure growth of electrigenic biofilms. It was not possible to obtain bioanodes directly on OECD medium. In acetate anolyte electrigens have immediate access to substrate and are able to grow. Conversely, in OECD, electrigens are deprived of substrate from the beginning. Fermenting bacteria have the ability to break down organic polymers present in the anolyte but at the beginning of the first cycle they are low in abundance. Inoculum older than 6 days was unusable proving that electrigenic bacteria cannot survive periods of inactivity for that amount of time. Consequently, by the time the fermenters grow in abundance the electrigens will have died. This explains why bioanodes cannot be obtained directly in OECD medium.

The chronopotentiometry (CP) profiles for acetate include 4 cycles. During the first cycle, cell voltages are the lowest suggesting that biofilms are still growing during this time and will reach maturity with the second cycle. This is not observed for OECD cells because biofilm growth has occurred during pre-feeding. The average cycle length for acetate cells was 13.52 ± 1.86 days and for OECD cells was 8.75 ± 2.56 days. The difference in cycle length is attributed to substrate. In OECD medium, the COD content is lower compared to acetate and additionally the activity of non-electrigens causes a decrease in substrate concentration. Equally plausible is the accumulation of end-products from fermentation which can inhibit bacterial metabolism. On the other hand, acetate is not fermentable, therefore the electrigens are not competing for substrate explaining the longer cycle length in acetate cells. Cycle length does not vary with A/C ratio.

Both GDE and the membrane that formed the MEA were proven to be permeable to oxygen by monitoring DO in a reactor previously sparged with nitrogen and sealed. The increase in DO inside the reactor is shown in figure 9.6 in the appendix. Consequently cycle length is also limited by oxygen permeation through the membrane-electrode assemble (MEA). COD content in the anolyte is consumed heterotrophically continuously at a small but constant rate.

Cell voltages were converted to electrical current values using Ohms's law. The average current per cycle in the stable region (higher than 90% of maximum current) was extracted for all cells and plotted in figure 6.1. Currents in the first cycle for acetate cells and in the pre-feeding cycle for OECD cells were excluded because biofilms were still growing in this phase. Currents are bigger on acetate cells by roughly 2 times compared to OECD cells.

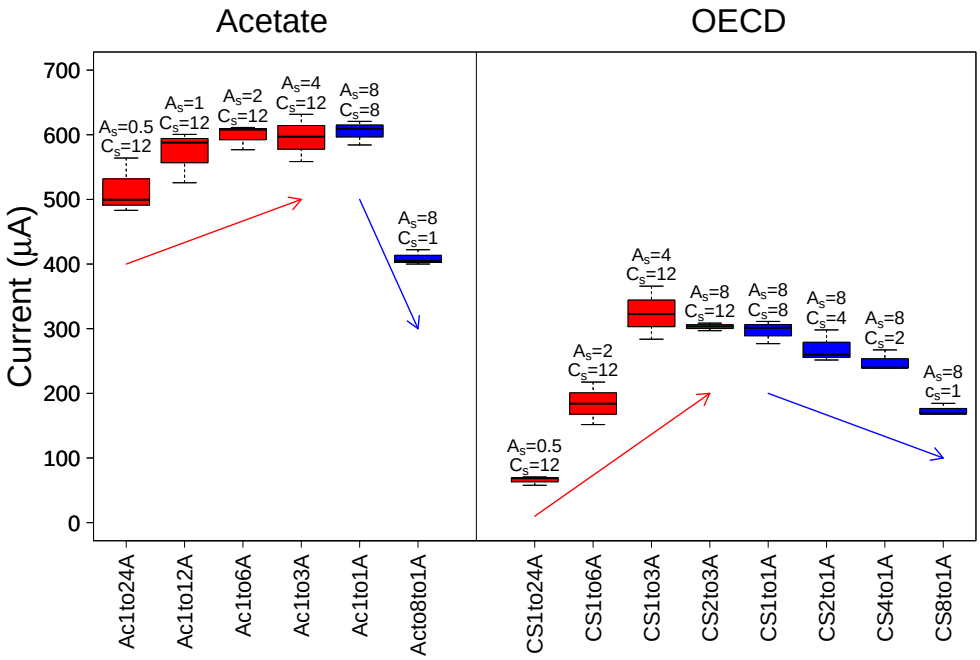

Figure 6.1: Average current output during mid-cycles stable regions. Surface areas of anodes (A_s) and cathodes (C_s) are indicated in cm^2 for each MFC. Each boxplot includes 3 values (one per cycle). The vertical line separates acetate-fed MFCs at left from OECD anolyte-fed MFCs at right. Within each substrate group, boxplots are arranged from left to right in increasing order of A/C. Red color indicates SCMFCs with constant cathode area and variable anode area. Blue color indicates SCMFCs with constant anode area and variable cathode area. A/C anode to cathode surface area ratio; A_s anode surface area; C_s cathode surface area;

The currents corresponding to AcCC and CSCC groups are shown in red in figure 6.1. For both substrate types, current increases with anode area when the cathode area is held constant at 12 cm^2 as shown by the blue arrows in figure 6.1. This increase in current shows a plateauing trend for both substrate types but is steeper for the OECD cells. This suggests cathode limitation in acetate medium at lower A/C ratios. In OECD cells, it is the anode which is the limiting electrode. This is also supported by the higher anode potentials displayed by CSCC cells.

In the case of AcCC cells, the increase in current is not proportional to anode area. In the CSCC group current increases fast with anode area until an A/C ratio of 1:3. Above this ratio current has not increased further suggesting cathode becomes limiting. In OECD medium, the anode was the limiting electrode up to a ratio of 1:3 where the anode area is 4 cm^2. Increasing the anode area further does not bring any increase in current. When the cathode is held constant at 12 cm^2 the anode becomes limiting at a lower A/C ratio in acetate cells. This is because currents are higher when acetate is the electron donor.

By dividing current to anode surface area anodic current densities are obtained. These are plotted in figure 6.2. Current density decreases continuously with increasing A/C ratio for both substrate types. Anode material is in excess in acetate cells at ratios above 1:6 and in OECD cells above 1:3.

For both types of substrate beyond the above mentioned ratios current does not increase any longer while current density decreases fast.

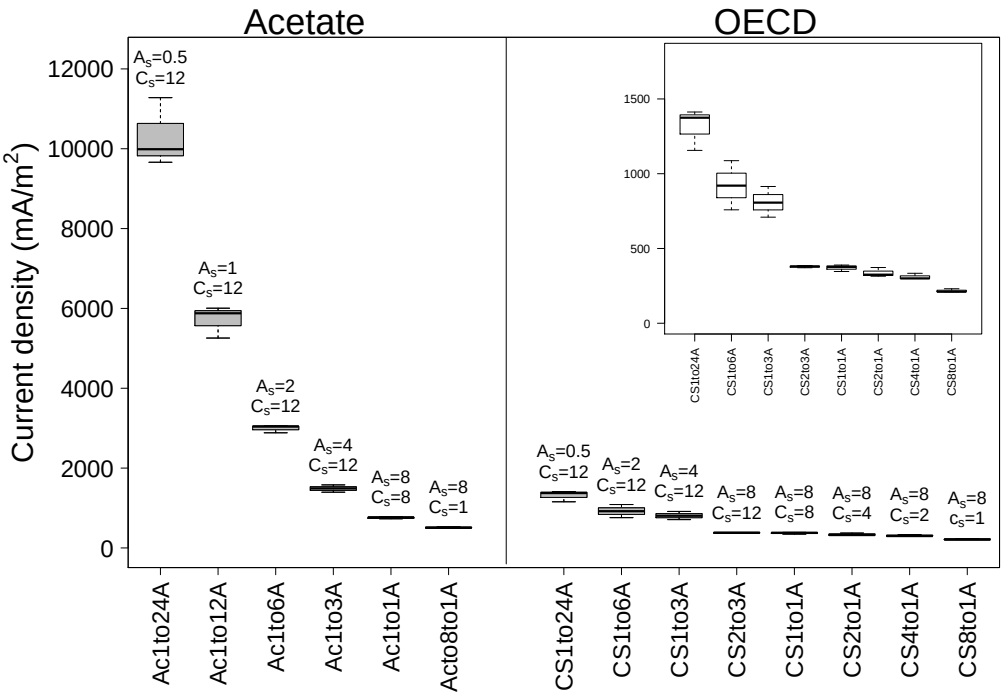

Figure 6.2: Comparison of current densities based on A/C ratio and substrate type. (A_s) and cathodes (C_s) are indicated in cm^2 for each MFC. The vertical line separates acetate-fed MFCs at left from OECD anolyte-fed MFCs at right. Within each substrate group, boxplots are arranged from left to right in increasing order of A/C. Inset figure shows current densities of only OECD cells.

CEs are shown in figure 6.3. Acetate cells have low CE in the first cycle when the biofilms were still growing. Acetate cells are characterised by higher CEs compared to OECD cells. Because acetate is readily available to electrigens, higher currents were possible when using this substrate.

In OECD medium, due to the complexity of the substrate, fermentation takes place producing organic chemicals that take longer to be metabolised or they cannot be used by bacteria at all. Cycle length may also influence COD removal rates due to oxygen permeation through the MEA. The longer the cycle the more oxygen can get through the MEA which is used by bacteria to lower the COD content. COD removal rates and CE values are show in table 9.6 in the appendix. COD removal rate does not show any dependence on A/C ratio. Instead COD removal is higher in acetate cells (90.32 $\pm$ 6.04 %) compared to OECD cells (84.73 $\pm$ 7.54 %).

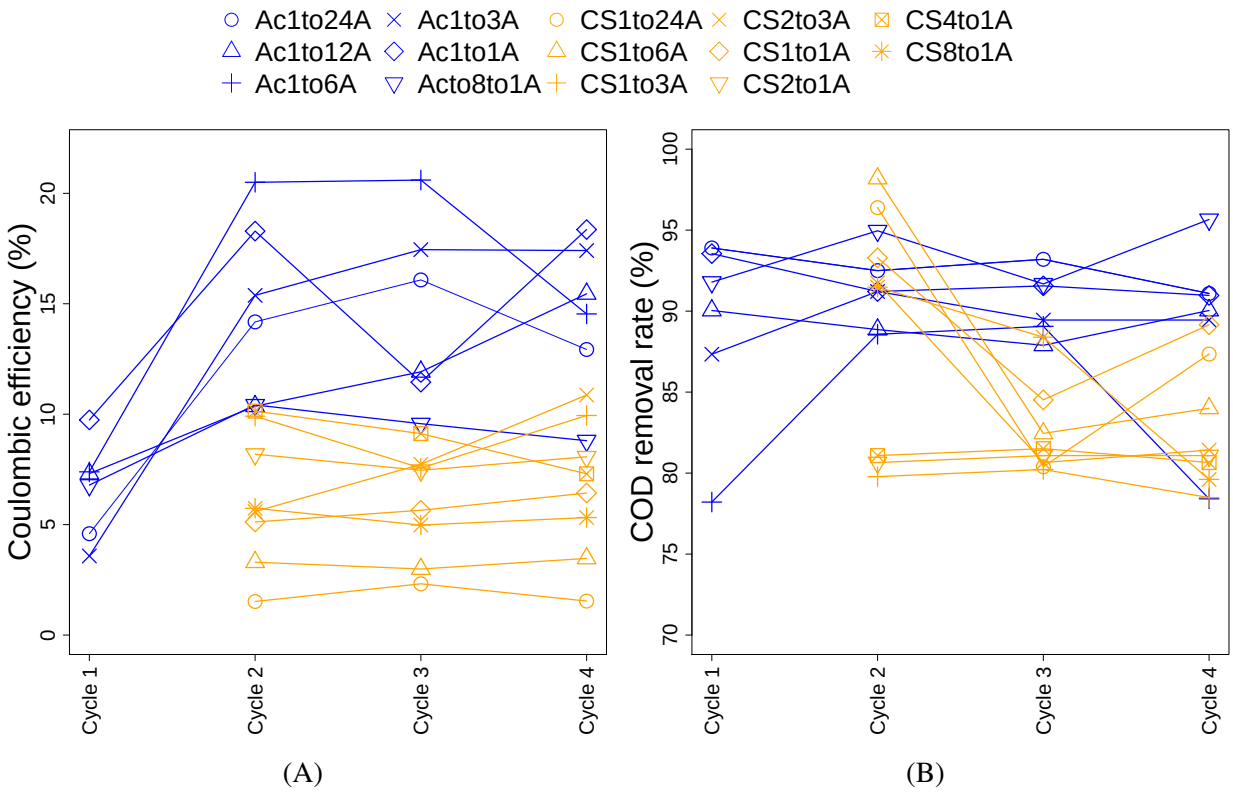

Figure 6.3: Coulombic efficiencies (A) and COD removal rates (B) per cycle. Acetate cells are shown in blue and OECD cells are shown in orange.

6.3.2 The effect of A/C ratio on community composition

Community percentage composition is shown in figure 6.4. For a better visualisation of the main differences regarding taxa composition between the 2 substrate types the first 20 most abundant genera are plotted in figure 9.7 in the appendix. Communities grown in acetate cells are characterised by higher percentages of *Porphyromonadaceae* (family), *Comamonas* (genus), *Rhizobiaceae* (family), *Bacteroidetes* (phylum) and *Sedimentibacter* (genus). Communities grown in OECD medium show higher percentages of *Bacteroidales* (order), *Dysgonomonas* (genus), *Azospirillum* (genus), *Sphaerochaeta* (genus), the uncultured bacterium *Blvii28* and *Magnetospirillum* (genus). Not all of the above mentioned taxons were identified down to genus level. The lowest taxon level of identification is written in brackets after each taxon. The uncultured *Blvii28* was found to belong to the family *Rikenellaceae* from the *Bacteroidetes* phylum [268]. This is a hydrogen producing bacterium previously isolated from wastewater and sludge. *Magnetospirillum* has been previously isolated from other MESs [269] and has been described as being able to survive in low-oxygen environment. *Sedimentibacter* is commonly identified in bioanodes started from wastewater inoculum [270].

In acetate substrate the A/C ratio has a clear impact on the percentage of taxons. At class level

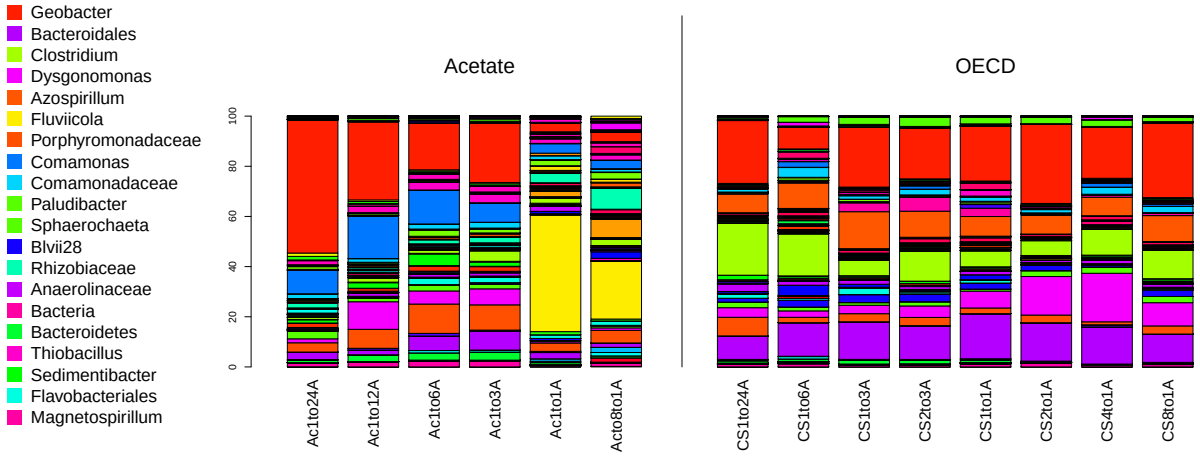

Figure 6.4: Percentage community composition. Vertical line separates acetate bioanodes at left from OECD bioanodes at right. Legends include first 20 most abundant genera. Taxons are identified to genus level. Where this was not possible the next classification level is shown (family, order or class).

acetate cells show a clear trend of decreasing *Deltaproteobacteria* with A/C ratio. *Deltaproteobacteria* are almost exclusively represented by *Geobacter*. Within the AcCC group *Geobacter* percentage decreases with anode area. Non-electrigens may not be important for electricity production. Instead they might have been carried over from inoculum and can grow feeding on biomass produced by *Geobacter*. The AcCA group exhibit very low *Geobacter* and a high percentage of *Fluviicola*. It is not clear what role the latter plays or if its high percentage is an effect of the A/C ratio. Its presence in other acetate bioanodes is very low although all were started from the same inoculum. Communities grown on OECD medium have a more uniform distribution of class-level taxons and their percentage shows no clear dependence on A/C ratio down to genus level.

Shannon and Simpson biodiversity indices were calculated and are plotted in figure 6.5A and 6.5B respectively. Their values are shown in the appendix in table 9.4. Shannon index measures species richness and Simpson index measures species evenness [265]. OECD cells show higher diversity of bacteria compared to acetate cells. This is due to the substrate complexity within OECD anolyte which promotes many types of metabolism and therefore a wider range of bacteria species identified in the corresponding cells.

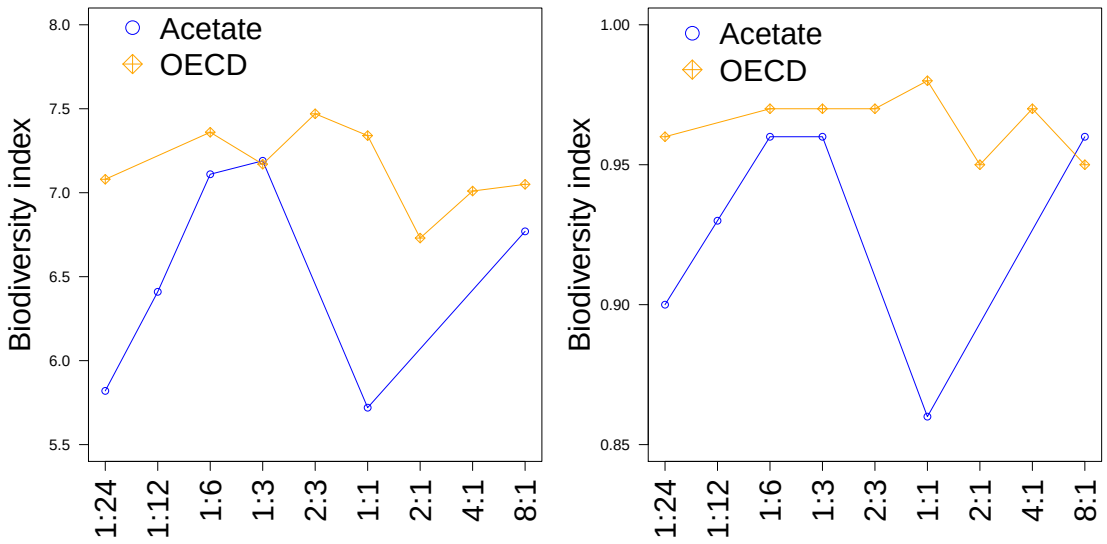

Figure 6.5: Biodiversity of bioanode communities. A: Shannon index; B: Simpson index; Acetate bioanodes are shown in blue, and OECD bioanodes are shown in orange

6.3.3 Grouping of communities using ordination plots

Bioanode communities are grouped based on Bray-Curtis distances in figure 6.6A. This ordination of communities shows two gradients for each substrate type. The samples in acetate group are arranged in the direction of increasing A/C ratio. The acetate reactors with the smallest A/C ratios are placed at one end of the gradient closer to each other than to the rest of the bioanodes. At the opposite end of the gradient, the 2 bioanodes with the highest A/C ratio are placed and the distances between them is smaller compared with the rest of the bioanodes. This arrangement suggests that communities grown on acetate converge in both directions of varying the A/C ratio. This means that community is not influenced by A/C at extreme values. The OECD cells are also arranged in a gradient.

Ordination of bioanode communities based on Jaccard distance is shown in figure 6.6B. This distance considers only presence-absence data while ignoring cell abundance. Bioanodes cluster by substrate type. The arrangement of samples within each substrate type shows collinearity but the resulting gradients are not explained by A/C ratio. The order of samples in each group is poorly correlated with the A/C ratio. Within the acetate group 2 subclusters can be observed which correspond to the AcCC and AcCA groups. The sub clustering might be an artifact caused by the high percentage of *Fluviicola* in the AcCA group. This in turn decreases the abundance of other taxons below detection limit. The Jaccard distance-based ordination of bioanodes shows that substrate is the main factor that shapes the community. The direction of both gradients is parallel with the Y-axis in figure 6.6B which explains only 13.33% variation across the communities. Therefore it

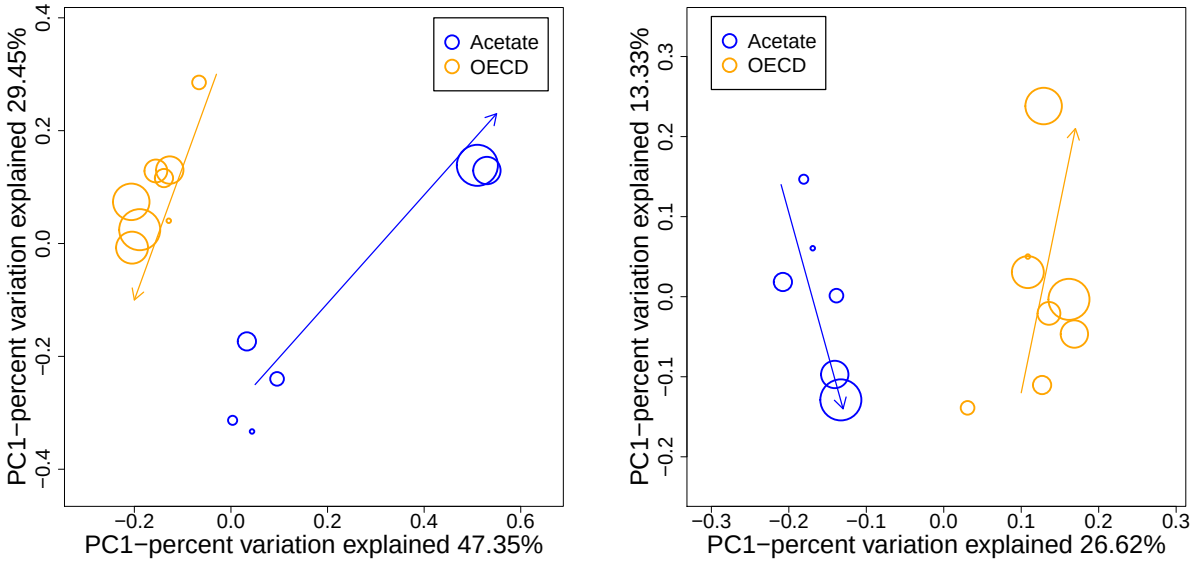

(A) (B)

Figure 6.6: Ordination of communities using Principal Coordinate Analysis (PCoA). A: PCoA based on Bray-Curtis distance; B: PCoA based on Jaccard distance. Each community is represented by an empty circle. Circle size increases with A/C ratio. Acetate bioanodes are shown in blue and OECD bioanodes are shown in orange. Blue arrows show gradients of acetate bioanode communities and orange arrows show gradients of OECD bioanode communities.

can be stated that A/C ratio does not impact on the presence-absence of taxons.

6.3.4 Electrigens activity and their abundance correlation to mean current and energy gain

For the AcCC group with each doubling of the anode area there is only a slight increase in current and for the CSCC current increase is less than proportional. Because of this it follows that the amount of energy harnessed by bacteria increases marginally with each doubling of anode area. Consequently it is expected that the density of bacteria cells decreases with A/C ratio. This trend is clearly visible for the constant cathode area groups as shown in figure 6.7 by the blue arrows.

Not all bacteria present on bioanodes are expected to be influenced by how much energy was gained from producing current. It is the number of electrigens that is expected to be better correlated to mean current. *Geobacter* is considered the only electrigen identified in the bacterial community. Its density was obtained by multiplying bacterial cell density presented in figure 6.7 with *Geobacter* percentage extracted from community analysis data. *Geobacter* density values for each bioanode are shown in figure 6.8.

For both types of substrate electrigen density decreases with increasing A/C ratio and does not reach a maximum limited by the available surface area provided by carbon felt. As the anode

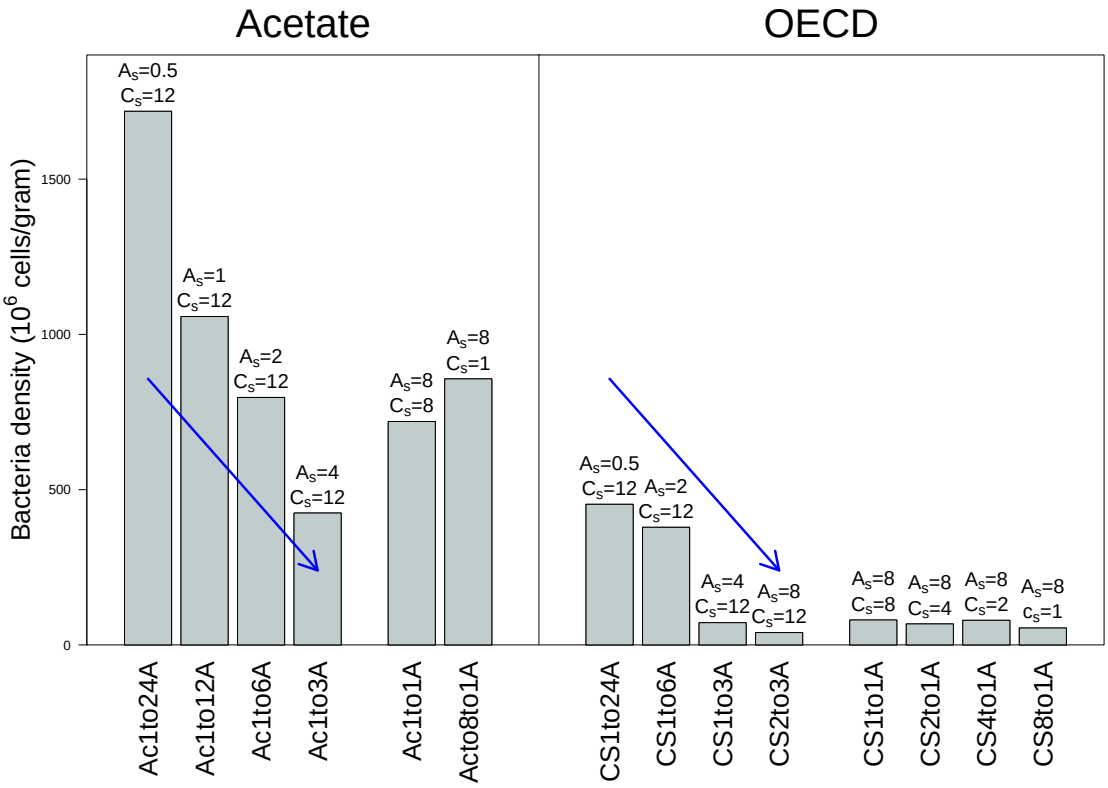

Figure 6.7: Bacterial cell density on bioanodes expressed as millions of cells per gram of wet electrode. Surface areas of anodes (A_s) and cathodes (C_s) are indicated in cm^2 above the corresponding bioanodes. The vertical line separates acetate-fed MFCs at left from OECD anolyte-fed MFCs at right. Within each substrate group, bars are arranged from left to right in increasing order of A/C. Vertical line separates acetate bioanodes at left and OECD bioanodes at right. Blue arrows show a decrease in bacterial densities within the constant cathode area groups.

becomes limiting its surface area is in excess of how many electrigens it can host. Consequently, a decrease in electrigens density with increasing A/C ratio is expected. This was confirmed for both acetate and OECD substrates as shown in figure 6.8. Excess anode area is not proportionally colonised with electrigens and instead it provides for more area for the growth of non-electrigens. It is possible that with increasing anode area and decreasing cathode area electrigens grow more dispersed across the anode and there is more available area for non-electrigens.

Current density was compared to both total cell density and electrigen density. Figure 6.9A shows current density plotted against bacterial cell density. This shows good correlation between the 2 factors. The points corresponding to reactors Ac1to1A and Ac8to1A are further from the fitted line than the rest of the points. Current density is better correlated to electrigen density as shown in figure 6.9B. This suggests that anodic communities include many bacteria that are not influenced by A/C ratio. Furthermore it was noticed that linearity is better within the acetate group ($R^2 = 0.96$) compared to the OECD group ($R^2 = 0.68$).

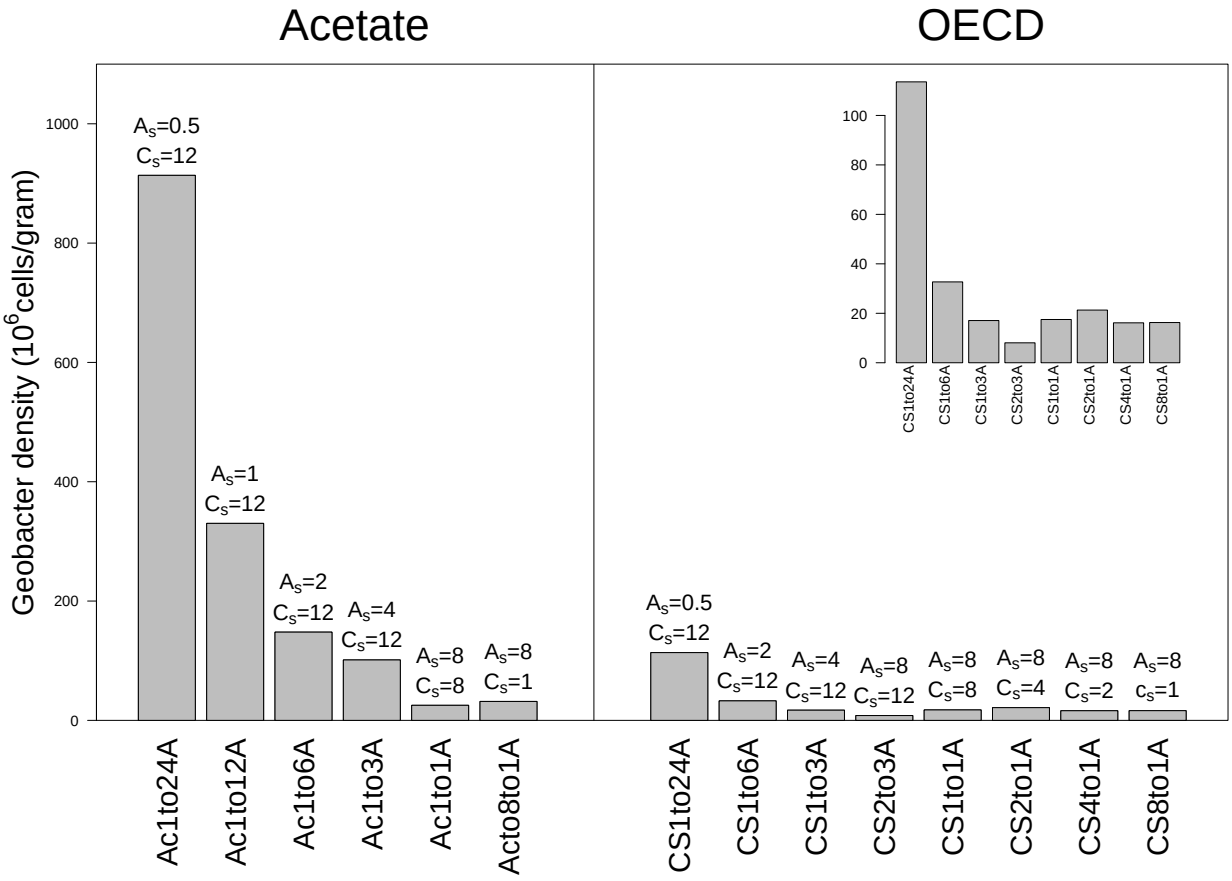

Figure 6.8: Density of *Geobacter* on bioanodes expressed as millions of cells per gram of wet electrode. Surface areas of anodes (A_s) and cathodes (C_s) are indicated in cm^2 above the corresponding bioanodes. Vertical line separates acetate bioanodes at left from OECD bioanodes at right. Within each substrate group, bars are arranged from left to right in increasing order of A/C. Inset figure shows a closer view of *Geobacter* densities on OECD bioanodes.

Total energy gain values were calculated according to equation 3.4 and are shown in table 9.5 in the appendix together with cell counts and maximum current per cycle. Total abundance of *Geobacter* is plotted against total gained energy in figure 6.10.

In the case of OECD cells, calculation of total gained energy includes pre-feeding cycles. For both substrate types total abundance of electrigens have increased with total gained energy. However the slope is smaller for OECD bioanodes suggesting a lower efficiency of growth in OECD medium. This can be explained by higher competition among bacteria in the OECD medium which sustains higher biodiversity. It should be mentioned that for calculating total gained energy for OECD medium it is assumed that electrigens are feeding with acetate resulting from fermentation. However this assumption may not be totaly correct because other low-molecular weight organics result from fermentation with different biological reduction/oxidation potentials. This would result in higher total gained energy for OECD bioanodes lowering further growth efficiency in these bioanodes.

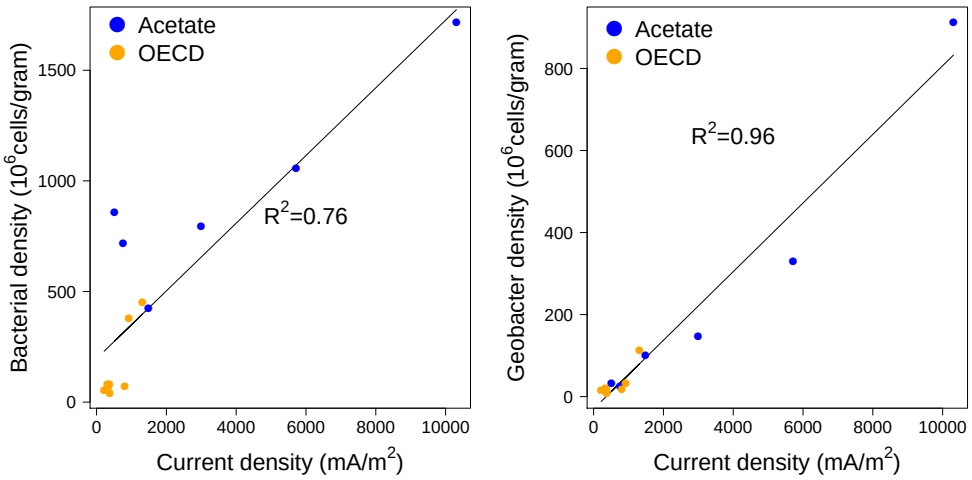

(A) (B)

Figure 6.9: Comparison of total bacterial density and *Geobacter* density to current density. A: scatter plot and linear fit between bacterial density and mean current density; B: scatter plot and linear fit between *Geobacter* density and mean current density; Points from acetate bioanodes are shown in blue and those from OECD bioanodes in orange.

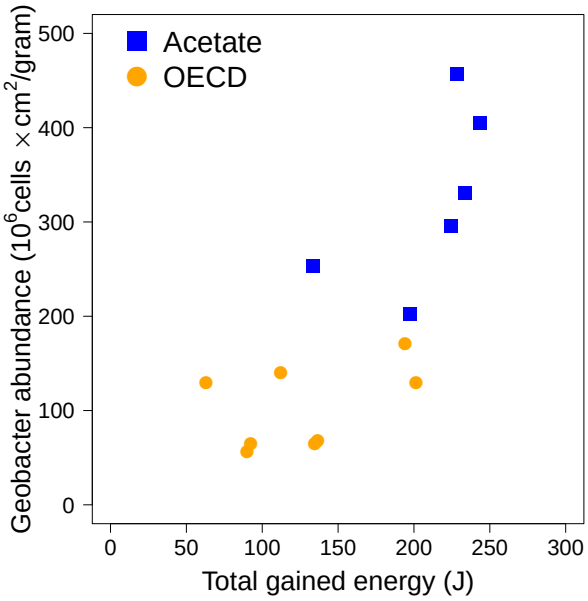

Figure 6.10: *Geobacter* abundance plotted against total gained energy. Acetate bioanodes are shown in blue and OECD bioanodes are shown in orange.

The possibility of using specific activity as a comparison parameter was investigated. Specific activity is defined as the amount of current produced by electrigenic cells. In order to use this parameter for comparing materials the first condition is that it stays constant for any anode to cathode ratio when anode material is the same. It can be calculated by dividing total current produced in a cell by total electrigen abundance. Electrigen density was normalised to anode area and it is plotted against mean current in figure 6.11A. Overall total electrigen abundance increases with mean

current. Yet linearity is poor especially for acetate bioanodes. This lack of linearity already signals that the condition of specific activity being invariable to A/C, is not satisfied. This could be due to accumulation of dead electrigens, a dependence of specific activity on A/C or a combination of both.

Next specific activity was obtained by dividing mean current density to electrigen density normalised to anode surface area, and it is shown in figure 6.11B. For both substrates within the constant cathode groups specific activity increases with anode area. Smaller bioanodes achieve higher current density which translates to higher overvoltage. This means that on bioanodes where electrigens grow in higher densities, their ability to produce current is reduced by higher overvoltage. This might be an explanation for the variation of specific activity with A/C.

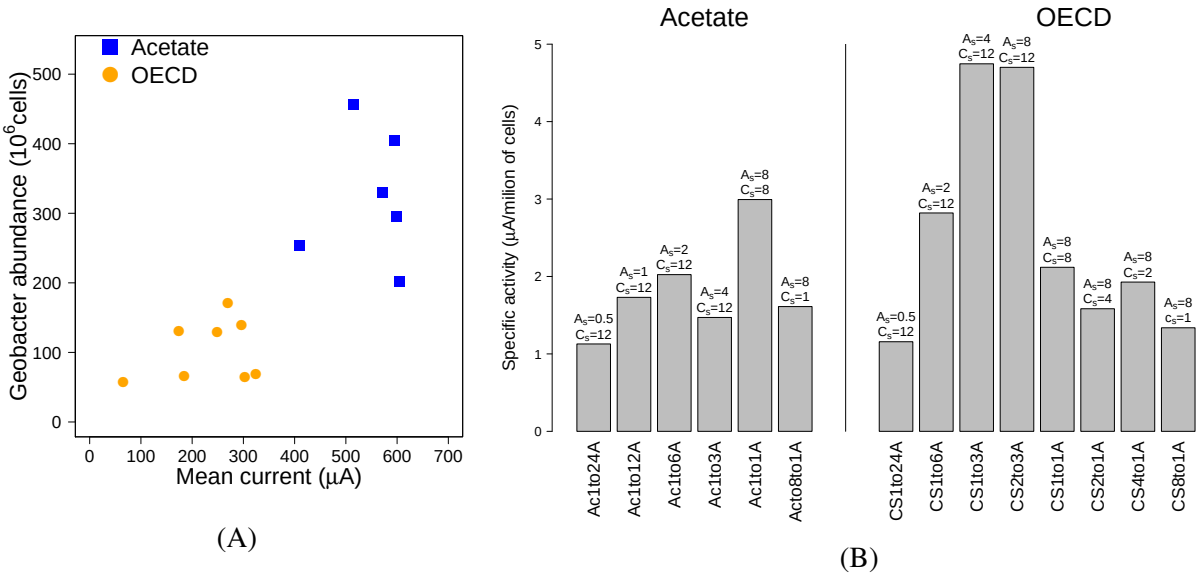

Figure 6.11: Evaluation of specific activity of electrigens on bioanodes. A: *Geobacter* abundance normalised to anode surface area plotted against mean current. Blue shows acetate bioanodes and orange OECD bioanodes. B: Barplot of specific activity obtained by dividing mean current to *Geobacter* normalised abundance. Surface areas of anodes (A_s) and cathodes (C_s) are indicated in cm^2 above the corresponding bioanodes. Vertical line separates acetate bioanodes at left from OECD bioanodes at right.

6.3.5 Interaction between electricity-producing bacteria and non-electrigens

Geobacter was the main known electrigen identified in the community composition of bioanodes. Other genera that may include electrigens were observed, such as *Bacillus*, *Desulfobulbus* and *Desulfovibrio*. However these were at low percentages (< 0.1%) and not present in all bioanode communities. Therefore only *Geobacter* will be included as electrigenic bacteria in all subsequent analysis. Correlation between abundance of electrigens and abundance of non-electrigens was assessed by linear regression. First density of non-electrigens was calculated as the difference

between total and *Geobacter* densities. On acetate bioanodes density of non-electrigens shows no correlation to electrigens density (adjusted R^2 = -0.09693, p-value = 0.4965). This can be visualised in figure 6.12A. However when considering the same relation only within the AcCC group linearity improves (adjusted R^2 = 0.2655, p-value=0.2856). Also density of non-electrigens shows a decreasing trend with anode area within the AcCC group (first 4 points from left in figure 6.13A). This suggests there may be a correlation between electrigens and non-electrigens but the number of acetate reactor is insufficient for concluding this.

Within the OECD bioanodes density of non-electrigens shows better correlation to electrigen density (adjusted R^2 = 0.5125, p-value = 0.02765). Their numbers increase together as shown in figure 6.12B. This means that non-electrigens abundance is lower at higher A/C ratio as confirmed in figure 6.13B. This suggest that in OECD anolyte density of electrigens is positively correlated to density of non-electrigens.

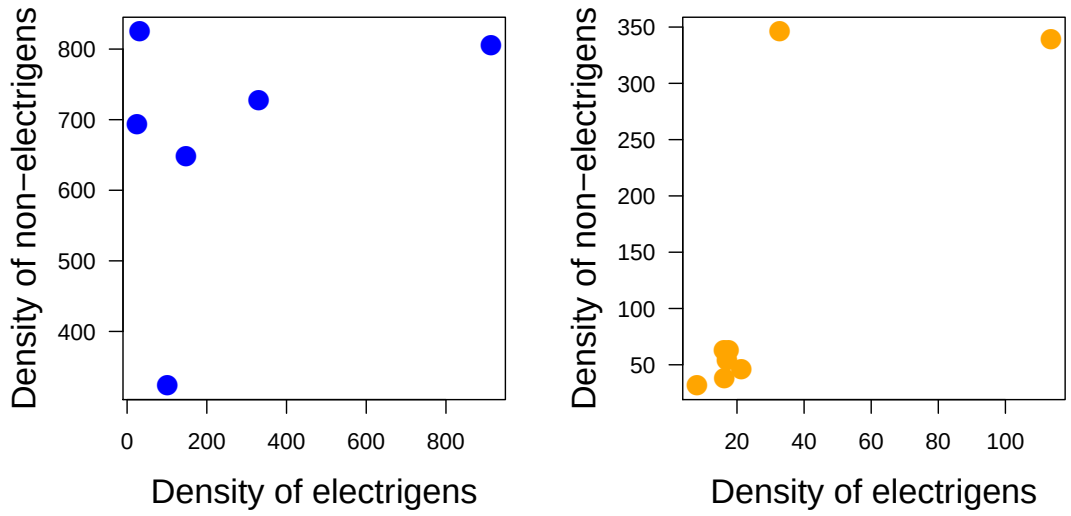

(A) (B)

Figure 6.12: Correlation between density of non-electrigens and density of electrigens ($\times 10^6$cells/gram). Acetate bioanodes are shown in blue (A) and OECD bioanodes are shown in orange (B).

Although the dependence of electrigens on non-electrigens for substrate in complex medium can be assumed, both groups of bacteria may benefit from growing together. In this context, fermenters will benefit the proximity of electrigens because the latter removes resulting fermentation products in the process of electricity generation.

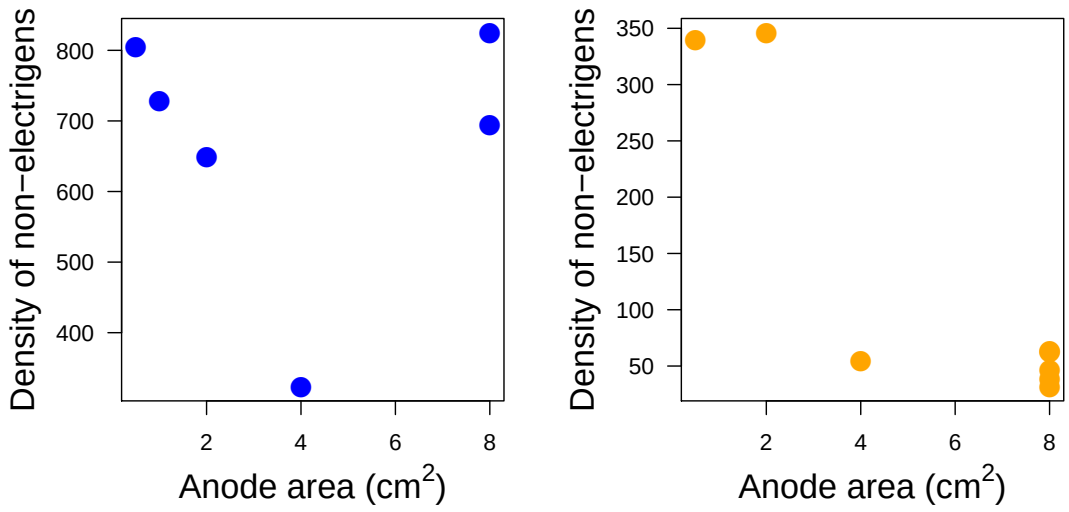

(A) (B)

Figure 6.13: Density of non-electrigens ($\times 10^6$cells/gram) vs anode area. A: Includes all acetate bioanodes shown in blue. Solid line shows fit between all values and dashed line shows fit only for the constant cathode area SCMFCs; B: Includes all OECD bioanodes shown in orange;

6.3.6 The effect of A/C ratio on performance

Polarisation curves were acquired on SCMFCs from set B of reactors. These are shown in figures 6.14 (Ac1to24B, Ac1to12B and Ac1to6B), 6.15 (Ac1to3B, Ac1to1 and Ac8to1B) and 6.16 (OECD1to3B, OECD2to1B and OECD4to1B). Cell voltage at infinite resistance (OCP) is a measure of the driving force of the reaction or the potential difference between the cathodic and anodic reaction [271]. For acetate cells, OCP was 617.5 $\pm$ 13.54 mV, and for OECD 609.6 $\pm$ 87.3 mV. The complexity of the OECD substrate may be responsible for the higher variation in OCP.

For the first highest external loads, cell voltage drops faster than in the middle of the curve. The sudden drop in cell voltage is needed to overcome barriers associated with electron transfer and is called overvoltage. The region is called activation polarization region. Most acetate cells showed an activation region between infinite resistance and 5480 Ω. The potential drop in this region is 94.8 $\pm$ 7.9 mV. For the Ac8to1B cell, the activation region stops at 9860 Ω and the potential drop is 154 mV. This drop is mostly attributed to the cathode high overvoltage associated with its small size. The activation region cannot be identified for the OECD cells. This is because OECD medium allows for lower currents than acetate. Identification of polarisation regions for these cells may require using more higher external loads.

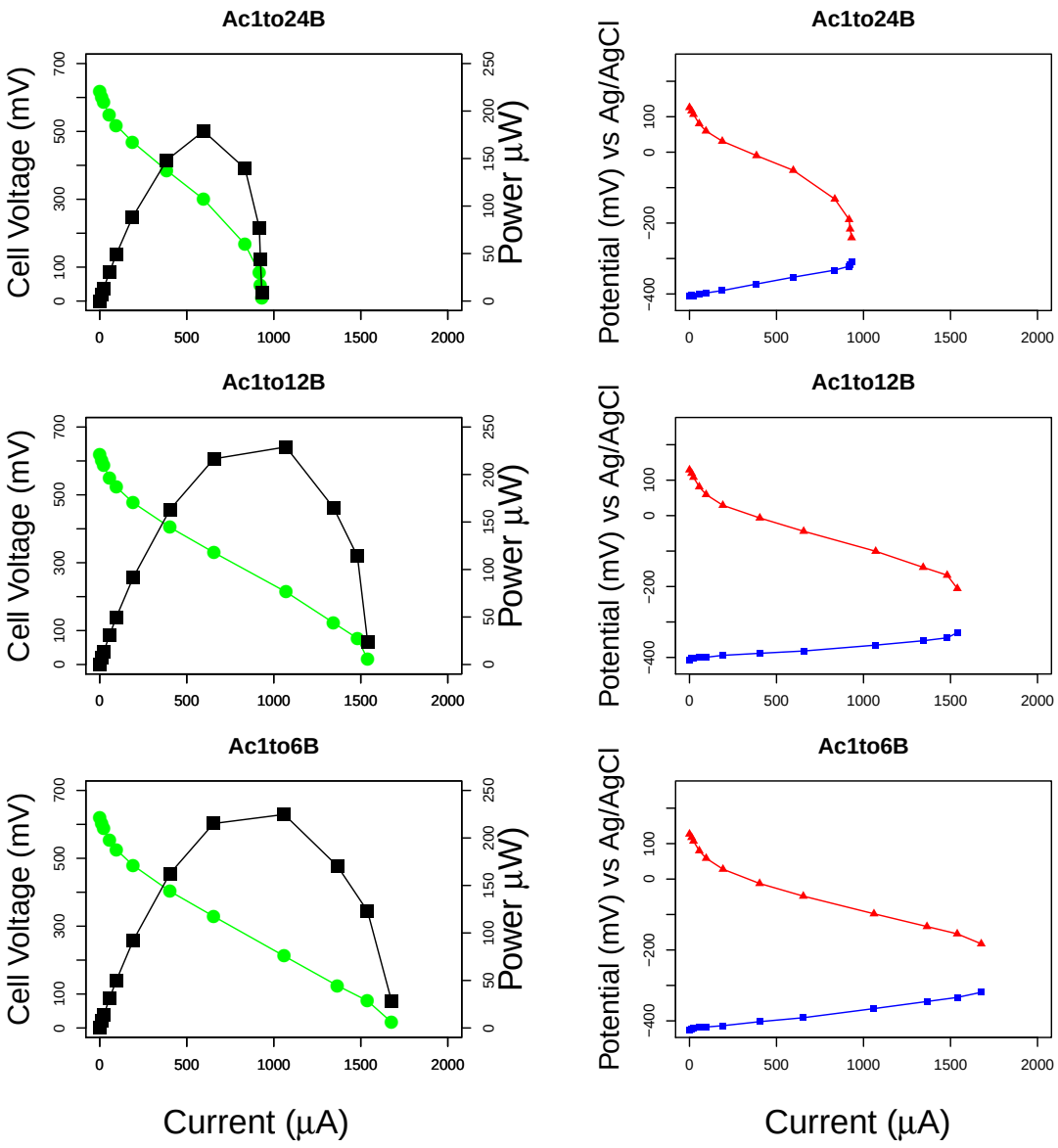

Figure 6.14: Polarisation curves on Ac1to24B, Ac1to12B and Ac1to6B acetate SCMFCs. Graphs in left column show cell voltages and power against current. Graphs in right column show anode and cathode potentials against current. The 2 graphs in each row shows data acquired from the same SCMFC. Cell voltages are shown in green, power in black, anode potentials in blue and cathode potentials in red.

The ohmic region is characterised by a linear relation between cell voltage and current. The slope inside the ohmic region can be used to calculated internal resistance. The range of external loads, calculated internal resistances and external load at peak power are shown in table 6.2. Acetate cells have much lower internal resistances as compared to OECD cells. External load at peak power is always the one closest to the value of internal resistance. The two resistances do not match exactly but that is because the external load was not varied at low enough increment.

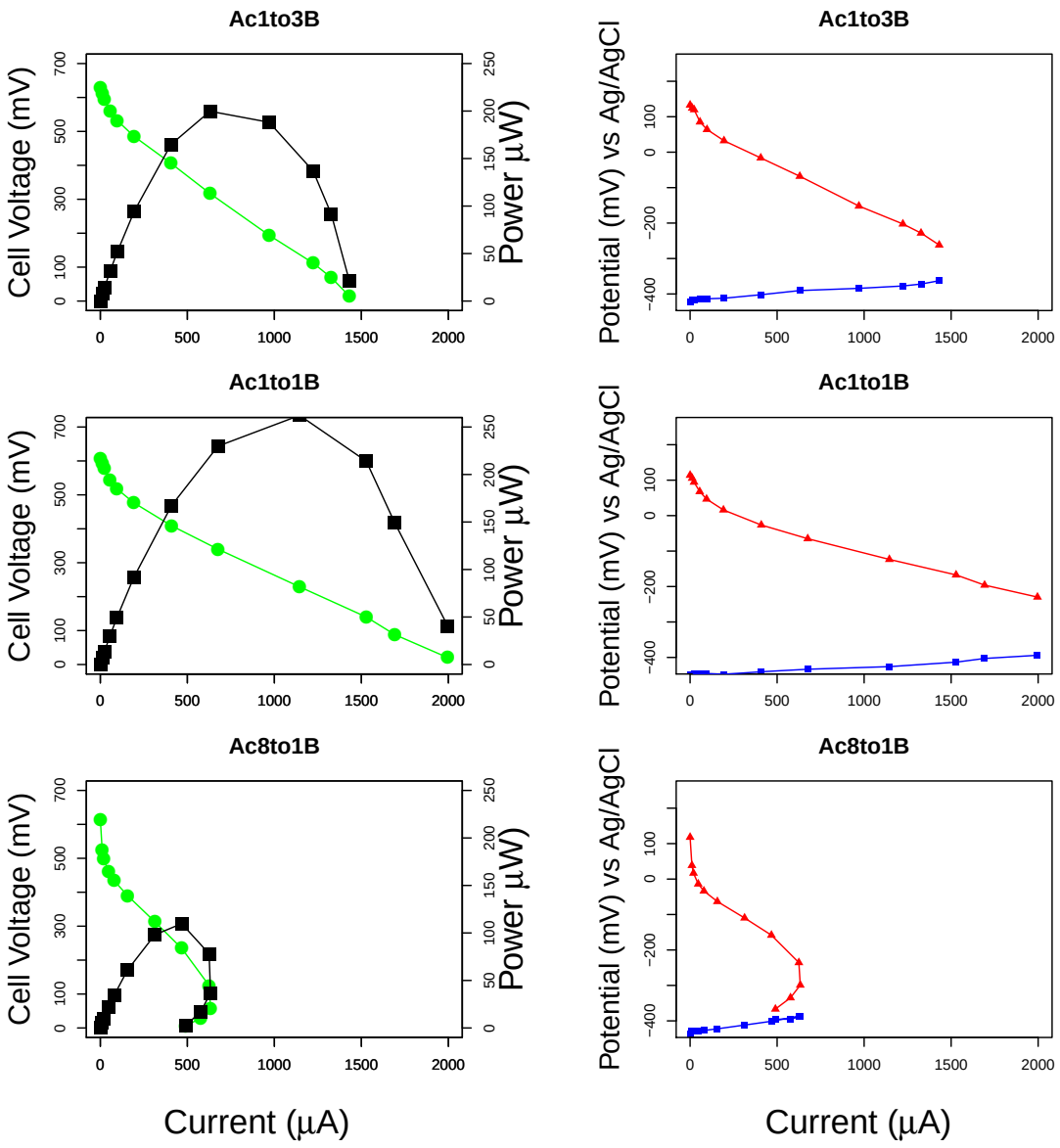

Figure 6.15: Polarisation curves on Ac1to3B, Ac1to1B and Ac8to1B acetate SCMFCs. Graphs in left column show cell voltages and power against current. Graphs in right column show anode and cathode potentials against current. The 2 graphs in each row shows data acquired from the same SCMFC. Cell voltages are shown in green, power in black, anode potentials in blue and cathode potentials in red.

Anode and cathode potentials plotted against current can be used to identify limitation associated with the A/C ratio in a fuel cell. In general, in acetate cells the cathode is responsible for most of the activation polarisation. Most of the potential drop in the mass transfer region is also caused by the cathode potential with the biggest drop for the Ac8to1B SCMFC. This shows that acetate bioanodes have better kinetics compared to their OECD counter parts.

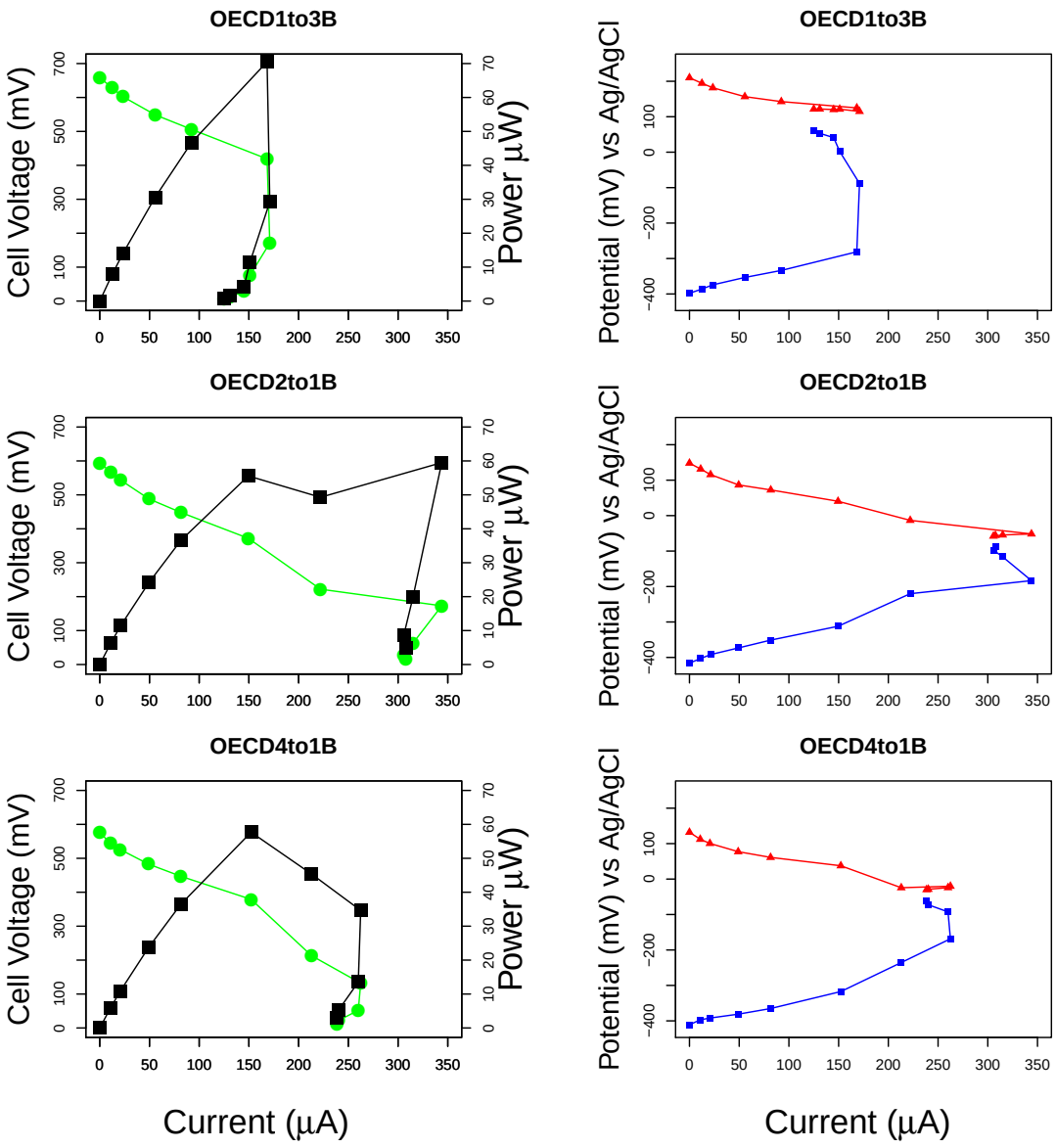

Figure 6.16: Polarisation curves on OECD1to3B, OECD2to1B and OECD4to1B OECD SCMFCs. Graphs in left column show cell voltages and power against current. Graphs in right column show anode and cathode potentials against current. The 2 graphs in each row shows data acquired from the same SCMFC. Cell voltages are shown in green, power in black, anode potentials in blue and cathode potentials in red.

On OECD cells, the anode participates more to the drop in cell voltage within the activation region than the cathode. Most of the voltage drop in the mass transfer region also comes from the anode. These show that on OECD cells the bioanode is the limiting electrode. Cell resistance decreases for higher A/C ratio therefore this is not the cause for decrease in power density.

Table 6.2: Ohmic region of polarisation curves. Horizontal mid line separates acetate SCMFCs above from OECD SCMFCs below.

Reactor	Linear region (Ω)	Internal resistance (Ω)	External load at peak power (Ω)
Ac1to24B	2490-200	462	503
Ac1to12B	2490-91.6	301	200
Ac1to6B	2490-52	293	200
Ac1to3B	2490-10.2	374	503
Ac1to1B	2490-10.2	249	200
Ac8to1B	2490-200	560	503
CS1to3B	50200-2490	1309	2490
CS2to1B	50200-503	1235	503
CS4to1B	50200-503	1600	2490

Power overshoot occurs on the acetate cell with the highest A/C ratio (Ac8to1B) and in all OECD cells. It seems that power overshoot arises when one of the electrode is massively limiting. In the case of Ac8to1B the cathode produces less current at its lowest potentials. Similarly OECD bioanodes produce less current at their highest anode potential. The fact that current drops beyond a certain potential might be the mechanistic reason for power overshoot. This may happen because current does not stabilise during the 20 minutes interval allowed for each resistance meaning that cell voltage acquired at higher external loads were overestimated. This explanation is also suggested by *Logan et al.* in [272]. In their study they found that power overshoot occurs in polarisation curves acquired at 20 and 100 days ruling out insufficient bioanode enrichment as the cause. However power overshoot was not detected when polarisation curves were collected in a multi-cycle approach where each resistance was kept for an entire cycle. In the present study power overshoot occurs on bioanodes with lower density of electrigens. It is therefore considered that power overshoot is associated with lack of current stabilisation during the 20 minutes interval particularly for bioanodes poorer in electrigens.

6.3.7 Biomass distribution

Cell abundance density was shown to decrease with increasing A/C ratio. Consequently, biomass density should follow a similar trend. Biomass distribution on bioanodes grown in acetate and at different A/C ratios is shown in figure 6.17. Bioanode Ac1to24B has a uniform distribution of biomass. Above this ratio biomass shows non-uniform distribution. The last 2 bioanodes at right (Ac1to1B and Ac8to1B) have lower biomass density but also non-uniform distribution. For example, bioanode Ac8to1B shows a few carbon threads with thick visible biofilms surrounding them while the rest of the anode is composed of very thin biofilms. The first 3 bioanodes from the left have so much biomass covering them that carbon threads cannot be distinguished as opposed to the rest of bioanodes.

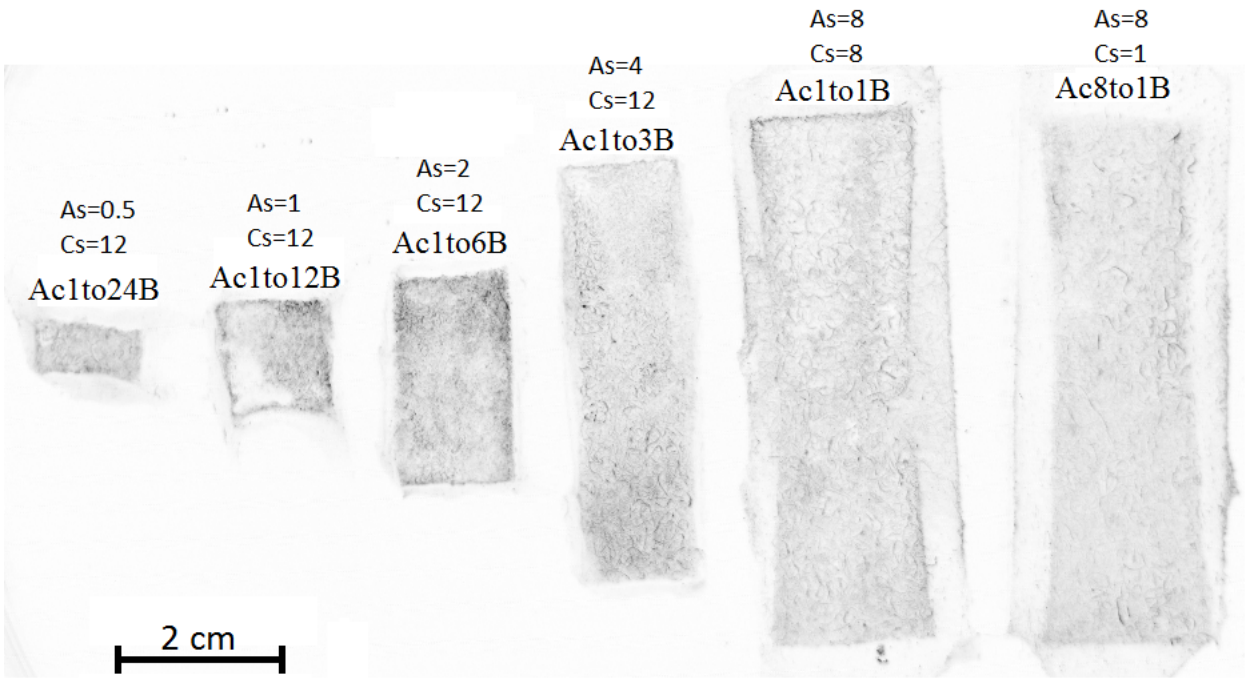

Figure 6.17: Biomass distribution on acetate-fed bioanodes. Surface areas of bioanodes (As) and their corresponding cathodes (Cs) are indicated above the bioanodes. Samples were stained with SYBR-Green, incubated for 30 minutes and imaged in fluorescence mode (excitation at 480 nm and emission at 485-655 nm, exposure time 30 seconds). Images were obtained in black and white and the colors were inverted for better visualisation.

Electrigens are competing with each other for anode surface because overvoltage increases with current density. This would drive the electrigens to spread evenly on anodes trying to get as far as possible from each other. On the other hand bacteria benefit from living together in a biofilm for many reasons. Coaggregation was found to benefit bacteria that are metabolically coupled by improving mass transfer between them [273]. In the case of electrigens one reason for local coaggregation is the need for a common network of cytochromes involved in electron transfer. This factor acts in the opposite direction as overvoltage, keeping electrigens closer together. In effect electrigens may benefit from growing closer to each other. As a result when the anode surface area is in excess islands of bacteria will prevail on the anode instead of a uniform distribution of biomass which would increase the average distance between bacteria. Another possible explanation for biomass uneven distribution might also be uneven colonisation of the bioanode. Air bubbles trapped in carbon felt creates an inhomogeneous environment explaining uneven colonisation. The regions with more colonised electrigens become regions of higher biomass density.

Current density may be limited by design which in turn limits how much biomass per anode area can be produced. Therefore growth in cell numbers is limited by how much current is physically possible for a given combination of anode and cathode surface areas. Bacterial cell number cannot grow indefinitely because this would lead to a decrease in how much current each bacterial cell can

produce. However the bioanodes presented in figure 6.17 have all been run for the same amount of time. What happens with biomass density and its distribution over longer periods of time remains unknown.

6.4 Conclusions

Results confirmed that current density and power density are higher at lower A/C ratio in acetate and complex medium as previously reported in the literature. The explanation is that bacteria forming anodic biofilms have the ability to adapt their abundance and specific activity in response to system design. On smaller bioanodes bacteria exhibit higher density and are therefore able to produce more current although at a lower specific activity. This plasticity is what sets apart the anodic biofilm from chemical catalysts and must be considered in the design of MESs.

Substrate type has a big impact on bacterial community and performance. Total cell abundance, electrigen abundance and current output are higher in acetate. Cell voltage and anode potential profiles show clear stable regions in mid-cycle in acetate but not in OECD anolyte. Also cycle length is shorter in OECD. Internal resistances are smaller for SCMFCs run on acetate. *Geobacter* percentage decreases with A/C only in acetate anolyte and shows no clear trend in OECD medium. Bioanode communities mainly cluster according to substrate type. Community composition is also affected by A/C especially in acetate anolyte.

Because complex substrate sustains lower currents than acetate the optimal A/C ratio differs between the 2 substrates. For the acetate cells current does not increase above the ratio of 1:6. For a constant cathode area any increase in anode area adds to the costs with marginal power increase. In the case of complex substrate current plateaus at a ratio of 1:3. The relative drop in current with A/C ratio is less steep compared to acetate cells. This suggests that the strategy for lowering materials costs depends on substrate properties. For acetate cells it is better to decrease the anode area relative to the cathode while for the OECD cells costs can be lowered on the cathode materials. For example current output in complex substrate at an A/C ratio of 4:1 was only slightly lower than at a ratio of 1:3. In this case using more anode material is compensated by lowering costs associated with smaller cathodes. As a generalisation costs can be lowered on the more active electrode which in turn depends on substrate type. Optimising A/C ratio when designing new MESs can benefit from the identification of the more active electrode because it reduces the number of combinations that need to be tested. The more active electrode can be predicted considering that this depends on organic substrate and on cathode catalyst. Varying the A/C ratio and using both acetate and complex substrate can also benefit the characterisation of novel cathodes. An improper A/C ratio may lead to anode limitations which does not allow comparison of different cathodes.

Specific activity of electrigens is not a good measure for comparing MESs of different designs.

Using specific activity as a parameter to compare reactor designs provides additional information but can suffer from similar drawbacks as using power density for the same purpose. A more accurate calculation of specific activity would also require the determination of the active fraction of electrigens. Biomass density decreased with A/C ratio and its distribution was not uniform. On bigger bioanodes local concentrations of biomass were observed suggesting an advantage in living closer together even when anode area is in excess. However the real distribution of electrigens across bioanodes remains unknown because SYBR-Green stains all bacteria.

Chapter 7. Colonisation and development of anodic biofilms on carbon felt electrodes

This chapter describes the bacterial community of anodic biofilms from colonisation to maturity. The research investigates the temporal dynamics of community composition, cell abundance and distribution of dead/live regions within biofilms. To ensure that all electrodes were subjected to the same conditions a novel multi-electrode reactor was developed and used for the tests. The study reports on the development of anodic biofilms from colonisation to maturity and examines the distribution of growth and community composition across bioanodes.

The objectives of this study are:

- Develop a multi-electrode reactor (MER) with shared anolyte to improve replication of running conditions.
- Investigate on anodic biofilm development and the identification of the steps in the formation of electrigenic community. This will provide a frame for future studies aimed at improving MES performance.
- Investigate biofilm growth on three-dimensional (3D) electrodes. Here it is hypothesised that 3D electrodes are subjected to gradients which affect biomass distribution with depth.
- Assess differences in community composition and biofilm structure across the surface of bioanodes.

7.1 Introduction

Increasing the power output of MESs requires a deeper understanding of the functions that are performed by bioanode electrigenic biofilms. Understanding the colonisation process and the long-term dynamics of bioanodes can provide the key for further increasing MES performance. It is important to establish an anode biofilm with stable communities for robust long term performance, and it is equally important to understand the evolution and ageing of bacteria communities during operation of the MES. It is useful to observe the evolution of the proportion of electrigens in a

community over time. Changes can signal if aging affects the anodic communities and if a regeneration procedure is needed. It also provides information on non-electrigens on their functions and interaction with electrigens. The electrigenic biofilm is fundamentally different from a chemical electrocatalyst. Unlike abiotic catalysts, electrigenic biofilms are not applied on electrodes; the anodic biofilm is a dynamic entity resulting from bacteria colonising and growing on the electrode surface. Therefore its study requires a different set of approaches combining microbiological and electrochemical methods.

The colonisation and long-term dynamics phenomena can manifest not only in community composition but also in spatial evolution of bacterial biomass. This especially applies to 3D electrodes which show more promise than flat electrodes due to a higher surface area available for attachment [274]. A 3D electrode is not a homogeneous environment. Gradients of chemical concentrations, current density, mass transfer and even electric potentials have been identified in 3D electrodes [275]. These gradients are larger on bigger electrodes predicting limitations on scaling up MESs. Bacteria may grow differently across a 3D electrode and their biomass distribution adds to the spatial heterogeneity already present. Heterogeneity also occurs on a smaller scale due to differentiation of regions within a biofilm [276]. Such regions differ in terms of chemical and bacterial composition, age and activity. Dead and live biovolumes were also shown to occur in anodic biofilms [221].

There have been studies that addressed community composition on anodes or assessed biofilm distribution on electrodes but none that correlated both. The 3D geometry of electrigenic biofilms has also been investigated using confocal microscopy [182, 221]. Such studies were based on endpoint characterization on systems that ran for pre-determined amounts of time. How the observed structures came into existence or if they would still change remained unknown. Temporal dynamics of bioanodes and response to substrate switching has been investigated by Zhang *et al.* [110]. This was done on the same reactor by subsampling the same anode at different points in time. In this approach community gradients across the electrode were not considered. Although a trend in *Geobacter* fraction across time was observed subsampling the same electrode does not take into account uneven growth across the electrode.

Temporal dynamics of community composition, cell abundance and distribution of dead/live regions within biofilms were investigated. The time frame covers changes from inoculum to the the colonisation community and then during growth of bioanodes. Electrodes were collected in duplicates at different points in time and subjected to community analysis and confocal microscopy imagining using dead-live staining. Bacterial composition was tracked in time using community analysis and cell counts data. The metabolic profile of bacterial communities through time was constructed using the metagenome which was retrieved from the community composition data. Such profiles help in interpreting changes in community composition from the point of view of selecting

for certain bacterial functions.

To ensure that all electrodes were subjected to the same conditions a novel MER was developed. This reactor was first validated for electrode equivalency in shared anolyte. Electrode equivalence makes the reactor suited for other types of studies that require high replication such as anode material testing. The design offers the advantage of running multiple electrodes in parallel avoiding the need for subsampling. This way results are not affected by gradients across electrodes. It was also shown that replication power measured as community divergence between replicated samples is better for the MER compared to separate reactors.

7.2 Experimental design and methodology

7.2.1 Development and validation of multi-electrode reactor

The MER designed specifically for this study has 8 anodes arranged in a symmetrical fashion. The cathodic and anodic chambers were separated by an anion-exchange membrane. The design is described in section 3.1.3. The MER was first optimised and assessed for electrode equivalency and inter-electrode interference. The MER was characterised by electrochemical methods and a running procedure was developed. Several runs were performed to check for cell resistances, uncompensated resistances, cell interference, current distribution among channels, and to explore the effect of the pump, air sparging and replacement of both catholyte and anolyte on cells performance.

As part of system-validation the MER was used as a platform for anode material testing. The reactor was run with 4 of the anodes made of carbon felt and the other 4 made of carbon cloth. The materials were alternated: anodes 1,3,5 and 7 were made of carbon felt and anodes 2,4,6 and 8 were made of carbon cloth. Current outputs in the stable region and power curves were used to compare the materials. Significance of differences were assessed by randomisation tests. Carbon cloth and carbon felt were analysed by FTIR to check if differences in carbon functionalization could have played a role. The objective was to test the replication power of the MER and to develop a running procedure that was implemented at the next run when biofilm dynamics was investigated. The impact of air-sparging and different strategies for replenishing the anolyte and catholyte were investigated. For these purposes the run lasted 35 days during which the reactor was fed on acetate until the 25^{th} day then on OECD anolyte. Power curves were collected 3 times and the results were used for comparing anode materials and substrates. The third set of power curves were collected when the system was running on OECD medium and were used to identify external resistance at peak power used in the next run for the study of biofilm dynamics.

7.2.2 Anodic biofilm dynamics on carbon felt electrodes

This was a study on the development of anodic electrigenic biofilms following the process from colonisation to maturity phase. Bioanodes were characterised in terms of community composition, total cell abundance and biofilm morphology assessed by confocal microscopy. Samples included inoculum, colonisation communities, electrodes sampled at different points in time and an OCP control.

Anodic currents were monitored and their average and standard deviation were calculated. Catholyte level was set to ensure all cathodes were immersed while splashing during air sparging was avoided. Sparging allows for aeration of the catholyte but also facilitates its slow evaporation. To avoid level drop due to evaporation, catholyte was replenished every 4-5 days.

Bioanodes were started by open circuit (OC) colonisation. In this procedure the anode is left in inoculum for 2 days without being connected to the cathode. After the colonisation step, inoculum is replaced with substrate-containing anolyte and the electrodes are connected by an external resistance. The bacteria that attach on the electrodes after the colonisation step will be referred to as colonisers. For example colonisers from primary inoculum refers to the bacterial community formed on electrodes that were incubated in primary inoculum for 2 days. If the anode is connected to the cathode during incubation in inoculum then the procedure is called closed circuit (CC) colonisation. This method was also explored but due to its frequent failure and need for re-inoculation it was not used in the present study.

Two types of inoculum were used: primary and secondary inoculum. Primary inoculum was a 1:1 mixture of wastewater and activated sludge. Secondary inoculum was represented by anolyte collected at the end of a cycle from a mature SCMFC. The OC colonisation communities resulting from using both inocula were characterized by community analysis.

The MER was run for 67 days inside a thermally insulated box. Temperature was held constant at 27° C and measured with a temperature logger. The external resistance was 1kΩ chosen based on power curves collected previously in the preliminary runs. Anolyte was changed in the external reservoir at 2-3 days interval with the purpose of avoiding substrate depletion. The OC colonisation was the method of choice due to its 100% success rate in starting bioanodes. Colonisation was followed by a short period (first 2 days) of pre-feeding on acetate before switching to OECD medium. The main reason for choosing OC colonisation in secondary inoculum and feeding on OECD medium was to eliminate time-variable diversity specific to primary inoculum and wastewater as feed. Secondly it was thought that the enriched inoculum minimises the proportion of bacteria that are not electrigens or do not interact (cooperation or competition) with ARBs. This choice was made in agreement with the aim of providing a reference model of biofilm development as stated in the introduction. This way the experiment is simplified and the chances of observing

interactions that shape the electrigenic community are increased.

The samples subjected to community analysis includes 8 anodes, secondary inoculum, OC colonisers from both primary and secondary inocula, an OCP control and sludge that accumulated inside the reactor. Samples and their analyses are summarised in table 7.1. Community analysis was performed on all samples. Confocal microscopy imaging was performed only on bioanode samples to investigate on growth patterns and correlate current output to biofilm morphology. Cell counts were done only on electrode-like samples. These excluded inocula and sludge. All samples were collected in duplicates except for the colonisers from secondary inoculum, OCP control and sludge. Lack of duplication for the above mentioned categories was caused by experimental limitation. The colonisers and OCP control samples were kept inside the anodic chamber. Duplicating these was limited by the available volume of the anodic chamber. Duplicating the sludge sample would have resulted in subsampling which qualifies as pseudo-replication.

Table 7.1: Summary of collected samples and investigation methods. CA-community analysis; CM-confocal microscopy; CC-cell counts;

Samples type and replication	**Time (days)**	**CA**	**CM**	**CC**
Secondary inoculum (2x)	NA	✓	X	X
Colonisers from primary inoculum (2x)	NA	✓	X	✓
Colonisers from secondary inoculum (1x)	0	✓	X	✓
Bioanodes 1&5 (2x)	9	✓	✓	✓
Bioanodes 2&6 (2x)	17	✓	✓	✓
Bioanodes 3&8 (2x)	33	✓	✓	✓
Bioanodes 4&7 (2x)	67	✓	✓	✓
OCP control (1x)	67	✓	X	✓
Sludge (1x)	67	✓	X	X

All 8 bioanodes together with two pieces of carbon felt were incubated in acetate end-anolyte from a previous SCMFC. The incubation was performed inside the anodic chamber. After this step one of the two free-floating pieces of carbon felt was homogenised and stored at -20°C. This sample provided for the OC colonisers community. Next the inoculum was replaced with OECD medium containing 1 g/L sodium acetate as part of the pre-feeding procedure. In all subsequent medium changes the OECD recipe was used and the reactor was run in recirculation mode. The second piece of carbon felt was collected at the end of the run and provided for the OCP control. During incubation anode potentials were monitored to provide information on colonisation efficiency.

In parallel two anodes were incubated at OCP in primary inoculum and their anode potentials were monitored. After the colonisation the two anodes were homogenised and stored at -20°C for downstream analysis. Independently a batch of 8 anodes were incubated in OECD end-anolyte and their anode potentials were monitored to allow comparison to anode profiles obtained in inocula that leads to anodic biofilm development.

For the present study the metagenomes were not directly available. The community composition was used to retrieve the metagenomes of samples using the R package Tax4Fun and the SILVA genome database. From the metagenome a table of all identified enzymes was obtained. Each had an abundance score that shows its percentage as part of the entire set of genes available in a metagenome. Enzymes were then grouped to form metabolic pathways. A total of 206 pathways were identified. The next step was to remove artifacts represented by pathways that are not present in prokaryotes. After this filtering, the pathways were sorted by category. For example all those involved in the degradation of a particular amino acid were grouped together to form a bigger group named amino-acid degradation.

Metabolic profiling was applied on inoculum, colonisers, electrodes and OCP control communities. 6 groups of pathways were chosen for revealing patterns in community dynamics that are driven by substrate as a selective factor. These are degradation of sugars, degradation of amino acids, degradation of polymers, degradation of lipids, bacterial motility and methane metabolism. The degradation pathways show how substrate shapes the community. Bacterial motility plays an important role in the initiation phase of biofilm development [277] therefore the presence of genes involved in this activity was included in the profiles. Methane metabolism was included due its association to conditions of high-organic loading and lack of oxygen which is typical for anodic chambers.

Electrodes were collected from the reactor 4 times. These were at 9^{th}, 17^{th}, 33^{th} and 67^{th} days respectively. Time 0 was represented by the OC colonisation community. The collected pairs of electrodes are 1 and 5, 2 and 6, 3 and 8, 4 and 7. The first two pairs form opposing electrodes. This pattern was stopped at the third time point when electrodes 3 and 8 were collected instead of electrodes 3 and 7. The reason was because at that point the biggest difference in current output occurred between electrodes 3 and 8. This allowed comparison of current output to biofilm morphology and community composition for 2 bioanodes that performed differently despite being subjected to the same treatment.

The present study also included a characterisation of biofilm distribution across bioanodes. This was done by two approaches. The first involved taking two samples per bioanode for confocal microscopy investigation, one from the top and one from the bottom of the bioanode. Secondly the 2 bioanodes that were collected at the end were split in two halves on the horizontal middle line and each part was investigated independently by community analysis to observe differences between the communities developed on the bottom and top halves respectively.

After collection, each bioanode had two pieces cut out to be visualised by confocal microscopy using dead/live staining. One piece was collected from the top and the other from the bottom. The rest of the electrode was homogenised inside a 2 ml tube using a stainless steel rod and then stored at -20^0 C in preparation for cell counts and community analysis.

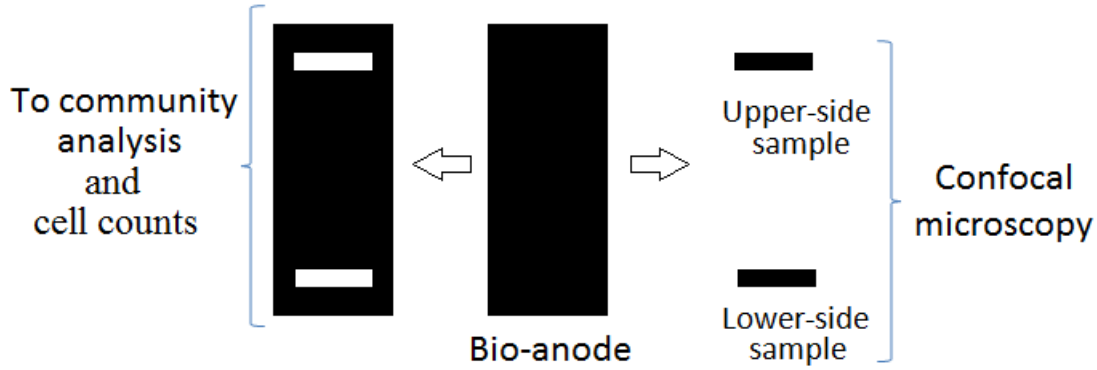

Figure 7.1: Bioanode preparation for downstream analyses. The middle black rectangle shows an entire bioanode after collection. 2 small pieces were cut from this, one from the lower half and the other from the upper half of the bioanode. The 2 pieces were imaged with a confocal microscope and the remaining bioanode was used entirely for community analysis and cell counts.

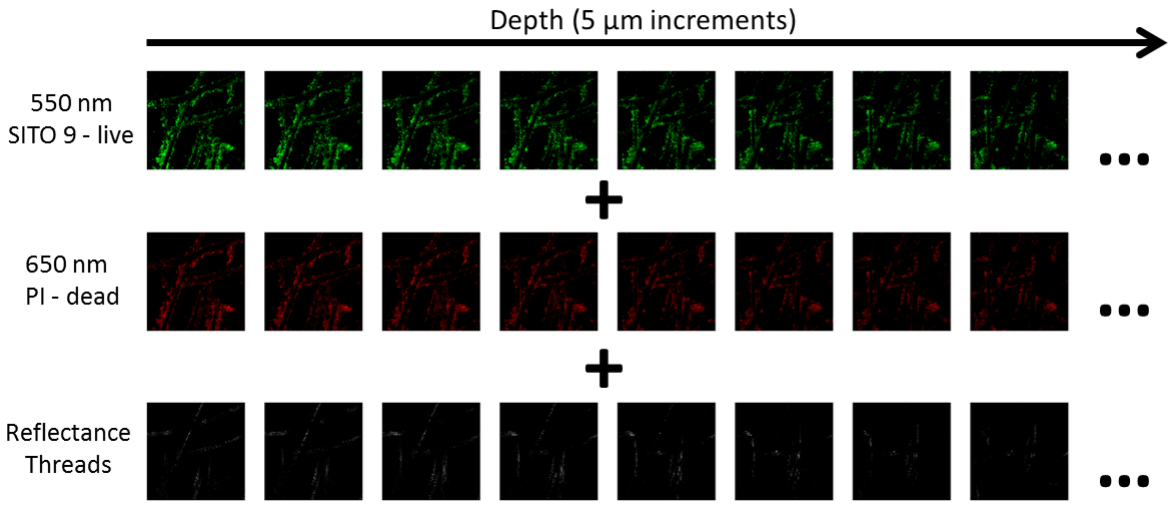

Figure 7.2: Optical sectioning with the confocal microscope. Columns contain 3 frames which show the same optical section. Frames positioned in the same row were taken using the same settings. These were: SYTO 9 fluorescence (upper row), propidium iodide fluorescence (middle row) and reflectance mode (lower row). Optical sections are arranged from left to right in decreasing order of bioanode depth. Depth-scan was conducted in increments of 5 µm as shown by the arrow at the top.

Splitting the anode for downstream analyses is shown in figure 7.1. 3 fields of view were randomly chosen from each preparation. Each field of view was subjected to optical sectioning in increments of 5 µm. Each slice was visualised in three modes: red fluorescence to identify exposed DNA, green fluorescence to identify live cells and reflectance to identify carbon threads. Optical sectioning is represented in figure 7.2. A total of 5500 images were generated which were then processed and analysed using ImageJ and Python Image Library.

7.3 Characterization and validation of the multi-electrode reactor

The MER was put through a series of tests checking if electrodes are equivalent and that inter-anode interference does not exist or is negligible. The anodic chamber and anolyte recirculation system was checked for leaks by running the entire system for 3 days with the cathode chamber being empty. This way any leaks in the membrane or the walls of the anode chamber could easily be noticed.

Inter-anode interference was assessed on mature bioanodes after currents reached stability. This was assessed by measuring changes in current output on a particular anode while the rest were switched on and off. Inter-electrode interference is show schematically in figure 7.3. For example when a channel was producing 940 μA, switching off any of its adjacent channels resulted in an increase in current of approx. 20 μA (2%). Conversely, switching off any of the 3 most distant channels resulted in a decrease of 20 μA. This could be explained by competition between adjacent electrodes for current-conducting anolyte space. Anode interference was not higher than 20 μA for currents around 1000 μA. When the anodes were producing lower currents (run on OECD substrate instead of acetate anolyte) the interference could not be measured.

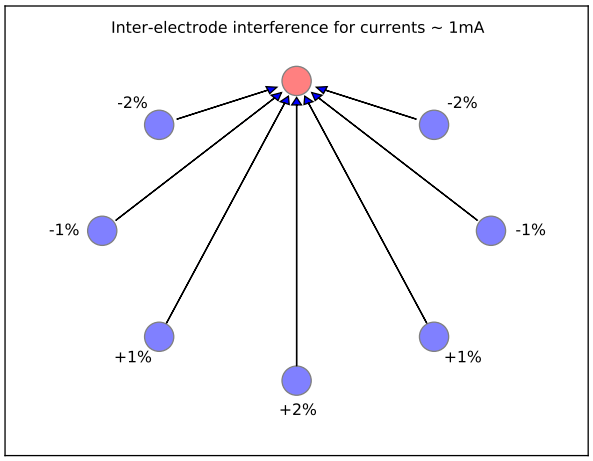

Figure 7.3: Inter-electrode interference. Each circle represents an anode (channel). The interference effect is shown on the anode represented by the red circle where all arrows are pointing. Percentage values next to each blue bioanode show the effect of that particular channel on the bioanode at the top.

Anodes' uncompensated resistances was estimated to be 12.01 Ω (σ=1.1 Ω). The average cell internal resistance was 36.18 Ω (σ=4.58 Ω) with uncolonised anodes. After growth occurred the average cell resistance increased to 52.71 Ω while its standard deviation decreased to 2.26 Ω. This suggest that biofilms add to cell resistance. The wider spread of cell resistances on fresh anodes

might be due to gas bubbles trapped in the mesh of the anode felt. When biofilms grow the bubbles disappear eliminating this cause of variation in cell resistances.

Cell voltages together with important events during the anode material testing run are shown in figure 7.4. Anodes were started by OC colonisation in acetate end-anolyte. Initially the reactor was fed on acetate medium and the external load for all channels was 5 kΩ. When the system reached stability the first set of power curves was recorded. Next the external loads were switched to 506 Ω and the system was again left to reach stability. Until this point catholyte was not changed or replenish but its level decreased due to evaporation. Two approaches were tried for catholyte refreshing. First catholyte level was brought to its initial value by adding deionised water. This led to a decrease in cell voltages and increase of variation in cell voltages across all channels. After 5 days the entire catholyte was changed with fresh solution. This was followed by a jump in cell voltages and a decrease in the spread of voltages across all channels. Based on these observations it was decided that catholyte replenishment with fresh solution is preferred over addition of deionised water. Also to minimise further evaporation loss, a cap was fitted on top of the cathodic chamber. The cap had ports for the cathodes connecting wires and sparging tubing and also holes allowing air to leave the chamber. Frequent change of the anolyte in the external reservoir and catholyte was considered to allow for constant chemical conditions during the run.

The external load was changed on the 22^{th} day to 104 Ω while still feeding on acetate medium. The air sparger was purposely switched off for a very short time. This lead to a sudden drop in cell voltages proving the need for continuous sparging. After the system stabilised a second set of power curves were collected. On the 25^{th} day anolyte was switched to OECD recipe and the external load was changed to 1 kΩ. The system was left to stabilise after which the third set of power curves was collected.

Figure 7.5 shows all 3 sets of power curves collected during the material testing run. Current and power densities were grouped by electrode materials. Power curves show averages and spread of current and power densities independently for carbon cloth and carbon felt bioanodes. Performance of carbon cloth bioanodes is consistently superior to those made from carbon felt. Peak power resistance shifted with growth of anodic biofilm from 1000 Ω to 200 Ω while the system was run on acetate. On substrate switching peak power resistance moved up to 1000 Ω.

Materials were compared using current outputs from all channels grouped by anode material. 4 sets of currents were extracted from the chronopotentiometry data. The first 3 are current obtained on acetate and on 3 different external loads: 5000 Ω, 500 Ω and 100 Ω respectively. The forth set was extracted from the part where the reactor was fed on OECD substrate and run at 1000 Ω external load. Differences between current averages on both substrate was tested for significance by permutation tests which are shown in figure 7.6.

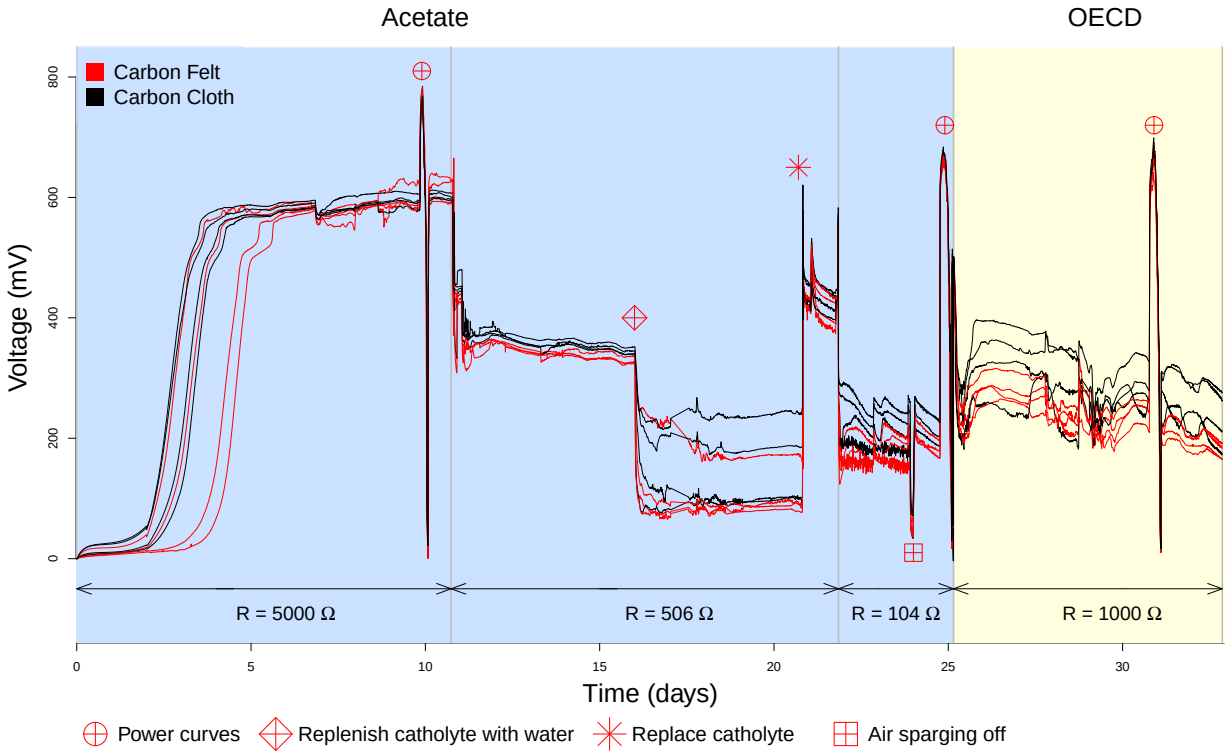

Figure 7.4: Cell voltages from the multi-electrode reactor during test run. 4 bioanodes were made from carbon felt and their corresponding cell voltages are shown in red. The other 4 bioanodes were made from carbon cloth and their corresponding cell voltages are shown in black. The blue background shows the first 25 days of the run when the system was fed on acetate. The orange background shows the period of OECD feeding. Substrate was switched to OECD medium on the 25th day. External resistance was changed at the 11th, 22nd and 25th day. Each period where a certain external resistance was used is indicated by double-ended arrows at the bottom of the graph. Polarisation curves were collected on the 10th, 25th and 32nd day. System response to catholyte replenishment with water, replacement of catholyte and turning off air sparging in the cathodic chamber were tested on the 16th, 21st and 24th day respectively.

The results of permutation tests show the effect of resistance on material comparison. The 5000 Ω external resistor was too big to reveal any difference between the bioanodes. Currents under these conditions were too small masking the effect of anode material. Still power curves collected at this point showed different performance between anode materials at resistances smaller than 5000 Ω (figure 7.5A). Lowering the external load to 500 Ω allows for bigger currents and shows clearly that carbon cloth performs better than felt. A further decrease to 100 Ω shows an even stronger difference between the two materials. At this external load all currents have increased but a bigger change in average current occurs for carbon cloth. At lower resistance the system becomes anode limited; this condition shows the difference between materials. Small p-values were obtained also when the system was run on OECD medium at 1000 Ω external load. Currents under these conditions are smaller and more spread as compared with feeding on acetate.

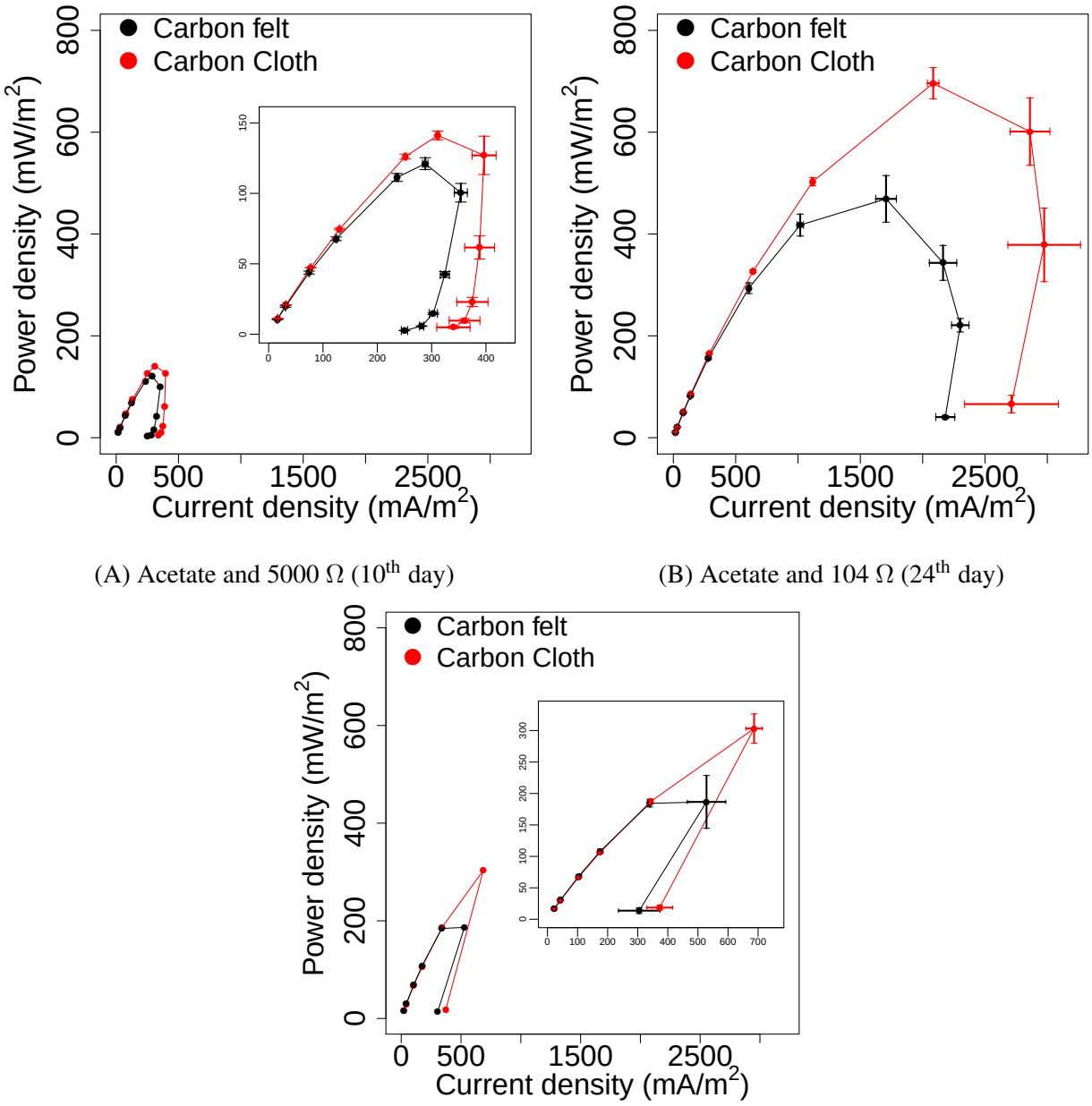

(A) Acetate and 5000 Ω (10th day)

(B) Acetate and 104 Ω (24th day)

(C) OECD and 1000 Ω (32nd day)

Figure 7.5: Power curves collected on the multi-electrode reactor during test run at different moments in time. A: 10th day (fed on acetate at an external resistance of 5000 Ω); B: 24th day (fed on acetate at an external resistance of 104 Ω); C: 32nd day (fed on OECD medium at an external resistance of 1000 Ω). Black curves show power density averaged over all 4 carbon felt bioanodes and red curves show power density averaged over all 4 carbon cloth bioanodes. Vertical error bars show twice the standard deviation of power density and horizontal error bars show twice the standard deviation of current density. All figures share the same x- and y-scale. Inset figures show close-up of the same data presented in the parent graph.

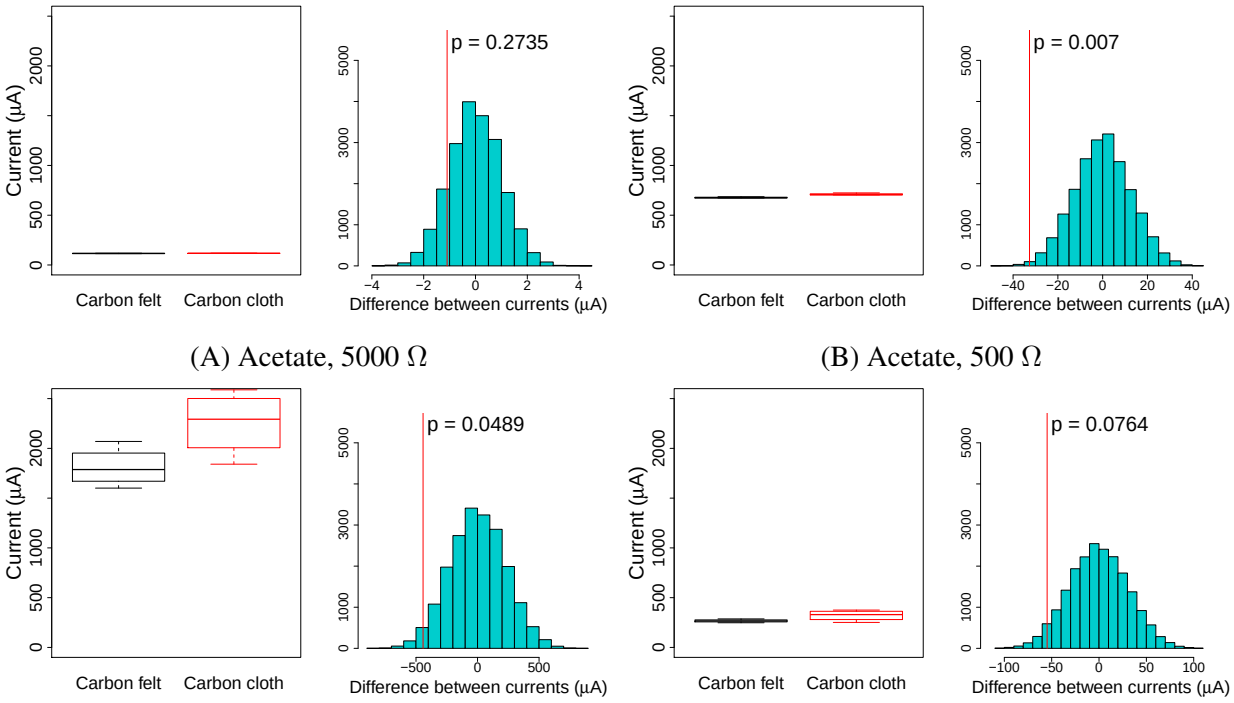

(A) Acetate, 5000 Ω

(B) Acetate, 500 Ω

(C) Acetate, 100 Ω

(D) OECD, 1000 Ω

Figure 7.6: Significance of difference between currents averaged by carbon felt and carbon cloth bioanodes calculated by permutation test. Currents were calculated from cell voltages measured during test run on multi-electrode reactor and averaged over stable regions. A: fed on acetate with external resistance of 5000 Ω, stable region 5.8-6.68 days; B: fed on acetate with external resistance of 500 Ω, stable region 12.44-15.78 days; C: fed on acetate with external resistance of 100 Ω, stable region 21.98-23.75 days; D: fed on OECD medium with external resistance of 1000 Ω, stable region 25.87-28.55 days; Each figure contains 2 graphs. Graph at left shows box-plots of currents grouped by anode material. Black indicates carbon felt and red indicates carbon cloth bioanodes. Graph at right shows histogram of probability of differences between average currents grouped by anode material. Vertical line shows position and p-value of actual difference.

The major difference between the materials is the packing of carbon threads. Carbon cloth is more dense than carbon felt and therefore has a bigger surface available for biofilm growth and possible smaller contact resistance. Although carbon cloth outperforms carbon felt the latter was used as anode material to investigate on anodic biofilm dynamics. This is because carbon felt having a loose packing of carbon threads is a 3D electrode and during confocal microscopy investigation can show biomass distribution with depth. Conversely carbon cloth would have limit the z-scan during confocal microscopy.

7.4 Development and dynamics of anodic biofilms: Results and discussion

7.4.1 Cell voltages and anode potentials of bioanodes used for the study of community dynamics

Cell voltages and anode potentials were monitored for all channels over a period of 67 days. CP profiles are shown in figure 7.7. During the run 4 events occurred and they are shown inside figure 7.7A. Event 1 signals substrate depletion which was quickly solved by changing the anolyte in the external reservoir. Event 2 is a pump failure and event 3 is data-logger failure which led to a lack of data during that time. Event 4 is a decrease in cell voltages which might be similar in nature to event 1. Any decrease in cell voltage is accompanied by an increase in anode potential (figure 7.7B) eliminating cathode activity decay as the reason for current drop. Channel 8 shows smaller current compared to other bioanodes. This is the reason why at the third sampling time anode 8 was collected instead of anode 7. The change in sampling order allowed for comparing community composition and biofilm morphological features between two bioanodes that differ in performance. Cell voltages were averaged across all bioanodes and the resulting current is plotted in figure 7.7C together with the error bars. Current variation decreases after the 33rd day when the least performing bioanode was removed from the reactor.

7.4.2 Bacterial community dynamics from inoculum to colonisers

The composition of communities in secondary inoculum, OC colonisers from primary and secondary inocula, all 8 anodes including top and bottom halves for the last two sampled bioanodes, OCP control and sludge are shown as bar plots in figure 7.8. The data is shown as percentages so all bars have the same height. Secondary inoculum shows small diversity and is dominated by *Azospirillum*. This is a free-living nitrogen fixing bacterium [278]. *Geobacter* average abundance in secondary inoculum is 1.94% and experiences a small decrease to 0.9% after colonisation. The OCP control shows a community composition very similar to that of the bioanodes from which it mainly differs by lack of *Geobacter*. Composition of OC colonisers from primary inoculum show the presence of *Geobacter* at an average abundance of 1.13% but also a higher diversity that any other sample. Comparing primary to secondary inoculum shows the impact of inoculum on the colonisation community. Wastewater and activated sludge are characterised by high diversity. When carbon felt is exposed to this mixture it will get colonised by many types of bacteria. Detection of *Geobacter* in OC colonisers from primary inoculum proves the usefulness of using OC colonisation for enriching ARBs.

Cell abundance was calculated as cell counts per gram of electrode and were used to weigh the community composition data. The resulting bar plot is shown in figure 7.9.

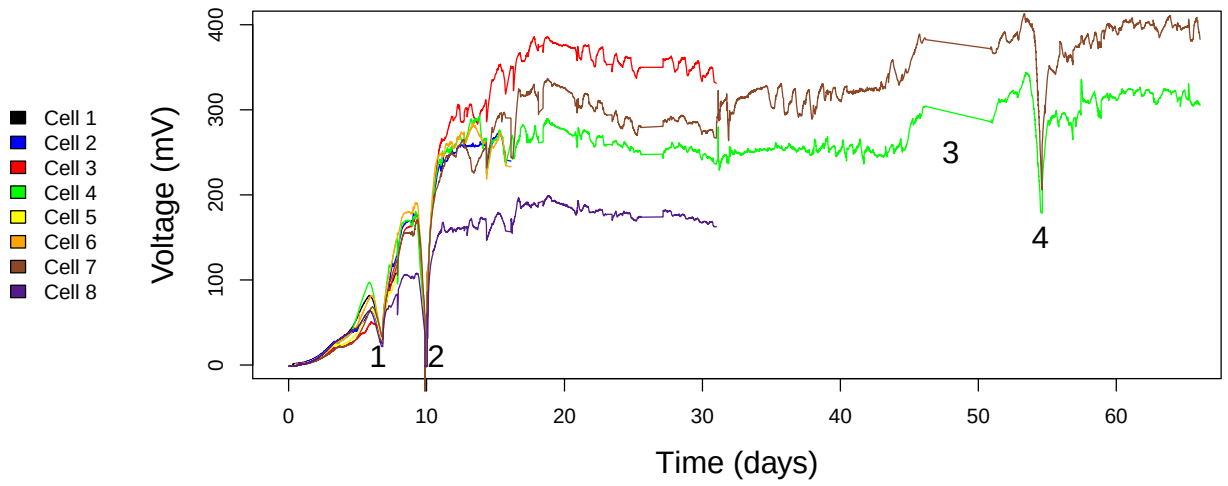

(A)

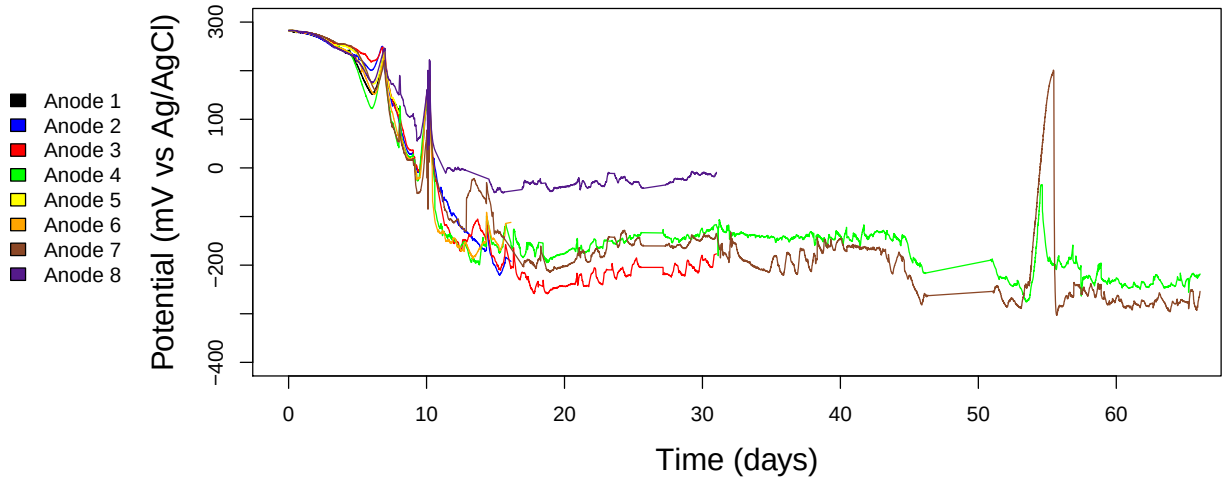

(B)

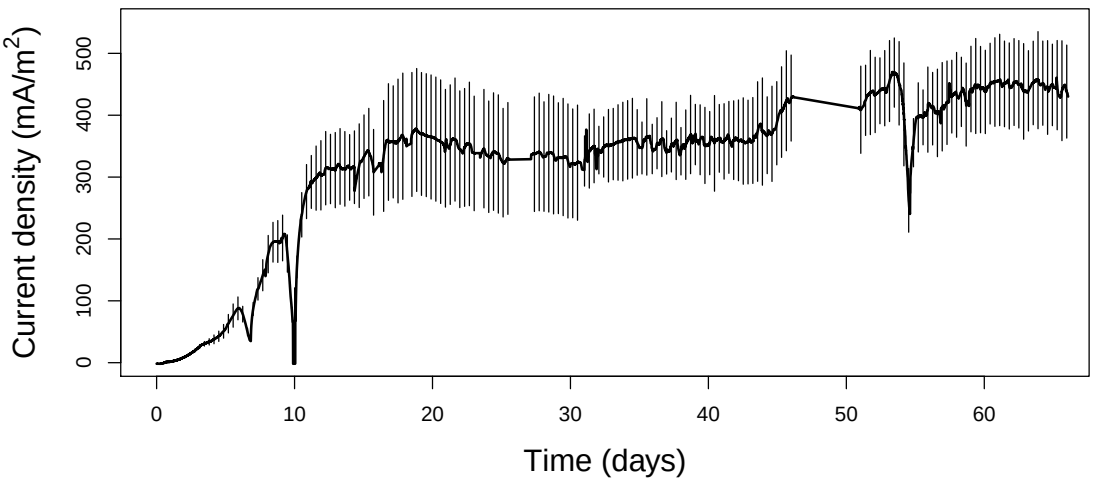

(C)

Figure 7.7: A: Cell voltages; event 1: substrate depletion; event 2: pump failure; event 3: data-logger failure; event 4: substrate depletion; B: Anode potentials measured against Ag/AgCl reference electrode; C: Current density averaged over all bioanodes in the multi-electrode reactor. Error bars show twice the standard deviation of current density.

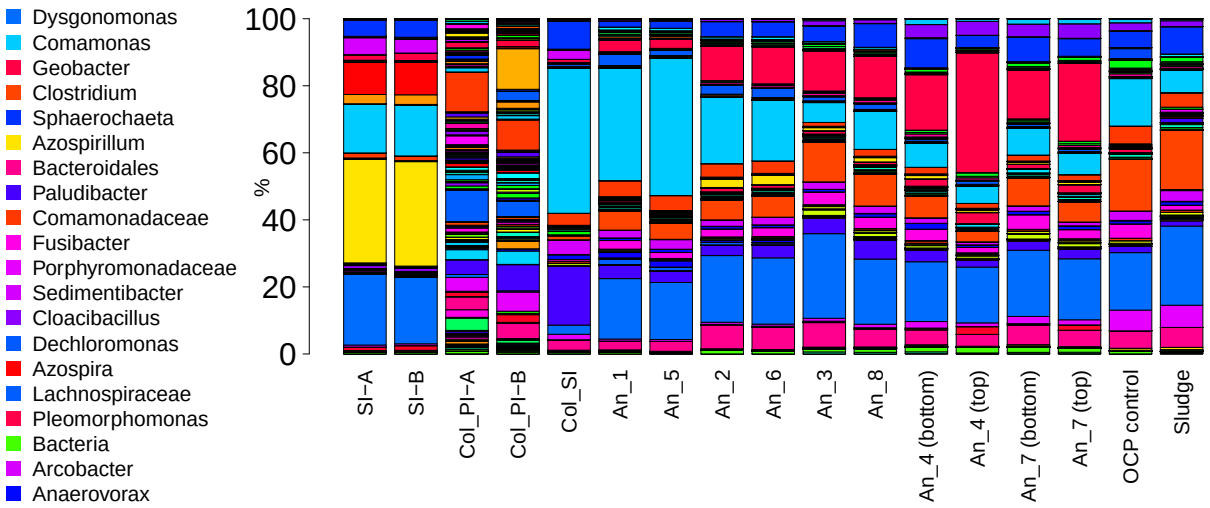

Figure 7.8: Community composition of secondary inoculum (SI), colonisers from primary inoculum (Col_PI), colonisers from secondary inoculum (Col_SI), bioanodes of different age (1 and 5 collected at 9 days, 2 and 6 collected at 17 days, 3 and 8 collected at 33 days, 4 and 7 collected at 67 days), sludge accumulated in the reactor over 67 days and OCP control. For bioanodes 4 and 7 the communities at the lower and upper halves are shown. Taxons are identified to genus level. Where this was not possible the next classification level is shown (family, order or class).

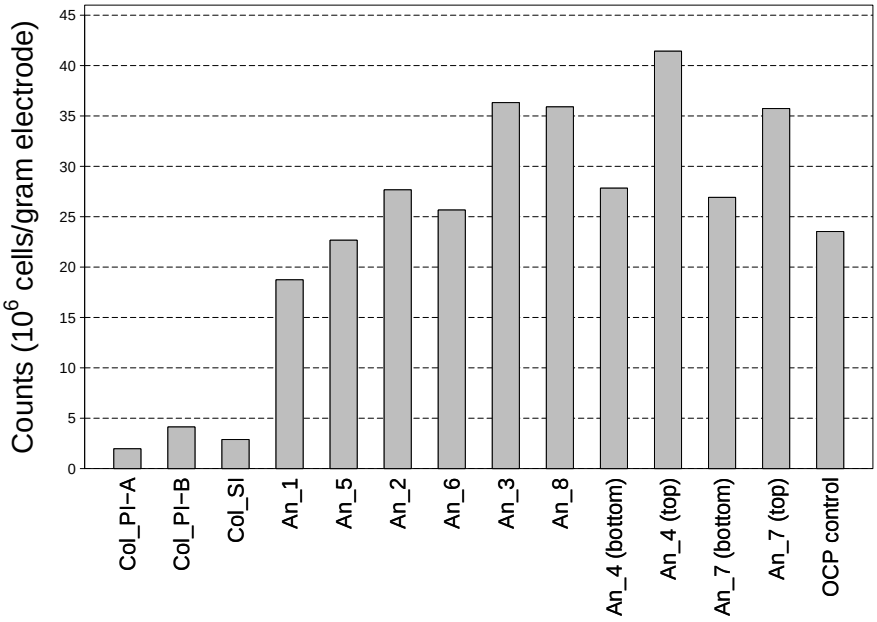

Figure 7.9: Cell abundances for each bioanode expressed as 10^6 bacterial cells per gram of wet electrode. Non-electrode samples (inocula and sludge) were excluded. Samples are arranged from left to right in increasing order of collection time. Cell counts for the lower and upper halves of bioanodes 4 and 7 are shown separately.

Figures 7.8 and 7.9 show that the upper halves of the last 2 bioanodes have higher cell abundance and higher *Geobacter* percentage. Community percentage data was weighted by bacterial cell counts and it shown in figure 7.10. Weighted data from both halves of each electrode were

combined by averaging abundance for each taxon. This shows the trend in community composition from OC colonisers and then across all bioanodes ordered according to the time of sampling. Overall bacteria abundance has increased from 2.9×10^6 cells/gram in OC colonisers community to 20.7×10^6 cells/gram in the first pair of bioanodes. This increase in bacterial number by 7 times occurred over 9 days. Abundance then increased by a factor of 1.7 over a period of 24 days reaching 36.1×10^6 cells/gram on the 32nd day. The last pair of bioanodes show slightly smaller abundance than the previous pair decreasing to 32.9×10^6 cells/gram.

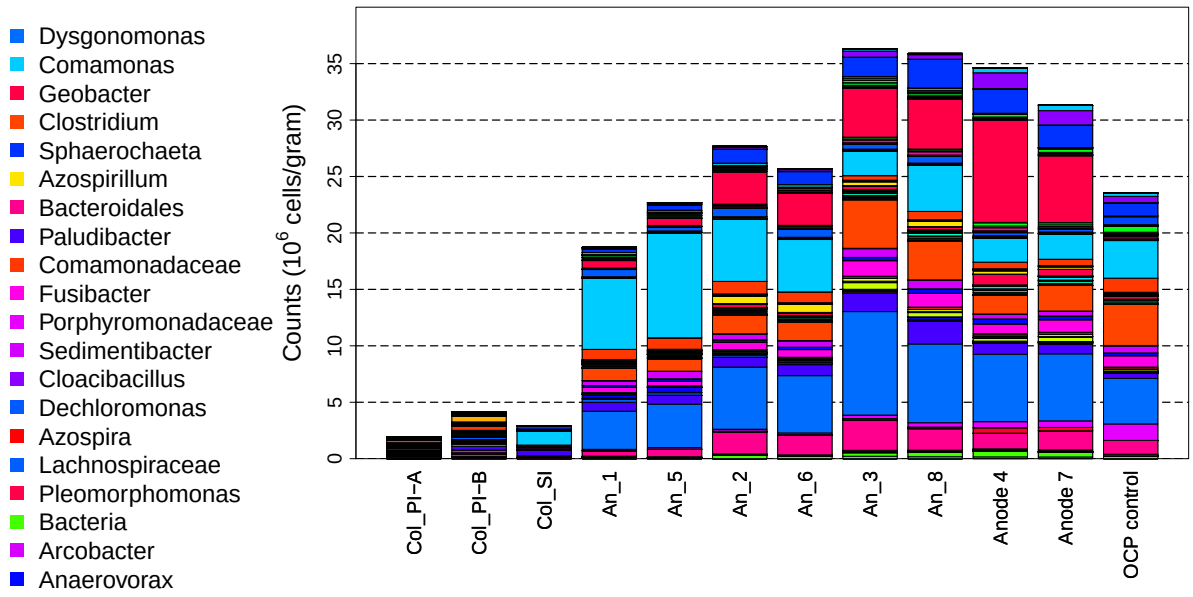

Figure 7.10: Community composition at genus-level weighted by bacterial cell counts in secondary inoculum (SI), colonisers from primary inoculum (Col_PI), colonisers from secondary inoculum (Col_SI), bioanodes of different age (1 and 5 collected at 9 days, 2 and 6 collected at 17 days, 3 and 8 collected at 33 days, 4 and 7 collected at 67 days), sludge accumulated in the reactor over 67 days and OCP control. Samples are arranged from left to right in increasing order of collection time. Upper and lower halves of bioanodes 4 and 7 were combined to generated the entire communities of these 2 bioanodes.

7.4.3 The colonisation process

To understand the colonisation process one must look at the percentage composition of enriched inoculum and the OC colonisation communities. The enriched inoculum contains *Geobacter* (1.63 % and 2.12 %) which provides for the initial pool of ARBs. Carbon felt displays a spongy-like structure under the microscope. Due to this property carbon felt can retain many small air bubbles which are not removed even after nitrogen sparging. These bubbles could be observed with the naked eye. This suggests that during colonisation the anode is a heterogeneous environment made of anaerobic and aerobic regions. It was previously proven that *Geobacter* can grow in presence of oxygen [279]. This implies that trapped air will not impede growth of *Geobacter*. The hetero-

geneous conditions within a fresh bioanode is reflected in the higher diversity of the colonisation community as compared with enriched inoculum.

Hydrogen peroxide forms as a result of oxygen reduction on carbon electrodes [280]. This process occurs in a certain potential window and its formal potential decreases with higher pH [281]. Electrochemical formation of peroxide on carbon felt can be used as a sterilisation procedure [282]. Hydrogen peroxide was proven to hinder bacterial colonisation and growth at carbon electrodes [27]. This may explain why the colonisation of carbon at closed circuit is more difficult. When the anodes are colonised at OCP, production of hydrogen peroxide is either avoided or decreased. This is because oxygen gets consumed heterotrophically by bacteria and does not result in formation of peroxide; instead oxygen promotes growth and attachment to the surface of the electrode. *Geobacter* might benefit from consumption of oxygen during respiration which gives it an advantage by allowing it to get more energy for growth during colonisation phase. Conversely during closed circuit colonisation, the anode is kept at a higher potential imposed by the cathode. Under these conditions peroxide is predicted to form over a longer time and on a bigger percentage of anode area.

How the anode potential changes during OC colonisation depends on the inoculum. When enriched inoculum is used the anode potential drops in less than 12 hours (figure 7.11C) reaching the typical bioanode OCP (-480 mV vs Ag/AgCl). In primary inoculum the anode potential also drops to the OCP value but this happens in a 2-step fashion (figure 7.11A). End-anolyte from cells fed on OECD medium was proven not to work as inoculum. In this situation the electrigens might be outcompeted in the planktonic community by fermenters making this type of anolyte unsuitable as inoculum. Anode potential during OC colonisation incubated in OECD end-anolyte also decreased but the profiles were not smooth as in the case of primary and secondary inocula (figure 7.11B).

Anode potential decrease during incubation is partially explained by a drop in oxygen level due to its consumption by heterotrophic bacteria. Profiles are smooth for inocula that leads to electrigenic biofilms but are erratic in OECD end-anolyte. The smooth pattern in anode potential profile might be due to growth of electrigens on the surface of anodes slowly driving the potential towards OCP values of mature bioanodes. It is considered that in OECD end-anolyte the anode potential is not driven by electrigens but instead reflects local redox potential of the anolyte. The presence of the smooth pattern may be useful as an indicator for successful colonisation.

Irrespective to what anolyte medium was used, one cycle of pre-feeding on acetate was proven mandatory for development. This aspect has already been mentioned in chapters 5 and 6. The need for acetate during colonisation has been reported before [151]. This can be explained by a smaller competitive advantage of *Geobacter* compared to fermentative bacteria in complex medium. *Geobacter* oxidises acetate and uses the anode as TEA. In complex medium acetate is the result of fermentation processes.

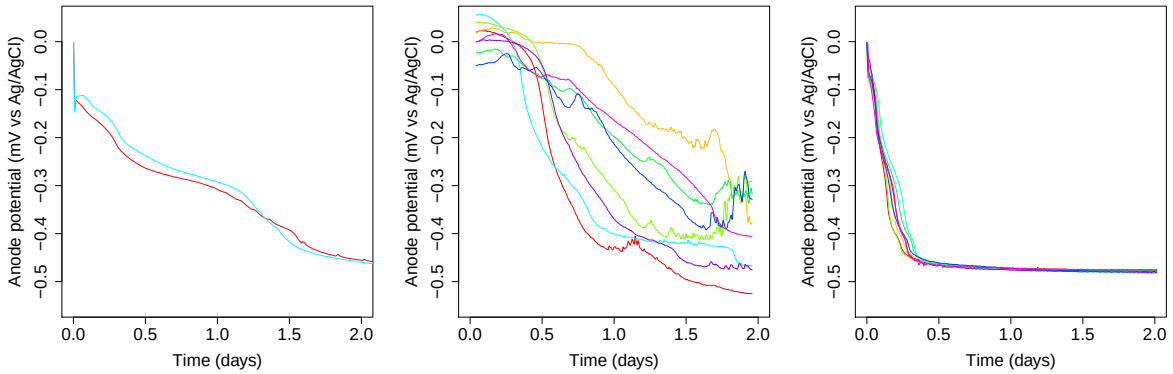

(A) Primary inoculum (B) OECD-secondary inoculum (C) Acetate-secondary inoculum

Figure 7.11: Anode potential measured against Ag/AgCl reference electrode during colonisation in 3 different inocula. Colonisation was done by incubating the bioanodes in inoculum for 2 days while being disconnected from the cathodes. A: primary inoculum (1:1 mix of wastewater and activated sludge); B: inoculum was end-cycle anolyte collected from a mature SCMFC fed on acetate; C: inoculum was end-cycle anolyte collected from a mature SCMFC fed on OECD medium;

Before *Geobacter* has access to its preferred substrate (acetate) other bacteria need to break down polymers and ferment the resulting monomers. If colonisation is started on complex medium the heterotrophic bacteria acquire a head start and can attach themselves to the anode excluding *Geobacter* from biofilm formation. That other bacteria can grow on the anode is evident when comparing the weighted community composition of OCP control with the mature bioanodes in figure 7.9. The bar plot shows that the main difference is lack of *Geobacter* in OCP control. Otherwise the community is similar in composition and even abundance with the electrodes. During pre-feeding on acetate *Geobacter* benefits from acetate while other competitive bacteria are disadvantaged by the lack of fermentable substrate.

7.4.4 The most abundant taxons forming electrigenic communities

The first 20 most abundant taxons plotted over time are shown in figure 7.12. Two main trends are visible in terms of abundance over time. In the first category there are taxons that experience continuous growth. This includes *Geobacter*, *Cloacibacilus*, *Pleomorphomonas*, an unidentified member of *Porphyromonadaceae*, an unidentified bacterium, an unidentified member of *Bacteroides* and *vadinCA02*. *Geobacter* is a well known ARB and it can be assumed this bacterium is responsible for electricity production. *Cloacibacilus* includes species that are commonly found in anaerobic environments such as wastewater treatment plants, anaerobic digesters and animal intestinal tract and are known to degrade amino acids and mucins [283].

The taxons included in the second group experience initial growth followed by a decreased in abundance by the end of the run. These taxons vary in terms of the time when growth stops.

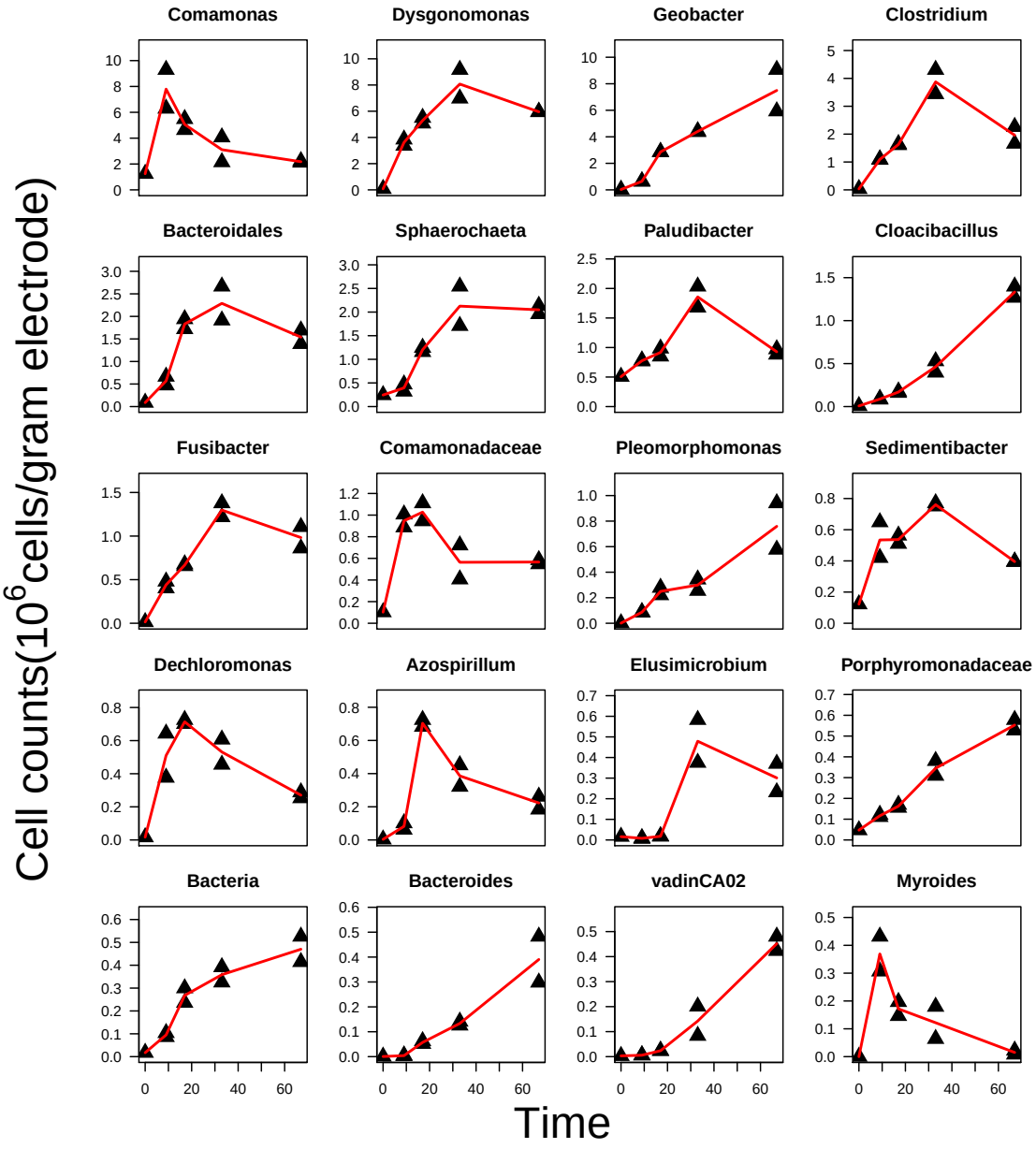

Figure 7.12: Absolute abundance of the first 20 most abundant bacteria genera vs time in bioanode communities of different age (9, 17, 33 and 67 days). Each plot shows abundance of one taxon and they all share the time-scale. To visualise trends over time, plots do not share the abundance scale. Plots are arranged from left to right and from top to bottom in decreasing order of maximum abundance. Each triangle represents one bioanode (2 for each time points). Red lines show local polynomial fits of abundance vs time.

For some the point of change is at time 1 (9^{th} day) while for others this occurs at time 3 (33^{rd} day). Although this classification cannot predict what will happen over a longer time period it is important to note here that 34 days have passed between time 3 and time 4 covering half of the run time. Taxons that have decreased after an initial increase are thought to have benefited when fed on complex substrate but on a longer time scale they are being excluded from the electrigenic

community as this reaches maturity. Their slow and continuous exclusion can be explained by a decrease in their competitive advantage as the biofilm reaches maturity.

Geobacter uses acetate or other low molecular weight products from fermentation for electrigenesis which are derived from the activity of other bacteria. The need for these bacteria for electrigenesis becomes obvious when the reactor is fed on complex substrates. This does not mean that the fermenting bacteria must be part of the electrigenic biofilm. They can perform their functions as part of the planktonic community and the products of their activity can reach *Geobacter* by diffusion only. Thus the apparent exclusion of some bacteria from the electrigenic biofilm can be interpreted as specialization of the biofilm for electrigenicity. As the biofilm reaches stability it develops as a niche for electrigenesis in interaction with the planktonic community. The growth of possible non-electrigenic taxons raises important questions regarding their interactions with electrigens and their roles. Non-electrigens could provide substrate for *Geobacter in-situ* but they could also find themselves in competition with electrigens for attachment area on the electrode.

7.4.5 Metabolic profiling reveal the selective forces that shape bioanode communities with time

Metabolic profiling is a method used for identifying all metabolic pathways present in the metagenome of a bacterial community. This procedure quantifies only the genetic potential of communities for certain functions. It does not imply correlation with real intensities of the corresponding functions. Still they can be used for comparing communities and interpreting changes in communities with time from the point of view of potential metabolic activities.

The resulting metabolic profiles are shown in figure 7.13. Inoculum, colonisers and the bioanodes collected at the first time point show big differences among them while profiles for anodes show trends across time. This suggest the community goes through 2 transitions. These are from inoculum to colonisers and from colonisers to bioanodes. Bioanode profiles show 2 trends. They are increasing for carbohydrate degradation pathways (sugar and starch) and decreasing for non-carbohydrate degradation pathways (amino-acids and lipids). Cell motility is poorly represented in the inoculum community but increased after colonisation phase. This suggests that motility was important during colonisation and it may have an important role in shaping the bioanode community.

Differences between metabolic profiles of communities developed on the top and bottom halves of anodes are shown in figure 7.14. They show that degradation pathways are less represented in the communities developed on the upper halves of bioanodes. The latter communities have higher percentage of *Geobacter* compared to the lower halves (figure 7.8). Differences between abundances of degradation pathways can be explained by a lower percentage of non-electrigenic bacteria in the upper halves.

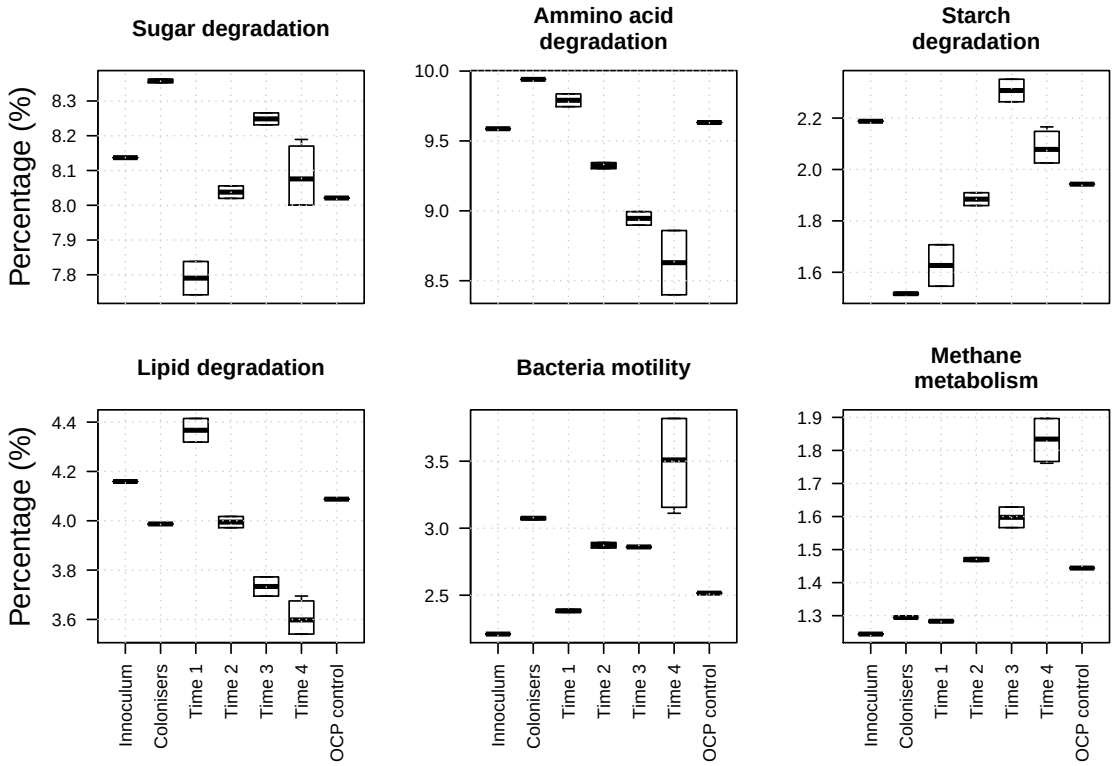

Figure 7.13: Metabolic profile of inoculum, colonisers, bioanodes and OCP control communities. Samples are arranged in increasing order of age. Vertical axis show percentage of enzymes involved in sugar degradation, amino acid degradation, starch degradation, lipid degradation, bacterial motility and methanane metabolism. Enzymes were identified from the metagenome of communities. The metagenome was retrieved based on 16S DNA sequencing data using Tax4Fun package in R.

It is important to note that these differences are relatively low so could equally be stochastic in nature. The potential for bacterial motility is better represented in the upper halves communities.

Overall metabolic profiling show two important features. First the bioanodes experience changes with time. Because the community composition shows uneven distribution among taxons these profiles might be driven by the main taxons. Secondly they suggest the existence of two key transition from inoculum to colonisers and from colonisers to bioanodes. The profile for bacterial motility suggest that this property may be important for in the initiation phase of the biofilm and later on for bacterial spread.

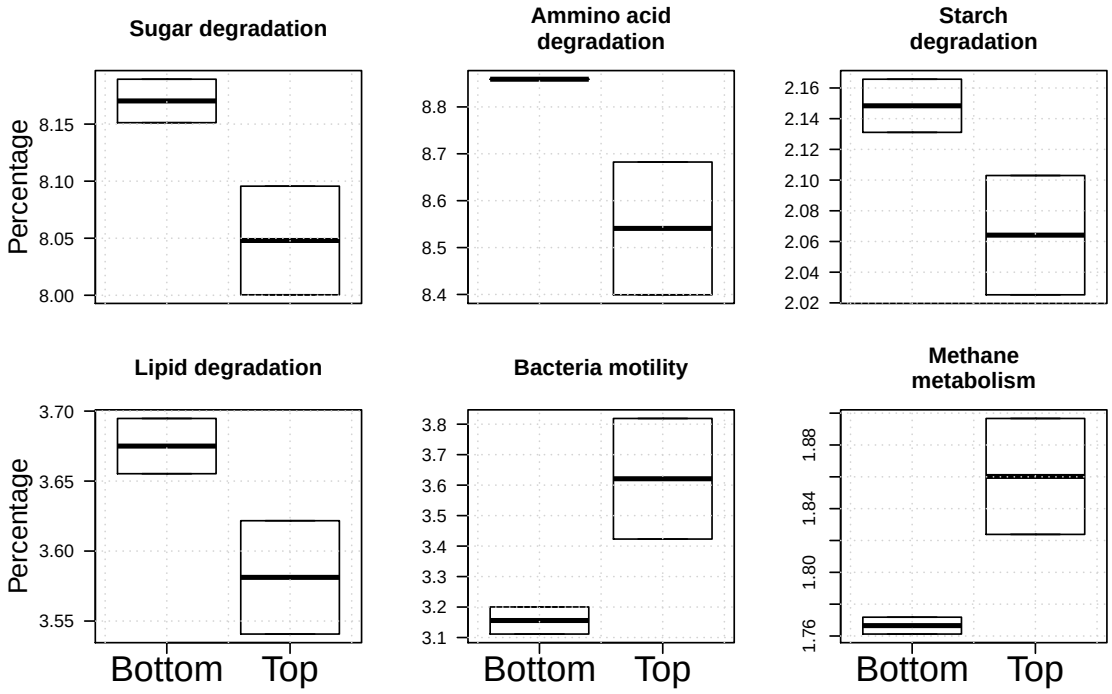

Figure 7.14: Comparison of metabolic profiles at lower and upper halves of bioanodes 4 and 7. Vertical axis show percentage of enzymes involved in sugar degradation, amino acid degradation, starch degradation, lipid degradation, bacterial motility and methane metabolism. Enzymes were identified from the metagenome of communities. The metagenome was retrieved based on 16S DNA sequencing data using Tax4Fun package in R.

7.4.6 Community dynamics is characterised by directional changes revealed by clustering methods

Clustering methods were applied on the community composition data to explore grouping of samples. Principal coordinate analysis (PCoA) plot using unweighted UniFrac distances is shown in figure 7.15. The enriched inoculum communities cluster close to each other (group 1). The OC colonisers from primary inoculum also cluster together (group 2). All the anode samples form a loose group which also includes the OCP control and sludge samples (group 3). Group 1, OC colonisers from secondary inoculum and group 3 are collinear suggesting time evolution across these groups. This pattern shows 2 main jumps in terms of phylogenetic composition. The first jump occurred at colonisation and the second jump occurred between the colonisation and biofilm development. Colonisation and the establishment of an electrigenic community are the main events that shape the phylogenetic composition. Within group 3 there is no apparent collinearity among electrodes. This suggests directional changes during biofilm growth are not driven by taxon composition. The main selective bottle neck is at substrate addition after which roughly the same taxons

will be found in all samples, both electrigenic (electrodes) and non-electrigenic (OCP control and sludge).

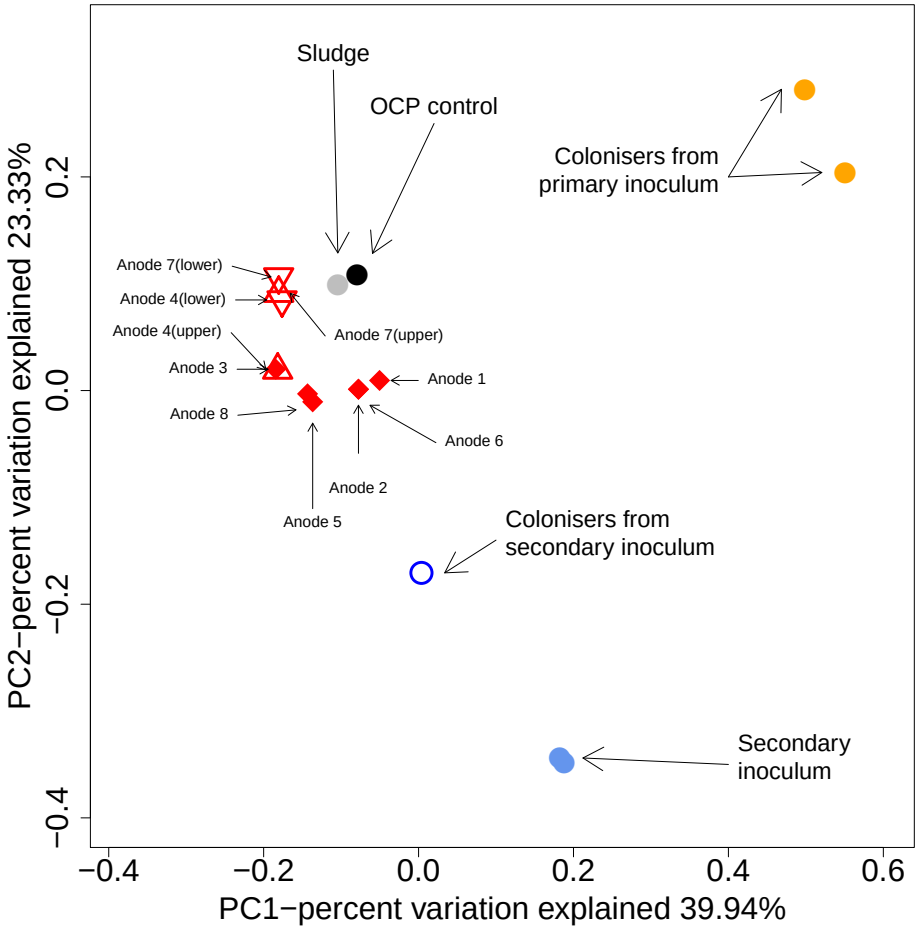

Figure 7.15: Ordination of bioanodes, inocula, sludge accumulated in the reactor and OCP control communities based on principal coordinate analysis. Distances between samples are unweighted UniFrac dissimilarities.

Figure 7.16A shows the PCoA plot using Jaccard distances between samples. The Jaccard distance is based only on presence-absence data and differs from UniFrac by not considering the branch distances between identified taxons on the phylogenetic tree. This plot shows similar grouping to figure 7.15 but the relative distances between groups are smaller. OC colonisers from secondary inoculum are closer to group 3 than in figure 7.15 suggesting that the taxons for which presence-absence data changed during growth event are phylogenetically distinct from the rest of the taxons. In other words the transition from colonisers to biofilm development affects certain branches of taxons. There is also a tendency for secondary inoculum, OC colonisers and bioanodes samples to be placed in a time series fashion suggesting that presence-absence data change directionally with time.

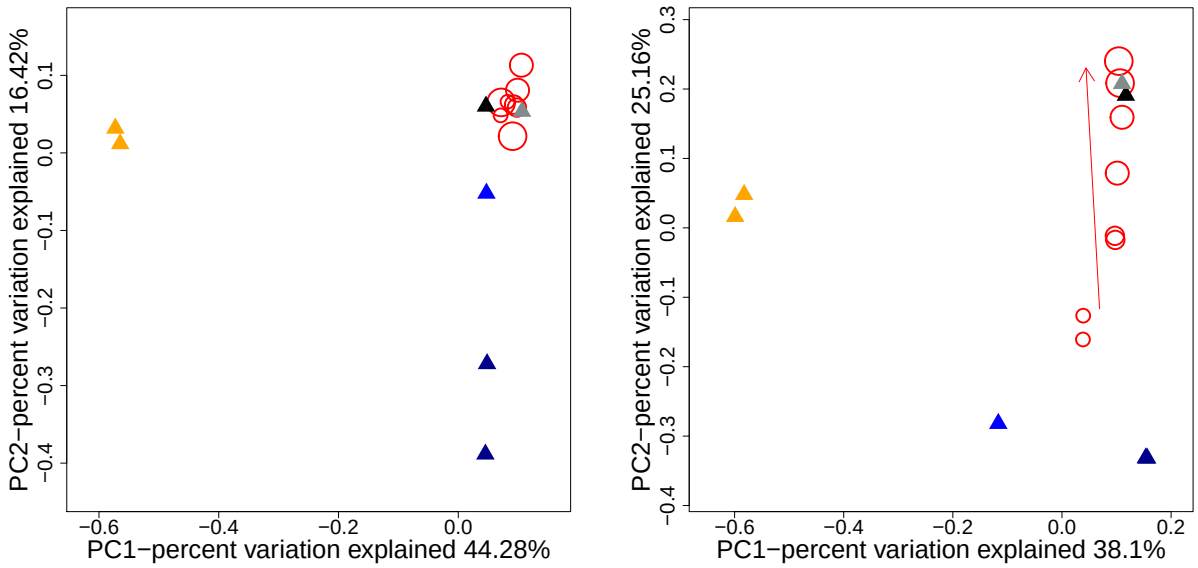

(A) (B)

Figure 7.16: Ordination of bioanodes, inocula, colonisers, sludge accumulated in the reactor and OCP control communities based on principal coordinate analysis. A: distances between samples was calculated using Jaccard dissimilarity index; B: distances between samples were calculated using Bray-Curtis dissimilarity index; Bioanodes are show as red circles with radius increasing with time of collection. Red arrow shows direction of time. Non-bioanode samples are shown as triangles. Orange triangles show communities of colonisers from primary inoculum. Dark-blue triangles show communities of colonisers from secondary inoculum. Black triangle indicates the OCP control community. Grey triangle shows the community of sludge accumulated in the multi-electrode reactor.

Weighted abundance data was used to build ordination plots showing a global view on the evolution in time of the bioanode community. Figure 7.16B shows the PCoA plot build on Bray-Curtis distance. This includes only electrode-like samples for which abundance can be expressed as cells/gram of carbon electrode. As opposed to Jaccard formula, Bray-Curtis distance takes into account the abundance of each taxon. A very important observation here is the arrangement of the electrode samples (OC colonisers from secondary inoculum and bioanodes) on a line in the same order as they were collected (shown by the red arrow in figure 7.16B). This pattern is called a time gradient and is typical for communities that change with time [284]. Collinearity occurs in this case because the abundance-based distance between initial and the developing community increases with time. It is important to observe the distance between time 3 and time 4 samples is smaller as compared to other successive sample pairs. The fact that the smaller distance is observed between the samples that are furthest apart in time signals that the community tends to a stable state. Electric currents have also stabilised during this time suggesting that the electrigenic biofilm has reached maturity.

7.4.7 Development of anodic biofilms assessed by confocal microscopy

Carbon felt has the 3D structure of a network made of crisscrossing loose threads with an average width of 20 μm. Therefore it provides for a representative material for building 3D electrodes. Carbon felt does not render itself to physical sectioning procedures due to its structure. Thin sections of carbon felt bioanodes fell apart due the loose packing of carbon threads. Optical sectioning does no suffer from this drawback. A piece of electrode is too thick to be placed between a microscopic slide and a glass slide. To accommodate for this a cassette was developed to fit samples of carbon felt electrodes. The cassette is shown in figure 3.11. Bioanode samples were treated with dead-live staining. The cassette and the mechanisms of dead-live staining were described in section 3.7.2.

For each field of view there are 3 sets of images, one for each color-channels which are shown in figure 7.2 as rows. Columns in figure 7.2 show images taken for each color channel corresponding to a z-scan depth value. Optical slices were obtained by joining images in each column. These show all biomass and carbon threads caught at a certain depth. All optical slices for a particular field of view can then be joined to create a general picture of the field of view in question. Figure 9.8 (appendix) shows all fields of view obtained in the upper halves of bioanodes and figure 9.9 (appendix) shows all field of views obtained in the lower half of the same bioanodes. These pictures give a perspective of each field of view showing red and green stained biomass surrounding carbon threads. They are useful for a general comparison of all fields of view. They show biofilms develop around carbon threads and the entire bioanode having the appearance of a biomat composed of numerous biofilms. The most obvious pattern is the consistent difference between biofilms developed on the lower half and upper half of the same bioanode. It was suggested that uneven coverage of bioelectrodes can occur in reactors with spatial heterogeneous conditions [285]. This could happen in the anodic chamber due to a range of factor such as anolyte flow regime or gas accumulation. It was also suggested that excess anode area can cause uneven and incomplete biomass coverage of bioanodes [208].

As seen in figure 7.17, there are 3 types of regions that can be identified. These are differentiated based on color (red, green and yellow). Where green and red channels overlap yellow regions result. Biofilms developed on the lower halves are thick and have a higher percentage of green regions. Conversely biofilms developed on the upper halves are thinner and are dominated by red regions. The interpretation of these regions is discussed in the following paragraph.

A close inspection shows the 3 regions are well separated spatially. The interpretation of what each region represents is based on the dead-live dying mechanism. Red fluorescence signals the presence of exposed DNA. This can be either from dead cells which are permeable to both dyes or from extraneous DNA. Many biofilms have DNA in their polymeric scaffold with structural roles [286–289]. DNA is negatively charged and can promote surface attachment directly or by other charged molecules that bind to it electrostatically [286]. Red regions are interpreted as dead biomass and/or structural DNA. Green fluorescence signals presence of compartmentalized DNA which could only exist as genomic DNA inside cells. Therefore green regions are allotted to live biomass. Yellow regions result from spatial overlap of green and red fluorescence. Because PI quenches SYTO 9 fluorescence it means that yellow regions contain a uniform mixture of compartmentalized DNA (live cells) and extraneous DNA. Yellow regions are interpreted as being the result of presence of live cells that are mixed with dead cells embedded in a scaffold which includes DNA with structural role.

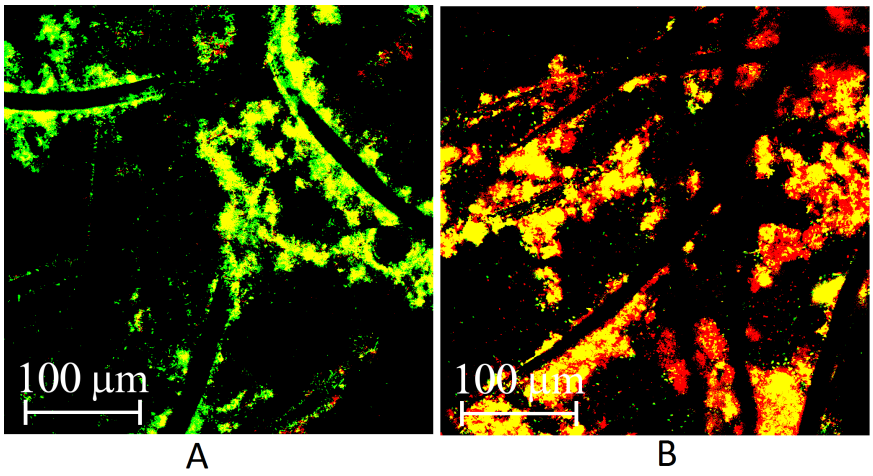

Figure 7.17: Identified regions in biofilms. Green shows live biomass, red shows dead biomass and yellow shows mixed biomass composed of both live and dead biomass. A: separation between live and mixed regions; B: separation between dead and mixed regions;

The perspective pictures (figures 9.8 and 9.9 in the appendix) show a mixture of green, red and yellow regions within the biofilms. Some spatial information is lost in the perspective view therefore the 3 regions cannot be well differentiated with this approach. Optical slices preservers that information. A few examples of optical slices are shown in figure 7.17. Yellow regions are present mainly inside biofilms.

7.4.8 Quantitative analysis of biofilm development on 3D electrodes

Cell numbers were extracted from microscopic images on biofilm but this method proved to be prone to errors. Cells in biofilm are close to each other leading to problems in their identification and an underestimation of their numbers. Furthermore the red channel images show smeared

regions which might originate from extraneous structural DNA or dead cells that have lost their integrity. Therefore extracting cell numbers by image processing is affected by errors.

Instead of cell numbers other parameters can be extracted from the images such biomass coverages and biovolumes [290–292]. Biomass coverage is calculated as the percentage of the total area in an optical slice occupied by biomass [292]. Biovolume in a field of view was estimated by summing over all optical slices in the given field of view the corresponding cell coverages multiplied by two factors: the z-scan step increment and total area of the optical slice [291]. The experimental design allows for visualising biofilm growth by following the evolution of biomass coverage and biovolumes over time.

Biomass coverages show percent of occupation of the entire biofilm by including live, dead and mixed regions. Carbon threads are not optically transparent as opposed to biomass. Because of this the visible portion in optical slices decreases with depth. To correct the coverage profiles first the percentage of visible portion in each optical slice was calculated. For this the area occupied by carbon threads in each slice was obtain. Next a series of images was created for each field of view to show cumulated carbon threads observed with depth. From these series the fraction of visible field in each optical slice was calculated as the number of pixels representing carbon threads minus total number of pixels present per optical slice. Coverage profiles were corrected by dividing coverage values by the fractions of visible field in the previous optical slice. The reason for using the visible fraction at the next slice in depth was because carbon threads detected in a certain optical slice do not cover biomass in the same slice but in the next.

Corrected profiles for the biomass coverage on the lower halves of the bioanodes are shown in figure 7.18. Figure 7.19 shows the same type of profiles extracted from the upper halves of the corresponding bioanodes. The common trend is that coverage increases initially, reaches a peak and then decreases with depth. The penetration power of the confocal microscope is limited by sample transparency. As the the z-scan proceeds the light from each optical slice is dimmed by top layers that include biomass and carbon threads.

The horizontal blue lines in figures 7.18 and 7.19 show the biomass centres. Their positions were averaged over each sample and are shown in figure 7.20. This shows that there is a tendency for biomass centers to move closer to the bioanode external face.

Biovolumes were extracted from the original images and are plotted in figure 7.21. Overall total biovolumes are bigger at the bottom of the electrodes than at the top. On the bottom halves of the bioanodes total biovolume has increased until time 3 and then experienced decrease at time 4. This decreased is mostly due to dead biovolume while the live biovolume has only slightly increased on average over the same period of time.

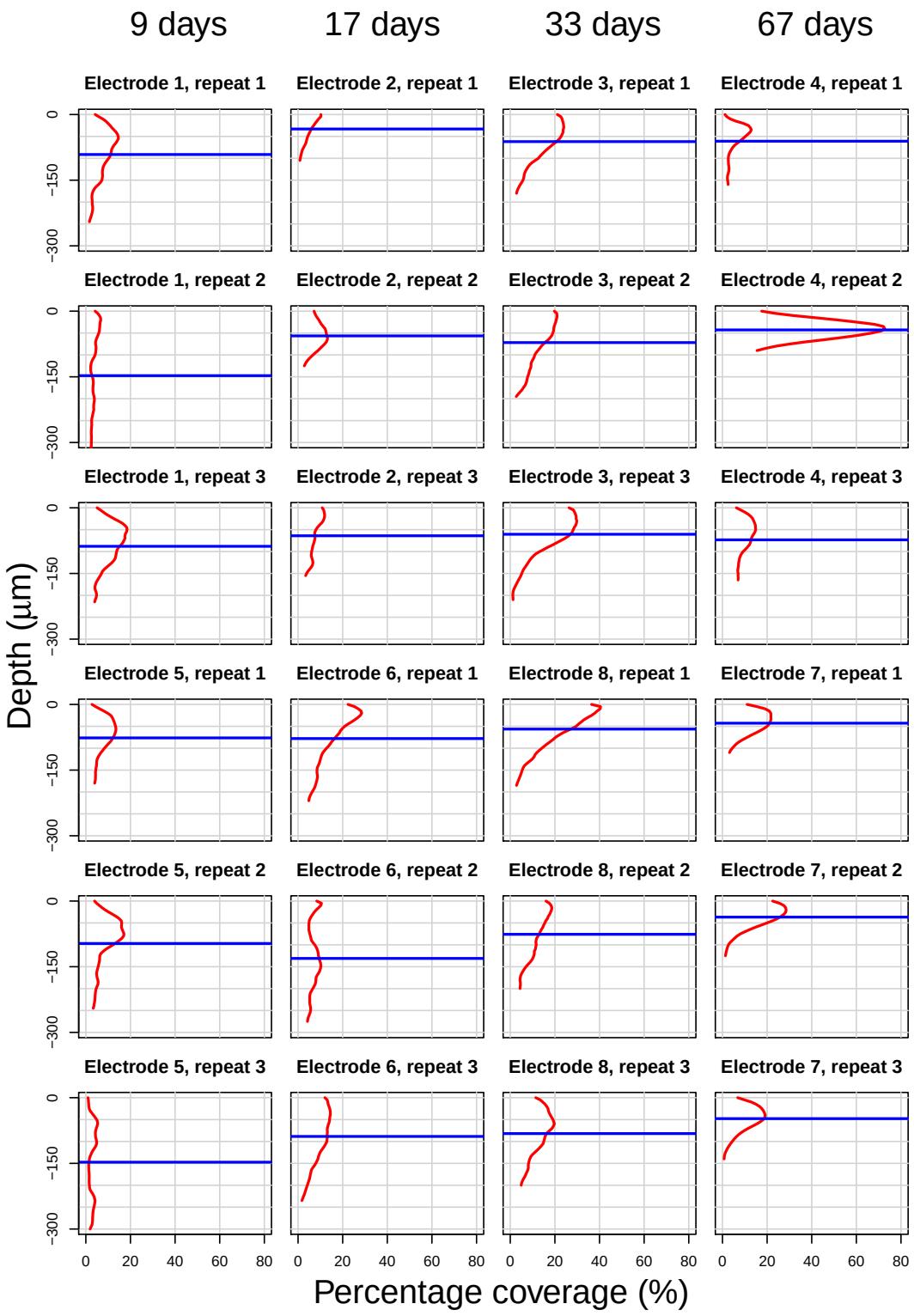

Figure 7.18: Biomass coverage profiles on the lower halves of the bioanodes. Columns are arranged from left to right in increasing order of time. All plots share the x-scale and y-scale. X-axis shows percentage of biomass coverage in an optical section. Y-axis shows depth in bioanode where an optical section was taken. Red lines show percentage of biomass coverage in optical sections with depth. Blue lines indicate position of biomass centers which separate equal biovolumes above and below.

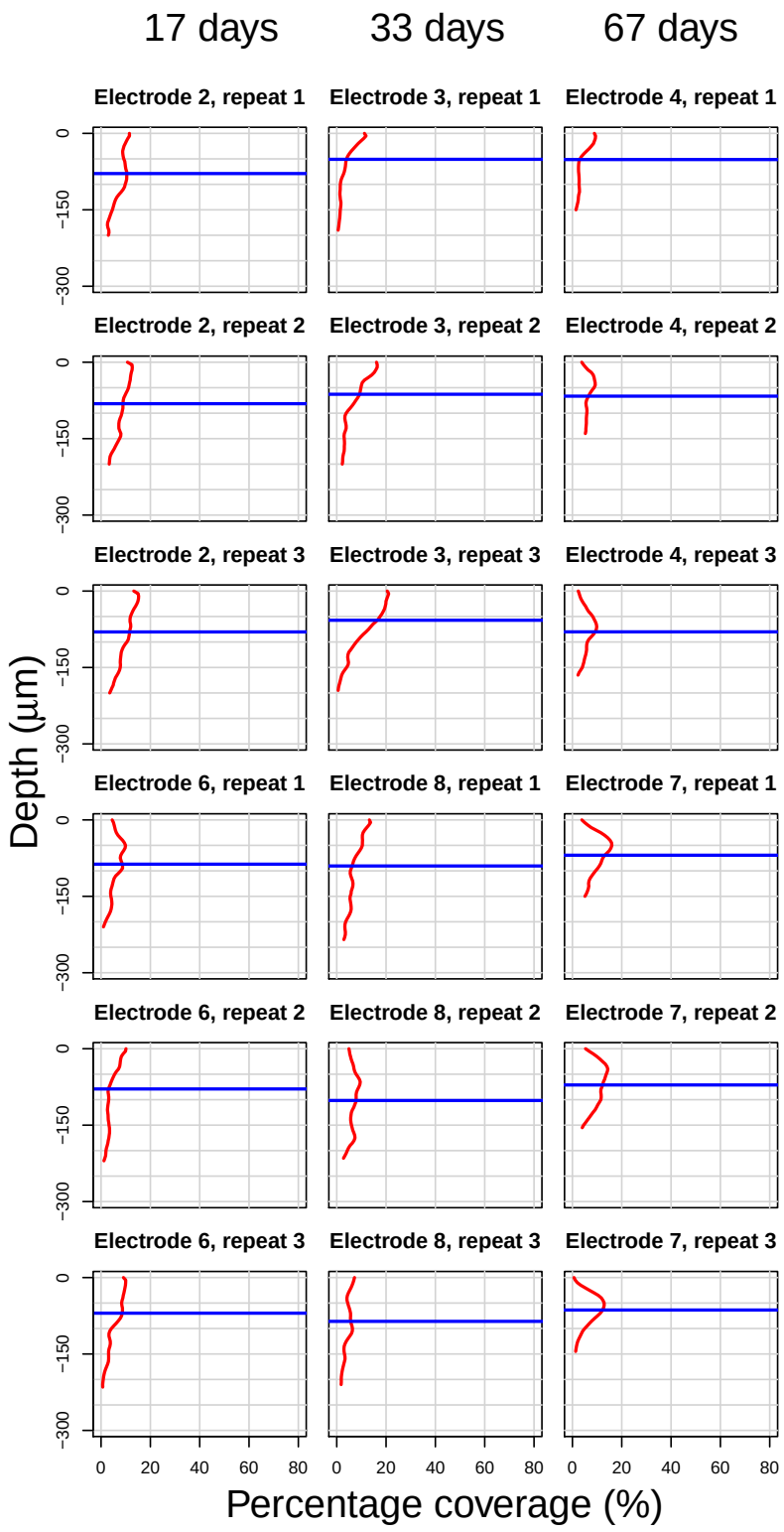

Figure 7.19: Biomass coverage profiles on the upper halves of the bioanodes. Columns are arranged from left to right in increasing order of time. All plots share the x-scale and y-scale. X-axis shows percentage of biomass coverage in an optical section. Y-axis shows depth in bioanode where an optical section was taken. Red lines show percentage of biomass coverage in optical sections with depth. Blue lines indicate position of biomass centers which separate equal biovolumes above and below.

Following the evolution of biomass centres in figure 7.20 one can notice that this has moved closer to the periphery of the electrode as biomass increased. Biovolumes are smaller at the top of the electrodes. Here the ratio between dead and live biomass is closer to 1 while at the bottom total biomass at the end of the run is dominated by the live fraction. Also the centre of the biomass has only slightly moved up to the periphery.

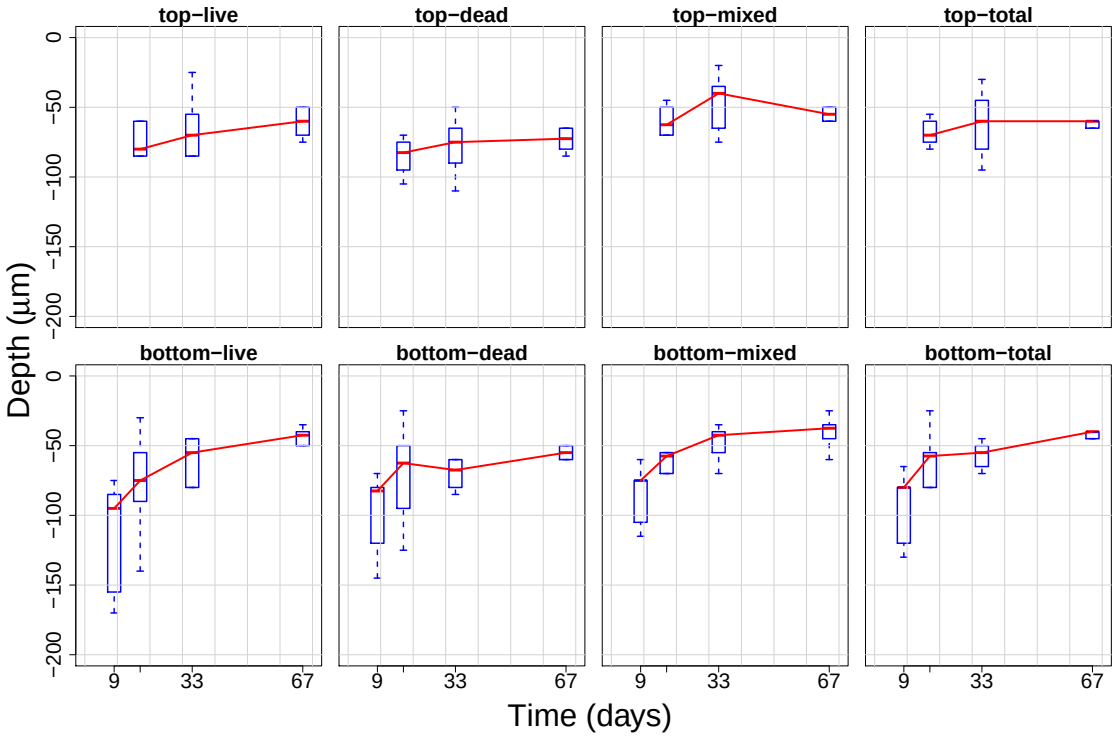

Figure 7.20: Evolution in time of dead, live, mixed and total biomass centers in the upper halves of bioanodes (top 4 plots) and lower halves of bioanodes (bottom 4 plots). Distribution of biomass centers is shown in blue. Red lines follow the evolution of center median with time.

The growth and distribution pattern of biomass can be explained by limitation in mass transfer inside the electrode. As biomass develops it limits the amount of substrate that can diffuse to the interior of the electrode hindering growth inside. Biomass acts both as a barrier to substrate diffusion and as a sink for substrate. The pattern is more pronounced at the lower halves of the bioanodes where total biovolume is bigger. At the top of the electrode biovolumes are smaller therefore are distributed deeper within the electrode. By the end of the run biomass centres at the top of electrode are placed at a depth of -60 µm and those from the bottom of the same electrodes are placed at -40 µm.

Younger biofilms (at 9 and 17 days) from the lower halves are dominated by dead biomass. In older biofilms (at 33 and 67 days) dead biomass has decreased while live and mixed biomass have increased. Also in older biofilms live regions surround mixed regions. This suggests that biofilms growth occur at their periphery.

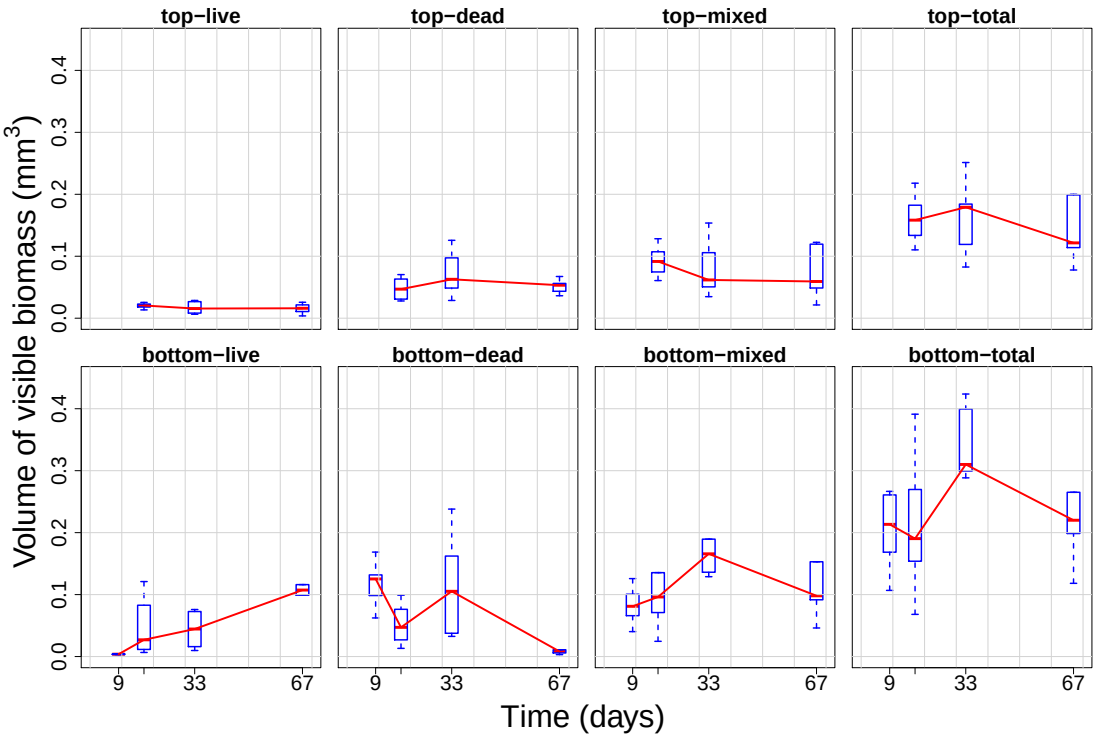

Figure 7.21: Evolution of dead, live, mixed and total biovolumes in the upper halves of bioanodes (top 4 plots) and lower halves of bioanodes (bottom 4 plots). Distribution of biovolumes is shown in blue. Red lines follow the evolution of biovolume median with time.

7.4.9 Correlations between current and biofilm development

The relation between current and biovolumes at the bottom and top sides of the anodes is shown as scatter plots in figure 7.22. Pearson correlations scores between current, biovolumes at the bottom side of bioanodes and total cell counts are shown in table 7.2. Current shows positive correlations to live, mixed and total biovolumes. The correlations are stronger for biovolumes measured at the bottom of the electrode. For both halves of the bioanodes current is better correlated to live and dead biovolumes and less correlated to total biovolume. Total biovolume is the sum of dead, live and mixed biovolumes each having a different trend in time therefore the smaller correlation between total biovolume and current. Current also shows poor correlation to total cell counts.

Dead and live biovolumes are negatively correlated. Figure 7.21 show that dead biovolume decreased over time while live and mixed biovolumes followed the opposite trend. This suggest that over time dead portions of the biofilm are removed and replaced by live cells. It is likely that the removal of dead biomass from biofilm is desirable for increasing current output from bioanodes.

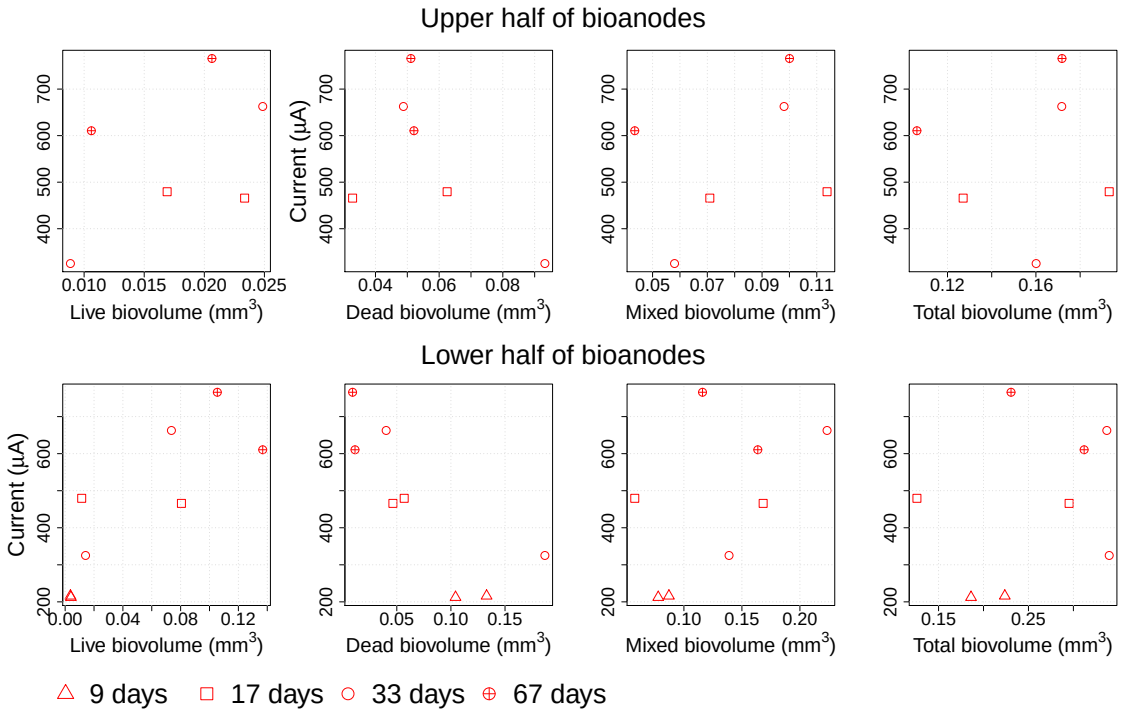

Figure 7.22: Correlation between current and live, dead, mixed and total biovolumes measured at the upper half of bioanodes (top 4 plots) and at the lower half of bioanodes (bottom 4 plots). Red symbols indicate bioanodes. Triangles - 9 day old bioanodes; Squares - 17 days old bioanodes; Circles - 33 days old bioanodes; Crossed circles - 67 days old bioanodes; Straight lines are linear fits.

Table 7.2: Pearson correlation matrix for current, cell counts and biovolumes at the lower halves of anodes (left side in each table cell) and upper halves of anodes (right side in each table cell)

	Current	Cell counts	Dead	Live	Mixed
Current	-				
Cell counts	0.639	-			
Dead biovolume	-0.816/-0.371	-0.207	-		
Live biovolume	0.819/0.485	0.518	-0.795/-0.885	-	
Mixed biovolume	0.512/0.371	0.637	-0.300/-0.085	0.615/0.428	-
Total biovolume	0.257/0.314	0.638	0.0587/0.2	0.470/0.2	0.887/0.943

As mentioned in section 7.2 at the third sampling time bioanodes 3 and 8 were collected because they showed the biggest difference in current output. Table 7.3 compares bioanode 3 and 8 in terms of current, cell counts and biovolumes. Cell counts and total biovolumes are very close to each other for both bioanodes. Bioanode 3 which produced the higher current is characterised by higher live biomass (0.07361 and 0.01413 mm^3 respectively) and lower dead biomass compared to bioanode 8 (0.04017 and 0.18682 mm^3 respectively). This pattern shows that current is strongly correlated to live and dead biomass but less to other parameters.

Table 7.3: Comparison between bioanodes 3 and 8

Bioanode	Current (μA)	Counts 10^6 cells/gram	Biovolume (mm^3) Dead	Live	Mixed	Total
3	662.63	36.2	0.04017	0.07361	0.2234	0.3371
8	325.23	35.9	0.18682	0.01413	0.1389	0.3398

7.5 Replication power of the multi-electrode reactor

Bioanodes grown in shared anolyte inside the MER showed smaller divergence as compared to bioanodes grown in replicate reactors. Divergence was measured here as UniFrac distances between replicates. A smaller divergence means better replication which is what the MER was designed for. UniFrac distances between pairs of replicates are plotted in figure 7.23.

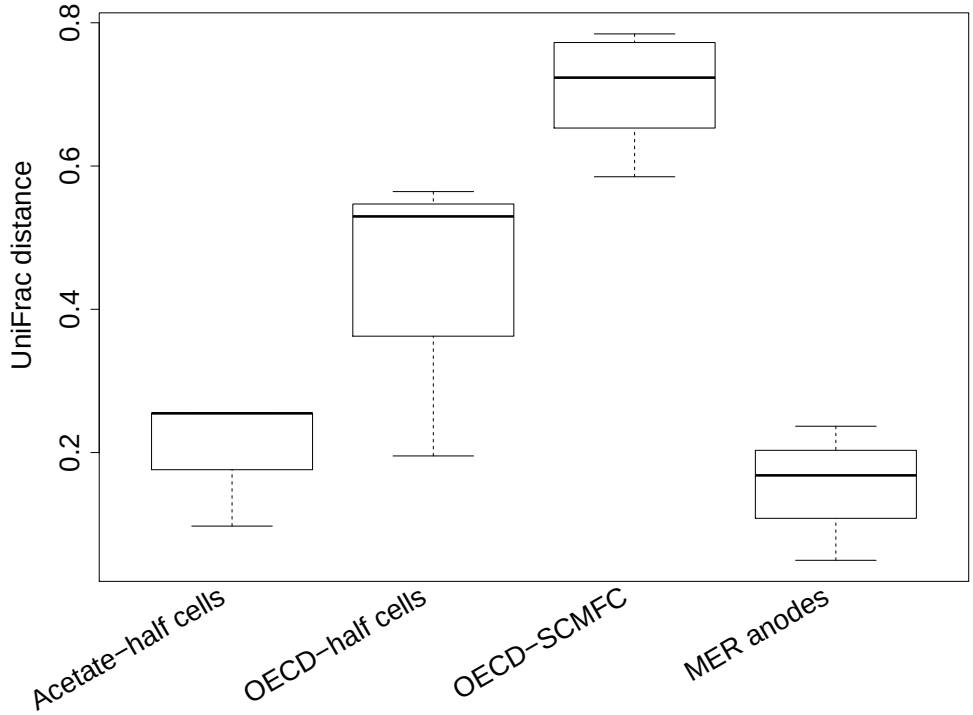

Figure 7.23: Comparison of replication between multi-electrode reactor (MER) and individual reactors based on UniFrac distances

The first two categories show the replication of the half-cells presented in chapter 5. The third category are distances between replicated SCMFCs used in chapter 6. The forth category are the distances between replicate bioanodes used in the study of biofilm dynamics presented in this chapter. Figure 7.23 shows that bioanodes grown in the MER have the smallest mean distances between replicates. Divergence is slightly higher for the anodes grown on acetate in half cells. The highest divergence is experienced by the SCMFCs fed on OECD anolyte. This shows that bioanodes grown

in shared anolyte experience less divergence and therefore a MER is a useful tool for studies that require to minimise differences between replicates.

7.6 Conclusions and future work

The MER has good replication power and can replace the use of separate reactors in studies that require many bioanodes. A MER needs less maintenance and ensures all bioanodes are exposed to the same treatment. Furthermore inter-electrode interference is negligible allowing for similar reactors to be build with higher number of bioanodes to increase replication. The MER was shown to be useful for material testing identifying carbon cloth as a better anode material than carbon felt.

The OC colonisation can enrich electrigens both from primary and secondary inocula. Acetate-end anolyte was proven to be a good inoculum unlike OECD anolyte. Also after the colonisation phase, bioanodes could not be fed directly on complex medium but instead they required a short period of pre-feeding on acetate.

Regarding biofilm development 3 phases can be identified characterised by changes in community composition and biofilm structure:

1. transition from inoculum to colonisers
2. transition from colonisers to anodic biofilms
3. bioanode maturation

Bacterial motility and presence of oxygen inside 3D electrodes are potentially important factors that drive the first transition. The current study was not able to catch the extent of the second transition as the bioanodes sampled at the 9^{th} day showed higher similarity to older bioanodes than to the coloniser samples regarding community composition and cell counts. This shows that important changes have occurred over a short time scale with high impact on anodic biofilms. The third phase includes less dramatic changes over a longer time scale. This transition is mainly characterised by changes that affect live and dead biomass, the distribution of biomass on electrodes and the percentage of *Geobacter*.

Total biovolume was relatively stable over all bioanodes, while dead biovolume experienced continuous decline accompanied by a continuous increase in live biovolume. Propidium iodide used in dead-live staining revealed granular regions which can be identified as dead cells but also smeared regions which opens the possibility that electrigenic biofilms have structural DNA in their composition. Further research is needed to investigate on the existence of structural DNA in anodic biofilms.

Over time the centre of biomass moved towards the periphery of the electrode suggesting that growth is limited by mass transfer. This observation has consequences on the design of 3D electrodes. 3D electrode materials are valued for their high surface area but the growth pattern of biofilms suggests that bioanode thickness can be decreased with no loss in performance. This can bring further improvements in the material costs of MESs.

Community composition has changed continuously from inoculum to the last bioanodes sampled. This changes were smallest between anodes collected at time 4 and the pair collected at time 3 although these time points are the farthest apart. This suggest that biofilms reach stability although *Geobacter* abundance has increased linearly with time. Biofilms developed on the lower and upper sides respectively, were consistently different. Community composition and cell counts also revealed differences between the two halves of the bioanodes. The uneven distribution of biomass on bioanodes remains unexplained and should be addressed by future research.

Chapter 8. Conclusions and future work

8.1 Summary

The main aim was to investigate how the anodic community is influenced by operational factors including light, anode poised potential, substrate and anode to cathode ratio. It was observed in all studies that the anodic community is highly variable in terms of composition and abundance. It was affected by substrate, time of sampling, anode poised potential, anode to cathode ratio and reactor type. Community analysis identified *Geobacter* as the main electrigenic genus of bacteria in all bioanodes. Other bacteria that were commonly found in bioanodes were *Dysgonomonas*, *Clostridium*, *Comamonas*, *Sphaerochaeta*, *Paludibacter*, *Cloacibacillus*, *Sedimentibacter*, *Azospira* and *Azospirillum*. These have also been commonly reported in the literature on bioanodes and should be viewed as components of anodic communities. Their functions and relation to electrigens remain unknown and should be the topic of future research.

The main findings together with practical implications, experimental limitations and recommendation for overcoming limitations are summarised below:

- Out of all operational factors investigated here, anolyte composition had the biggest impact on community and performance. This was observed in principal components analysis plots which showed that bioanodes were grouped first by substrate and secondly by anode poised potential or A/C ratio respectively. Bioanodes grown in acetate medium were characterised by higher bacterial densities, *Geobacter* abundance and current output. These could be explained by the higher COD content and conductivity of acetate anolyte compared to OECD anolyte.

- The practical outcome from the study of light effect was that all reactors used in the next 3 studies were protected from light. The fact that light leads to a decrease in *Geobacter* percentage accompanied by an increase in the percentage of anoxygenic photosynthetic bacteria supports the role of competitive exclusion in shaping the anodic community. An interesting observation was that light had no effect when the reactors were run for one cycle in the dark but resumed when 1 ml of a mixture of wastewater and activated sludge was added. This

is an example of an established electrigenic community that suffered from invading bacteria when conditions favour the latter. Other similar situations may be observed in the future and could also be explained using the principle of competitive exclusion.

- The study of anode potential effect has confirmed that abundance of electrigens increases with anode potential in acetate anolyte. Previous studies have reported on an increase in total biomass with anode potential. However they suffer from 2 factors. First they did not have access to true abundance of electrigens and secondly results were obtained by subsampling the same bioanodes. The present study does not suffer from the above mentioned drawbacks.

- A very important finding was the sudden increase in *Geobacter* abundance in acetate cell when anode potential was increased from -400 to -200 mV vs Ag/AgCl. Lack of linearity between anode poised potential and abundance of electrigens may be explained by the extension of electron transport chain (ETC) in response to higher anode potential. This in turn allows bacteria to harness more energy. This hypothesis can be tested in the future by exploring the effects at more anode potential values between -400 and -200 mV vs Ag/AgCl and by using specific inhibitors of ETC components.

- Total abundance and *Geobacter* percentage decreased with anode potential in OECD half cells but the cause of this remained unexplained. One possible explanation is that cell counts on OECD bioanodes were small enough to be affected by random variation. Therefore more work is required on investigating the effect of anode poised potential on bioanodes fed with complex substrate.

- It was observed that removing biomass from the surface of bioanodes resulted in increasing current output. It can be hypothesised here that dead biomass accumulates on bioanodes which then hinders current production. This aspect warrants a thorough investigation on the accumulation of dead biomass on bioanodes, its effects and ways of circumventing them. It may result in periodic bioanode regeneration by removing dead biomass as part of standard maintenance procedure for conserving/improving performance.

- In SCMFCs decreasing the anode area relatively to cathode area allowed for higher density of electrigens. This explains why power density decreases with anode area.

- The multi-electrode reactor used in this study showed better replication of bioanodes in terms of community composition compared to replicated reactors. Furthermore interference between anode-cathode pairs was negligible. The system required less maintenance compared to individual reactors and ensured that replicated bioanodes were exposed to similar environments as opposed to using a separate reactor for each replicate.

- The anodic community experienced the biggest changes during transition from inoculum

to colonisers and from colonisers to 9-days old bioanodes. More frequent sampling while the biofilms are still growing is required for investigating colonisation. Over 67 days the community composition stabilised accompanied by a decrease in the dead biovolume and an increase in live biovolume. This shows system stability over long periods of time which is necessary for BES applications. Also the study of community dynamics is important for the other 3 studies because it shows that bioanodes changed continuously. This suggest that bioanodes that were sampled after 30-50 days may not have reached maturity. The study of anodic community dynamics used sterile synthetic sewage and a time frame of only 67 days. For long term application of BESs it is necessary to investigate how the anodic community reacts when exposed to the biodiversity within real wastewater and how it behaves over longer periods of times.

- Biovolume was higher closer to the anolyte facing side of carbon felt bioanodes. This feature was more emphasized for older bioanodes. The fact that biomass grows closer towards the exterior of carbon felt was confirmed by imaging biomass across the entire depth of bioanodes. Electrigenic activity also decreased with depth. The reason behind this is that deeper within carbon felt electrigens are mass transfer limited. This suggests that using thinner anodes will decrease materials costs and also reduce unused volume inside scaled-up reactors.

- Biomass imaging on the entire bioanode showed that biomass did not grow uniformly on the surface of bioanodes. This was more pronounced in SCMFCs with limiting cathode but it also occurred in half-cells. It is possible that electrigens benefit from coaggregation which is one possible explanation for non-uniform biomass distribution. Other reasons might be due to chemical gradients formed inside the anodic chambers, non-uniform colonisation and the re-circulation of anolyte. Regarding the reason for uneven distribution of biomass on bioanodes this phenomenon deserves more investigation. Understanding it may bring further increase in performance and a reduction in material costs by minimising excess anode area.

8.2 Recommendations for future work

There are several important practical outcomes resulting from the work presented in this thesis:

1. Practical difficulties in replicating bioanodes can be circumvented by the use of multi-electrode reactors. This type of system deserve a place in the field of research on microbial electrochemical systems. Multi-electrode reactors can be applied for high-throughput electrode material testing. They could be upgraded in the future by increasing the number of electrode pairs or extend their application for replicating biocathodes as well.

2. The imaging technique presented here for visualising biomass on entire bioanodes will be very useful for future studies. The technique can be extended by including a calibration procedure that allows transformation of fluorescence measurements into biomass values. It will also benefit from using higher resolution cameras. It will be particular useful for scaling up efforts by providing investigators with information on how biomass distribution is influenced by local conditions inside reactors.

3. Biomass imaging on entire bioanodes has revealed that bioanodes are no covered uniformly with bacteria. Community analysis and confocal microscopy investigation have confirmed this observation. It is therefore recommended that future studies avoid subsampling of bioanodes because this can introduce unexplained variation.

4. Differences between using acetate and OECD complex substrate anolytes were noticed. In the case study of anode poised potential trends were opposite between the 2 anolytes. The implication is that care should be taken when generalising results acquired using acetate as electron donor. It is recommended that at least 2 anolyte composition to be used, one based on acetate and the other to contain a complex mixture that simulates wastewater or real wastewater.

5. Because light was shown to promote growth of bacteria that replace electrigens, it is recommended that proper measures should be taken to protect microbial electrochemical systems from light unless the aim of the study is to integrate light or study its effects on MESs. Real life MFC reactors will probably not be exposed to light due to practical reasons. However it is recommended that lab-scale MFC are protected from light because this can impact the conclusions and how they are extrapolated to upscaled reactors.

Chapter 9. Appendix A

Table 9.1: Total energy gain, cell counts and maximum current per cycle for bioanodes used for investigating the effect of anode poised potential.

Reactor	Total possible energy gain (J)	Cell counts $\times 10^6$ cells/gram	Maximum current (μA)		
			Cycle 1	Cycle 2	Cycle 3
-400AcA	365.91	248	1091	1004	1219
-400AcA	405.81	181	595	1151	1106
-200AcA	1173.38	1099	1914	2326	2310
-200AcB	1259.2	1448	2141	2385	2192
0AcA	1716.12	1419	2200	1986	1905
0AcB	1641.58	1441	2502	2075	1608
-400CSA	39.24	148	116	154	113
-400CSB	45.82	167	111	118	113
-200CSA	104.73	116	208	202	191
-200CSB	123.64	77	153	215	212
0CSA	149.42	53	130	124	148
0CSB	186.79	21	130	134	129

Table 9.2: Coulombic efficiency and COD removal rates per cycle for each bioanode used for investigating the effect of anode poised potential.

	Coulombic efficiency (%)			COD removal (%)		
Reactor	Cycle 1	Cycle 2	Cycle 3	Cycle 1	Cycle 2	Cycle 3
-400AcA	16.08	20.19	19.7	88.25	90.18	86.22
-400AcB	17.94	22.57	21.56	89.41	89.31	86.9
-200AcA	28.16	31.08	28.2	89.51	90.09	87.48
-200AcB	27.35	35.33	31.15	89.7	88.73	90.28
0AcA	23.53	25.44	35.56	91.44	87.67	89.8
0AcB	21.39	23.38	36.09	69.97	83.03	90.09
-400CSA	4.29	4.07	4.86	77.97	76.69	74.13
-400CSB	5.61	4.68	5.14	74.13	76.48	72
-200CSA	5.03	6.09	6.08	77.76	71.58	74.77
-200CSB	5.25	7.49	7.56	76.26	79.89	76.05
0CSA	5.36	5.3	5.55	71.36	74.77	78.61
0CSB	6.72	5.71	7.83	77.76	76.26	79.67

Table 9.3: Biodiversity indices of bioanodes used for investigating the effect of anode poised potential. Mid horizontal line separates acetate bioanodes from OECD bioanodes.

Reactor	Shannon	Simpson
-400AcA	4.96	0.81
-400AcB	5.28	0.82
-200AcA	5.37	0.85
-200AcB	4.23	0.72
0AcA	4.35	0.75
0AcB	4.57	0.78
-400CSA	6.88	0.95
-400CSB	7.36	0.96
-200CSA	5.68	0.85
-200CSB	6.37	0.92
0CSA	6.55	0.94
0CSB	6.58	0.94

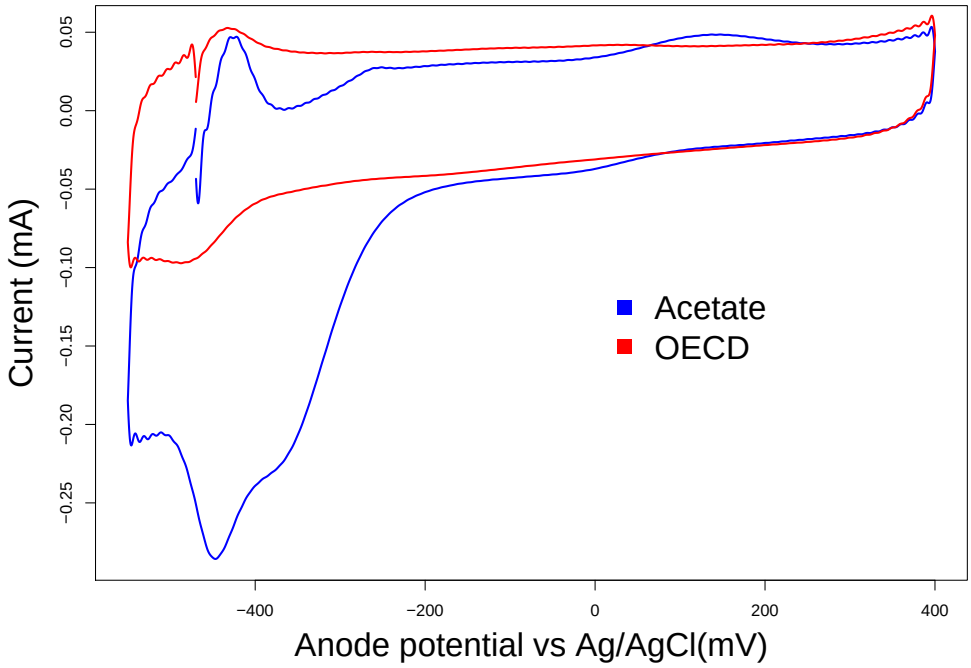

Figure 9.1: Control CVs at 5 mV/s

Table 9.4: Biodiversity indices of bioanodes used for investigating the effect of anode to cathode surface area ratio. Mid horizontal line separates acetate bioanodes from OECD bioanodes.

Reactor	Shannon index	Simpson index
Ac1to24A	5.82	0.9
Ac1to12A	6.41	0.93
Ac1to6A	7.11	0.96
Ac1to3A	7.19	0.96
Ac1to1A	5.72	0.86
Acto8to1A	6.77	0.96
CS1to24A	7.08	0.96
CS1to6A	7.36	0.97
CS1to3A	7.17	0.97
CS2to3A	7.47	0.97
CS1to1A	7.34	0.98
CS2to1A	6.73	0.95
CS4to1A	7.01	0.97
CS8to1A	7.05	0.95

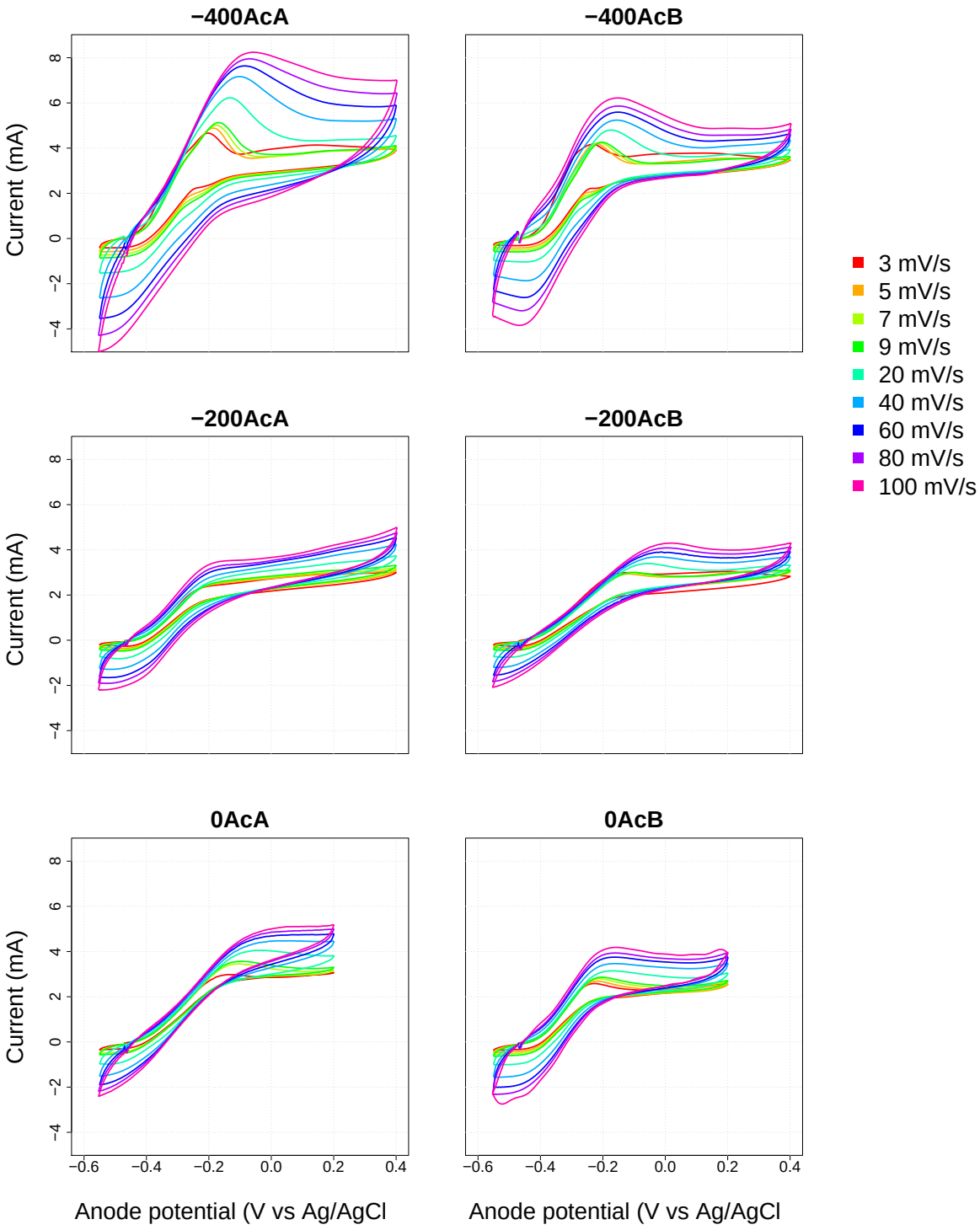

Figure 9.2: All CVs on acetate cell from potential study

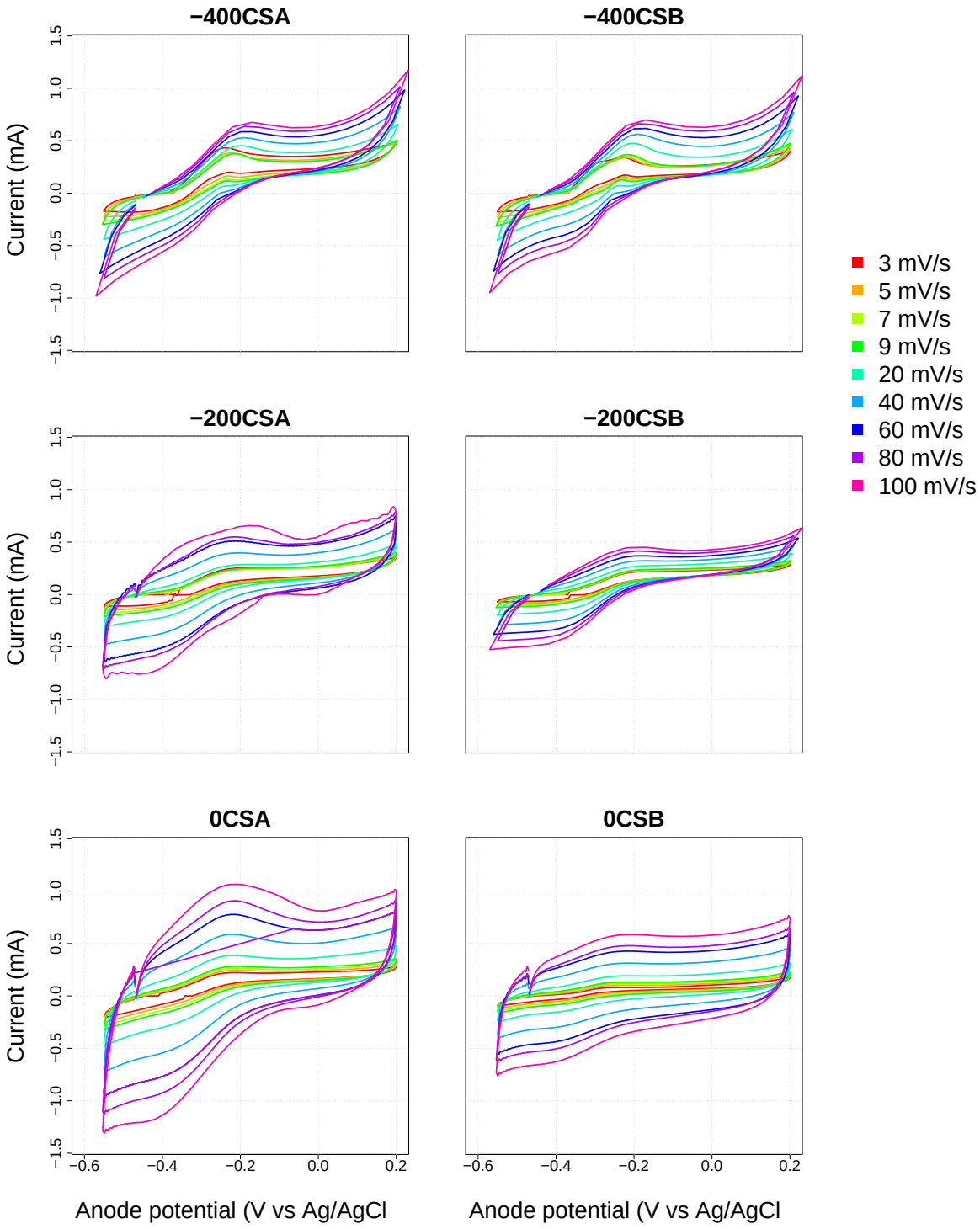

Figure 9.3: All CVs on OECD cell from potential study

Table 9.5: Total energy gain, cell counts and maximum current per cycle for bioanodes used for investigating the effect of anode to cathode surface area ratio. Mid horizontal line separates acetate bioanodes from OECD bioanodes.

Reactor	Total possible energy gain (J)	Cell counts $\times 10^6$ cells/gram	Maximum current (μA)			
			Cycle 1	Cycle 2	Cycle 3	Cycle 4
Ac1to24A	228.67	1718	250.31	483.09	563.98	499.41
Ac1to12A	233.68	1057	449.54	525.76	600.55	587.81
Ac1to6A	224.38	796	394.98	607.89	611.31	576.86
Ac1to3A	243.50	424	425.69	558.52	631.63	597.00
Ac1to1A	197.42	719	548.85	620.71	609.21	584.21
Acto8to1A	133.26	756	456.88	422.15	404.81	400.01
CS1to24A	89.90	425	68.72	70.63	57.80	-
CS1to6A	92.48	378	217.44	151.70	184.03	-
CS1to3A	136.56	71	365.80	322.63	283.75	-
CS2to3A	134.57	39	308.59	303.58	296.94	-
CS1to1A	112.27	80	301.35	311.26	276.89	-
CS2to1A	194.10	67	298.12	259.79	251.59	-
CS4to1A	201.47	79	267.22	239.73	239.77	-
CS8to1A	62.96	54	184.55	168.73	168.51	-

Table 9.6: COD removal rates for SCMFCs used for investigating the effect of anode to cathode surface area ratio.

Reactor	COD removal rate (%)				Coulombic efficiency (%)			
	Cycle1	Cycle2	Cycle3	Cycle4	Cycle1	Cycle2	Cycle3	Cycle4
Ac1to24A	93.9	92.5	93.2	91.09	4.59	14.18	16.08	12.93
Ac1to12A	90.04	88.86	87.89	90.04	7.31	10.36	11.92	15.45
Ac1to6A	78.21	88.57	89.06	78.41	7.39	20.5	20.6	14.54
Ac1to3A	87.34	91.21	89.45	89.45	3.58	15.38	17.45	17.41
Ac1to1A	93.55	91.21	91.56	90.97	9.74	18.29	11.45	18.36
Ac8to1A	91.79	94.96	91.68	95.66	6.79	10.42	9.57	8.8
CS1to24A	96.39	80.39	87.35	-	1.52	2.32	1.54	-
CS1to6A	98.19	82.45	84	-	3.3	2.99	3.47	-
CS1to3A	79.78	80.22	78.49	-	9.91	7.56	9.94	-
CS2to3A	91.74	80.65	81.42	-	5.59	7.73	10.87	-
CS1to1A	93.29	84.52	89.16	-	5.12	5.65	6.43	-
CS2to1A	80.65	81.08	81.08	-	8.19	7.46	8.07	-
CS4to1A	81.08	81.51	80.65	-	10.14	9.12	7.3	-
CS8to1A	91.48	88.39	79.61	-	5.74	4.98	5.32	-

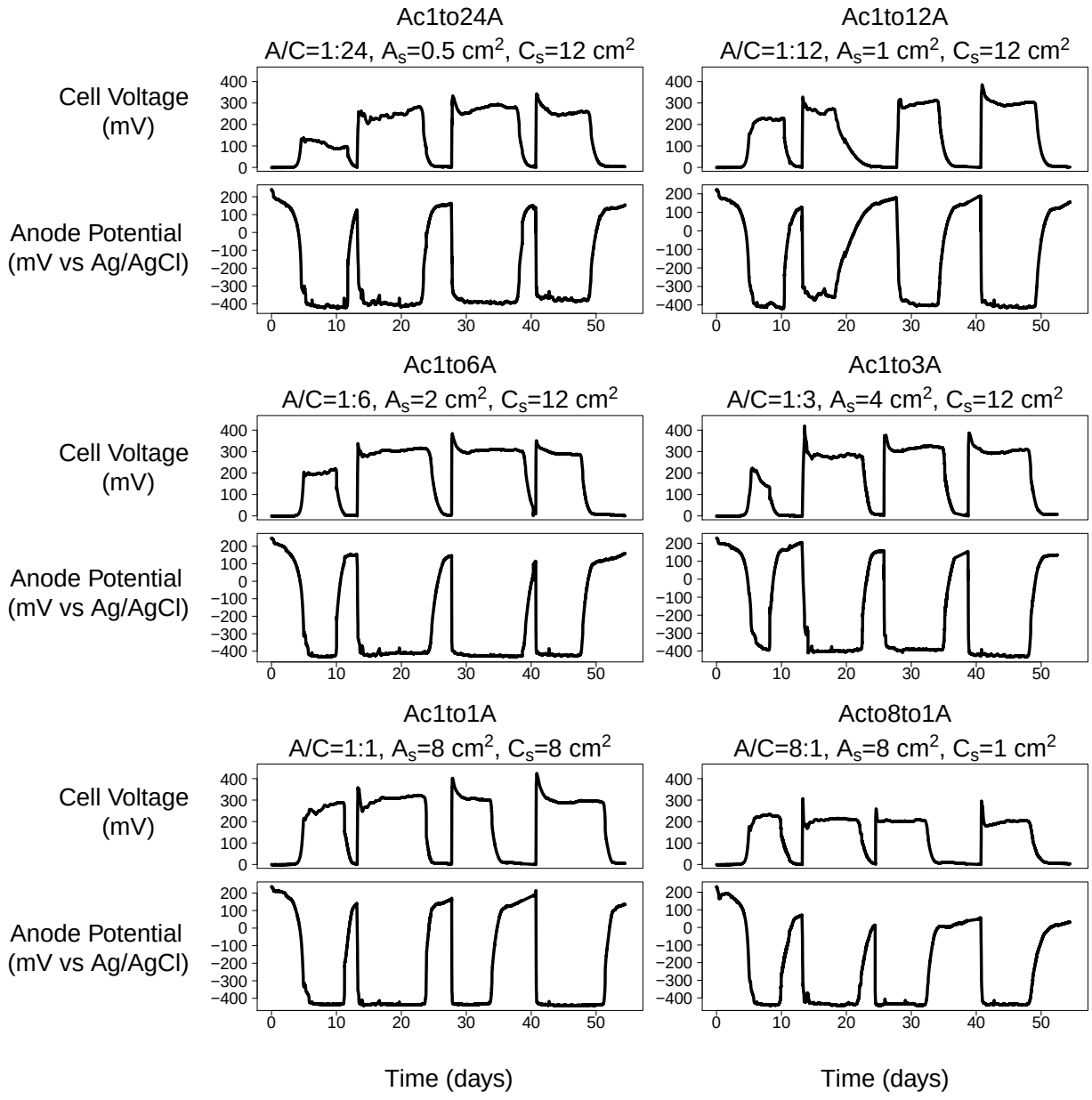

Figure 9.4: CP profiles for acetate SCMFCs. Cell voltages are placed above their corresponding anode potentials for each bioanode. A/C anode to cathode surface area ratio; A_s anode area; C_s cathode area;

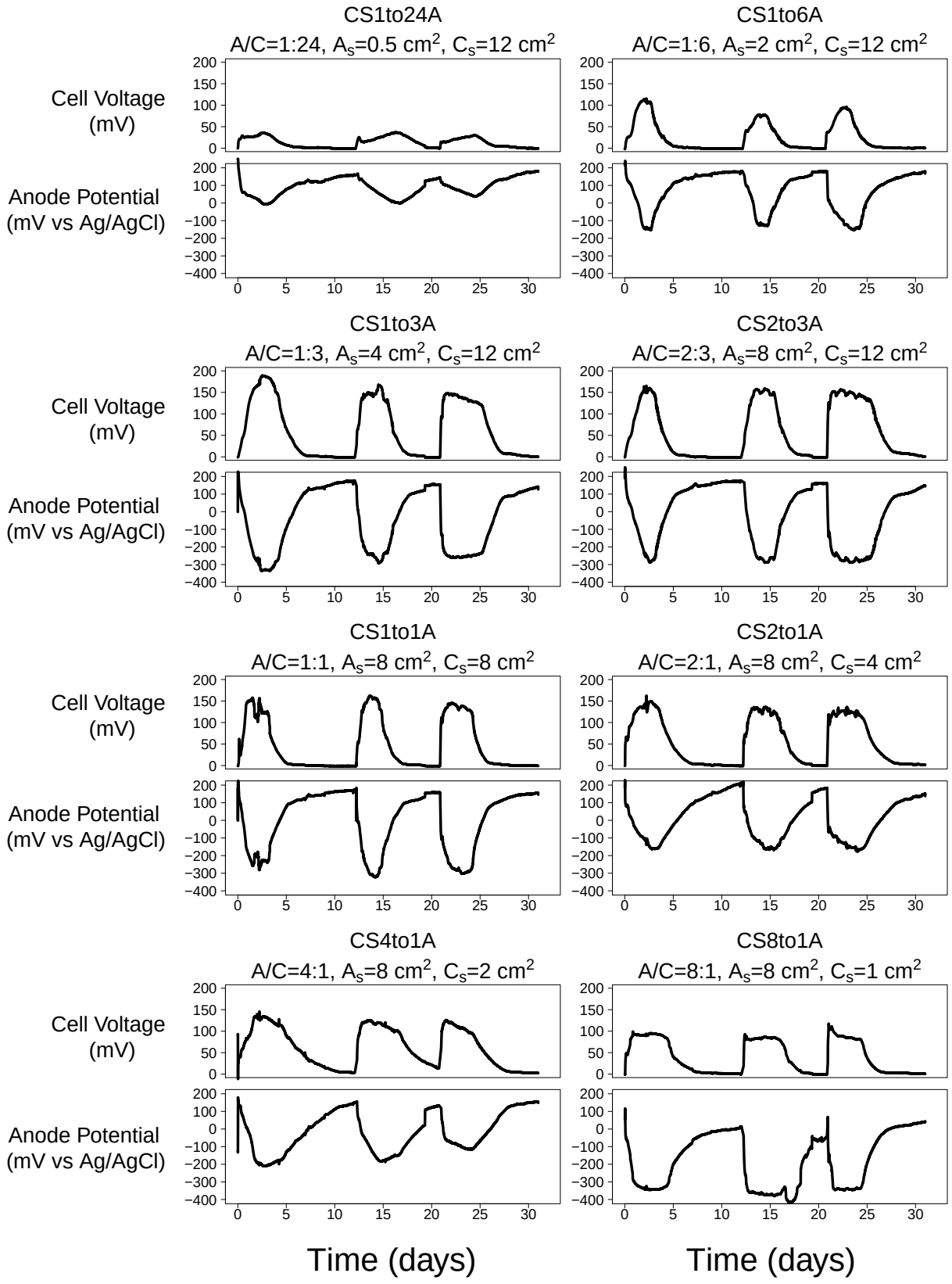

Figure 9.5: CP profiles for OECD SCMFCs. Pre-feeding cycles are not included. Cell voltages are placed above their corresponding anode potentials for each bioanode. A/C anode to cathode surface area ratio; A_s anode area; C_s cathode area;

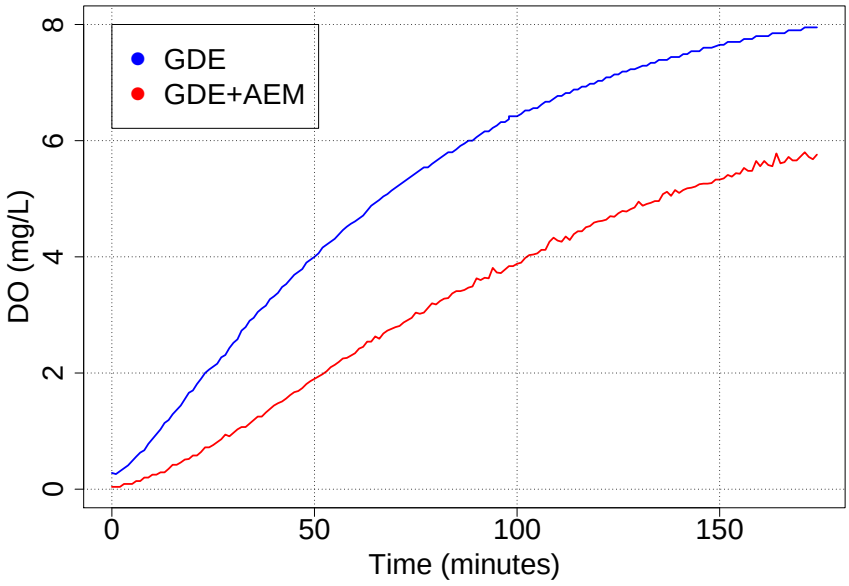

Figure 9.6: Oxygen influx through GDE and AEM

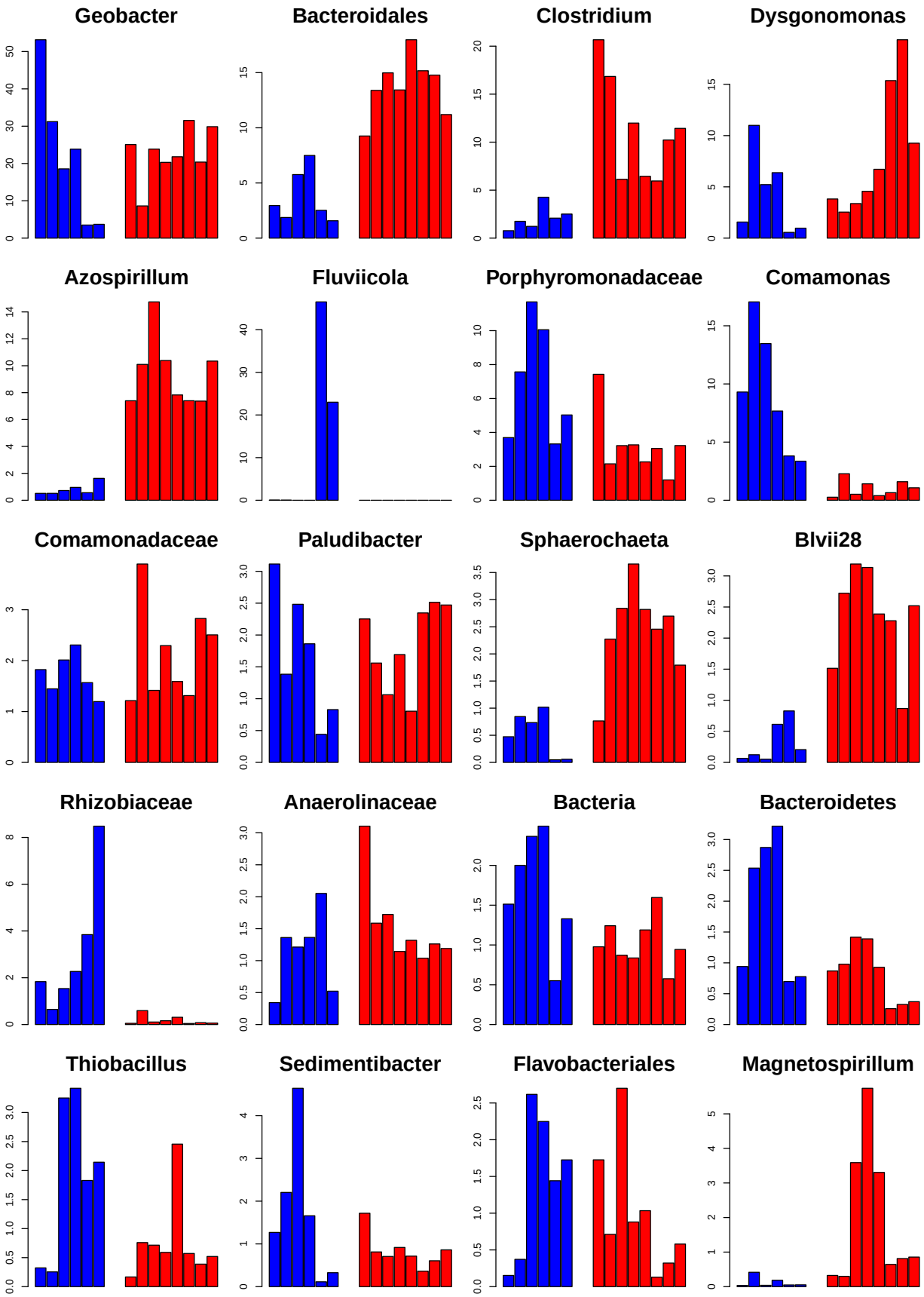

Figure 9.7: First 20 most abundant genus-level taxons in A/C study. Acetate cells are shown in blue and OECD cells are shown in red.

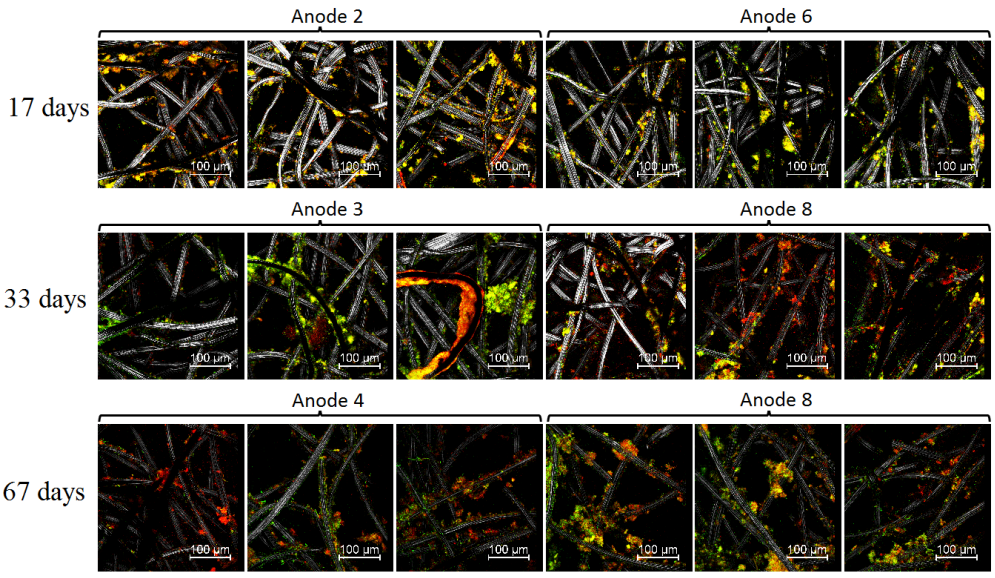

Figure 9.8: Perspective pictures of the fields of view obtained on the upper halves of bioanodes. Rows are arranged from top to bottom in increasing order of the time of sampling. Each perspective picture was obtained by combining all optical sections taken from the same field of view.

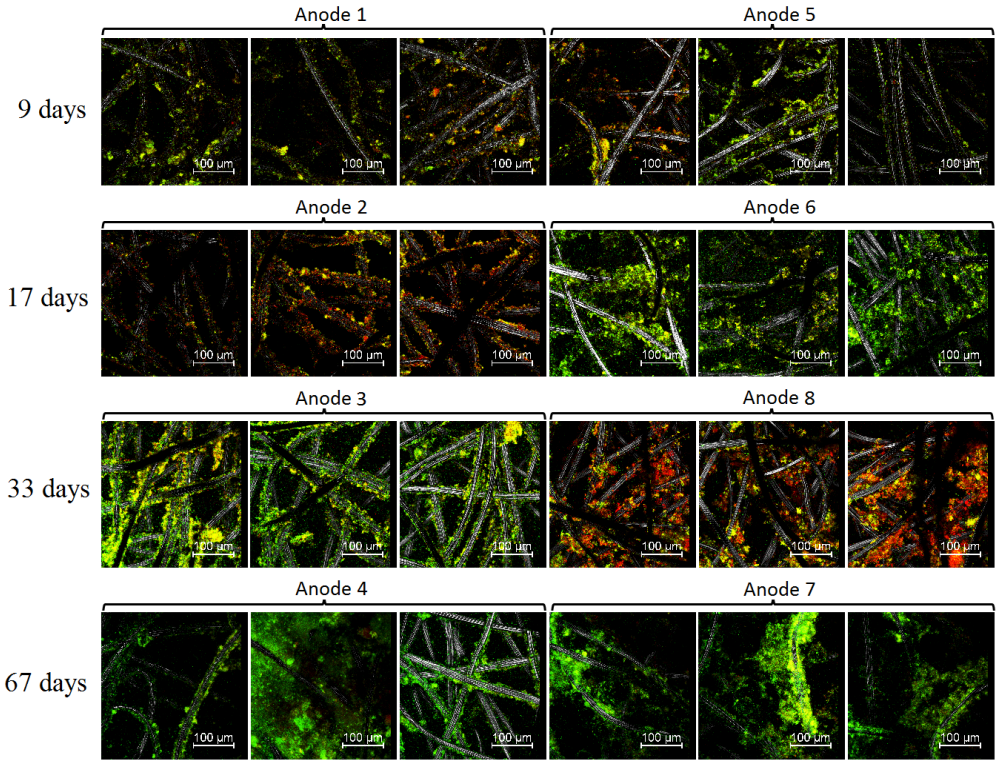

Figure 9.9: Perspective pictures of the fields of view visualised on the bottom halves of bioanodes. Rows are arranged from top to bottom in increasing order of the time of sampling. Each perspective picture was obtained by combining all optical sections taken from the same field of view.

References

[1] Bruce Logan. Harvesting energy from wastewater treatment. *Penn State University. http://www. engr. psu. edu/ce/enve/logan/web presentations/Logan-BuschAward-10-5-04. pdf*, 2004.

[2] Peter Aelterman, Korneel Rabaey, Peter Clauwaert, and Willy Verstraete. Microbial fuel cells for wastewater treatment. *Water Science & Technology*, 54(8):9–15, 2006.

[3] Lars Peter Nielsen, Nils Risgaard-Petersen, Henrik Fossing, Peter Bondo Christensen, and Mikio Sayama. Electric currents couple spatially separated biogeochemical processes in marine sediment. *Nature*, 463(7284):1071–1074, 2010.

[4] Korneel Rabaey and René A Rozendal. Microbial electrosynthesis revisiting the electrical route for microbial production. *Nature Reviews Microbiology*, 8(10):706–716, 2010.

[5] Liang Su, Wenzhao Jia, Changjun Hou, and Yu Lei. Microbial biosensors: a review. *Biosensors and Bioelectronics*, 26(5):1788–1799, 2011.

[6] Jose Rodrigo, Karina Boltes, and Abraham Esteve-Nuñez. Microbial-electrochemical bioremediation and detoxification of dibenzothiophene-polluted soil. *Chemosphere*, 101:61–65, 2014.

[7] Heming Wang and Zhiyong Jason Ren. A comprehensive review of microbial electrochemical systems as a platform technology. *Biotechnology advances*, 31(8):1796–1807, 2013.

[8] Souichiro Kato. Biotechnological aspects of microbial extracellular electron transfer. *Microbes and Environments*, 30(2):133, 2015.

[9] Michael J McInerney, Jessica R Sieber, and Robert P Gunsalus. Syntrophy in anaerobic global carbon cycles. *Current opinion in biotechnology*, 20(6):623–632, 2009.

[10] Ximena C Abrevaya, Pablo JD Mauas, and Eduardo Cortón. Microbial fuel cells applied to the metabolically based detection of extraterrestrial life. *Astrobiology*, 10(10):965–971, 2010.

[11] Mohamed Y El-Naggar, Yuri A Gorby, Wei Xia, and Kenneth H Nealson. The molecular density of states in bacterial nanowires. *Biophysical journal*, 95(1):L10–L12, 2008.

[12] M Rosenbaum, MT Agler, JJ Fornero, A Venkataraman, and LT Angenent. Integrating bes in the wastewater and sludge treatment line. *Bioelectrochemical Systems: From Extracellular Electron Transfer to Biotechnological Application*, pages 393–421, 2010.

[13] Igor Bodik and MIROSLAVA Kubaská. Energy and sustainability of operation of a wastewater treatment plant. *Environment Protection Engineering*, 39(2):15–24, 2013.

[14] Bruce E Logan. *Microbial fuel cells*. John Wiley & Sons, 2008.

[15] Yue Dong, Youpeng Qu, Weihua He, Yue Du, Jia Liu, Xiaoyu Han, and Yujie Feng. A 90-liter stackable baffled microbial fuel cell for brewery wastewater treatment based on energy self-sufficient mode. *Bioresource technology*, 195:66–72, 2015.

[16] Zheng Ge, Liao Wu, Fei Zhang, and Zhen He. Energy extraction from a large-scale microbial fuel cell system treating municipal wastewater. *Journal of Power Sources*, 297:260–264, 2015.

[17] Firas Khaled, Olivier Ondel, and Bruno Allard. Microbial fuel cells as power supply of a low-power temperature sensor. *Journal of Power Sources*, 306:354–360, 2016.

[18] Avinash Shantaram, Haluk Beyenal, Raaja Raajan Angathevar Veluchamy, and Zbigniew Lewandowski. Wireless sensors powered by microbial fuel cells. *Environmental science & technology*, 39(13):5037–5042, 2005.

[19] Ioannis Ieropoulos, John Greenman, and Chris Melhuish. Microbial fuel cells based on carbon veil electrodes: stack configuration and scalability. *International Journal of Energy Research*, 32(13):1228–1240, 2008.

[20] Kun Dong, Boyang Jia, Chaoling Yu, Wenbo Dong, Fangzhou Du, and Hong Liu. Microbial fuel cell as power supply for implantable medical devices: a novel configuration design for simulating colonic environment. *Biosensors and Bioelectronics*, 41:916–919, 2013.

[21] Fernanda Leite Lobo, Heming Wang, Casey Forrestal, and Zhiyong Jason Ren. Ac power generation from microbial fuel cells. *Journal of Power Sources*, 297:252–259, 2015.

[22] Alim Dewan, Conrad Donovan, Deukhyoun Heo, and Haluk Beyenal. Evaluating the performance of microbial fuel cells powering electronic devices. *Journal of Power Sources*, 195(1):90–96, 2010.

[23] Wei-Eng Thung, Soon-An Ong, Li-Ngee Ho, Yee-Shian Wong, Fahmi Ridwan, Yoong-Ling Oon, Yoong-Sin Oon, and Harvinder Kaur Lehl. A highly efficient single chambered up-

flow membrane-less microbial fuel cell for treatment of azo dye acid orange 7-containing wastewater. *Bioresource technology*, 197:284–288, 2015.

[24] Ke Han, Pei-Lin Yueh, Lian-Jie Qin, Chuan-Chung Hsueh, and Bor-Yann Chen. Deciphering synergistic characteristics of microbial fuel cell-assisted dye decolorization. *Bioresource technology*, 196:746–751, 2015.

[25] Bor-Yann Chen, Bin Xu, Pei-Lin Yueh, Ke Han, Lian-Jie Qin, and Chung-Chuan Hsueh. Deciphering electron-shuttling characteristics of thionine-based textile dyes in microbial fuel cells. *Journal of the Taiwan Institute of Chemical Engineers*, 51:63–70, 2015.

[26] Bor-Yann Chen, Chih-Ming Ma, Ke Han, Pei-Lin Yueh, Lian-Jie Qin, and Chuan-Chung Hsueh. Influence of textile dye and decolorized metabolites on microbial fuel cell-assisted bioremediation. *Bioresource technology*, 200:1033–1038, 2016.

[27] Jeffrey M Foley, René A Rozendal, Christopher K Hertle, Paul A Lant, and Korneel Rabaey. Life cycle assessment of high-rate anaerobic treatment, microbial fuel cells, and microbial electrolysis cells. *Environmental science & technology*, 44(9):3629–3637, 2010.

[28] Abhilasha Singh Mathuriya and JV Yakhmi. Microbial fuel cells to recover heavy metals. *Environmental chemistry letters*, 12(4):483–494, 2014.

[29] Sebastià Puig, Marc Serra, Ariadna Vilar-Sanz, Marina Cabré, Lluís Bañeras, Jesús Colprim, and M Dolors Balaguer. Autotrophic nitrite removal in the cathode of microbial fuel cells. *Bioresource technology*, 102(6):4462–4467, 2011.

[30] Yan Li, Isaiah Williams, Zhiheng Xu, Baikun Li, and Baitao Li. Energy-positive nitrogen removal using the integrated short-cut nitrification and autotrophic denitrification microbial fuel cells (mfcs). *Applied Energy*, 163:352–360, 2016.

[31] Peter Clauwaert, Korneel Rabaey, Peter Aelterman, Liesje De Schamphelaire, The Hai Pham, Pascal Boeckx, Nico Boon, and Willy Verstraete. Biological denitrification in microbial fuel cells. *Environmental science & technology*, 41(9):3354–3360, 2007.

[32] Bernardino Virdis, Korneel Rabaey, Zhiguo Yuan, and Jürg Keller. Microbial fuel cells for simultaneous carbon and nitrogen removal. *Water research*, 42(12):3013–3024, 2008.

[33] Yong Jiang, Peng Liang, Changyong Zhang, Yanhong Bian, Xufei Yang, Xia Huang, and Peter R Girguis. Enhancing the response of microbial fuel cell based toxicity sensors to cu (ii) with the applying of flow-through electrodes and controlled anode potentials. *Bioresource technology*, 190:367–372, 2015.

[34] Michelle Rasmussen and Shelley D Minteer. Long-term arsenic monitoring with an enterobacter cloacae microbial fuel cell. *Bioelectrochemistry*, 106:207–212, 2015.

[35] Zhidan Liu, Jing Liu, Baoming Li, Yuanhui Zhang, and Xin-Hui Xing. Focusing on the process diagnosis of anaerobic fermentation by a novel sensor system combining microbial fuel cell, gas flow meter and ph meter. *International Journal of Hydrogen Energy*, 39(25):13658–13664, 2014.

[36] Hyung Joo Kim, Moon Sik Hyun, In Seop Chang, and Byung Hong Kim. A microbial fuel cell type lactate biosensor using a metal-reducing bacterium, shewanella putrefaciens. *J. Microbiol. Biotechnol*, 9(3):365–367, 1999.

[37] Kui Hyun Kang, Jae Kyung Jang, Hyunsoo Moon, In Seop Chang, Byung Hong Kim, et al. A microbial fuel cell with improved cathode reaction as a low biochemical oxygen demand sensor. *Biotechnology letters*, 25(16):1357–1361, 2003.

[38] Yinghua Feng and Willie F Harper. Biosensing with microbial fuel cells and artificial neural networks: laboratory and field investigations. *Journal of environmental management*, 130:369–374, 2013.

[39] RT Gill, Michael John Harbottle, JWN Smith, and SF Thornton. Electrokinetic-enhanced bioremediation of organic contaminants: A review of processes and environmental applications. *Chemosphere*, 107:31–42, 2014.

[40] Lu Lu, Tyler Huggins, Song Jin, Yi Zuo, and Zhiyong Jason Ren. Microbial metabolism and community structure in response to bioelectrochemically enhanced remediation of petroleum hydrocarbon-contaminated soil. *Environmental science & technology*, 48(7):4021–4029, 2014.

[41] De-Yin Huang, Shun-Gui Zhou, Qing Chen, Bo Zhao, Yong Yuan, and Li Zhuang. Enhanced anaerobic degradation of organic pollutants in a soil microbial fuel cell. *Chemical engineering journal*, 172(2):647–653, 2011.

[42] Carolina Cruz Viggi, Enrica Presta, Marco Bellagamba, Saulius Kaciulis, Santosh K Balijepalli, Giulio Zanaroli, Marco Petrangeli Papini, Simona Rossetti, and Federico Aulenta. The oil-spill snorkel: an innovative bioelectrochemical approach to accelerate hydrocarbons biodegradation in marine sediments. *Frontiers in microbiology*, 6, 2015.

[43] Junyeong An, Bongkyu Kim, Jonghyeon Nam, How Yong Ng, and In Seop Chang. Comparison in performance of sediment microbial fuel cells according to depth of embedded anode. *Bioresource technology*, 127:138–142, 2013.

[44] Liam Doherty, Yaqian Zhao, Xiaohong Zhao, Yuansheng Hu, Xiaodi Hao, Lei Xu, and Ranbin Liu. A review of a recently emerged technology: Constructed wetland–microbial fuel cells. *Water research*, 85:38–45, 2015.

[45] Yan-Li Zhou, Hui-Fang Wu, Zai-Sheng Yan, Hai-Yuan Cai, and He-Long Jiang. The enhanced survival of submerged macrophyte potamogeton malaianus by sediment microbial fuel cells. *Ecological Engineering*, 87:254–262, 2016.

[46] Kirsten JJ Steinbusch, Hubertus VM Hamelers, Joris D Schaap, Christel Kampman, and Cees JN Buisman. Bioelectrochemical ethanol production through mediated acetate reduction by mixed cultures. *Environmental science & technology*, 44(1):513–517, 2009.

[47] Rene A Rozendal, Adriaan W Jeremiasse, Hubertus VM Hamelers, and Cees JN Buisman. Hydrogen production with a microbial biocathode. *Environmental Science & Technology*, 42(2):629–634, 2007.

[48] A Escapa, R Mateos, EJ Martínez, and J Blanes. Microbial electrolysis cells: An emerging technology for wastewater treatment and energy recovery. from laboratory to pilot plant and beyond. *Renewable and Sustainable Energy Reviews*, 55:942–956, 2016.

[49] Michael S Rappe and Stephen J Giovannoni. The uncultured microbial majority. *Annual Reviews in Microbiology*, 57(1):369–394, 2003.

[50] Guo-Wei Chen, Soo-Jung Choi, Jae-Hwan Cha, Tae-Ho Lee, and Chang-Won Kim. Microbial community dynamics and electron transfer of a biocathode in microbial fuel cells. *Korean Journal of Chemical Engineering*, 27(5):1513–1520, 2010.

[51] César Iván Torres. On the importance of identifying, characterizing, and predicting fundamental phenomena towards microbial electrochemistry applications. *Current opinion in biotechnology*, 27:107–114, 2014.

[52] Bruce E Logan. Exoelectrogenic bacteria that power microbial fuel cells. *Nature Reviews Microbiology*, 7(5):375–381, 2009.

[53] Derek R Lovley. Bug juice: harvesting electricity with microorganisms. *Nature Reviews Microbiology*, 4(7):497–508, 2006.

[54] Doo Hyun Park and J Gregory Zeikus. Electricity generation in microbial fuel cells using neutral red as an electronophore. *Applied and environmental microbiology*, 66(4):1292–1297, 2000.

[55] Hengduo Xu and Xiangchun Quan. Anode modification with peptide nanotubes encapsulating riboflavin enhanced power generation in microbial fuel cells. *International Journal of Hydrogen Energy*, 2015.

[56] Enrico Marsili, Daniel B Baron, Indraneel D Shikhare, Dan Coursolle, Jeffrey A Gralnick, and Daniel R Bond. Shewanella secretes flavins that mediate extracellular electron transfer. *Proceedings of the National Academy of Sciences*, 105(10):3968–3973, 2008.

[57] Korneel Rabaey, Nico Boon, Monica Höfte, and Willy Verstraete. Microbial phenazine production enhances electron transfer in biofuel cells. *Environmental science & technology*, 39(9):3401–3408, 2005.

[58] Yan Qiao, Ya-Juan Qiao, Long Zou, Cai-Xia Ma, and Jian-Hua Liu. Real-time monitoring of phenazines excretion in pseudomonas aeruginosa microbial fuel cell anode using cavity microelectrodes. *Bioresource Technology*, 198:1–6, 2015.

[59] Arvind Venkataraman, Miriam Rosenbaum, Jan BA Arends, Rayko Halitschke, and Largus T Angenent. Quorum sensing regulates electric current generation of pseudomonas aeruginosa pa14 in bioelectrochemical systems. *Electrochemistry Communications*, 12(3):459–462, 2010.

[60] Hyung Joo Kim, Hyung Soo Park, Moon Sik Hyun, In Seop Chang, Mia Kim, and Byung Hong Kim. A mediator-less microbial fuel cell using a metal reducing bacterium, shewanella putrefaciens. *Enzyme and Microbial Technology*, 30(2):145–152, 2002.

[61] Uwe Schröder. Anodic electron transfer mechanisms in microbial fuel cells and their energy efficiency. *Physical Chemistry Chemical Physics*, 9(21):2619–2629, 2007.

[62] Daniel R Bond, Sarah M Strycharz-Glaven, Leonard M Tender, and César I Torres. On electron transport through geobacter biofilms. *ChemSusChem*, 5(6):1099–1105, 2012.

[63] Jessica E Butler, Franz Kaufmann, Maddalena V Coppi, Cinthia Núñez, and Derek R Lovley. Maca, a diheme c-type cytochrome involved in fe (iii) reduction by geobacter sulfurreducens. *Journal of bacteriology*, 186(12):4042–4045, 2004.

[64] Zarath M Summers, Heather E Fogarty, Ching Leang, Ashley E Franks, Nikhil S Malvankar, and Derek R Lovley. Direct exchange of electrons within aggregates of an evolved syntrophic coculture of anaerobic bacteria. *Science*, 330(6009):1413–1415, 2010.

[65] T Proft and EN Baker. Pili in gram-negative and gram-positive bacteria - structure, assembly and their role in disease. *Cellular and molecular life sciences*, 66(4):613–635, 2009.

[66] Numfon Eaktasang, Christina S Kang, Heejun Lim, Oh Sung Kwean, Suyeon Cho, Yohan Kim, and Han S Kim. Production of electrically-conductive nanoscale filaments by sulfate-reducing bacteria in the microbial fuel cell. *Bioresource Technology*, 2016.

[67] Rachel M Snider, Sarah M Strycharz-Glaven, Stanislav D Tsoi, Jeffrey S Erickson, and Leonard M Tender. Long-range electron transport in geobacter sulfurreducens biofilms is redox gradient-driven. *Proceedings of the National Academy of Sciences*, 109(38):15467–15472, 2012.

[68] Hana Yi, Kelly P Nevin, Byoung-Chan Kim, Ashely E Franks, Anna Klimes, Leonard M Tender, and Derek R Lovley. Selection of a variant of geobacter sulfurreducens with enhanced capacity for current production in microbial fuel cells. *Biosensors and Bioelectronics*, 24(12):3498–3503, 2009.

[69] Gemma Reguera, Kevin D McCarthy, Teena Mehta, Julie S Nicoll, Mark T Tuominen, and Derek R Lovley. Extracellular electron transfer via microbial nanowires. *Nature*, 435(7045):1098–1101, 2005.

[70] Ashley E Franks, Kelly P Nevin, Hongfei Jia, Mounir Izallalen, Trevor L Woodard, and Derek R Lovley. Novel strategy for three-dimensional real-time imaging of microbial fuel cell communities: monitoring the inhibitory effects of proton accumulation within the anode biofilm. *Energy & Environmental Science*, 2(1):113–119, 2009.

[71] Jerome T Babauta, Hung Duc Nguyen, and Haluk Beyenal. Redox and ph microenvironments within shewanella oneidensis mr-1 biofilms reveal an electron transfer mechanism. *Environmental science & technology*, 45(15):6654–6660, 2011.

[72] Jinwei Zhang, Enren Zhang, Keith Scott, and J Grant Burgess. Enhanced electricity production by use of reconstituted artificial consortia of estuarine bacteria grown as biofilms. *Environmental science & technology*, 46(5):2984–2992, 2012.

[73] Rachel A Yoho, Sudeep C Popat, Laura Rago, Albert Guisasola, and César I Torres. Anode biofilms of geoalkalibacter ferrihydriticus exhibit electrochemical signatures of multiple electron transport pathways. *Langmuir*, 31(45):12552–12559, 2015.

[74] Renata Toczylowska-Maminska, Karolina Szymona, Hubert Madej, Wan Zhen Wong, Agnieszka Bala, Wojciech Brutkowski, Krzysztof Krajewski, Paik San H'ng, and Mariusz Maminski. Cellulolytic and electrogenic activity of enterobacter cloacae in mediatorless microbial fuel cell. *Applied Energy*, 160:88–93, 2015.

[75] Hyung Soo Park, Byung Hong Kim, Hyo Suk Kim, Hyung Joo Kim, Gwang Tae Kim, Mia Kim, In Seop Chang, Yong Keun Park, and Hyo Ihl Chang. A novel electrochemically active

and fe (iii)-reducing bacterium phylogenetically related to clostridium butyricum isolated from a microbial fuel cell. *Anaerobe*, 7(6):297–306, 2001.

[76] J Vilas Boas, VB Oliveira, LRC Marcon, DP Pinto, M Simões, and AMFR Pinto. Effect of operating and design parameters on the performance of a microbial fuel cell with lactobacillus pentosus. *Biochemical Engineering Journal*, 104:34–40, 2015.

[77] Eliseo Herrero-Hernández, TJ Smith, and Robert Akid. Electricity generation from wastewaters with starch as carbon source using a mediatorless microbial fuel cell. *Biosensors and Bioelectronics*, 39(1):194–198, 2013.

[78] Chin-Yu Lee, Kuo-Ling Ho, Duu-Jong Lee, Ay Su, and Jo-Shu Chang. Electricity harvest from nitrate/sulfide-containing wastewaters using microbial fuel cell with autotrophic denitrifier, pseudomonas sp. c27. *international journal of hydrogen energy*, 37(20):15827–15832, 2012.

[79] Qian Fu, Hajime Kobayashi, Hideo Kawaguchi, Javier Vilcaez, Tatsuki Wakayama, Haruo Maeda, and Kozo Sato. Electrochemical and phylogenetic analyses of current-generating microorganisms in a thermophilic microbial fuel cell. *Journal of bioscience and bioengineering*, 115(3):268–271, 2013.

[80] Dawn E Holmes, Daniel R Bond, and Derek R Lovley. Electron transfer by desulfobulbus propionicus to fe (iii) and graphite electrodes. *Applied and Environmental Microbiology*, 70(2):1234–1237, 2004.

[81] Christina S Kang, Numfon Eaktasang, Dae-Young Kwon, and Han S Kim. Enhanced current production by desulfovibrio desulfuricans biofilm in a mediator-less microbial fuel cell. *Bioresource technology*, 165:27–30, 2014.

[82] Daniel R Bond and Derek R Lovley. Evidence for involvement of an electron shuttle in electricity generation by geothrix fermentans. *Applied and environmental microbiology*, 71(4):2186–2189, 2005.

[83] Prathap Parameswaran, Tyson Bry, Sudeep C Popat, Bradley G Lusk, Bruce E Rittmann, and César I Torres. Kinetic, electrochemical, and microscopic characterization of the thermophilic, anode-respiring bacterium thermincola ferriacetica. *Environmental science & technology*, 47(9):4934–4940, 2013.

[84] Kelly C Wrighton, Peter Agbo, Falk Warnecke, Karrie A Weber, Eoin L Brodie, Todd Z DeSantis, Philip Hugenholtz, Gary L Andersen, and John D Coates. A novel ecological role of the firmicutes identified in thermophilic microbial fuel cells. *The ISME journal*, 2(11):1146–1156, 2008.

[85] Yi Zuo, Defeng Xing, John M Regan, and Bruce E Logan. Isolation of the exoelectrogenic bacterium ochrobactrum anthropi yz-1 by using a u-tube microbial fuel cell. *Applied and environmental microbiology*, 74(10):3130–3137, 2008.

[86] Cuong Anh Pham, Sung Je Jung, Nguyet Thu Phung, Jiyoung Lee, In Seop Chang, Byung Hong Kim, Hana Yi, and Jongsik Chun. A novel electrochemically active and fe (iii)-reducing bacterium phylogenetically related to aeromonas hydrophila, isolated from a microbial fuel cell. *FEMS Microbiology Letters*, 223(1):129–134, 2003.

[87] Carlo Santoro, Sofia Babanova, Kateryna Artyushkova, Jose A Cornejo, Linnea Ista, Orianna Bretschger, Enrico Marsili, Plamen Atanassov, and Andrew J Schuler. Influence of anode surface chemistry on microbial fuel cell operation. *Bioelectrochemistry*, 106:141–149, 2015.

[88] Shun'ichi Ishii, Kazuya Watanabe, Soichi Yabuki, Bruce E Logan, and Yuji Sekiguchi. Comparison of electrode reduction activities of geobacter sulfurreducens and an enriched consortium in an air-cathode microbial fuel cell. *Applied and environmental microbiology*, 74(23):7348–7355, 2008.

[89] Ruud A Timmers, Michael Rothballer, David PBTB Strik, Marion Engel, Stephan Schulz, Michael Schloter, Anton Hartmann, Bert Hamelers, and Cees Buisman. Microbial community structure elucidates performance of glyceria maxima plant microbial fuel cell. *Applied microbiology and biotechnology*, 94(2):537–548, 2012.

[90] Prathap Parameswaran, Husen Zhang, César I Torres, Bruce E Rittmann, and Rosa Krajmalnik-Brown. Microbial community structure in a biofilm anode fed with a fermentable substrate: the significance of hydrogen scavengers. *Biotechnology and bioengineering*, 105(1):69–78, 2010.

[91] Dawn E Holmes, Kelly P Nevin, Oona L Snoeyenbos-West, Trevor L Woodard, Justin N Strickland, and Derek R Lovley. Protozoan grazing reduces the current output of microbial fuel cells. *Bioresource technology*, 193:8–14, 2015.

[92] CE Reimers, P Girguis, HA Stecher, LM Tender, N Ryckelynck, and P Whaling. Microbial fuel cell energy from an ocean cold seep. *Geobiology*, 4(2):123–136, 2006.

[93] Lu Lu, Defeng Xing, and Zhiyong Jason Ren. Microbial community structure accompanied with electricity production in a constructed wetland plant microbial fuel cell. *Bioresource technology*, 195:115–121, 2015.

[94] DE Holmes, DR Bond, RA O'neil, CE Reimers, LR Tender, and DR Lovley. Microbial communities associated with electrodes harvesting electricity from a variety of aquatic sediments. *Microbial ecology*, 48(2):178–190, 2004.

[95] Na Song, He-Long Jiang, Hai-Yuan Cai, Zai-Sheng Yan, and Yan-Li Zhou. Beyond enhancement of macrophyte litter decomposition in sediments from a terrestrialized shallow lake through bioanode employment. *Chemical Engineering Journal*, 279:433–441, 2015.

[96] Xiaojing Li, Xin Wang, Zhiyong Jason Ren, Yueyong Zhang, Nan Li, and Qixing Zhou. Sand amendment enhances bioelectrochemical remediation of petroleum hydrocarbon contaminated soil. *Chemosphere*, 141:62–70, 2015.

[97] Yeng Fung Choo, Jiyoung Lee, In Seop Chang, and Byung Hong Kim. Bacterial communities in microbial fuel cells enriched with high concentrations of glucose and glutamate. *Journal of microbiology and biotechnology*, 16(9):1481, 2006.

[98] Guangli Liu, Shuxian Yu, Haiping Luo, Renduo Zhang, Shiyu Fu, and Xiaonan Luo. Effects of salinity anions on the anode performance in bioelectrochemical systems. *Desalination*, 351:77–81, 2014.

[99] Sokhee Jung and John M Regan. Influence of external resistance on electrogenesis, methanogenesis, and anode prokaryotic communities in microbial fuel cells. *Applied and environmental microbiology*, 77(2):564–571, 2011.

[100] Jian Sun, Wanjun Li, Youming Li, Yongyou Hu, and Yaping Zhang. Redox mediator enhanced simultaneous decolorization of azo dye and bioelectricity generation in air-cathode microbial fuel cell. *Bioresource technology*, 142:407–414, 2013.

[101] Shun'ichi Ishii, Shino Suzuki, Trina M Norden-Krichmar, Angela Wu, Yuko Yamanaka, Kenneth H Nealson, and Orianna Bretschger. Identifying the microbial communities and operational conditions for optimized wastewater treatment in microbial fuel cells. *Water research*, 47(19):7120–7130, 2013.

[102] Hao-Yi Cheng, Bin Liang, Yang Mu, Min-Hua Cui, Kun Li, Wei-Min Wu, and Ai-Jie Wang. Stimulation of oxygen to bioanode for energy recovery from recalcitrant organic matter aniline in microbial fuel cells (mfcs). *Water research*, 81:72–83, 2015.

[103] Cuijie Feng, Anyi Hu, Shaohua Chen, and Chang-Ping Yu. A decentralized wastewater treatment system using microbial fuel cell techniques and its response to a copper shock load. *Bioresource technology*, 143:76–82, 2013.

[104] Guotao Sun, Anders Thygesen, and Anne S Meyer. Acetate is a superior substrate for microbial fuel cell initiation preceding bioethanol effluent utilization. *Applied microbiology and biotechnology*, 99(11):4905–4915, 2015.

[105] Shun'ichi Ishii, Shino Suzuki, Trina M Norden-Krichmar, Tony Phan, Greg Wanger, Kenneth H Nealson, Yuji Sekiguchi, Yuri A Gorby, and Orianna Bretschger. Microbial popula-

tion and functional dynamics associated with surface potential and carbon metabolism. *The ISME journal*, 8(5):963–978, 2014.

[106] Yanmei Sun, Jincheng Wei, Peng Liang, and Xia Huang. Electricity generation and microbial community changes in microbial fuel cells packed with different anodic materials. *Bioresource technology*, 102(23):10886–10891, 2011.

[107] Urania Michaelidou, Annemiek ter Heijne, Gerrit Jan W Euverink, Hubertus VM Hamelers, Alfons JM Stams, and Jeanine S Geelhoed. Microbial communities and electrochemical performance of titanium-based anodic electrodes in a microbial fuel cell. *Applied and environmental microbiology*, 77(3):1069–1075, 2011.

[108] Sokhee Jung and John M Regan. Comparison of anode bacterial communities and performance in microbial fuel cells with different electron donors. *Applied microbiology and biotechnology*, 77(2):393–402, 2007.

[109] Lihong Liu, Olga Tsyganova, Duu-Jong Lee, Ay Su, Jo-Shu Chang, Aijie Wang, and Nanqi Ren. Anodic biofilm in single-chamber microbial fuel cells cultivated under different temperatures. *international journal of hydrogen energy*, 37(20):15792–15800, 2012.

[110] Husen Zhang, Xi Chen, Daniel Braithwaite, and Zhen He. Phylogenetic and metagenomic analyses of substrate-dependent bacterial temporal dynamics in microbial fuel cells. *PloS one*, 9(9):e107460, 2014.

[111] A Bridier, E Desmond-Le Quemener, C Bureau, P Champigneux, L Renvoise, J-M Audic, E Blanchet, A Bergel, and T Bouchez. Successive bioanode regenerations to maintain efficient current production from biowaste. *Bioelectrochemistry*, 106:133–140, 2015.

[112] Hui Yu, Chunhua Feng, Xiaoping Liu, Xiaoyun Yi, Yuan Ren, and Chaohai Wei. Enhanced anaerobic dechlorination of polychlorinated biphenyl in sediments by bioanode stimulation. *Environmental Pollution*, 211:81–89, 2016.

[113] Pan Yu Wong, Ka Yu Cheng, Anna H Kaksonen, David C Sutton, and Maneesha P Ginige. Enrichment of anodophilic nitrogen fixing bacteria in a bioelectrochemical system. *Water research*, 64:73–81, 2014.

[114] Bibiana Cercado, Nathalie Byrne, Marie Bertrand, Diana Pocaznoi, Mickaël Rimboud, Wafa Achouak, and Alain Bergel. Garden compost inoculum leads to microbial bioanodes with potential-independent characteristics. *Bioresource technology*, 134:276–284, 2013.

[115] Paul G Dennis, Kun Guo, Michael Imelfort, Paul Jensen, Gene W Tyson, and Korneel Rabaey. Spatial uniformity of microbial diversity in a continuous bioelectrochemical system. *Bioresource technology*, 129:599–605, 2013.

[116] Stephanie F Ketep, Alain Bergel, Marie Bertrand, Wafa Achouak, and Eric Fourest. Lowering the applied potential during successive scratching/re-inoculation improves the performance of microbial anodes for microbial fuel cells. *Bioresource technology*, 127:448–455, 2013.

[117] Stéphanie F Ketep, Alain Bergel, Marie Bertrand, Mohamed Barakat, Wafa Achouak, and Eric Fourest. Forming microbial anodes with acetate addition decreases their capability to treat raw paper mill effluent. *Bioresource technology*, 164:285–291, 2014.

[118] Narcís Pous, Alessandro A Carmona-Martínez, Anna Vilajeliu-Pons, Erika Fiset, Lluis Bañeras, Eric Trably, M Dolors Balaguer, Jesús Colprim, Nicolas Bernet, and Sebastià Puig. Bidirectional microbial electron transfer: Switching an acetate oxidizing biofilm to nitrate reducing conditions. *Biosensors and Bioelectronics*, 75:352–358, 2016.

[119] Elise Blanchet, Elie Desmond, Benjamin Erable, Arnaud Bridier, Théodore Bouchez, and Alain Bergel. Comparison of synthetic medium and wastewater used as dilution medium to design scalable microbial anodes: Application to food waste treatment. *Bioresource technology*, 185:106–115, 2015.

[120] César I Torres, Rosa Krajmalnik-Brown, Prathap Parameswaran, Andrew Kato Marcus, Greg Wanger, Yuri A Gorby, and Bruce E Rittmann. Selecting anode-respiring bacteria based on anode potential: phylogenetic, electrochemical, and microscopic characterization. *Environmental science & technology*, 43(24):9519–9524, 2009.

[121] Korneel Rabaey, Nico Boon, Steven D Siciliano, Marc Verhaege, and Willy Verstraete. Biofuel cells select for microbial consortia that self-mediate electron transfer. *Applied and environmental microbiology*, 70(9):5373–5382, 2004.

[122] Yunlong Li, Baogang Zhang, Ming Cheng, Yalong Li, Liting Hao, and Huaming Guo. Spontaneous arsenic (iii) oxidation with bioelectricity generation in single-chamber microbial fuel cells. *Journal of hazardous materials*, 306:8–12, 2016.

[123] Nelli J Beecroft, Feng Zhao, John R Varcoe, Robert CT Slade, Alfred E Thumser, and Claudio Avignone-Rossa. Dynamic changes in the microbial community composition in microbial fuel cells fed with sucrose. *Applied microbiology and biotechnology*, 93(1):423–437, 2012.

[124] Shun'ichi Ishii, Takefumi Shimoyama, Yasuaki Hotta, and Kazuya Watanabe. Characterization of a filamentous biofilm community established in a cellulose-fed microbial fuel cell. *Bmc Microbiology*, 8(1):1, 2008.

[125] Guodong Zhang, Yan Jiao, and Duu-Jong Lee. A lab-scale anoxic/oxic-bioelectrochemical reactor for leachate treatments. *Bioresource technology*, 186:97–105, 2015.

[126] Nina Kircheva, Jonathan Outin, Gérard Perrier, Julien Ramousse, Gérard Merlin, and Emilie Lyautey. Bio-electrochemical characterization of air-cathode microbial fuel cells with microporous polyethylene/silica membrane as separator. *Bioelectrochemistry*, 106:115–124, 2015.

[127] Byung Hong Kim, HS Park, HJ Kim, GT Kim, IS Chang, J Lee, and NT Phung. Enrichment of microbial community generating electricity using a fuel-cell-type electrochemical cell. *Applied Microbiology and Biotechnology*, 63(6):672–681, 2004.

[128] Guoqiang Zhan, Lixia Zhang, Yong Tao, Yujian Wang, Xiaoyu Zhu, and Daping Li. Anodic ammonia oxidation to nitrogen gas catalyzed by mixed biofilms in bioelectrochemical systems. *Electrochimica Acta*, 135:345–350, 2014.

[129] Waheed Miran, Mohsin Nawaz, Jiseon Jang, and Dae Sung Lee. Conversion of orange peel waste biomass to bioelectricity using a mediator-less microbial fuel cell. *Science of The Total Environment*, 547:197–205, 2016.

[130] Shanshan Wang, Liping Huang, Linlin Gan, Xie Quan, Ning Li, Guohua Chen, Lu Lu, Defeng Xing, and Fenglin Yang. Combined effects of enrichment procedure and non-fermentable or fermentable co-substrate on performance and bacterial community for pentachlorophenol degradation in microbial fuel cells. *Bioresource technology*, 120:120–126, 2012.

[131] Liping Huang, Qiang Wang, Xie Quan, Yaxuan Liu, and Guohua Chen. Bioanodes/biocathodes formed at optimal potentials enhance subsequent pentachlorophenol degradation and power generation from microbial fuel cells. *Bioelectrochemistry*, 94:13–22, 2013.

[132] Liping Huang, Yuliang Sun, Yaxuan Liu, and Ning Wang. Mineralization of 4-chlorophenol and analysis of bacterial community in microbial fuel cells. *Procedia Environmental Sciences*, 18:534–539, 2013.

[133] Pierangela Cristiani, Andrea Franzetti, Isabella Gandolfi, Edoardo Guerrini, and Giuseppina Bestetti. Bacterial dgge fingerprints of biofilms on electrodes of membraneless microbial fuel cells. *International Biodeterioration & Biodegradation*, 84:211–219, 2013.

[134] Hongsuck Kim, Byunggoon Kim, Jiyeon Kim, Taeho Lee, and Jaecheul Yu. Electricity generation and microbial community in microbial fuel cell using low-ph distillery wastewater at different external resistances. *Journal of biotechnology*, 186:175–180, 2014.

[135] Elise Blanchet, Sophie Pécastaings, Benjamin Erable, Christine Roques, and Alain Bergel. Protons accumulation during anodic phase turned to advantage for oxygen reduction during cathodic phase in reversible bioelectrodes. *Bioresource technology*, 173:224–230, 2014.

[136] Sokhee P Jung, Mi-Hwa Yoon, Seung-Mok Lee, Sang-Eun Oh, Hojeong Kang, and Jae-Kyu Yang. Power generation and anode bacterial community compositions of sediment fuel cells differing in anode materials and carbon sources. *Int. J. Electrochem. Sci*, 9:315–326, 2014.

[137] Nguyet Thu Phung, Jiyoung Lee, Kui Hyun Kang, In Seop Chang, Geoffrey Michael Gadd, and Byung Hong Kim. Analysis of microbial diversity in oligotrophic microbial fuel cells using 16s rdna sequences. *FEMS microbiology letters*, 233(1):77–82, 2004.

[138] Qian Fu, Hajime Kobayashi, Hideo Kawaguchi, Javier Vilcaez, and Kozo Sato. Identification of new microbial mediators for electromethanogenic reduction of geologically-stored carbon dioxide. *Energy Procedia*, 37:7006–7013, 2013.

[139] Jing Cai, Ping Zheng, Yajuan Xing, and Mahmood Qaisar. Effect of electricity on microbial community of microbial fuel cell simultaneously treating sulfide and nitrate. *Journal of Power Sources*, 281:27–33, 2015.

[140] Kyungmi Chung and Satoshi Okabe. Continuous power generation and microbial community structure of the anode biofilms in a three-stage microbial fuel cell system. *Applied microbiology and biotechnology*, 83(5):965–977, 2009.

[141] Jianmei Luo, Ming Li, Minghua Zhou, and Youshuang Hu. Characterization of a novel strain phylogenetically related to kocuria rhizophila and its chemical modification to improve performance of microbial fuel cells. *Biosensors and Bioelectronics*, 69:113–120, 2015.

[142] Vianey Ruiz, Zehra Esra Ilhan, Dae-Wook Kang, Rosa Krajmalnik-Brown, and Germán Buitrón. The source of inoculum plays a defining role in the development of mec microbial consortia fed with acetic and propionic acid mixtures. *Journal of biotechnology*, 182:11–18, 2014.

[143] GT Kim, G Webster, JWT Wimpenny, Byung Hong Kim, HJ Kim, and Andrew John Weightman. Bacterial community structure, compartmentalization and activity in a microbial fuel cell. *Journal of applied microbiology*, 101(3):698–710, 2006.

[144] Nils Risgaard-Petersen, André Revil, Patrick Meister, and Lars Peter Nielsen. Sulfur, iron-, and calcium cycling associated with natural electric currents running through marine sediment. *Geochimica et Cosmochimica Acta*, 92:1–13, 2012.

[145] Ugo Marzocchi, Daniela Trojan, Steffen Larsen, Rikke Louise Meyer, Niels Peter Revsbech, Andreas Schramm, Lars Peter Nielsen, and Nils Risgaard-Petersen. Electric cou-

pling between distant nitrate reduction and sulfide oxidation in marine sediment. *ISME J*, 8(8):1682–1690, 2014.

[146] Regina Schauer, Nils Risgaard-Petersen, Kasper U Kjeldsen, Jesper J Tataru Bjerg, Bo B Jørgensen, Andreas Schramm, and Lars Peter Nielsen. Succession of cable bacteria and electric currents in marine sediment. *The ISME journal*, 8(6):1314–1322, 2014.

[147] Atsushi Kouzuma, Souichiro Kato, and Kazuya Watanabe. Microbial interspecies interactions: recent findings in syntrophic consortia. *Frontiers in microbiology*, 6, 2015.

[148] Ralf Cord-Ruwisch, Derek R Lovley, and Bernhard Schink. Growth of geobacter sulfurreducens with acetate in syntrophic cooperation with hydrogen-oxidizing anaerobic partners. *Applied and environmental microbiology*, 64(6):2232–2236, 1998.

[149] Shawn E McGlynn, Grayson L Chadwick, Christopher P Kempes, and Victoria J Orphan. Single cell activity reveals direct electron transfer in methanotrophic consortia. *Nature*, 526(7574):531–535, 2015.

[150] Souichiro Kato, Kazuhito Hashimoto, and Kazuya Watanabe. Microbial interspecies electron transfer via electric currents through conductive minerals. *Proceedings of the National Academy of Sciences*, 109(25):10042–10046, 2012.

[151] David A Finkelstein, Leonard M Tender, and J Gregory Zeikus. Effect of electrode potential on electrode-reducing microbiota. *Environmental science & technology*, 40(22):6990–6995, 2006.

[152] Daniel R Bond, Dawn E Holmes, Leonard M Tender, and Derek R Lovley. Electrode-reducing microorganisms that harvest energy from marine sediments. *Science*, 295(5554):483–485, 2002.

[153] Natacha Ryckelynck, Hilmar A Stecher III, and Clare E Reimers. Understanding the anodic mechanism of a seafloor fuel cell: interactions between geochemistry and microbial activity. *Biogeochemistry*, 76(1):113–139, 2005.

[154] Nicolas Chabert, Oulfat Amin Ali, and Wafa Achouak. All ecosystems potentially host electrogenic bacteria. *Bioelectrochemistry*, 106:88–96, 2015.

[155] Baikun Li and Paul L Bishop. Micro-profiles of activated sludge floc determined using microelectrodes. *Water research*, 38(5):1248–1258, 2004.

[156] Masahiko Morita, Nikhil S Malvankar, Ashley E Franks, Zarath M Summers, Ludovic Giloteaux, Amelia E Rotaru, Camelia Rotaru, and Derek R Lovley. Potential for di-

rect interspecies electron transfer in methanogenic wastewater digester aggregates. *MBio*, 2(4):e00159–11, 2011.

[157] Miriam Rosenbaum, Zhen He, and Largus T Angenent. Light energy to bioelectricity: photosynthetic microbial fuel cells. *Current Opinion in Biotechnology*, 21(3):259–264, 2010.

[158] Xiaoxin Cao, Xia Huang, Peng Liang, Nico Boon, Mingzhi Fan, Lin Zhang, and Xiaoyuan Zhang. A completely anoxic microbial fuel cell using a photo-biocathode for cathodic carbon dioxide reduction. *Energy & Environmental Science*, 2(5):498–501, 2009.

[159] Luísa Gouveia, Carole Neves, Diogo Sebastião, Beatriz P Nobre, and Cristina T Matos. Effect of light on the production of bioelectricity and added-value microalgae biomass in a photosynthetic alga microbial fuel cell. *Bioresource technology*, 154:171–177, 2014.

[160] Araceli Gonzalez del Campo, Jose F Perez, Pablo Cañizares, Manuel A Rodrigo, Francisco J Fernandez, and Justo Lobato. Characterization of light/dark cycle and long-term performance test in a photosynthetic microbial fuel cell. *Fuel*, 140:209–216, 2015.

[161] Qingjie Hou, Haiyan Pei, Wenrong Hu, Liqun Jiang, and Ze Yu. Mutual facilitations of food waste treatment, microbial fuel cell bioelectricity generation and chlorella vulgaris lipid production. *Bioresource Technology*, 203:50–55, 2016.

[162] Iwona Gajda, John Greenman, Chris Melhuish, and Ioannis Ieropoulos. Self-sustainable electricity production from algae grown in a microbial fuel cell system. *Biomass and Bioenergy*, 82:87–93, 2015.

[163] Ramesh Kakarla, Jung Rae Kim, Byong-Hun Jeon, and Booki Min. Enhanced performance of an air–cathode microbial fuel cell with oxygen supply from an externally connected algal bioreactor. *Bioresource technology*, 195:210–216, 2015.

[164] John M Pisciotta, YongJin Zou, and Ilia V Baskakov. Light-dependent electrogenic activity of cyanobacteria. *PloS one*, 5(5):e10821, 2010.

[165] Kien B Lam, Mu Chiao, and Liwei Lin. A micro photosynthetic electrochemical cell. In *Micro Electro Mechanical Systems, 2003. MEMS-03 Kyoto. IEEE The Sixteenth Annual International Conference on*, pages 391–394. IEEE, 2003.

[166] Yuri A Gorby, Svetlana Yanina, Jeffrey S McLean, Kevin M Rosso, Dianne Moyles, Alice Dohnalkova, Terry J Beveridge, In Seop Chang, Byung Hong Kim, Kyung Shik Kim, et al. Electrically conductive bacterial nanowires produced by shewanella oneidensis strain mr-1 and other microorganisms. *Proceedings of the National Academy of Sciences*, 103(30):11358–11363, 2006.

[167] Jonathan P Badalamenti, César I Torres, and Rosa Krajmalnik-Brown. Light-responsive current generation by phototrophically enriched anode biofilms dominated by green sulfur bacteria. *Biotechnology and bioengineering*, 110(4):1020–1027, 2013.

[168] YK Cho, TJ Donohue, I Tejedor, MA Anderson, KD McMahon, and DR Noguera. Development of a solar-powered microbial fuel cell. *Journal of applied microbiology*, 104(3):640–650, 2008.

[169] Miriam Rosenbaum, Uwe Schröder, and Fritz Scholz. In situ electrooxidation of photobiological hydrogen in a photobioelectrochemical fuel cell based on rhodobacter sphaeroides. *Environmental science & technology*, 39(16):6328–6333, 2005.

[170] Miriam Rosenbaum, Uwe Schröder, and Fritz Scholz. Utilizing the green alga chlamydomonas reinhardtii for microbial electricity generation: a living solar cell. *Applied microbiology and biotechnology*, 68(6):753–756, 2005.

[171] David PBTB Strik, Ruud A Timmers, Marjolein Helder, Kirsten JJ Steinbusch, Hubertus VM Hamelers, and Cees JN Buisman. Microbial solar cells: applying photosynthetic and electrochemically active organisms. *Trends in biotechnology*, 29(1):41–49, 2011.

[172] Zhen He, Jinjun Kan, Florian Mansfeld, Largus T Angenent, and Kenneth H Nealson. Self-sustained phototrophic microbial fuel cells based on the synergistic cooperation between photosynthetic microorganisms and heterotrophic bacteria. *Environmental science & technology*, 43(5):1648–1654, 2009.

[173] David PBTB Strik, Hubertus VM Hamelers, and Cees JN Buisman. Solar energy powered microbial fuel cell with a reversible bioelectrode. *Environmental science & technology*, 44(1):532–537, 2009.

[174] Paul S Dobbin, Louise H Warren, Nicola J Cook, Alastair G McEwan, Anne K Powell, and David J Richardson. Dissimilatory iron (iii) reduction by rhodobacter capsulatus. *Microbiology*, 142(4):765–774, 1996.

[175] Xiaoxin Cao, Xia Huang, Nico Boon, Peng Liang, and Mingzhi Fan. Electricity generation by an enriched phototrophic consortium in a microbial fuel cell. *Electrochemistry Communications*, 10(9):1392–1395, 2008.

[176] Defeng Xing, Yi Zuo, Shaoan Cheng, John M Regan, and Bruce E Logan. Electricity generation by rhodopseudomonas palustris dx-1. *Environmental Science & Technology*, 42(11):4146–4151, 2008.

[177] Xin Wang, Yujie Feng, Nanqi Ren, Heming Wang, He Lee, Nan Li, and Qingliang Zhao. Accelerated start-up of two-chambered microbial fuel cells: effect of anodic positive poised potential. *Electrochimica Acta*, 54(3):1109–1114, 2009.

[178] Rachel C Wagner, Douglas F Call, and Bruce E Logan. Optimal set anode potentials vary in bioelectrochemical systems. *Environmental science & technology*, 44(16):6036–6041, 2010.

[179] Jieun Song, Daisuke Sasaki, Kengo Sasaki, Souichiro Kato, Akihiko Kondo, Kazuhito Hashimoto, and Shuji Nakanishi. Comprehensive metabolomic analyses of anode-respiring geobacter sulfurreducens cells: The impact of anode-respiration activity on intracellular metabolite levels. *Process Biochemistry*, 51(1):34–38, 2016.

[180] Andrew Kato Marcus, César I Torres, and Bruce E Rittmann. Conduction-based modeling of the biofilm anode of a microbial fuel cell. *Biotechnology and Bioengineering*, 98(6):1171–1182, 2007.

[181] Ka Yu Cheng, Goen Ho, and Ralf Cord-Ruwisch. Affinity of microbial fuel cell biofilm for the anodic potential. *Environmental science & technology*, 42(10):3828–3834, 2008.

[182] Hyung-Sool Lee, César I Torres, and Bruce E Rittmann. Effects of substrate diffusion and anode potential on kinetic parameters for anode-respiring bacteria. *Environmental science & technology*, 43(19):7571–7577, 2009.

[183] Rachel A Yoho, Sudeep C Popat, and César I Torres. Dynamic potential-dependent electron transport pathway shifts in anode biofilms of geobacter sulfurreducens. *ChemSusChem*, 7(12):3413–3419, 2014.

[184] Juan Pablo Busalmen, Abraham Esteve-Nuñez, Antonio Berná, and Juan Miguel Feliu. Atrseiras characterization of surface redox processes in g. sulfurreducens. *Bioelectrochemistry*, 78(1):25–29, 2010.

[185] Xiuping Zhu, Matthew D Yates, and Bruce E Logan. Set potential regulation reveals additional oxidation peaks of geobacter sulfurreducens anodic biofilms. *Electrochemistry Communications*, 22:116–119, 2012.

[186] Laurence Soussan, Benjamin Erable, Marie-Line Délia, and Alain Bergel. The open circuit potential of geobacter sulfurreducens bioanodes depends on the electrochemical adaptation of the strain. *Electrochemistry Communications*, 33:35–38, 2013.

[187] Jincheng Wei, Peng Liang, Xiaoxin Cao, and Xia Huang. A new insight into potential regulation on growth and power generation of geobacter sulfurreducens in microbial fuel cells based on energy viewpoint. *Environmental science & technology*, 44(8):3187–3191, 2010.

[188] David White, James T Drummond, and Clay Fuqua. *The physiology and biochemistry of prokaryotes*. Oxford University Press New York, 1995.

[189] Peter Aelterman, Stefano Freguia, Jurg Keller, Willy Verstraete, and Korneel Rabaey. The anode potential regulates bacterial activity in microbial fuel cells. *Applied microbiology and biotechnology*, 78(3):409–418, 2008.

[190] Xiuping Zhu, Matthew D Yates, Marta C Hatzell, Hari Ananda Rao, Pascal E Saikaly, and Bruce E Logan. Microbial community composition is unaffected by anode potential. *Environmental science & technology*, 48(2):1352–1358, 2014.

[191] Yujie Feng, Qiao Yang, Xin Wang, and Bruce E Logan. Treatment of carbon fiber brush anodes for improving power generation in air–cathode microbial fuel cells. *Journal of Power Sources*, 195(7):1841–1844, 2010.

[192] Yang-Yang Yu, Chun Xian Guo, Yang-Chun Yong, Chang Ming Li, and Hao Song. Nitrogen doped carbon nanoparticles enhanced extracellular electron transfer for high-performance microbial fuel cells anode. *Chemosphere*, 140:26–33, 2015.

[193] Mengmeng Liu, Minghua Zhou, Huijia Yang, Gengbo Ren, and Yingying Zhao. Titanium dioxide nanoparticles modified three dimensional ordered macroporous carbon for improved energy output in microbial fuel cells. *Electrochimica Acta*, 190:463–470, 2016.

[194] Fatima AlZahra'a Alatraktchi, Yifeng Zhang, Jafar Safaa Noori, and Irini Angelidaki. Surface area expansion of electrodes with grass-like nanostructures and gold nanoparticles to enhance electricity generation in microbial fuel cells. *Bioresource technology*, 123:177–183, 2012.

[195] Xiangchun Quan, Bo Sun, and Hengduo Xu. Anode decoration with biogenic pd nanoparticles improved power generation in microbial fuel cells. *Electrochimica Acta*, 182:815–820, 2015.

[196] Michael Bunge, Lina S Søbjerg, Amelia-Elena Rotaru, Delphine Gauthier, Anders T Lindhardt, Gerd Hause, Kai Finster, Peter Kingshott, Troels Skrydstrup, and Rikke L Meyer. Formation of palladium (0) nanoparticles at microbial surfaces. *Biotechnology and bioengineering*, 107(2):206–215, 2010.

[197] In Ho Park, Maria Christy, Pil Kim, and Kee Suk Nahm. Enhanced electrical contact of microbes using fe 3 o 4/cnt nanocomposite anode in mediator-less microbial fuel cell. *Biosensors and Bioelectronics*, 58:75–80, 2014.

[198] Akshay Modi, Shiv Singh, and Nishith Verma. In situ nitrogen-doping of nickel nanoparticle-dispersed carbon nanofiber-based electrodes: Its positive effects on the performance of a microbial fuel cell. *Electrochimica Acta*, 190:620–627, 2016.

[199] Celal Erbay, Xiong Pu, Woongchul Choi, Mi-Jin Choi, Yeontack Ryu, Huijie Hou, Furong Lin, Paul de Figueiredo, Choongho Yu, and Arum Han. Control of geometrical properties of carbon nanotube electrodes towards high-performance microbial fuel cells. *Journal of Power Sources*, 280:347–354, 2015.

[200] Celal Erbay, Gang Yang, Paul de Figueiredo, Reza Sadr, Choongho Yu, and Arum Han. Three-dimensional porous carbon nanotube sponges for high-performance anodes of microbial fuel cells. *Journal of Power Sources*, 298:177–183, 2015.

[201] Shuiliang Chen, Guanghua He, Qin Liu, Falk Harnisch, Yan Zhou, Yu Chen, Muddasir Hanif, Suqin Wang, Xinwen Peng, Haoqing Hou, et al. Layered corrugated electrode macrostructures boost microbial bioelectrocatalysis. *Energy & Environmental Science*, 5(12):9769–9772, 2012.

[202] Shuiliang Chen, Guanghua He, Xiaowu Hu, Mingyun Xie, Suqin Wang, Daojie Zeng, Haoqing Hou, and Uwe Schröder. A three-dimensionally ordered macroporous carbon derived from a natural resource as anode for microbial bioelectrochemical systems. *ChemSusChem*, 5(6):1059–1063, 2012.

[203] Jun Zhang, Jun Li, Dingding Ye, Xun Zhu, Qiang Liao, and Biao Zhang. Tubular bamboo charcoal for anode in microbial fuel cells. *Journal of Power Sources*, 272:277–282, 2014.

[204] Felix Offei, Anders Thygesen, Moses Mensah, Kwame Tabbicca, Dinesh Fernando, Irina Petrushina, and Geoffrey Daniel. A viable electrode material for use in microbial fuel cells for tropical regions. *Energies*, 9(1):35, 2016.

[205] Mengmeng Liu, Minghua Zhou, Huijia Yang, Gengbo Ren, and Yingying Zhao. Titanium dioxide nanoparticles modified three dimensional ordered macroporous carbon for improved energy output in microbial fuel cells. *Electrochimica Acta*, 2015.

[206] Mirella Di Lorenzo, Keith Scott, Tom P Curtis, and Ian M Head. Effect of increasing anode surface area on the performance of a single chamber microbial fuel cell. *Chemical Engineering Journal*, 156(1):40–48, 2010.

[207] Lihong Liu, Tzu-Yang Chou, Chin-Yu Lee, Duu-Jong Lee, Ay Su, and Juin-Yih Lai. Performance of freshwater sediment microbial fuel cells: Consistency. *International Journal of Hydrogen Energy*, 2015.

[208] Timothy D Harrington, Jerome T Babauta, Emily K Davenport, Ryan S Renslow, and Haluk Beyenal. Excess surface area in bioelectrochemical systems causes ion transport limitations. *Biotechnology and bioengineering*, 112(5):858–866, 2015.

[209] Alim Dewan, Haluk Beyenal, and Zbigniew Lewandowski. Scaling up microbial fuel cells. *Environmental science & technology*, 42(20):7643–7648, 2008.

[210] Naroa Uría, David Sánchez, Roser Mas, Olga Sánchez, Francesc Xavier Munoz, and Jordi Mas. Effect of the cathode/anode ratio and the choice of cathode catalyst on the performance of microbial fuel cell transducers for the determination of microbial activity. *Sensors and Actuators B: Chemical*, 170:88–94, 2012.

[211] G Hernández-Flores, HM Poggi-Varaldo, O Solorza-Feria, MT Ponce Noyola, T Romero-Castañón, and N Rinderknecht-Seijas. Tafel equation based model for the performance of a microbial fuel cell. *International Journal of Hydrogen Energy*, 40(48):17421–17432, 2015.

[212] E Martinucci, F Pizza, D Perrino, A Colombo, SPM Trasatti, A Lazzarini Barnabei, A Liberale, and P Cristiani. Energy balance and microbial fuel cells experimentation at wastewater treatment plant milano-nosedo. *International Journal of Hydrogen Energy*, 40(42):14683–14689, 2015.

[213] Li Xiao, Zheng Ge, Patrick Kelly, Fei Zhang, and Zhen He. Evaluation of normalized energy recovery (ner) in microbial fuel cells affected by reactor dimensions and substrates. *Bioresource technology*, 157:77–83, 2014.

[214] Jiseon You, Carlo Santoro, John Greenman, Chris Melhuish, Pierangela Cristiani, Baikun Li, and Ioannis Ieropoulos. Micro-porous layer (mpl)-based anode for microbial fuel cells. *International Journal of Hydrogen Energy*, 39(36):21811–21818, 2014.

[215] Bingchuan Liu, Isaiah Williams, Yan Li, Lei Wang, Amvrossios Bagtzoglou, Jeffrey McCutcheon, and Baikun Li. Towards high power output of scaled-up benthic microbial fuel cells (bmfcs) using multiple electron collectors. *Biosensors and Bioelectronics*, 79:435–441, 2016.

[216] Howard W Harris, Mohamed Y El-Naggar, Orianna Bretschger, Melissa J Ward, Margaret F Romine, AY Obraztsova, and Kenneth H Nealson. Electrokinesis is a microbial behavior that requires extracellular electron transport. *Proceedings of the National Academy of Sciences*, 107(1):326–331, 2010.

[217] Victor Burke and Fred O Gibson. The gram reaction and the electric charge of bacteria. *Journal of bacteriology*, 26(2):211, 1933.

[218] Ravinder Kumar, Lakhveer Singh, and AW Zularisam. Exoelectrogens: Recent advances in molecular drivers involved in extracellular electron transfer and strategies used to improve it for microbial fuel cell applications. *Renewable and Sustainable Energy Reviews*, 56:1322–1336, 2016.

[219] Seokheun Choi and Junseok Chae. Optimal biofilm formation and power generation in a micro-sized microbial fuel cell (mfc). *Sensors and Actuators A: Physical*, 195:206–212, 2013.

[220] Bernardino Virdis, Diego Millo, Bogdan C Donose, and Damien J Batstone. Real-time measurements of the redox states of c-type cytochromes in electroactive biofilms: A confocal resonance raman microscopy study. *PloS one*, 9(2):e89918, 2014.

[221] Kelly P Nevin, H Richter, SF Covalla, JP Johnson, TL Woodard, AL Orloff, H Jia, M Zhang, and DR Lovley. Power output and columbic efficiencies from biofilms of geobacter sulfurreducens comparable to mixed community microbial fuel cells. *Environmental microbiology*, 10(10):2505–2514, 2008.

[222] Bruce E Logan and John M Regan. Electricity-producing bacterial communities in microbial fuel cells. *TRENDS in Microbiology*, 14(12):512–518, 2006.

[223] Krishna Katuri, M Luisa Ferrer, María C Gutiérrez, Ricardo Jiménez, Francisco del Monte, and Dónal Leech. Three-dimensional microchanelled electrodes in flow-through configuration for bioanode formation and current generation. *Energy & Environmental Science*, 4(10):4201–4210, 2011.

[224] James P Stratford, Nelli J Beecroft, Robert CT Slade, André Grüning, and Claudio Avignone-Rossa. Anodic microbial community diversity as a predictor of the power output of microbial fuel cells. *Bioresource technology*, 156:84–91, 2014.

[225] Tonia Tommasi, Adriano Sacco, Caterina Armato, Diana Hidalgo, Livio Millone, Alessandro Sanginario, Elena Tresso, Tiziana Schilirò, and Candido Fabrizio Pirri. Dynamical analysis of microbial fuel cells based on planar and 3d-packed anodes. *Chemical Engineering Journal*, 288:38–49, 2016.

[226] Audrey S Commault, Gavin Lear, and Richard J Weld. Maintenance of geobacter-dominated biofilms in microbial fuel cells treating synthetic wastewater. *Bioelectrochemistry*, 106:150–158, 2015.

[227] Jayesh M Sonawane, Arpit Gupta, and Prakash C Ghosh. Multi-electrode microbial fuel cell (memfc): a close analysis towards large scale system architecture. *international journal of hydrogen energy*, 38(12):5106–5114, 2013.

[228] Yongtae Ahn, Marta C Hatzell, Fang Zhang, and Bruce E Logan. Different electrode configurations to optimize performance of multi-electrode microbial fuel cells for generating power or treating domestic wastewater. *Journal of Power Sources*, 249:440–445, 2014.

[229] Bingchuan Liu, Alyssa Weinstein, Michael Kolln, Caleb Garrett, Lei Wang, Amvrossios Bagtzoglou, Udayarka Karra, Yan Li, and Baikun Li. Distributed multiple-anodes benthic microbial fuel cell as reliable power source for subsea sensors. *Journal of Power Sources*, 286:210–216, 2015.

[230] Daehee Kim, Junyeong An, Bongkyu Kim, Jae Kyung Jang, Byung Hong Kim, and In Seop Chang. Scaling-up microbial fuel cells: Configuration and potential drop phenomenon at series connection of unit cells in shared anolyte. *ChemSusChem*, 5(6):1086–1091, 2012.

[231] Junyeong An, Bongkyu Kim, Jae Kyung Jang, Hyung-Sool Lee, and In Seop Chang. New architecture for modulization of membraneless and single-chambered microbial fuel cell using a bipolar plate-electrode assembly (bea). *Biosensors and Bioelectronics*, 59:28–34, 2014.

[232] Lijiao Ren, Yongtae Ahn, Huijie Hou, Fang Zhang, and Bruce E Logan. Electrochemical study of multi-electrode microbial fuel cells under fed-batch and continuous flow conditions. *Journal of Power Sources*, 257:454–460, 2014.

[233] César I Torres, Andrew Kato Marcus, and Bruce E Rittmann. Proton transport inside the biofilm limits electrical current generation by anode-respiring bacteria. *Biotechnology and Bioengineering*, 100(5):872–881, 2008.

[234] Falk Harnisch, Uwe Schröder, and Fritz Scholz. The suitability of monopolar and bipolar ion exchange membranes as separators for biological fuel cells. *Environmental science & technology*, 42(5):1740–1746, 2008.

[235] Ampai Kumlanghan, Proespichaya Kanatharana, Punnee Asawatreratanakul, Bo Mattiasson, and Panote Thavarungkul. Microbial bod sensor for monitoring treatment of wastewater from a rubber latex industry. *Enzyme and microbial technology*, 42(6):483–491, 2008.

[236] Feng Zhao, Robert CT Slade, and John R Varcoe. Techniques for the study and development of microbial fuel cells: an electrochemical perspective. *Chemical Society Reviews*, 38(7):1926–1939, 2009.

[237] Sharon B Velasquez-Orta, Tom P Curtis, and Bruce E Logan. Energy from algae using microbial fuel cells. *Biotechnology and bioengineering*, 103(6):1068–1076, 2009.

[238] P. Stiefel, S. Schmidt-Emrich, K. Maniura-Weber, and Q. Ren. Critical aspects of using bacterial cell viability assays with the fluorophores SYTO9 and propidium iodide. *BMC Microbiol.*, 15:36, 2015.

[239] Noha Youssef, Cody S Sheik, Lee R Krumholz, Fares Z Najar, Bruce A Roe, and Mostafa S Elshahed. Comparison of species richness estimates obtained using nearly complete fragments and simulated pyrosequencing-generated fragments in 16s rrna gene-based environmental surveys. *Applied and environmental microbiology*, 75(16):5227–5236, 2009.

[240] Marcus J Claesson, Qiong Wang, Orla O'Sullivan, Rachel Greene-Diniz, James R Cole, R Paul Ross, and Paul W O'Toole. Comparison of two next-generation sequencing technologies for resolving highly complex microbiota composition using tandem variable 16s rrna gene regions. *Nucleic acids research*, page 873, 2010.

[241] Christopher Quince, Anders Lanzen, Russell J Davenport, and Peter J Turnbaugh. Removing noise from pyrosequenced amplicons. *BMC bioinformatics*, 12(1):1, 2011.

[242] Micah Hamady, Jeffrey J Walker, J Kirk Harris, Nicholas J Gold, and Rob Knight. Error-correcting barcoded primers allow hundreds of samples to be pyrosequenced in multiplex. *Nature methods*, 5(3):235, 2008.

[243] Nils Johan Fredriksson, Malte Hermansson, and Britt-Marie Wilén. The choice of pcr primers has great impact on assessments of bacterial community diversity and dynamics in a wastewater treatment plant. *PloS one*, 8(10):e76431, 2013.

[244] J Gregory Caporaso, Justin Kuczynski, Jesse Stombaugh, Kyle Bittinger, Frederic D Bushman, Elizabeth K Costello, Noah Fierer, Antonio Gonzalez Pena, Julia K Goodrich, Jeffrey I Gordon, et al. Qiime allows analysis of high-throughput community sequencing data. *Nature methods*, 7(5):335–336, 2010.

[245] Daniel McDonald, Jose C Clemente, Justin Kuczynski, Jai Ram Rideout, Jesse Stombaugh, Doug Wendel, Andreas Wilke, Susan Huse, John Hufnagle, Folker Meyer, et al. The biological observation matrix (biom) format or: how i learned to stop worrying and love the ome-ome. *GigaScience*, 1(1):7, 2012.

[246] Thomas Kuilman, Arno Velds, Kristel Kemper, Marco Ranzani, Lorenzo Bombardelli, Marlous Hoogstraat, Ekaterina Nevedomskaya, Guotai Xu, Julian de Ruiter, Martijn P Lolkema, et al. Copywriter: Dna copy number detection from off-target sequence data. *Genome Biol*, 16(1):49, 2015.

[247] Kathrin P Aßhauer, Bernd Wemheuer, Rolf Daniel, and Peter Meinicke. Tax4fun: predicting functional profiles from metagenomic 16s rrna data. *Bioinformatics*, 31(17):2882–2884,

2015.

[248] Mariusz Jankowski. Erosion, dilation and related operators. *Department of Electrical EngineeringUniversity of Southern Maine Portland, Maine, USA*, 2006.

[249] Stefan Van Der Walt, Johannes L Schönberger, Juan Nunez-Iglesias, François Boulogne, Joshua D Warner, Neil Yager, Emmanuelle Gouillart, and Tony Yu. scikit-image: image processing in python. *PeerJ*, 2:e453, 2014.

[250] Bruce E Logan, Bert Hamelers, René Rozendal, Uwe Schröder, Jürg Keller, Stefano Freguia, Peter Aelterman, Willy Verstraete, and Korneel Rabaey. Microbial fuel cells: methodology and technology. *Environmental science & technology*, 40(17):5181–5192, 2006.

[251] Rudolf K Thauer, Kurt Jungermann, and Karl Decker. Energy conservation in chemotrophic anaerobic bacteria. *Bacteriological reviews*, 41(1):100, 1977.

[252] Garrett Hardin et al. The competitive exclusion principle. *science*, 131(3409):1292–1297, 1960.

[253] Michael T Madigan and Deborah O Jung. An overview of purple bacteria: systematics, physiology, and habitats. In *The purple phototrophic bacteria*, pages 1–15. Springer, 2009.

[254] David PBTB Strik, Jan FH Snel, Cees JN Buisman, et al. Green electricity production with living plants and bacteria in a fuel cell. *International Journal of Energy Research*, 32(9):870–876, 2008.

[255] Hai-Long Tian, Jie-Yu Zhao, Hong-Yu Zhang, Chang-Qiao Chi, Bao-An Li, and Xiao-Lei Wu. Bacterial community shift along with the changes in operational conditions in a membrane-aerated biofilm reactor. *Applied microbiology and biotechnology*, 99(7):3279–3290, 2015.

[256] Dan MacIsaac, Gary Kanner, and Graydon Anderson. Basic physics of the incandescent lamp (lightbulb). *The Physics Teacher*, 37(9):520–525, 1999.

[257] Frank W Larimer, Patrick Chain, Loren Hauser, Jane Lamerdin, Stephanie Malfatti, Long Do, Miriam L Land, Dale A Pelletier, J Thomas Beatty, Andrew S Lang, et al. Complete genome sequence of the metabolically versatile photosynthetic bacterium rhodopseudomonas palustris. *Nature biotechnology*, 22(1):55–61, 2004.

[258] Pietro Carlozzi, Benjamin Pushparaj, Alessandro Degl Innocenti, and Antonella Capperucci. Growth characteristics of rhodopseudomonas palustris cultured outdoors, in an underwater tubular photobioreactor, and investigation on photosynthetic efficiency. *Applied microbiology and biotechnology*, 73(4):789–795, 2006.

[259] Xiuping Zhu, Justin C Tokash, Yiying Hong, and Bruce E Logan. Controlling the occurrence of power overshoot by adapting microbial fuel cells to high anode potentials. *Bioelectrochemistry*, 90:30–35, 2013.

[260] Hong Liu, Shaoan Cheng, and Bruce E Logan. Production of electricity from acetate or butyrate using a single-chamber microbial fuel cell. *Environmental science & technology*, 39(2):658–662, 2005.

[261] Hanno Richter, Kelly P Nevin, Hongfei Jia, Daniel A Lowy, Derek R Lovley, and Leonard M Tender. Cyclic voltammetry of biofilms of wild type and mutant geobacter sulfurreducens on fuel cell anodes indicates possible roles of omcb, omcz, type iv pili, and protons in extracellular electron transfer. *Energy & Environmental Science*, 2(5):506–516, 2009.

[262] Anne Willems, Paul De Vos, and Jozef De Ley. The genus comamonas. *The Prokaryotes: a handbook on the biology of bacteria, ecophysiology, isolation, identification and applications, 2nd edition.*, 3:2583–2590, 1992.

[263] Jan Vanbrabant, Paul De Vos, Marc Vancanneyt, Jan Liessens, Willy Verstraete, and Karel Kersters. Isolation and identification of autotrophic and heterotrophic bacteria from an autohydrogenotrophic pilot-plant for denitrification of drinking water. *Systematic and applied microbiology*, 16(3):471–482, 1993.

[264] Yumiko Kodama, Takefumi Shimoyama, and Kazuya Watanabe. Dysgonomonas oryzarvi sp. nov., isolated from a microbial fuel cell. *International journal of systematic and evolutionary microbiology*, 62(Pt 12):3055–3059, 2012.

[265] Harini Nagendra. Opposite trends in response for the shannon and simpson indices of landscape diversity. *Applied Geography*, 22(2):175–186, 2002.

[266] Sarah M Strycharz, Anthony P Malanoski, Rachel M Snider, Hana Yi, Derek R Lovley, and Leonard M Tender. Application of cyclic voltammetry to investigate enhanced catalytic current generation by biofilm-modified anodes of geobacter sulfurreducens strain dl1 vs. variant strain kn400. *Energy & Environmental Science*, 4(3):896–913, 2011.

[267] Sang-Eun Oh and Bruce E Logan. Proton exchange membrane and electrode surface areas as factors that affect power generation in microbial fuel cells. *Applied Microbiology and Biotechnology*, 70(2):162–169, 2006.

[268] Xiao-Li Su, Qi Tian, Jie Zhang, Xian-Zheng Yuan, Xiao-Shuang Shi, Rong-Bo Guo, and Yan-Ling Qiu. Acetobacteroides hydrogenigenes gen. nov., sp. nov., an anaerobic hydrogen-producing bacterium in the family rikenellaceae isolated from a reed swamp. *International journal of systematic and evolutionary microbiology*, 64(9):2986–2991, 2014.

[269] J Cameron Thrash, Sarir Ahmadi, Tamas Torok, and John D Coates. Magnetospirillum bellicus sp. nov., a novel dissimilatory perchlorate-reducing alphaproteobacterium isolated from a bioelectrical reactor. *Applied and environmental microbiology*, 76(14):4730–4737, 2010.

[270] Hamid Rismani-Yazdi, Ann D Christy, Burk A Dehority, Mark Morrison, Zhongtang Yu, and Olli H Tuovinen. Electricity generation from cellulose by rumen microorganisms in microbial fuel cells. *Biotechnology and bioengineering*, 97(6):1398–1407, 2007.

[271] Jay B Benziger, M Barclay Satterfield, Warren HJ Hogarth, James P Nehlsen, and Ioannis G Kevrekidis. The power performance curve for engineering analysis of fuel cells. *Journal of Power Sources*, 155(2):272–285, 2006.

[272] Valerie J Watson and Bruce E Logan. Analysis of polarization methods for elimination of power overshoot in microbial fuel cells. *Electrochemistry Communications*, 13(1):54–56, 2011.

[273] Shun'ichi Ishii, Tomoyuki Kosaka, Katsutoshi Hori, Yasuaki Hotta, and Kazuya Watanabe. Coaggregation facilitates interspecies hydrogen transfer between pelotomaculum thermopropionicum and methanothermobacter thermautotrophicus. *Applied and environmental microbiology*, 71(12):7838–7845, 2005.

[274] Jincheng Wei, Peng Liang, and Xia Huang. Recent progress in electrodes for microbial fuel cells. *Bioresource technology*, 102(20):9335–9344, 2011.

[275] JJ Hwang and PY Chen. Heat/mass transfer in porous electrodes of fuel cells. *International journal of heat and mass transfer*, 49(13):2315–2327, 2006.

[276] Paula Watnick and Roberto Kolter. Biofilm, city of microbes. *Journal of bacteriology*, 182(10):2675–2679, 2000.

[277] Trevor Roger Garrett, Manmohan Bhakoo, and Zhibing Zhang. Bacterial adhesion and biofilms on surfaces. *Progress in Natural Science*, 18(9):1049–1056, 2008.

[278] Oda Steenhoudt and Jos Vanderleyden. Azospirillum, a free-living nitrogen-fixing bacterium closely associated with grasses: genetic, biochemical and ecological aspects. *FEMS microbiology reviews*, 24(4):487–506, 2000.

[279] WC Lin, Maddalena V Coppi, and DR Lovley. Geobacter sulfurreducens can grow with oxygen as a terminal electron acceptor. *Applied and Environmental Microbiology*, 70(4):2525–2528, 2004.

[280] Vijay A Sethuraman, John W Weidner, Andrew T Haug, Sathya Motupally, and Lesia V Protsailo. Hydrogen peroxide formation rates in a pemfc anode and cathode effect of humidity and temperature. *Journal of The Electrochemical Society*, 155(1):B50–B57, 2008.

[281] Biljana Šljukić, Craig E Banks, Slavko Mentus, and Richard G Compton. Modification of carbon electrodes for oxygen reduction and hydrogen peroxide formation: The search for stable and efficient sonoelectrocatalysts. *Physical Chemistry Chemical Physics*, 6(5):992–997, 2004.

[282] P Drogui, S Elmaleh, M Rumeau, C Bernard, and A Rambaud. Oxidising and disinfecting by hydrogen peroxide produced in a two-electrode cell. *Water Research*, 35(13):3235–3241, 2001.

[283] Akila Ganesan, Sebastien Chaussonnerie, Anne Tarrade, Catherine Dauga, Theodore Bouchez, Eric Pelletier, Denis Le Paslier, and Abdelghani Sghir. Cloacibacillus evryensis gen. nov., sp. nov., a novel asaccharolytic, mesophilic, amino-acid-degrading bacterium within the phylum 'synergistetes', isolated from an anaerobic sludge digester. *International journal of systematic and evolutionary microbiology*, 58(9):2003–2012, 2008.

[284] RE Mahony, U Helmke, and JB Moore. Gradient algorithms for principal component analysis. *The Journal of the Australian Mathematical Society. Series B. Applied Mathematics*, 37(04):430–450, 1996.

[285] Mieke CAA Van Eerten-Jansen, Anna B Veldhoen, Caroline M Plugge, Alfons JM Stams, Cees JN Buisman, and Annemiek Ter Heijne. Microbial community analysis of a methane-producing biocathode in a bioelectrochemical system. *Archaea*, 2013, 2013.

[286] Theerthankar Das, Shama Sehar, and Mike Manefield. The roles of extracellular dna in the structural integrity of extracellular polymeric substance and bacterial biofilm development. *Environmental microbiology reports*, 5(6):778–786, 2013.

[287] Sasha J Rose, Lmar M Babrak, and Luiz E Bermudez. Mycobacterium avium possesses extracellular dna that contributes to biofilm formation, structural integrity, and tolerance to antibiotics. *PloS one*, 10(5):e0128772, 2015.

[288] Morten Harmsen, Martin Lappann, Susanne Knøchel, and Søren Molin. Role of extracellular dna during biofilm formation by listeria monocytogenes. *Applied and environmental microbiology*, 76(7):2271–2279, 2010.

[289] Irit Gilan and Alex Sivan. Extracellular dna plays an important structural role in the biofilm of the plastic degrading actinomycete rhodo-coccus ruber. *Advances in Microbiology*, 2013, 2013.

[290] Robin T Merod, Jennifer E Warren, Hope McCaslin, and Stefan Wuertz. Toward automated analysis of biofilm architecture: bias caused by extraneous confocal laser scanning microscopy images. *Applied and environmental microbiology*, 73(15):4922–4930, 2007.

[291] Martin Kuehn, Martina Hausner, Hans-Joachim Bungartz, Michael Wagner, Peter A Wilderer, and Stefan Wuertz. Automated confocal laser scanning microscopy and semiautomated image processing for analysis of biofilms. *Applied and environmental microbiology*, 64(11):4115–4127, 1998.

[292] JB Xavier, DC White, and JS Almeida. Automated biofilm morphology quantification from confocal laser scanning microscopy imaging. *Water Science & Technology*, 47(5):31–37, 2003.